THE UNIVERSITY OF
SYDNEY

COPYRIGHT AND USE OF THIS THESIS

This thesis must be used in accordance with the provisions of the Copyright Act 1968.

Reproduction of material protected by copyright may be an infringement of copyright and copyright owners may be entitled to take legal action against persons who infringe their copyright.

Section 51 (2) of the Copyright Act permits an authorized officer of a university library or archives to provide a copy (by communication or otherwise) of an unpublished thesis kept in the library or archives, to a person who satisfies the authorized officer that he or she requires the reproduction for the purposes of research or study.

The Copyright Act grants the creator of a work a number of moral rights, specifically the right of attribution, the right against false attribution and the right of integrity.

You may infringe the author's moral rights if you:

- fail to acknowledge the author of this thesis if you quote sections from the work
- attribute this thesis to another author
- subject this thesis to derogatory treatment which may prejudice the author's reputation

For further information contact the University's Director of Copyright Services

sydney.edu.au/copyright

CLINICAL, PATHOLOGICAL AND GENETIC BASIS OF BICUSPID AORTIC VALVE DISEASE

Ratnasari Padang

A thesis submitted in fulfilment of the requirements for the degree of

Doctor of Philosophy

Faculty of Medicine

University of Sydney

August 2014

DECLARATION

The work described within this thesis was carried out at the Agnes Ginges Centre for Molecular Cardiology, Centenary Institute, and the Department of Cardiology and Cardiothoracic Surgery, Royal Prince Alfred Hospital, under the supervisions of Professor Christopher Semsarian, Professor Paul G. Bannon, Doctor Richard Bagnall and Doctor Rajesh Puranik between February 2011 and July 2014. Unless otherwise acknowledged, this work was carried out by the author. This thesis has not been submitted, in either whole or part, for the purposes of obtaining any other degree.

Ratnasari Padang

August 2014

ACKNOWLEDGEMENTS

Prof. Christopher Semsarian, Dr. Richard Bagnall, Prof. Paul Bannon and Dr. Rajesh Puranik – all of you are supervisors like no other. There are no words to express my gratitude for the things that you have taught and given me.

A/Prof. David Richmond – for inspiring me into this project, sharing with me your knowledge and passion for research, for your time, mentorship and unconditional support. My deepest and utmost appreciation.

To all the patients who have participated in the project – the works in this thesis will not even be remotely possible without your participations. Your generosity and trust in my work really humble me.

Ms. Lisa Turner, Ms. Ann Madden, all the cardiothoracic surgeons, cardiologist, operating theatre 21 and 22 nurses and cardiothoracic anaesthetists at RPAH – for your unconditional support to this project, from case referrals and recruitments, to assistance with intraoperative specimens collections. The recruitment process would not have gone as smoothly without your help.

My family and friends at Centenary and RPAH – for being there for me and for supporting me through the ups and downs in the past 3.5 years.

NHMRC and NHF of Australia – for funding and supporting this project.

And finally, My husband, Sergei – for believing in me and for supporting me. You know what you are: my rock and my world. This thesis is dedicated to you.

Thank You.

TABLE OF CONTENTS

ABSTRACT

Bicuspid aortic valve (BAV) is the most common congenital heart defect. It is a clinically heterogeneous disorder with valve dysfunction and related aortopathy being the major complications. Familial clustering and genetic studies have established that BAV is a highly heritable trait, indicating an underlying genetic basis. However, the underlying genetic basis of BAV disease in humans is mostly undetermined. The gene and molecular pathways that underlie the development of structural valve degeneration (SVD) and valvular dysfunction in BAV are also not well understood. Further, identification of patients with BAV who are at the highest risk for developing aortic complications presents a challenging task for most clinicians today. Hence, the work carried out in this thesis aimed to address these gaps in our present knowledge of BAV disease.

To investigate the genetics underlying BAV development, candidate gene approach and whole exome sequencing were performed on sporadic and familial cases of BAV, respectively. In the candidate gene study, the relationship between *GATA5* and *Nkx2-5* gene variations and BAV disease were investigated amongst 100 unrelated cases of BAV. Whilst screening of *Nkx2-5* failed to identify disease-causing mutations in the study cohort, analysis of the *GATA5* gene screening identified the presence of 4 rare non-synonymous variants located in the transcriptional activator domains I and II of *GATA5*, of which 3 affected highly evolutionarily conserved amino acid residues, specifically Gln3Arg, Ser19Trp and Tyr142His. These non-

synonymous variants may alter the transcriptional activity of *GATA5*, and therefore may contribute to the development of BAV in humans. Meanwhile, exome sequencing approach was adopted to investigate the genetics underlying BAV development in 2 large Caucasian families with preponderance for BAV and the related aortopathy. Variants prioritisation and the subsequent co-segregation analyses revealed a completely different list of shared candidate gene variants between the 2 families. While the composition of the lists of shared candidate gene variants within the 2 families, apart from the causative variant itself, was mostly determined by chance, the fact that the lists were completely different between the 2 families, and assuming that the causative variant was present within the lists, implied that the causative variant responsible for BAV development in Family A and B would be different and unique to each family. Accordingly, this finding supported a previous observation that suggested the presence of mutations in diverse genes (i.e. genetic heterogeneity) to be responsible for the development of BAV in different families. Also, the study incidentally identified mutations in the GDNF-related pathway to be mutually occurring in both families, thus providing some clues toward its potential regulatory role in BAV development, which warranted further investigation.

A genome-wide transcriptome profiling was performed using RNA sequencing to investigate the differential gene expression underlying SVD in human BAV compared to the normal trileaflet aortic valve (TAV). The study identified that differential gene expression profiles existed even within the BAV group, dividing them into those with calcification predominant disease and those with primarily

redundant leaflet degeneration. It also demonstrated the shared upregulation of inflammatory pathways and downregulation of *NOTCH1* signalling within calcified human BAV and TAV leaflets, indicating a common mechanism of calcific leaflet degenerations in human aortic valve. Further, a unique pattern of dysregulation of foetal gene programs was also identified amongst the different study subgroups. Taken together, these findings indicated the presence of distinct gene expression signatures that marked the different type of SVD in BAV, compared to TAV, supporting an emerging theory that BAV is heterogeneous with respect to molecular events in disease progression.

The project also investigated the role of CMR imaging in the evaluation of differential aortic wall mechanical properties between patients with BAV and TAV in response to exercise, in attempt to identify novel imaging biomarkers to predict those with a more aggressive BAV-related aortic disease phenotype. In this pilot study, free-breathing real-time CMR imaging was shown to provide the necessary spatial and temporal resolution to allow accurate dynamic structural assessment of the aorta. This study however failed to detect a statistically significant difference in aortic mechanical properties between patients with BAV and TAV during exercise, possibly related to the limitation created by a small sample size. An alternative explanation to this observation is that there is, in fact, no true difference between the 2 groups, i.e. the null hypothesis is correct. Interestingly, the study identified an immediate reduction of aortic elastic properties amongst patients with BAV in response to a brief period of resistance exercise, which may have important implications during exercise prescription amongst individuals with BAV.

In summary, the studies presented in this thesis have contributed to the present understanding of the underlying genetic and molecular basis of BAV disease in humans, and identified important questions that require continued investigations. The project also has laid an important foundation for future real-time exercise CMR imaging-based work in efforts to identify novel imaging biomarkers that can be used to better risk stratify those with BAV-related aortopathy. Overall, the work in this thesis have provided an important step forward in our efforts to gain a greater understanding on the pathogenetic basis of BAV disease and one step closer towards our ultimate goal in reducing the overall health burden created by this complex, albeit common, human disease.

PUBLICATIONS ARISING FROM THIS THESIS

Padang R, Bannon PG, Jeremy R, Richmond DR, Semsarian C, Vallely M, Wilson M, Yan TD. The genetic and molecular basis of bicuspid aortic valve associated thoracic aortopathy: a link to phenotype heterogeneity. *Ann Cardiothorac Surg* 2013; 2(1):83-91.

Padang R, Bagnall R, Semsarian C. Genetic basis of familial valvular heart disease. *Circ Cardiovasc Genet* 2012;5(5):569-80.

Padang R, Bagnall R, Richmond D, Bannon P, Semsarian C. Rare non-synonymous variations in the transcriptional activation domains of GATA5 in bicuspid aortic valve disease. *J Mol Cell Cardiol* 2012;53(2):277-81.

PRESENTATIONS

Poster presentation. **Padang R**, Bagnall R, Richmond D, Bannon P, Semsarian C. Rare non-synonymous variations in the transcriptional activation domains of GATA5 in bicuspid aortic valve disease. 60th CSANZ Annual Scientific Meeting, Brisbane (2012).

Poster presentation. Sherrah A, Andvik S, Bannon PG, **Padang R**, Jeremy R. Predictors of survival in heritable thoracic aortic aneurysm. 60th CSANZ Annual Scientific Meeting, Brisbane (2012).

Poster presentation. Mollahajian H, **Padang R**, Rahnavardi M, Yan TD, Bannon PG. Valve sparing aortic root surgery in bicuspid aortic valve: a systematic review. 59th CSANZ Annual Scientific Meeting, Perth (2011).

LIST OF FIGURES

CHAPTER 1

CHAPTER 3

CHAPTER 4

CHAPTER 5

CHAPTER 6

CHAPTER 7

LIST OF TABLES

CHAPTER 1

CHAPTER 2

CHAPTER 3

CHAPTER 4

CHAPTER 5

CHAPTER 6

APPENDICES

LIST OF ABBREVIATIONS

1kG	1000 Genomes Project
2D	2-dimensional
3D	3-dimensional
aa	amino acid
A-P	anterior – posterior (leaflet orientation)
AVR	aortic valve replacement
BAV	bicuspid aortic valve
BAM	Binary sequence Alignment/Map format
bp	base pairs
cDNA	complementary deoxyribonucleic acid
CHD	congenital heart disease
Chr	chromosome
CMR	cardiac magnetic resonance
Ct	comparative threshold
DAVID	Database for Annotation, Visualisation and Integrated Discovery
DEPC	diethylpyrocarbonate
del	deletion
DEGs	Differentially expressed genes
DMSO	dimethyl sulfoxide
DNA	deoxyribonucleic acid
dNTP	deoxynucleoside triphosphates
ECG	electrocardiogram
ECM	extracellular matrix
EVS	Exome Variant Server
GERP	Genomic evolutionary rate profiling
GO	Gene Ontology
IGV	Integrative Genomics Viewer
Indels	insertion / deletions
IPA	Ingenuity Pathway Analysis

L-N	left-non (coronary leaflets fusion pattern)
MAF	minor allele frequency
$MgCl_2$	magnesium chloride
miRNA	microRNA
MMP	matrix metalloproteinase, protein
mRNA	messenger RNA
NCBI	National Centre for Biotechnology Information
NGS	Next Generation Sequencing
NHLBI	National Heart, Lung and Blood Institute
PCR	polymerase chain reaction
qPCR	quantitative PCR
R-L	right-left (coronary leaflets fusion pattern or leaflet orientation)
R-N	right-non (coronary leaflets fusion pattern)
RNA	ribonucleic acid
RNA-seq	RNA sequencing
RPAH	Royal Prince Alfred Hospital
RT-PCR	reverse transcription PCR
SAM	Sequence Alignment/Map format
SD	standard deviation
SNV	single nucleotide variation
SVD	structural valve degeneration
T_a	annealing temperature
TAA	thoracic aortic aneurysm
TAV	tricuspid aortic valve
TDW	triple distilled water
TGF_β	Transforming Growth Factor β, protein
TTE	transthoracic echocardiography
U	units
UTR	untranslated region
VHD	valvular heart disease
VSMC	vascular smooth muscle cells
VUS	variant of uncertain significance

CHAPTER 1: INTRODUCTION

1.1. VALVULAR HEART DISEASE

Worldwide, valvular heart disease (VHD) is a major cause of disability, diminished quality of life and premature death from cardiovascular disease (Mensah, 2009), making it an important clinical entity. Despite a dramatic decline in the incidence of rheumatic heart disease in industrialised countries, VHD remains highly prevalent and yet, is often under-diagnosed and its health burden underappreciated (Nkomo et al., 2006). It is estimated that significant VHD affects over 2.5% of the US population and its prevalence increases with age (Iung and Vahanian, 2011). Recent improvements in diagnostic imaging modalities and advancement in pharmacotherapies, interventional cardiology and surgical approaches have contributed to improved survival of patients with VHD, further increasing its prevalence and rendering it a growing public-health problem (Nkomo et al., 2006).

While many VHDs are acquired during adult life, congenital forms present with abnormal valve structures at birth, yet may not manifest as valvular dysfunction and disease until later in life (Lincoln and Yutzey, 2011, Markwald et al., 2010). Furthermore, familial clustering and heritability have been noted for common heart valve defects, such as bicuspid aortic valve and myxomatous mitral valve prolapse, implying an underlying genetic basis (Garg et al., 2005, Hinton et al., 2006, Lincoln and Yutzey, 2011). These familial VHDs can occur in isolation (non-syndromic) or present as part of a clinical genetic syndrome, such as Marfan, Turner and Noonan syndromes (Pierpont et al., 2007).

Traditionally, well-characterised multigeneration families have been invaluable for determining the genetic basis of disease, because they are amenable to marker-based genome-wide linkage analysis. However, the identification of causal genes in VHD has been hampered by complex genetic and phenotypic heterogeneity, incomplete penetrance, and the likely contribution of genetic modifier loci. Although *in-vitro* studies and transgenic animal models that recapitulate the human phenotype have provided insights into the genetic basis of VHD, these findings do not always translate to humans. Therefore, concurrent studies on the molecular pathways regulating valvulogenesis have sought to highlight gene networks relevant to VHD.

The work presented in this thesis focuses on non-syndromic bicuspid aortic valve (BAV) disease (Figure 1.1), the commonest form of congenital heart disease, and specifically, it aims to investigate the underlying clinicopathological and genetic basis of this complex and highly heritable disorder.

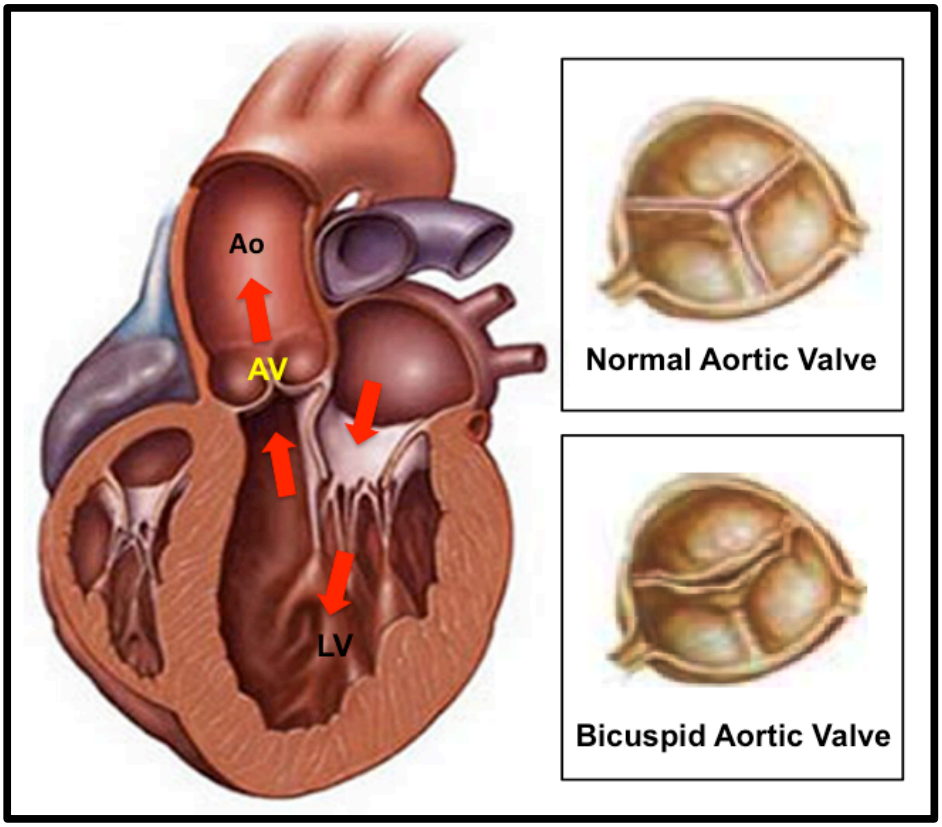

Figure 1. 1. Internal view of the heart.
Insets illustrate the superior view of a normal aortic valve (with three leaflets) versus a bicuspid aortic valve (with two leaflets). AV, aortic valve; Ao, aorta; LV, left ventricle; red arrow demonstrates direction of blood flow. Image adapted with modifications from The Mayo Foundation for Medical Education and Research (www.mayoclinic.org) and The Agnes Ginges Centre for Molecular Cardiology's Familial Bicuspid Aortic Valve Patient Information Sheet.

Given the developmental nature of BAV, which predisposes to premature calcification and adult aortic valve dysfunction, understanding of the molecular pathways and genetic factors that control normal heart valve development becomes important as they may give clues into the pathogenesis of BAV disease.

1.2. OVERVIEW OF DEVELOPMENT OF CARDIAC VALVES

A key aspect of cardiac development is the formation and function of the cardiac valves. An overview of this process, specifically that relating to aortic valve development, is summarised in Figure 1.2. Cardiac valve development begins immediately following cardiac looping, at embryonic day 31-35 in humans, with the formation of endocardial cushions in the atrioventricular canal and outflow tract (Butcher and Markwald, 2007, Combs and Yutzey, 2009). Normal *UDP-glucose dehydrogenase* (*UGDH*) gene activity to synthesise glycosaminoglycan is critical for the early cell signalling events that establish the boundaries of these cushion-forming regions (Walsh and Stainier, 2001). Cardiac cushion formation involves the transformation of a subset of endothelial cells into mesenchymal cells in the cushion-forming area, which is induced by Bone Morphogenetic Protein-2 (*BMP2*) signals derived from adjacent myocardial cells (Combs and Yutzey, 2009). The mesenchymal progenitor cells migrate into the intervening cardiac jelly and proliferate to form swellings of valve primordial (Figure 1.2.A), which eventually give rise to valvuloseptal structures and adult valvular interstitial cells (Liu et al., 2007, Schoen, 2008, Combs and Yutzey, 2009, Hinton and Yutzey, 2011).

The atrioventricular cushions contribute to atrioventricular (mitral and tricuspid) valve leaflets, whereas the outflow tract cushions contribute to semilunar (aortic and pulmonary) valve leaflets (Lincoln and Yutzey, 2011, Combs and Yutzey, 2009). The outflow tract and semilunar valve development are complex and involve coordinated interactions between the endocardial-derived mesenchyme,

cardiac and smooth muscle progenitors from the anterior or secondary heart field and the cardiac neural crest (de la Pompa and Epstein, 2012). Whereas the secondary heart field progenitor cells contribute to the outflow tract myocardium, a population of neural crest-derived cells migrate into the distal (truncal) part of the outflow tract cushions, which subsequently divide the outflow tract into aortic and pulmonary trunks (Figure 1.2.B), and differentiate into the vascular smooth muscle layer of the aortic arch (Butcher and Markwald, 2007, Niessen and Karsan, 2008, de la Pompa and Epstein, 2012). A number of signalling pathways including *Wnt/β-catenin, NOTCH, TGF-β, BMP, VEGF, NFATc1* and *MAPK,* and transcription factors including *Twist1, Tbx20, Msx1/2* and *Sox9* are active during this early stage of valvulogenesis (Figure 1.2.C). These pathways are collectively important in the regulation of cell migration, proliferation and extracellular matrix expression in the developing valves (Benson, 2008, Chakraborty et al., 2010, Combs and Yutzey, 2009, Hinton and Yutzey, 2011).

Later in embryonic valve development, cell proliferation decreases and the fused endocardial cushions remodel and thin out to form mature valve leaflets, which are characterised by increasing complexity and organisation of the extracellular matrix, and compartmentalisation of valvular interstitial cells (Combs and Yutzey, 2009, Hinton and Yutzey, 2011). The molecular pathway which regulates this later stage of valvulogenesis is less well understood, but it involves periostin, a component of the extracellular matrix protein (Norris et al., 2008). The *periostin* gene has been identified as a molecular switch that promotes endocardial cushion cells differentiation into a fibroblastic cell lineage,

rather than into myocardial or osteochondral cell lines, and regulates cushion remodelling, separation of the developing atrioventricular valve from the underlying myocardium, and its transformation into mature valve leaflet and the supporting apparatus (Butcher and Markwald, 2007, Norris et al., 2008).

The mature valve leaflets are stratified into three layers with distinct mechanical properties arranged in orientation to the blood flow: a flexible elastin-rich atrialis / ventricularis layer, a central shock-absorbing proteoglycan-rich spongiosa layer, and a tensile collagen-rich fibrosa layer (Lincoln et al., 2006). The process of valve compartmentalisation and remodelling occurs at late gestation and continues into postnatal life, suggesting that mechanisms of prenatal valve development persist during postnatal valve growth and maintenance (Hinton et al., 2006)' (Liu et al., 2007). Furthermore, evidence suggests that developmental signalling pathways are shared between heart valves and the precursors of cartilage, tendon and bone, playing a critical role at this later stage of valve maturation / remodelling (Lincoln et al., 2006). These pathways include *BMP2*-mediated induction of *Sox9* and aggrecan, *receptor activator of NFκB ligand* (*RANKL*)-mediated induction of *NFATc1*, and *FGF4*-mediated induction of *Scleraxis* and tenascin (Lin et al., 2012b, Chakraborty et al., 2010, Lincoln et al., 2006).

Cardiac valve development during embryogenesis is therefore complex, with an integrated mechanism of genetic factors, activation of signalling pathways, as well as external environmental factors, such as the physical forces of blood flow. Since many of the signalling pathways and transcription factors

responsible for valve development are reactivated in paediatric and adult valve diseases (Lincoln and Yutzey, 2011, Wirrig and Yutzey, 2011), the insights gained from understanding normal valvulogenesis have provided a platform to identify potential candidate genes involved in familial BAV.

Figure 1. 2. Semilunar (aortic and pulmonary) valve development.

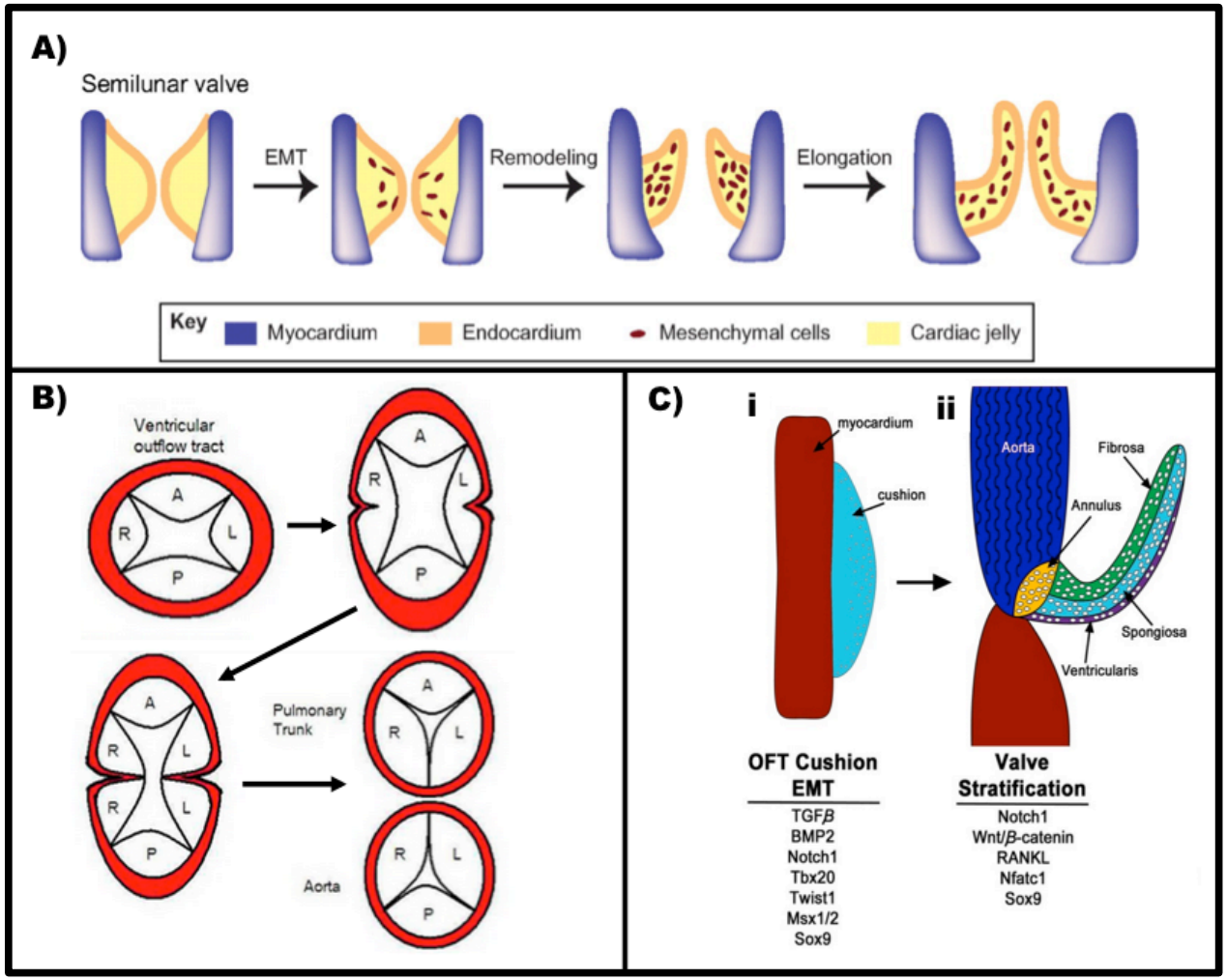

A) Diagramatic representation of epithelial-to-mesenchymal transformation (EMT), semilunar valve elongation and maturation into thin valve leaflets; B). Ventricular outflow tract (OFT) cushion septation and maturation into pulmonary valve and aortic valve; C) Summary of molecular pathways that are active during endocardial cushion development and valve stratification. Adapted from (Lin et al., 2012a, Wirrig, 2013) and UNSW Faculty of Medicine website (http://php.med.unsw.edu. au/medwiki/index.php?title=Development_of_the_heart_and_common_genetic_abnormalities_of_heart_function).

1.3. BICUSPID AORTIC VALVE DISEASE

1.3.1. Clinical significance of BAV disease

BAV occurs when the aortic valve has two cusps, rather than three, and represents the most common form of congenital cardiac malformation, affecting approximately 1.3% of the general population (Michelena et al., 2011, Roger et al., 2012). BAV has a male predominance of approximately 3:1 (Siu and Silversides, 2010), and at least 35% of those affected develop serious complications including aortic stenosis and/or regurgitation requiring valve replacement, endocarditis, ascending aortic aneurysm and dissection (Vallely et al., 2008). BAV underlies 70-85% of stenotic aortic valve in children and at least 50% of aortic stenosis in adults (Schoen, 2008, Cripe et al., 2004). Thoracic aortic enlargement is also common in BAV, reported in up to 50-60% of affected individuals (Tzemos et al., 2008, Nistri et al., 1999, Ward, 2000). Furthermore, BAV carries an 8-fold increased risk of aortic dissection and over a 25-year period, the risk of valve replacement is 53%, aneurysm formation is 26%, and aortic surgery is 25% (Michelena et al., 2011). As such, BAV represents a greater burden of disease than all other congenital heart diseases combined (Siu and Silversides, 2010, Ward, 2000).

In up to 62.5% to 80% of cases, BAV reportedly occurs sporadically as an isolated birth defect (Cripe et al., 2004, Deshpande and Kinare, 1991, Garg, 2006, Michelena et al., 2011). However, it can be familial and can occur as part of a syndrome with more global clinical manifestations, such as Turner, Williams-Beuren and Andersen syndromes. Furthermore, BAV is also

recognised to coexist with other congenital cardiovascular malformations, most commonly with coarctation of the aorta, but also with cardiac septal defects, aberrant coronary artery anatomy or the genetically-related hypoplastic left heart syndrome (Siu and Silversides, 2010, Hinton et al., 2009, Cripe et al., 2004). This suggests that BAV is not only a disorder of valvulogenesis, but also represents a more complex coexistent genetic disease of the aorta and/or cardiac development (Cripe et al., 2004, Siu and Silversides, 2010).

1.3.2. Anatomy and diagnosis of BAV

Disorders of aortic valvulogenesis tend to be regarded in the context of a phenotypic continuum, ranging from aortic valves with a single leaflet to those with four leaflets (Vallely et al., 2008). Within this continuum, BAV exists and demonstrates a wide morphological variation (Figure 1.3), as seen in human cases of BAV (Figure 1.4) and observed in BAV of Syrian hamsters (Fernandez et al., 2009). BAV morphological phenotypes range from the typical form with 2 unequal-sized leaflets and the larger leaflet having a central raphe due to commissural fusion (ie. functionally bicuspid), to the less common form with 2 approximately symmetrical leaflets without a raphe (ie. anatomically bicuspid) (Sievers and Schmidtke, 2007, Siu and Silversides, 2010). Fusion of the right and left coronary (R-L) cusps is the most common pattern of BAV and is associated with coarctation of the aorta, whilst fusion of the right and noncoronary (R-N) cusps, the second commonest form, is associated with more cuspal pathology (Siu and Silversides, 2010).

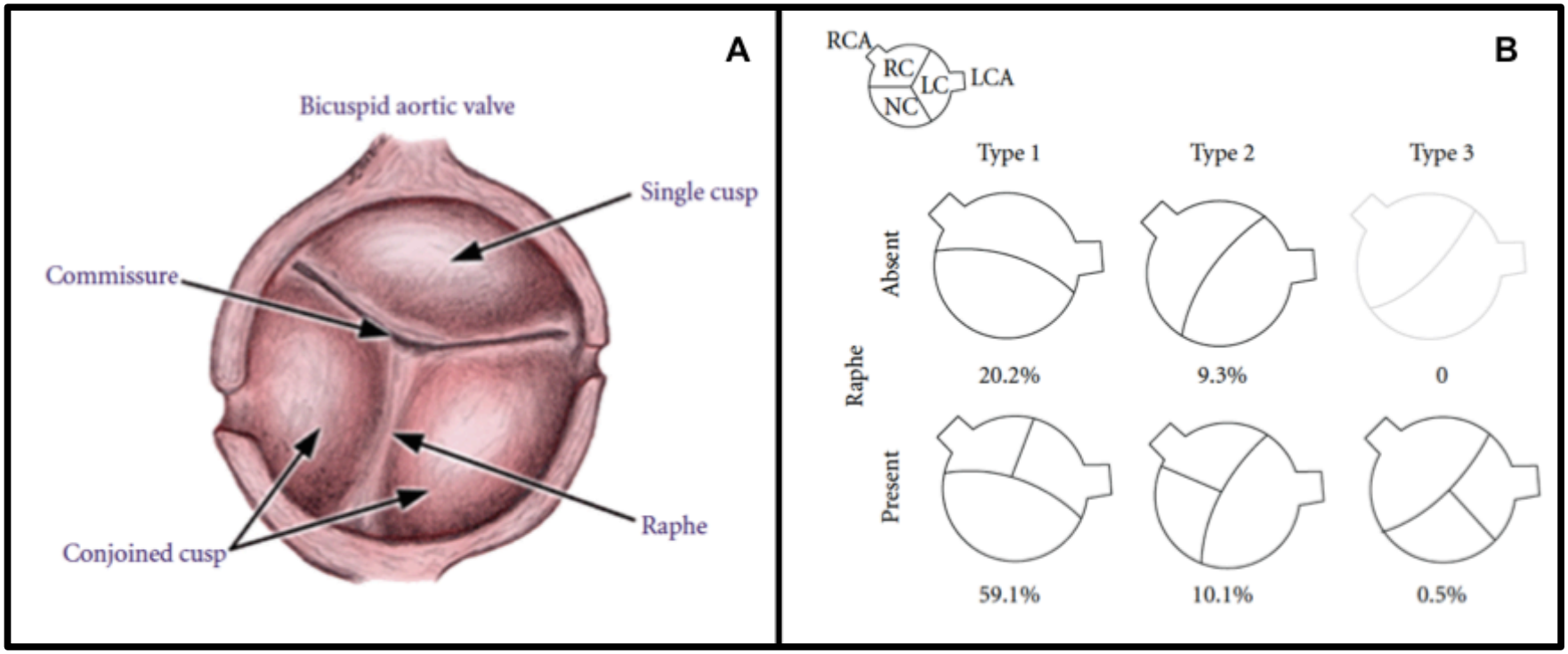

Figure 1. 3. Bicuspid aortic valve.

A) The basic anatomy of BAV; B) The classification and incidence of BAV according to site of cusp fusion as seen from a parasternal short axis view on echocardiography. RCA, right coronary artery; LCA, left coronary artery; RC, right coronary cusp; LC, left coronary cusp; NC, non-coronary cusp. Adapted from (Mordi and Tzemos, 2012, Schaefer et al., 2008).

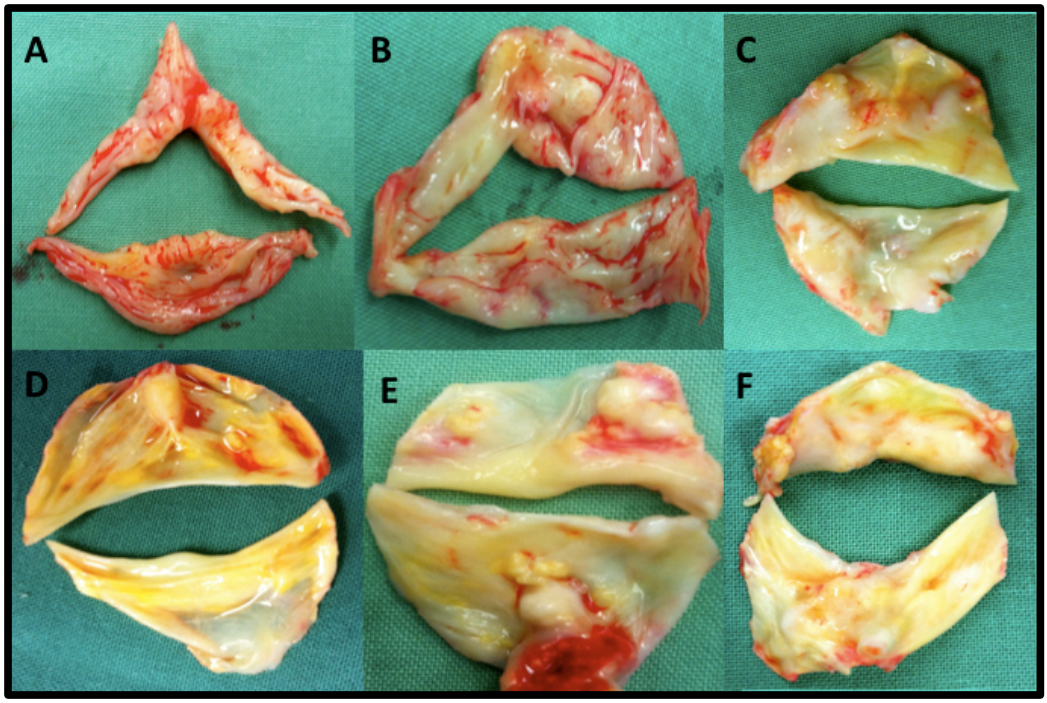

Figure 1. 4. Different phenotypic spectrum of human BAV morphology.
A) Tri-leaflet aortic valve with complete fusion of the right and left (R-L) coronary cusps; B) Tri-leaflet aortic valve with complete fusion of the R-L coronary cusps and partial fusion of the right and non coronary cusps; C) and D) Bi-leaflet aortic valve with extensive raphe in the fused leaflet; E) Bi-leaflet aortic valve with a vestigial raphe; F) True bicuspid aortic valve without raphe. Figure A and B are classified as functionally bicuspid and the remaining are classified as anatomically ("true") bicuspid.

While clinical auscultatory findings may suggest the presence of associated murmurs of aortic stenosis, incompetence or, when present, coarctation of the aorta, the mainstay of diagnosis of BAV is echocardiography (transthoracic or transoesophageal). When adequate echocardiographic images are obtained, figures of up to 92% sensitivity and 96% specificity have been reported for detecting BAV anatomy (Siu and Silversides, 2010). The presence of heavy leaflet calcification however can hamper echocardiographic diagnosis. Whilst

transoesophageal echocardiography can sometimes improve visualisation of the leaflets (Figure 1.5), it is not uncommon that the final diagnosis can only be made during direct inspection of the leaflets at time of valve surgery. In some instances, alternative cardiac imaging such as cardiac magnetic resonance (CMR) imaging or computer tomography (CT) can assist to confirm BAV anatomy, but usually, these modalities are used to evaluate the thoracic aorta for the presence of associated aortopathy or co-existent coarctation of the aorta (Figure 1.5).

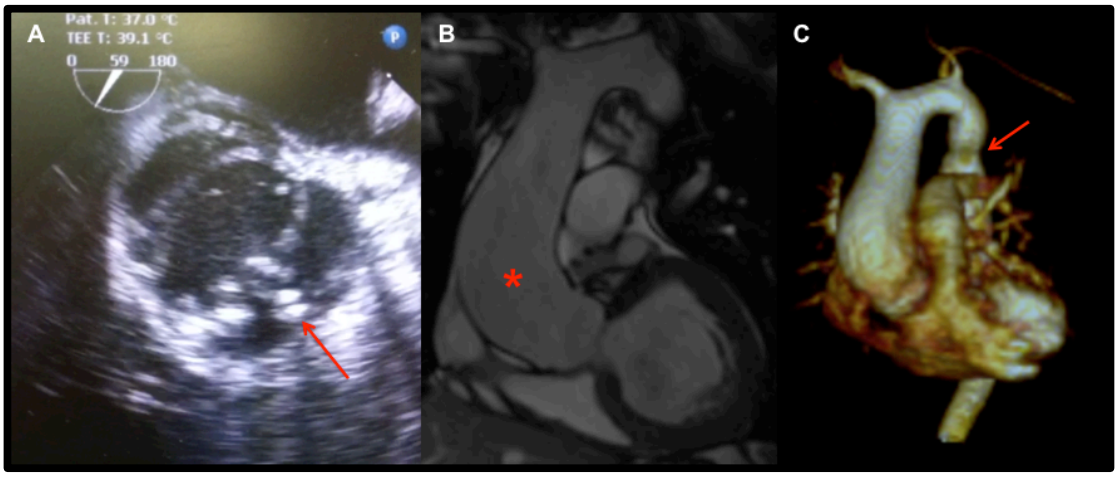

Figure 1. 5. Images of BAV and the aorta.

A) Transoesophageal echocardiography short axis view of a BAV with a right and left cusps fusion. The image was taken during cardiac systole and the aortic valve orifice has a characteristic “fish mouthed” appearance. The red arrow points to the raphe, which was heavily calcified. B) Cine cardiac magnetic resonance (CMR) image of the thoracic aorta. The asterix denotes ascending aortic dilatation. C) 3D CMR reconstruction of the thoracic aorta. The red arrow points to the mild narrowing at the site of previous coarctation repair.

1.3.3. Pathogenesis of BAV

Despite its high prevalence, the aetiology of BAV is largely undetermined, although gene mutations leading to alterations in cell migration and signal transduction, in conjunction with non-genetic factors such as blood flow during valvulogenesis may contribute to its formation prenatally (Lincoln and Yutzey, 2011). Since the relationship of the individual valve cusps to specific endocardial cushion progenitors is not known (Combs and Yutzey, 2009), BAV could result from a failure of separation of primordial cusps (Lincoln and Yutzey, 2011). Meanwhile, the pathogenesis of aortic valve dysfunction in BAV is thought to be the result of dysregulation in the complex molecular hierarchies controlling late valve development, which continues into postnatal life and results in the chronic process of valve tissue remodelling, leading to abnormal leaflet architecture, valvular thickening, and abnormal biomechanics (Figure 1.6) (Hinton et al., 2006, Koullias et al., 2004, Martin et al., 2007). With increasing age, BAV leaflets are prone to develop premature fibrosis and calcification in response to hemodynamic shear stress (Fedak et al., 2002, Rajamannan, 2011), an active process that involves inflammation, endothelial dysfunction, lipoprotein and calcium deposition, and results in ossification of the leaflets and valvular stenosis (Siu and Silversides, 2010). Meanwhile, the aetiology of aortic regurgitation in BAV patients is more complex. It is often a consequence of an intrinsic leaflet(s) redundancy or prolapse of the larger of the unequally sized cusps; however, it can also occur secondary to other external factors, such as endocarditis, after balloon valvuloplasty, or concomitant dilatation of the aortic root (Siu and Silversides, 2010, Koullias et al., 2004, Fedak et al., 2002).

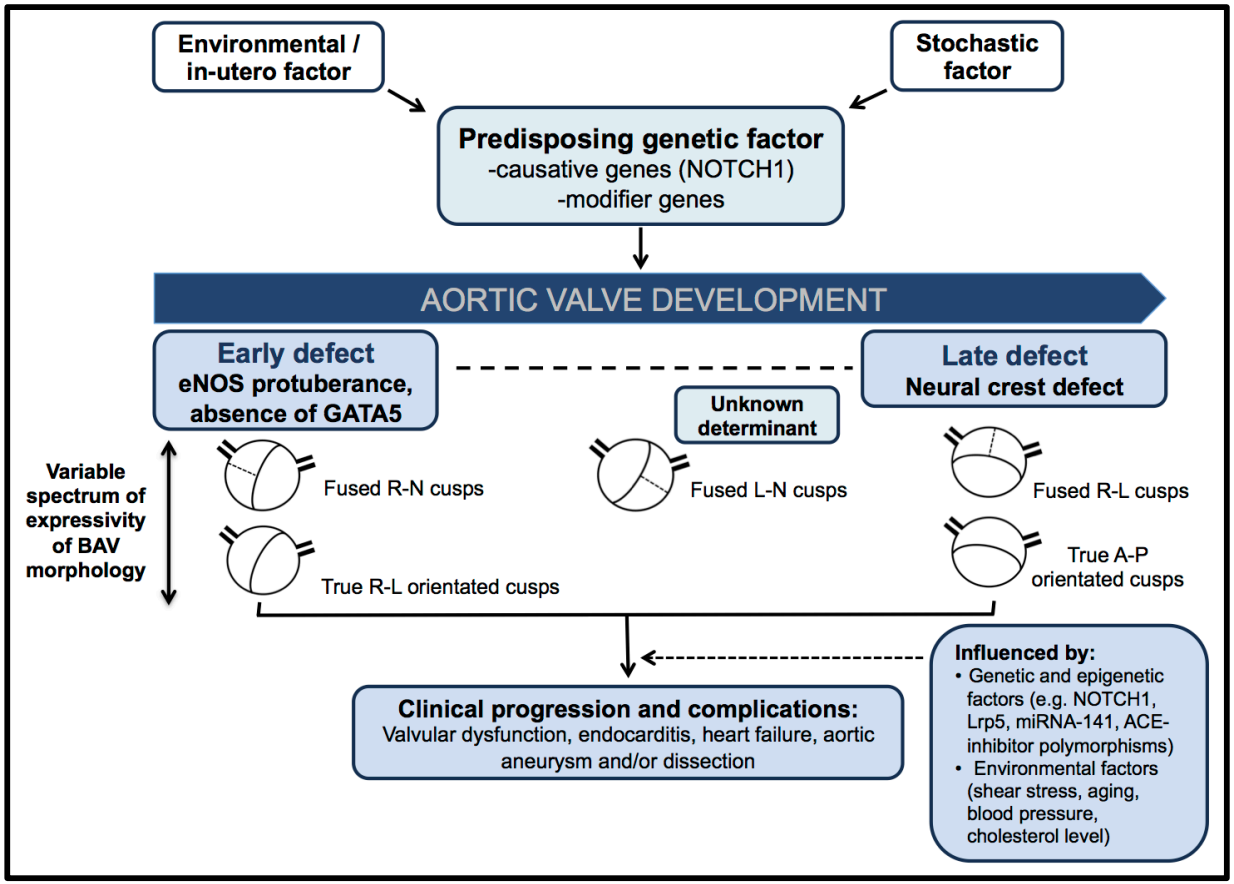

Figure 1. 6. Proposed pathogenetic mechanism of BAV.

Although BAV is largely genetically determined, both environmental and stochastic factors play a contributory role in determination of BAV morphogenesis and later manifestation of valve dysfunction and complication. It is likely that different BAV morphology to have different aetiological entities (Padang et al., 2012b).

Histological examination of BAV tissue from paediatric patients revealed excessive extracellular matrix production and trilaminar matrix disorganisation, with fragmentation and reduction in elastin content, and accumulation of collagen and proteoglycan (Hinton et al., 2006). BAV leaflets also show valvular interstitial cell disarray and varying degrees of inflammatory cell infiltrates, which secrete proteolytic enzymes implicated in collagen and elastin degradation in abdominal aortic aneurysm, such as MMP-2 and MMP-9 (Koullias et al., 2004). Supporting this, tissue microarray and immunohistochemical analysis of BAV leaflets demonstrated higher levels of MMP-2 and -9, and lower level of the MMP inhibitor, TIMP1 (Koullias et al., 2004). The increased MMP activity extends to the aortic annulus and/or ascending aorta and may contribute to the related aortopathy (Tadros et al., 2009).

1.3.4. Genetic basis of BAV

Familial clustering demonstrates that BAV is heritable, with 9% prevalence in first-degree relatives of patients with BAV, and up to 24% in families with more than 1 person affected (Siu and Silversides, 2010, Ward, 2000, Cripe et al., 2004). While autosomal dominant transmission of BAV has been observed in several 3-generation pedigrees, there is however no single-gene model that can definitively explained BAV inheritance (Prakash et al., 2014). In fact, it is likely that mutations in diverse genes with dissimilar inheritance patterns to be responsible for the development of BAV in different families (Cripe et al., 2004). Table 1.1 summarises the key genetic findings in BAV identified to date.

Genetic heterogeneity in BAV is demonstrated by the involvement of mutations in diverse genes encoding transcription factors, extracellular matrix proteins and signalling pathways that regulate cell proliferation, differentiation, adhesion or apoptosis (Ward, 2000, Martin et al., 2007, Garg, 2006).

Table 1. 1. Gene mutations in human and animal models of BAV.

Human	Mouse
Non-syndromic (familial and sporadic) BAV	*Nos3* (*eNOS*) deficiency
NOTCH1 missense and frame shift mutations	*Nkx2.5* haploinsufficiency
Linkage to locus on Chr 5q, 13q, 18q	Targeted deletion of *Gata5*
Syndromic BAV or BAV with other cardiovascular malformation:	Endocardial cushion tissue-specific deletion of *Alk2*
Andersen syndrome - *KCNJ2* mutation (Chr 17q)	
Thoracic Aortic Aneurysm and Dissection syndrome (TAAD) - *ACTA2* mutation (Chr 10q)	
Marfan syndrome - *Fibrillin1* mutation (Chr 15q)	
William Beuren syndrome – *Elastin* mutation (Chr 7q)	
Turner syndrome (45XO karyotype)	

Chr = chromosome

To date, only the transcriptional regulator *NOTCH1* gene at chromosome 9q34.3 has been linked to the development and calcific progression of non-syndromic BAV in humans, in a limited number of familial cases and ~4% of sporadic cases (Garg et al., 2005, Mohamed et al., 2006). The Notch signalling pathway is highly conserved and plays a critical role in cell fate determination and differentiation during organogenesis (Garg, 2006). NOTCH1 transcripts are abundant in the mesenchyme of the outflow tract and the developing aortic valve leaflets, which probably underlie the role of Notch signalling in aortic valve development (Garg et al., 2005). *NOTCH1* signalling represses *BMP2* and the

downstream osteogenic gene, *RUNX2*, a central transcriptional regulator of osteoblast cell fate (Garg et al., 2005, Nigam and Srivastava, 2009). Recently, *NOTCH1* signalling has been shown to regulate the expression of Sox9, a key chondrogenic transcription factor and regulator of extracellular matrix genes that is required for normal valve development and maintenance (Acharya et al., 2011). While inhibition of *NOTCH1* signalling downregulates Sox9 expression and promotes valvular calcification *in-vitro*, overexpression of Sox9 markedly attenuates the calcific process that occurs with *NOTCH1* inhibition (Acharya et al., 2011). *NOTCH1* mutations are therefore associated with both defective development of the aortic valve and, later, de-repression of an osteoblast gene program and dysregulation of valvular extracellular matrix genes, via a Sox9-dependent mechanism, leading to accelerated aortic valve calcification.

Further evidence of specific gene mutations as a cause of BAV has come from genome-wide marker-based linkage analyses. Families showing autosomal dominant inheritance of BAV and/or associated cardiovascular malformations have shown linkage to chromosomes 18q, 5q and 13q, whereas families with BAV and ascending aortic aneurysms have shown linkage to chromosome 15q25-26 (Vallely et al., 2008, Martin et al., 2007). The causal gene(s) however are yet to be identified. Furthermore, mutations in the *ACTA2* gene on chromosome 10q, which encodes smooth muscle alpha-actin (ACTA2), cause thoracic aortic aneurysm and, in some instances, BAV (Siu and Silversides, 2010). It has been suggested that the different phenotypes of BAV-associated aortopathy may be caused by unique pathogenetic mechanisms (Girdauskas et al., 2011b). A missense mutation in the *TGFBR2* gene, c.1159G>A, which

destabilises the protein structure, was segregated in a family with non-syndromic BAV with proximal aortic involvement (Girdauskas et al., 2011b), although the true incidence of *TGFBR* mutation in overall BAV populations is probably very low (Arrington et al., 2008). Associations have also been reported between aneurysm risks in BAV patients with polymorphisms in *eNOS, ACE, MMP-9* and *MMP-2* genes (Pisano et al., 2011, Foffa et al., 2012). Furthermore, downregulation of the *ubiquitin fusion degradation 1-like* gene (*UFD1L*), which is highly expressed in the cardiac outflow tract during embryogenesis, has also been noted in BAV, and may represent a candidate gene (Mohamed et al., 2005).

In addition to the above studies in humans, animal studies have shed light on the genetic basis of BAV. In mice, homozygous deletion of the endothelial nitric oxide synthase (*Nos3*) gene, and haploinsufficiency for the cardiac homeobox gene *Nkx2-5,* are associated with a higher incidence of BAV (Biben et al., 2000, Lee et al., 2000). Recently, tissue-specific deletion of Activin Receptor Type I gene (*Alk2* or *Acvr1*) in the endocardial cushion mesenchyme of developing murine heart has been shown to result in formation of aortic valve defects, including BAV of R-N morphology (Thomas et al., 2012). However, none of these genes have been associated with BAV in humans (Laforest et al., 2011, Majumdar et al., 2006). Furthermore, targeted deletion of the transcription factor *Gata5* in mice leads to partially penetrant BAV with fusion of the right and non-coronary cusps (Laforest et al., 2011). An essential role of GATA5 in cardiac morphogenesis and aortic valve development has only recently been reported, whereby it regulates several pathways involved in endocardial cell

differentiation, including those directed by *Bmp4*, *Tbx20*, and, notably, *NOS3* and *NOTCH1* (Laforest et al., 2011). Downregulation of *Nos3* expression and attenuation of the *Notch* pathway are observed in *Gata5*$^{-/-}$ mice (Laforest et al., 2011), which may underlie the development of BAV as mutations in *Nos3* and *NOTCH1* are associated with BAV in mice and humans, respectively.

Animal studies are also at the forefront of research into the hypothesis that the different BAV morphologies have a different etiological basis. *Gata5*$^{-/-}$ mice, *eNOS* knock-out mice and inbred Syrian hamsters each display a high incidence of BAV, but with different valve morphologies. BAV with fusion of the right coronary and non-coronary leaflets may result from morphogenetic defects that happen before outflow tract septation, which probably relies on an exacerbated nitric oxide-dependent endothelial-to-mesenchymal transformation. BAV with fusion of right and left coronary leaflets may result from the anomalous septation of the proximal portion of the outflow tract, due to distorted behaviour of neural crest cells (Fernandez et al., 2009). This anomalous behaviour of the cardiac neural crest is believed to explain the association of the right and left coronary leaflet fusion BAV morphology with coarctation of the aorta and the more pronounced aortic wall degeneration, compared to BAV with fusion of the right and non-coronary leaflets (Fernandez et al., 2009).

Interestingly, Sans-Coma et al. recently demonstrated that BAV in Syrian hamsters are expressions of a quantitative trait, subject to polygenic inheritance, with reduced penetrance and variable expressivity (Sans-Coma et al., 2012). Furthermore, examination of aortic valve morphology in virtually

isogenic Syrian hamsters produced by systematic inbreeding through full-sib mating, with the probability of homozygosity being 0.999 or higher, demonstrated the presence of BAV in up to five-sixths of the hamsters studied, whilst the remaining one-sixth had a tri-leaflet aortic valve. This suggests that the same underlying genotype, which accounts for the whole range of valve morphology, including BAV, must be acting together with factors other than genetic ones during embryonic life, creating “developmental noise”, to influence the definitive anatomic configuration of the valve (Sans-Coma et al., 2012). Further, no significant association was noted between the valvular phenotype in the parents and the offspring produced by crossing genetically alike hamster, with the probability of homozygosity of at least 0.989. Taken together, these findings support a complex inheritance pattern, as seen in human BAV, and may explain the relatively low recurrence rate of BAV in first-degree relatives, despite its common prevalence within the general population (Sans-Coma et al., 2012). The findings also provide a potential explanation regarding aortic valve anatomy in monozygotic twins where BAV was present in one twin but tricuspid aortic valve in the other (Lewis and Henderson, 1990).

While specific gene mutations can cause BAV in mice and humans, the variability in BAV morphology and its disease manifestations cannot be entirely explained. MicroRNAs (miRNAs) are a class of evolutionarily conserved small, non-coding RNAs that regulate gene expression in development and disease. Reduced expression of miR-26a, miR-30b and miR-195 in stenotic BAV associated with calcification, compared to a regurgitant phenotype, has been reported (Nigam et al., 2010). *In-vitro* transfection of each of these miRNAs into

human aortic valvular interstitial cells indirectly modulated the expression of several calcification-related genes, including *RUNX2*, *BMP2*, alkaline phosphatase (*ALPL*), *SMAD1* and *SMAD3* (Nigam et al., 2010). Patients with BAV-associated aortic stenosis have also been shown to have attenuated expression of miRNA-141, a repressor of *BMP-2* (Yanagawa et al., 2012). Together, these studies suggest miRNA dysregulation contributes to aortic stenosis in BAV, and that miRNAs represent a potential new therapeutic target to limit progressive aortic valve calcification and dysfunction.

Collectively, these findings support a genetic basis for BAV, although it remains undetermined in the majority of cases. Nevertheless, BAV pathogenesis is likely to involve a complex interplay between specific gene mutations, modifier loci, aberrant signalling pathways, abnormal neural crest migrations, environmental influences in-utero, and stochastic factors. The balance of this interaction is likely to have major influence on phenotypic heterogeneity, BAV disease progression and severity, including aortic valve dysfunction and aortic complications.

1.3.5. BAV related aortopathy

As mentioned previously, over 50% of individuals with BAV present with concurrent dilatation of the proximal aorta (Vallely et al., 2008, Fedak et al., 2002). Significant phenotype heterogeneity of BAV related thoracic aortic enlargement has been described (Figure 1.7), which may occur independently of the underlying valvular morphology and function (Tzemos et al., 2008, Ward,

2000, Nistri et al., 1999, Jackson et al., 2011). This most commonly manifests as asymmetric ascending aortic dilatation beyond the sinotubular junction with variable arch involvement and/or varying degrees of annuloaortic ectasia, predisposing to aortic dissection or rupture, a feared complication.

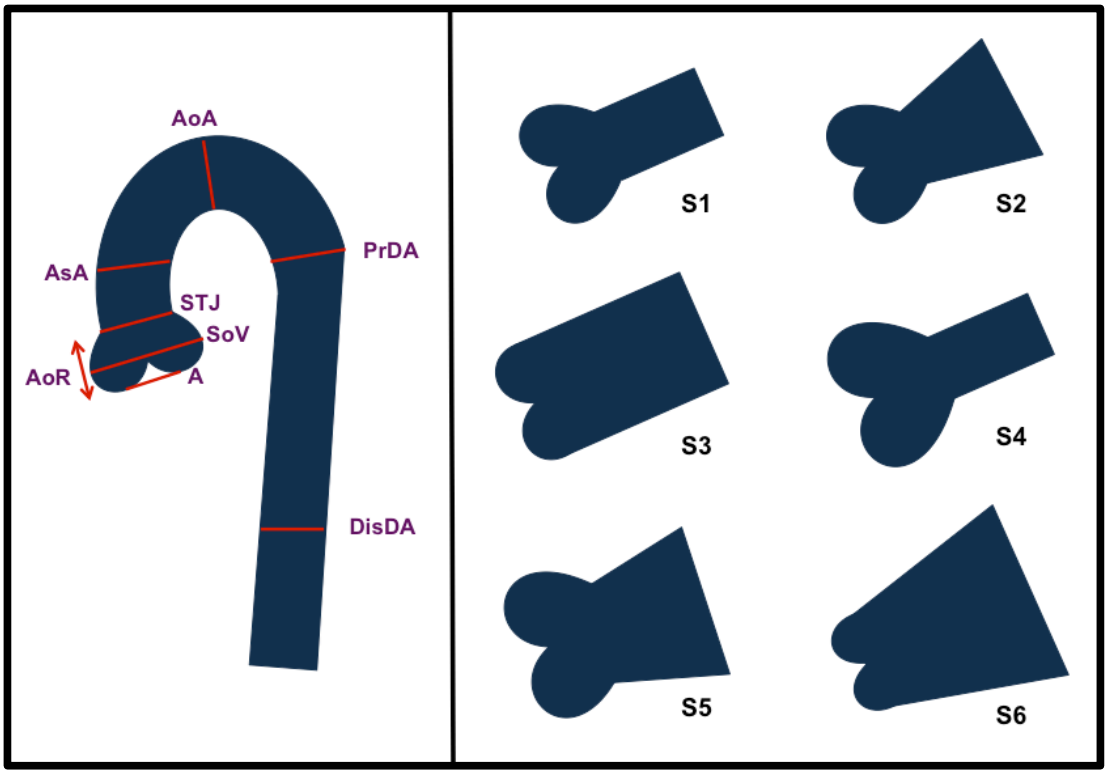

Figure 1. 7. Different morphologies of BAV-related aortopathy.
The left panel depicts the different reference levels used in the assessment of thoracic aorta dimension. The panel on the right (adapted with modifications from (Mart, 2013)) demonstrates the different aortic dilatation pattern seen in patients with BAV: S1 – normal shape; S2 – ascending aorta dilatation; S3 – effacement of the sinotubular junction; S4 – enlargement of the aortic root, Marfan-like; S5 – enlarged sinus of Valsalva and ascending aorta; S6 – normal annulus and proximal sinus of Valsalva, enlarged distal sinus of Valsalva, sinotubular junction and ascending aorta. A, aortic annulus; AoR, aortic root; SoV, sinus of Valsalva; STJ, sinotubular junction; AsA, tubular portion of the ascending aorta; AoA, aortic arch; PrDA, proximal descending aorta; DisDA, distal descending aorta.

Presently, some controversies exist in the literature regarding the underlying pathogenesis of BAV related aortopathy (Girdauskas et al., 2011a), specifically whether it is genetic or hemodynamic in origin. This is of major clinical relevance because it will have an influence on the surgical management of the valve and the ascending aorta.

1.3.5.1. Genetic underpinnings of BAV related aortopathy

The developmental nature of BAV related aortopathy has been suggested by various studies, which indicates the presence of an underlying genetic defect causing inherent structural abnormality of the arterial wall. This is based on the observation that aortic root and ascending aortic dilatation have been documented in children with BAV (Gurvitz et al., 2004, Fernandes et al., 2012, Holmes et al., 2007), suggesting that BAV related aortopathy is a process that begins early in life. Progressive aortic dilatation can also occur in patients with normally functioning BAV and even following aortic valve replacement (Aicher et al., 2007, Gurvitz et al., 2004, Tadros et al., 2009, Michelena et al., 2008, Yasuda et al., 2003), implying the presence of an intrinsically 'weaker' aorta. In addition, the presence of valve dysfunction alone does not necessarily account for the degree or rate of progression of aortic dilatation in BAV patients (Keane et al., 2000, Nistri et al., 1999, Tadros et al., 2009), suggesting that factors, other than hemodynamic, are at play. Notably, an inherent structural alteration has been described in the ascending aorta of BAV patients, irrespective of the underlying valve haemodynamic (Fedak et al., 2003). Histological examination of dilated aortas of BAV patients demonstrate accelerated aortic media degeneration with focal matrix disruption, altered collagen content, greater

elastin fragmentation, accumulation of mucopolysaccharide ground substance and higher rates of vascular smooth muscle cell (VSMC) apoptosis (Figure 1.8) (Bonderman et al., 1999, Tadros et al., 2009). These findings are also present in the non-dilated aortas of BAV patients and similar to those observed in the aortas of Marfan syndrome patients with Fibrillin-1 gene mutation (Blunder et al., 2012, Bonderman et al., 1999, Tadros et al., 2009). In fact, deficiency of fibrillin-1, which occurs independently of aortic diameter, and increased matrix metalloproteinase-2 (MMP2) activity have been reported in BAV aortic tissue (Fedak et al., 2003).

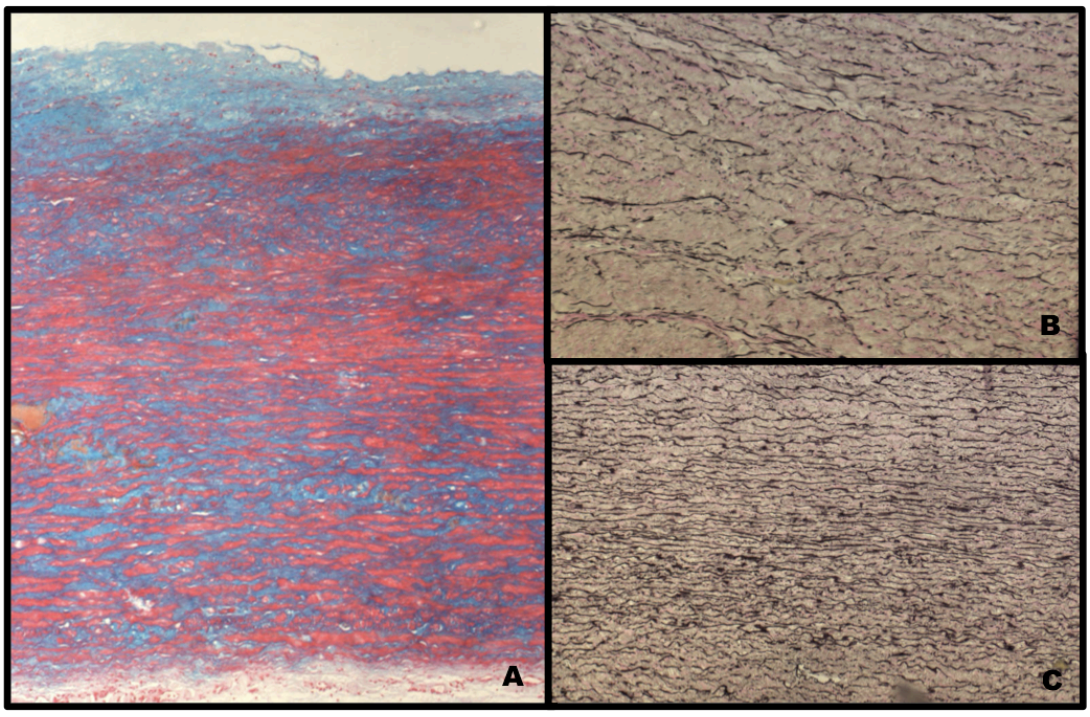

Figure 1. 8. Common histological findings in aneurysmal aortas of BAV patients.

A) Extensive medial degenerative changes, with accumulation of basophilic mucopolysaccharide ground substance, as demonstrated using an alcian-blue stain. B) Significant reduction of elastin content with fragmentation, thinning and disarray of elastin fibres, particularly in areas of maximum aortic dilatation. C) In

contrast to Figure B, this image demonstrated a normal elastin content and organisation within the non-dilated aortic segment. These images are courtesy of Dr. Geoff Watson, Department of Anatomical Pathology, Royal Prince Alfred Hospital, Sydney, Australia.

Further supporting the genetic basis of BAV related aortopathy is the observation that inherent abnormality of aortic elasticity is commonly seen in BAV patients, even at the non-dilated stage and irrespective of aortic size (Nistri et al., 2008). It has thereby been hypothesised that loss of fibrillin-1 microfibrils in BAV aortas, presumably from an underlying heritable microfibrillar gene defect, may cause detachment of VSMC from the elastic laminae, resulting in accelerated cell death and the release of pathological MMPs species with subsequent matrix degradation, weakening of aortic wall structural integrity, loss of aortic elasticity, progressive aortic dilatation, aneurysm and/or dissection (Figure 1.9) (Fedak et al., 2003, Verma and Siu, 2014). Interestingly, fibrillin-1 deficiency is also observed in the pulmonary arteries of BAV patients and main pulmonary artery dilatation has been noted to occur in association with BAV in the absence of pulmonary valve abnormality (Fedak et al., 2003, Kutty et al., 2010). It is therefore speculated that both aortic and main pulmonary artery dilatation in BAV may be the result of a common developmental abnormality as the great arteries originate from a common embryonic truncus (Fedak et al., 2003).

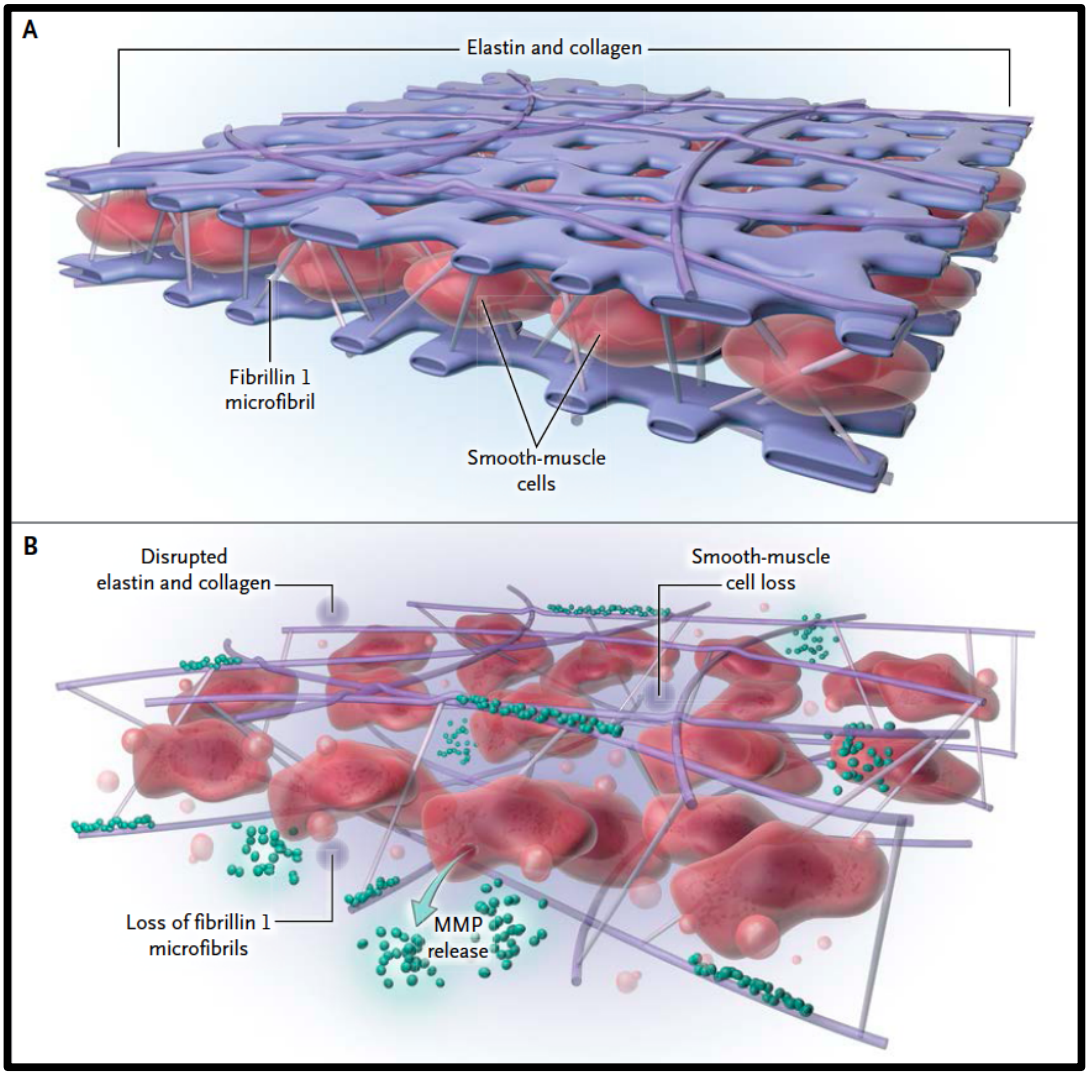

Figure 1. 9. Pathophysiological features of Bicuspid Aortopathy.

Structural support and elasticity are afforded to the aorta by means of alternating layers of elastic lamellae and smooth-muscle cells (SMCs). A) At the histologic level, the smooth-muscle cells in the aorta in persons with tricuspid valves are secured to the adjacent elastin and collagen matrix by fibrillin 1 microfibrils. B) The aorta in persons with BAV may be deficient in fibrillin 1. This deficiency culminates in a disrupted architecture whereby SMCs detach, accompanied by a surge in local levels of matrix metalloproteinases (MMPs), leading to loss of integrity in the extracellular matrix and the accumulation of apoptotic cells. These events may lead to an aorta with weakened structural integrity and reduced elasticity. Adapted from (Verma and Siu, 2014).

Most recently, global gene expression levels have been compared in aortic tissue from patients with a bicuspid or tricuspid aortic valve, with and without thoracic aortic aneurysm (Folkersen et al., 2011). Only seven genes were differentially expressed between the non-dilated BAV and non-dilated tricuspid groups; the 4 upregulated genes were *LEFTY2* (left-right determination factor 2; a TGF-β family member), *FRAS1* (Fraser syndrome 1; a member of the extracellular matrix family of protein), *SHC4* (Src homology 2 domain containing family, member 4) and *DAPK3* (death-associated protein kinase 3; a proapoptotic gene), and the 3 downregulated genes were *VEGFC* (a member of the vascular endothelial growth factor family), *NFASC* (neurofascin homolog; a member of the L1 family of cell adhesion molecule), and *LSP1* (lymphocyte-specific protein 1). Given the possible shared genetic underpinnings of BAV and related aortopathy, an investigation of these genes in BAV is warranted. The study also showed immune responsive genes were upregulated in tricuspid valve patients with a dilated aorta, compared to those with a dilated aorta and BAV, suggesting that immune response genes are not directly involved in BAV related aneurysms. Rather, BAV patients with aortic dilation showed an almost exclusive expression of the *TGF-β* binding proteins *LTBP3/4*, ADAMTSL1 and an alternatively spliced isoform of *Fibronectin-1* (*FN1)* (Folkersen et al., 2011). A common extracellular matrix component of the vessel wall, fibronectin is a glycoprotein that influences cell migration and proliferation, thus central to normal tissue repair / remodelling and maintenance of tissue integrity in response to injury. Patients with BAV-related aortopathy appear to have impaired TGF-β-mediated splicing mechanisms of fibronectin transcript, thereby leading to altered fibronectin expression in the aortic aneurysm tissue and

consequently contributing to the increased susceptibility to aortopathy development in BAV patients (Paloschi et al., 2011). Interestingly, a diverging alternative splicing fingerprint of the TGF-β pathways has been observed within ascending aortic dilatation in bicuspid versus tricuspid aortic valve patients (Kurtovic et al., 2011), resulting in differential downstream gene expression and signalling. Different epigenetic modification of the chromatin structure may be responsible for the observed differential splicing pattern of TGF-β (Kurtovic et al., 2011), which may play an important contributory role in modifying phenotypic heterogeneity of thoracic aneurysm pattern in BAV. Importantly, these findings highlight the central role of TGF-β as the key regulator of vascular matrix remodelling and VSMC activity, and that dysregulation of TGF-β signalling and its downstream pathways appears to be a common mechanism involved in aneurysm formation, including in BAV related aortopathy. Overall, these findings suggest an underlying genetic defect in the pathogenesis of aortic dilatation in BAV.

1.3.5.2. Hemodynamic contributions in BAV related aortopathy

There is emerging evidence to support the hypothesis that BAV-related aortopathy is a haemodynamic phenomenon, in which the structurally defective valve, or even a 'normally' functioning one, is in fact morphologically stenotic, as a result of restricted mobility / opening of the conjoined leaflet, producing a nonaxial transvalvular turbulent flow jet within the aortic root (Robicsek et al., 2004, Girdauskas et al., 2012, Della Corte et al., 2012). This in turn creates abnormal biomechanics and helical flow alterations that propagate eccentrically

inside the proximal aorta, resulting uneven wall stress distribution and promoting aortic dilatation / aneurysm, which, in BAV, preferentially bulges asymmetrically toward the right-anterior aortic wall (i.e. aortic convexity) (Hope et al., 2011). A positive correlation has also been demonstrated between the degree of restriction in the conjoint cusp systolic motion (the so-called “conjoint cusp opening angle”), and the consequent eccentricity of the transvalvular systolic flow, with the severity and growth rate of the ascending aortic dilatation (Della Corte et al., 2012, den Reijer et al., 2010, Hope et al., 2012). Furthermore, in support of the hemodynamic theory, different aortic leaflet fusion patterns have been shown to generate specific jet orientations in the proximal aorta (Hope et al., 2011, Mahadevia et al., 2014), with distinct patterns of asymmetry in the aneurysms that develop, different rates of aortopathy progression, and unique MMPs and TIMPs (MMP inhibitors) signatures (Ikonomidis et al., 2012, Russo et al., 2008). Relatively recently, using sophisticated 4D flow cardiac MRI (Figure 1.10), fusion of the right and left coronary leaflets (R-L BAV), the most common type of BAV, has been shown to produce a right-anteriorly directed helical systolic flow jet with marked peripheral skewing towards the ascending aortic convexity (Hope et al., 2011, Mahadevia et al., 2014). This may explain the larger aortic root dimension and asymmetric dilatation of the mid-ascending aorta, commonly seen in these BAV patients, and the more severe degree of ascending aortic wall degeneration with enhanced proteolytic indices relative to the other BAV subtypes (Girdauskas et al., 2012, Ikonomidis et al., 2012, Russo et al., 2008). Meanwhile, fusion of the right and noncoronary leaflets (R-N BAV), the second commonest type of BAV, is associated with left-posteriorly directed eccentric

flow jet with propagation further towards the proximal aortic arch, which might explain its association with isolated ascending aortic dilatation (without aortic root involvement) and increased aortic arch dimensions seen in this subgroup of BAV patients (Girdauskas et al., 2012, Fazel et al., 2008).

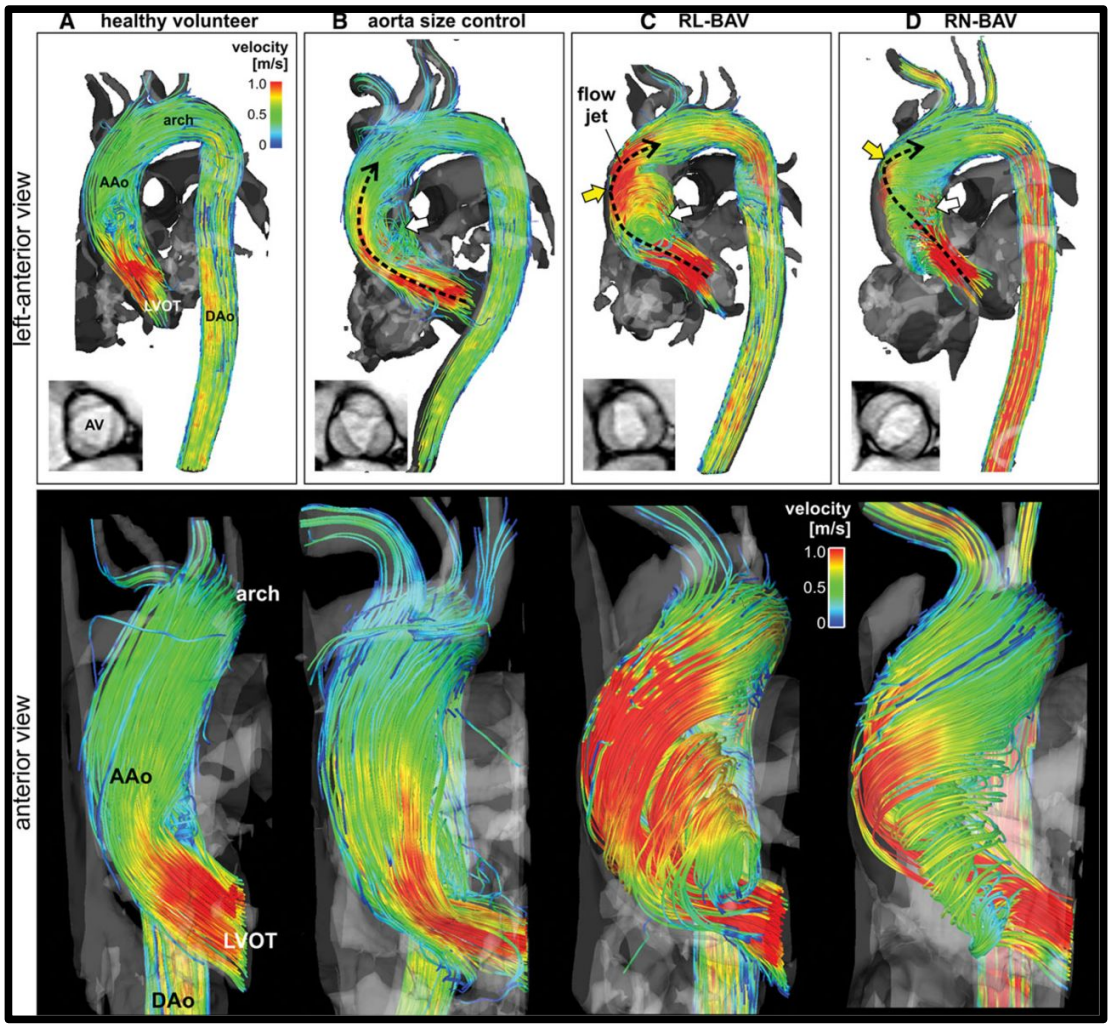

Figure 1. 10. Visualisation of peak systolic blood flow in patients with BAV (C (R-L BAV) and D (R-N BAV)) in comparison with an aorta sized-matched control subjects (B) and a healthy volunteer (A) using 4D flow CMR imaging.

Adapted from (Mahadevia et al., 2014). **Top panel**, note the presence of distinctly different 3D outflow flow jet patterns (black dashed arrows) in the

ascending aorta (AAo) for patients **B** and **C**. **Bottom panel**, 3D flow patterns in the left ventricular outflow tract (LVOT) and AAo distal to the aortic valve. Note the different systolic aortic valve outflow flow jet patterns (red indicating high velocities > 1 m/s) and wall impingement zones that correspond to variable exertion of high wall shear forces between different valve groups (**C** and **D**) and aorta size–matched controls (**B**) and healthy volunteers (**A**). AV, aortic valve; DAo, descending aorta; m/s, metre per second.

Further support for the importance of flow in BAV-related aortopathy pathogenesis has also arisen from *in-vivo* studies, which show that aberrant shear stress, such as that produced by BAV leaflets, is able to modulate expression of genes that regulate MMP production, matrix remodelling and VSMC apoptosis, thus predisposing to aneurysm formation (Dolan et al., 2011, Ruddy et al., 2010). This is substantiated by the increased expression of MMP2 and a higher MMP2 to TIMP1 activity in tissue samples from aortic aneurysms in BAV patients (Tadros et al., 2009), as well as a higher apoptosis rate of cultured VSMC derived from the dilated aorta of BAV patients compared to controls (Bonderman et al., 1999). Furthermore, BAV aortic aneurysm tissues exhibit reduction of endothelial nitric oxide synthase (eNOS) protein expression, with site-dependent variability, which is probably triggered by variations in shear stress along the aortic wall (Aicher et al., 2007, Mohamed et al., 2012). Simulated reduction of eNOS expression in the cultured VSMCs of BAV-related aneurysm tissue, by treatment with NOS inhibitor L-NAME, results in cytosolic accumulation of HTRA2/Omi, a proapoptotic mitochondrial serine protease, which presumably mediates VSMC apoptosis in BAV aortas (Mohamed et al., 2012), thereby conferring susceptibility to aneurysm formation. Moreover,

structural alteration of the extracellular matrix in itself can also result in transmission of proapoptotic cues to the VSMCs (Della Corte et al., 2008). Extracellular matrix remodelling occurs early in BAV, evident even in the nonaneurysmal BAV aortas, with maximum changes observed at the convexity, and is characterised by collagen and laminin reduction and increased in fibronectin and tenascin expression (Della Corte et al., 2008, Della Corte et al., 2006). These changes are associated with enhanced VSMC apoptotic indices, also primarily at the convexity, even prior to overt aortic dilatation, and, interestingly, increased Bcl-2-modifying factor-Bcl-2 binding (Bmf-Bcl2), a known matrix-dependent proapoptotic signalling mechanism (Della Corte et al., 2008). Therefore, it is speculated that stress-induced extracellular matrix changes within the aortic convexity of BAV patients may trigger cytoskeletal rearrangement of VSMCs that lead to early local apoptosis of these cells. This is presumably mediated by Bmf-Bcl2 binding, resulting in progressive, typically asymmetric aortic enlargement seen in BAV related aortopathy (Della Corte et al., 2008). These studies support the important role of haemodynamic in the initiation and progression of BAV-related aortopathy.

1.3.5.3.Phenotype heterogeneity in BAV related aortopathy

Not all patients with BAV will develop aortic dilatation over time, regardless of the underlying valvular function. There is also a highly heterogeneous expression of aortopathy in BAV disease even amongst patients with specific valve fusion pattern and similar levels of valve dysfunction (Barker et al., 2012). Furthermore, there is a small subset of BAV patients, mostly young males, who

present with predominantly symmetric dilatation of the aortic root at an early age. This is associated with annular dilatation and varying degrees of aortic insufficiency (Nistri et al., 1999) and may represent a predominantly genetic form of BAV disease less influenced by hemodynamic factors.

Therefore, these studies suggest that BAV-related aortopathy is a product of the interaction between genetic and hemodynamic factors. BAV-related aortopathy could be associated with a congenital anomaly of some component of a matrix signalling pathway, thereby conferring inherent genetic susceptibility. Meanwhile, the hemodynamic disturbances, produced by the genetically determined, anatomically abnormal valve, then act after birth as a triggering and accelerating factor to the locally degenerative process within the aortic media, leading to progressive asymmetric aortic dilatation and aneurysm formation (Della Corte et al., 2008). Ultimately, the clinical heterogeneity seen in BAV-related aortopathy may be explained by individual variable combinations of coexisting genetic susceptibilities, the severity of haemodynamic alteration and other yet-to-be-identified environmental factors in modifying the final phenotype manifestation of the aortopathy.

Overall, current evidence points to BAV disease being a final common pathway for a wide variety of altered molecular and genetic defects. Determination of the genetic basis underlying BAV disease is complex. Not only that there are large number of genes involved in valvulogenesis (genetic heterogeneity) but epigenetic, haemodynamic, and stochastic factors are also important in modulating phenotype expression and thus contributing to the wide spectrum of

disease manifestations (clinical heterogeneity). Recent advances in the fields of valve development and BAV disease, combined with major developments in genetic analysis technologies, place the field at the precipice of accelerated discovery into the causative and pathogenetic mechanisms responsible for this common heart valve defect. Furthermore, the present limitation of pharmacological therapy in delaying or stopping disease progression has left surgical therapies as the most effective cure for many cases of BAV disease. Improved understanding of the genetic basis, molecular pathways, and cellular mediators involved in the pathogenesis of BAV disease will create great opportunities for the development of novel pharmacological treatment and prevention strategies. This knowledge has the potential to also be used to stratify treatment modalities, time surgical intervention, and guide management of at-risk family members, in terms of diagnostic, therapeutic, and prevention strategies, with the overall aim of reducing the health burden of BAV disease.

1.4. STRATEGIES TO IDENTIFY PATHOGENESIS OF BAV

A common feature of nearly all types of genetic heart disease, including BAV, is the phenotype heterogeneity observed between affected individuals, even within the same family. This can largely be explained by the considerable genetic diversity and the heterogeneity of genetic modifiers that may influence the ultimate phenotypic manifestation of these conditions. Elucidating the genetic basis of diseases therefore becomes a fundamental starting point for studies of disease mechanisms, pathways and molecular targets for potential therapeutic interventions (McCarthy and Hirschhorn, 2008).

Over the past few decades, many genetic techniques have been developed to assist with identification of causative mutation(s) for a Mendelian disease, as summarised in Table 1.2. Whilst traditional gene mapping approaches, such as karyotyping, linkage analysis, candidate gene, and copy number variation analysis, have lead to great insights into many Mendelian disorders, they are unable to detect all forms of genomic variation (Gilissen et al., 2011). Fortunately, researchers within genetic fields have received a boost over the past few years by the introduction of new technologies that enable DNA sequencing at much higher throughput and at much lower costs than previously possible (Gilissen et al., 2011), such as whole exome and whole genome sequencing.

This project utilised a combination of candidate gene analysis and whole exome sequencing to investigate the underlying pathogenetic basis of BAV disease.

This project also employed RNA sequencing (transcriptome sequencing) technology to assess the effects of BAV disease states on gene expression within the aortic valve, which may give insights into disease mechanisms and pathways. These approaches will be briefly discussed in the following sections.

Table 1. 2. Mendelian disease gene identification approaches.

Approach	Applies to	Advantages	Disadvantages
Candidate gene	Any disease	Easy to perform for one or two genes; requires no mapping, can directly identify the causative variant/ mutation	Relies heavily on current biological knowledge; success rate very low
Genetic mapping by karyotyping	Any disease	Easy to perform; no familial cases required; can detect (large) balanced events	Low resolution, only detects large chromosomal aberrations; mutation detection requires second step
Genetic mapping by linkage analysis	Inherited disease	Easy to perform	Requires large families, often identifies large loci; mutation detection requires second step
Genetic mapping by homozygosity mapping	Recessive monogenic diseases	Small families can be used	Most useful for consanguineous families; often identifies large loci; mutation detection requires second step
Genetic mapping by CNV analysis	Monogenic/ monolocus disease	High resolution CNV screening; no familial cases required; can potentially identify small loci	Only investigates CNVs; cannot detect balanced events, no base-pair resolution; mutation detection requires second step
Whole exome sequencing	Any disease	Base-pair resolution exome-wide; detects most types of genomic variation; can directly identify the causative variant/mutation	Unable to detect non-coding variants; limited resolution for CNVs and other structural variation; coverage variability due to enrichment process; relatively expensive
Whole genome sequencing	Any disease	Base-pair resolution genome-wide; detects all types of genomic variation; can directly identify the causative variant/mutation	Data analysis complex; even more expensive than exome sequencing

Adapted from (Gilissen et al., 2011). Highlighted in grey are the techniques employed in this project.

1.4.1. Candidate gene approach

Candidate gene studies have been at the forefront in the field of genetic epidemiology, where they have been used to identify genes with modest effect and the association of a genetic variant with a particular disease or clinical trait (Patnala et al., 2013). Candidate gene approach is relatively cheap and quick to perform, although it can be labour intensive and cost inefficient when genes with large number of exons are involved. It generally begins with selection of a putative candidate gene based on its relevance in the mechanism of disease being investigated. It is therefore dependent on *a priori* knowledge of the candidate gene's biological function.

Candidate gene approach is traditionally performed using Sanger sequencing (i.e. direct DNA sequencing). This is achieved by amplifying all exons along with intron/exon borders of the selected candidate gene of interests using PCR, followed by sequencing of the entire coding regions (Chapter 2.4.1). When DNA sequence variation is detected, the variation is then analysed for its functional significance and therefore the likely pathogenicity. The following are some of the criteria that can be used to support causality of the putative gene variants in the disease pathogenesis (Kuhlenbaumer et al., 2011): (1) variant co-segregation with disease within the family; (2) gene variants lead to a non-synonymous amino acid substitution, splicing aberration or protein truncation; (3) unknown or novel variants that are neither found in controls or public databases (e.g. dbSNP); (4) different mutations in the same gene are found in unrelated cohort with the same disease phenotype; and (5) functional evidence from animal or *in-vitro* models.

Whilst candidate gene approach has been used successfully in identifying a number of single gene defects, it is subject to a fundamental limitation. The major challenge with the candidate gene approach is how much is known of the biology of the disease being investigated and thus, the ability of the current knowledge to sufficiently predict causative genes. Since genetic heterogeneity is more the rule than the exception in many genetic disease, therefore, if only a small number of genes are considered, it is likely that only a subset of genes involved in a disease are identified (Tabor et al., 2002). This contributes to the generally low success rate of this approach.

1.4.2. Whole exome sequencing

With the advent of next-generation sequencing (NGS) technologies, fundamental limitations posed by candidate gene sequencing and other traditional approaches have been surmounted, assisting with the identification of causative genes at an accelerated rate. The NGS has the potential to identify all kinds of genetic variation at base-pair resolution throughout the human genome in a single experiment, hence a much faster and more cost efficient strategy compared to traditional techniques (Gilissen et al., 2011). There are 2 unbiased sequencing approaches for detecting genetic variation within an individual, namely whole genome sequencing and whole exome sequencing. Whilst whole genome sequencing is the ultimate approach for detecting all genomic variation in a patient's genome in a single experiment, it poses a significant bioinformatics analysis challenge and its regular application is

currently cost-prohibitive for many laboratories (Gilissen et al., 2011). Therefore, a more cost-efficient sequencing strategy is to study the approximately 1% of human genome that is protein-coding (the exome) by means of whole exome sequencing. This is supported by the fact that approximately 85% of mutations with large effects in Mendelian diseases reside within the exons (Choi et al., 2009), hence, making this a powerful strategy for identifying genes that underlie Mendelian disorders in circumstances in which conventional approaches have failed.

The overall exome sequencing workflow is summarised in Figure 1.11 and Figure 1.12 further details the basic computational workflow and the online-tools or software used in the bioinformatics and single nucleotide variations (SNV) calling pipelines. The specifics of the process involved with this technique are described in greater details in Chapter 2.4.3.

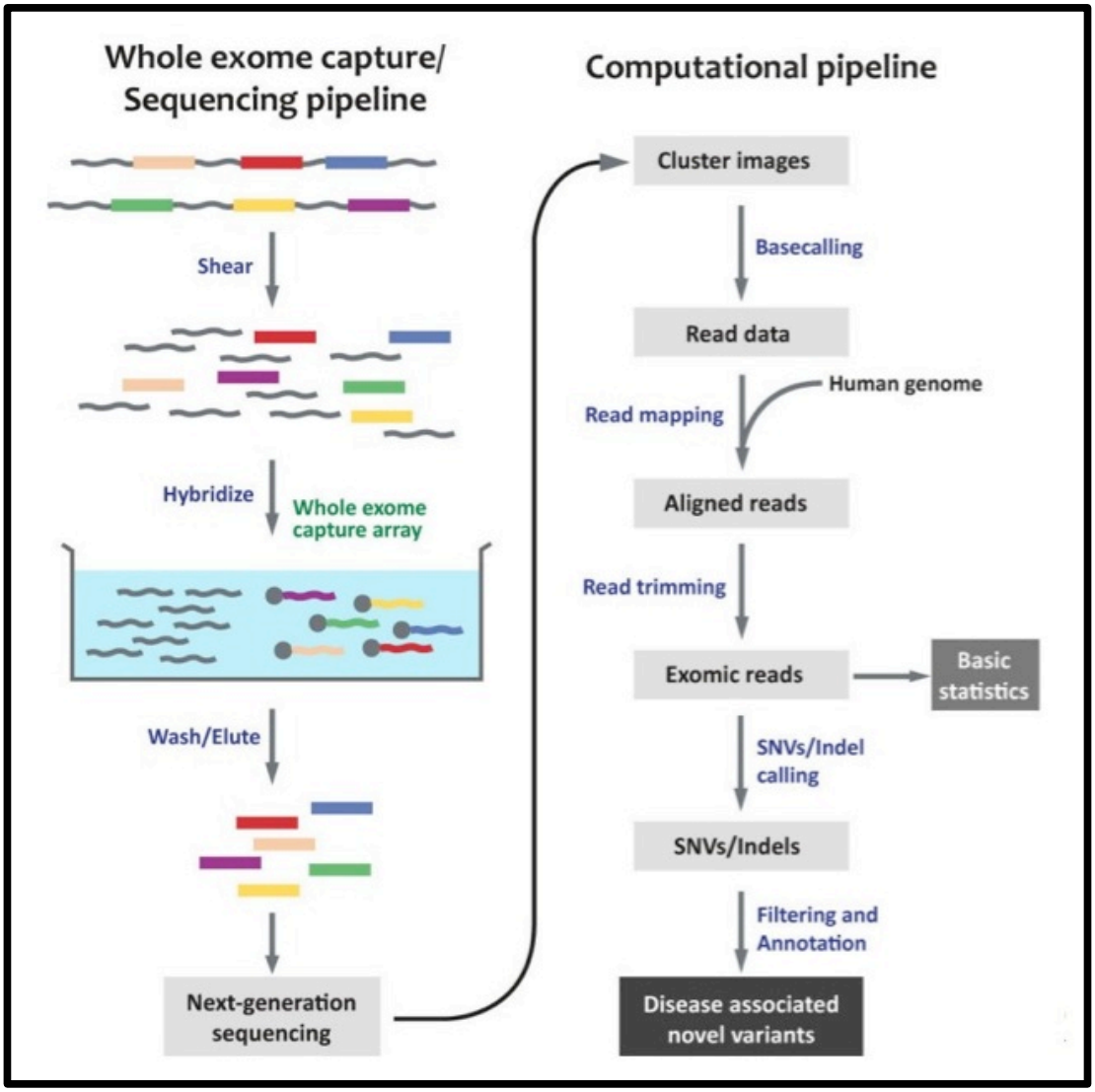

Figure 1. 11. Whole exome sequencing workflow.

Adapted from (Goh and Choi, 2012).

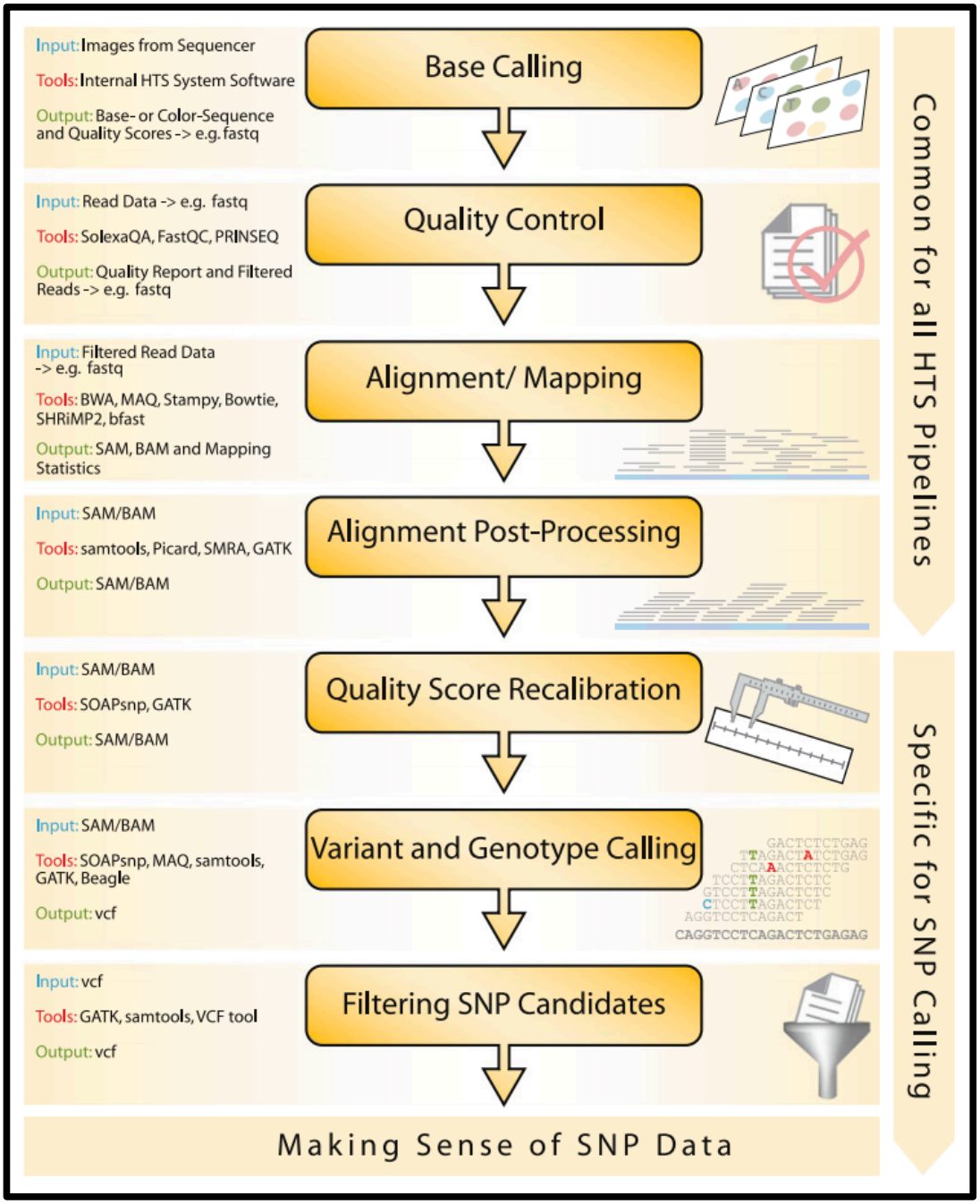

Figure 1. 12. Overview of bioinformatics and SNV calling pipelines.
Adapted from (Altmann et al., 2012).

Whilst many examples are available in the literature that provide proof-of-concept of exome sequencing strategies for identification of disease-causing mutations for various recessive and dominant disorders, the technique is

subject to a number of technical and analytical limitations. These include the inability of exome sequencing to detect non-coding regulatory variants (i.e. promoters, enhancers and microRNAs), its limited resolution for analysis of copy number variations and other structural variation, and the variability of exome coverage depending on the enrichment process, which may lead to inadequate coverage of the region that contains a causal variant and even failure to accurately call a variant, due to the strict filtering process (Gilissen et al., 2011, Bamshad et al., 2011). Mismapped reads or errors in alignment, due to paralogous genes, pseudogenes or sequences that exhibit high sequence similarities in the genome, may also lead to false variants in a gene being called, leading to false positive findings. Meanwhile, false negative results can arise when part or the entire causative gene is not in the target definition (Bamshad et al., 2011); for example, it is not known to be a gene (i.e. unannotated exons) and thus not targeted in the current capture method. Additionally, some exonic regions with high GC content or repetitive sequences (up to 10-15% of the exome) can also be very difficult to target with the current exome sequencing approach (Ware et al., 2012). Therefore, presently Sanger sequencing will continue to be used as a complementary strategy to cover these poorly covered target regions and to validate exome sequencing findings. Nonetheless, despite these limitations, exome sequencing is well justified as a valuable strategy to search for causative alleles underlying Mendelian disorders (Ng et al., 2010).

1.4.3. RNA sequencing (Transcriptome sequencing)

A transcriptome is a collection of all the transcripts or messenger RNA (mRNA) present in a given cell or tissue of an organism. Therefore, RNA sequencing or transcriptome sequencing is very useful in providing a snapshot of the current state of a cell or tissue and the possible effects of disease states on gene expressions (transcriptome) (Churko et al., 2013). RNA sequencing also provides information on the differences between the transcriptome and the exome as a result of RNA editing (Churko et al., 2013). Whilst hybridisation-based microarray profiling has revolutionised the study of transcriptomics and proved useful in determining gene expression profiles, transcriptome analysis using RNA sequencing is becoming the preferred method of choice (Kogenaru et al., 2012). This is because RNA sequencing is more sensitive, provides absolute quantity levels, offers a large dynamic range of expression that is not affected by on-chip sequence biases, and gives additional information on gene expression levels and splice junction variants (Churko et al., 2013). Furthermore, RNA sequencing requires a relatively small amount of total RNA compared to microarray for quantification (Kogenaru et al., 2012), making it a more attractive technique to employ. Figure 1.13 illustrates the overall RNA sequencing workflow for transcriptome quantification and functional analysis. The specific process involved in RNA sequencing is detailed on Chapter 2.4.4.

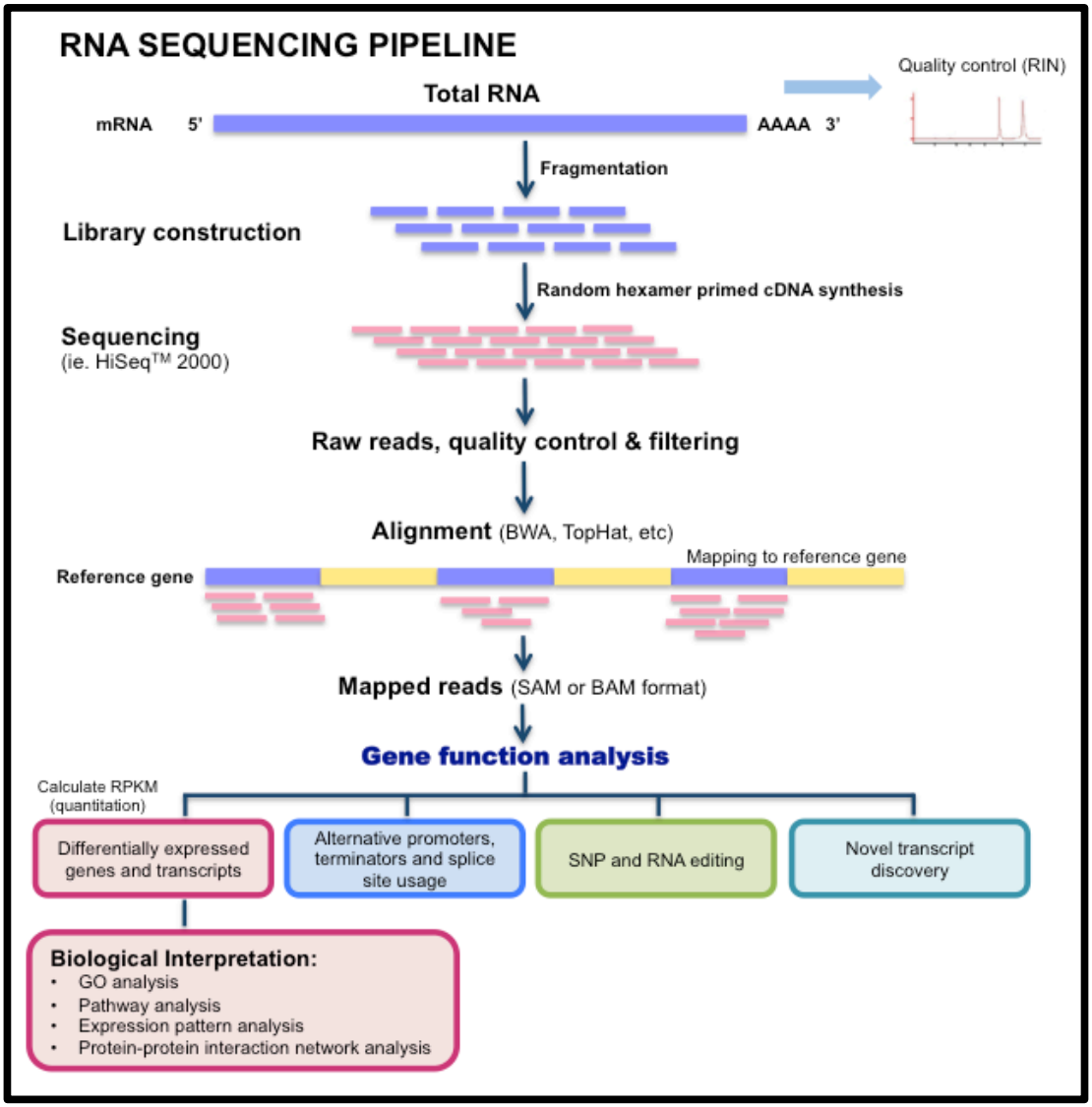

Figure 1. 13. RNA sequencing workflow.

Figure adapted with modification from http://www.bioinfo.mc.vanderbilt.edu/NGS/rna-seq.html.

Evaluation of transcriptome using RNA sequencing plays a valuable role in cardiovascular medicine because transcriptome changes can identify how cardiovascular diseases changes with time (Churko et al., 2013). Thus, RNA sequencing provides a means for understanding the genetic and epigenetic consequences that produce and influence the actual disease phenotype

(Schnabel et al., 2012), highlighting molecular pathways that are important in disease pathogenesis. In turn, it provides us with a better understanding of disease mechanisms and an opportunity to develop targets for potential therapeutic interventions.

1.4.4. Cardiac Magnetic Resonance (CMR) imaging in BAV-related aortopathy

Whilst echocardiography (transthoracic and/or transoesophageal when indicated) remains the first-line diagnostic imaging modality for the detection of BAV, evaluation of its morphological feature and assessment of related valvular and aortic complications in the majority of patients, its use can be challenging in those with poor acoustic windows or extensive leaflets calcifications. Further, adequate echocardiographic views of the mid and distal ascending aorta and aortic arch, the usual sites of maximum dilatation in BAV disease, can be difficult to assess (Ko et al., 2012) and therefore, clinically important aortic dilatation can potentially be missed.

In the last decade, CMR imaging has emerged as a powerful adjunctive modality in the assessment of BAV patients (Shenoy et al., 2014), especially in those with suboptimal echocardiography images and when conflicting/ambiguous echo measurements are obtained, which can critically impact on clinical management and interventional planning. In BAV, CMR imaging can be used for comprehensive assessment of aortic valve structure, left ventricular volume and function, accurate quantification of aortic

regurgitation, and detection of other coexistent congenital cardiac malformation. Further, CMR imaging provides a complete assessment of the entire thoracic aorta, allowing anatomical, morphological and dynamic/functional evaluation of BAV-related aortic abnormalities (Evangelista, 2014), including aneurysm, dissection and aortic coarctation. Given the need for life-long routine aortic imaging surveillance in these patients and the lack of radiation exposure that is associated with CT angiography (CTA), CMR imaging appears to be the imaging modality of choice in the long-term follow-up of aortic pathologies in BAV patients. However, the major limitations of CMR imaging are limited availability, lack of portability, relatively long acquisition time, high cost and contraindications to use in certain patients, i.e. those with implanted cardiac pacemakers/defibrillators or claustrophobia. Table 1.3 summarised comparative strengths and limitations between the different imaging modalities that are currently available for the assessment of various aortic pathologies, including echocardiography, CTA, and CMR imaging.

Table 1. 3. Comparative advantages of imaging modalities for aortic diseases assessment.

Advantages of modality	TTE	TOE	CTA	CMR
Readily available	+++	+	+++	+
Quickly performed	+++	++	++	+
Non-invasive	+++	+	+++	+++
No iodinated contrast	+++	+++	-	+++^
No radiation	+++	+++	-	+++
Overall aorta segment assessment	+*	++$	+++	+++
3D multiplanar and high resolution	-	-	+++	+++
Dynamic and functional information	++	++	-	+++
Measurement accuracy	+*	+*	+++	++
Branch vessel involvement	+	+	+++	+++
Presence of AR and mechanisms	+++	+++	-	++
Assessment of LV function	+++	+++	+	+++

* good in ascending aorta; $ good in thoracic aorta; ^using gadolinium (Gd)-based contrast medium; +++, excellent; ++, good; + limited; -, bad; CTA, CT angiography; CMR, cardiac magnetic resonance imaging; TOE, transoesophageal echocardiography; TTE, transthoracic echocardiography; AR, aortic regurgitation; LV, left ventricle. Adapted from (Evangelista, 2014).

Typically, a comprehensive CMR examination of the aorta includes the following imaging sequences (Evangelista, 2014): (1) basic black-blood imaging using spin-echo sequences, which provide significant morphological information on the aortic wall and adjacent structures; (2) cine-MR images or non-contrast white-blood imaging with high temporal resolution to obtain images of multiple phases and visualise blood flow during systole and diastole; (3) MR imaging contrast-enhanced angiography (MRA) with intravenous gadolinium, which provides accurate information on aortic diameter, aneurysm extent and its relationship with the main arterial branches; (4) the phase-contrast imaging

technique, which can provide functional data, including quantification of forward and reverse aortic flow in case of aortic regurgitation; and (5) 3D isotropic whole-heart imaging, using FIESTA (fast imaging employing steady state acquisition)-based sequence, to provide complementary evaluation of the great vessels and intracardiac anatomy. These imaging sequences are conventionally acquired with ECG-gating and breath-holding, in order to obtain CMR images with high temporal and spatial resolutions, as data are acquired over a number of cardiac cycles. Thus, regular heart rhythm and consistent cardiac position are important during CMR image acquisition. Figure 1.14 illustrates an example of a recommended CMR protocol for the overall assessment of BAV and BAV-related aortic abnormalities (Shenoy et al., 2014). Recently, advancement in CMR imaging technique has resulted in the development of a free-breathing real-time phase contrast CMR sequence with good spatiotemporal resolution, which allows instantaneous assessments of physiological blood flow and cardiac dynamics (Lin et al., 2012c, Sohns et al., 2013).

This project utilised state-of-the-art real time exercise CMR imaging techniques to evaluate the differential aortic wall mechanical properties between patients with BAV and TAV and ultimately, to identify novel imaging biomarker(s) that can potentially be used to predict for the development of adverse aortic outcome in those with BAV disease. The specifics of the process involved with this technique are described briefly in Chapter 2.5 and in greater details in Chapter 6.2.

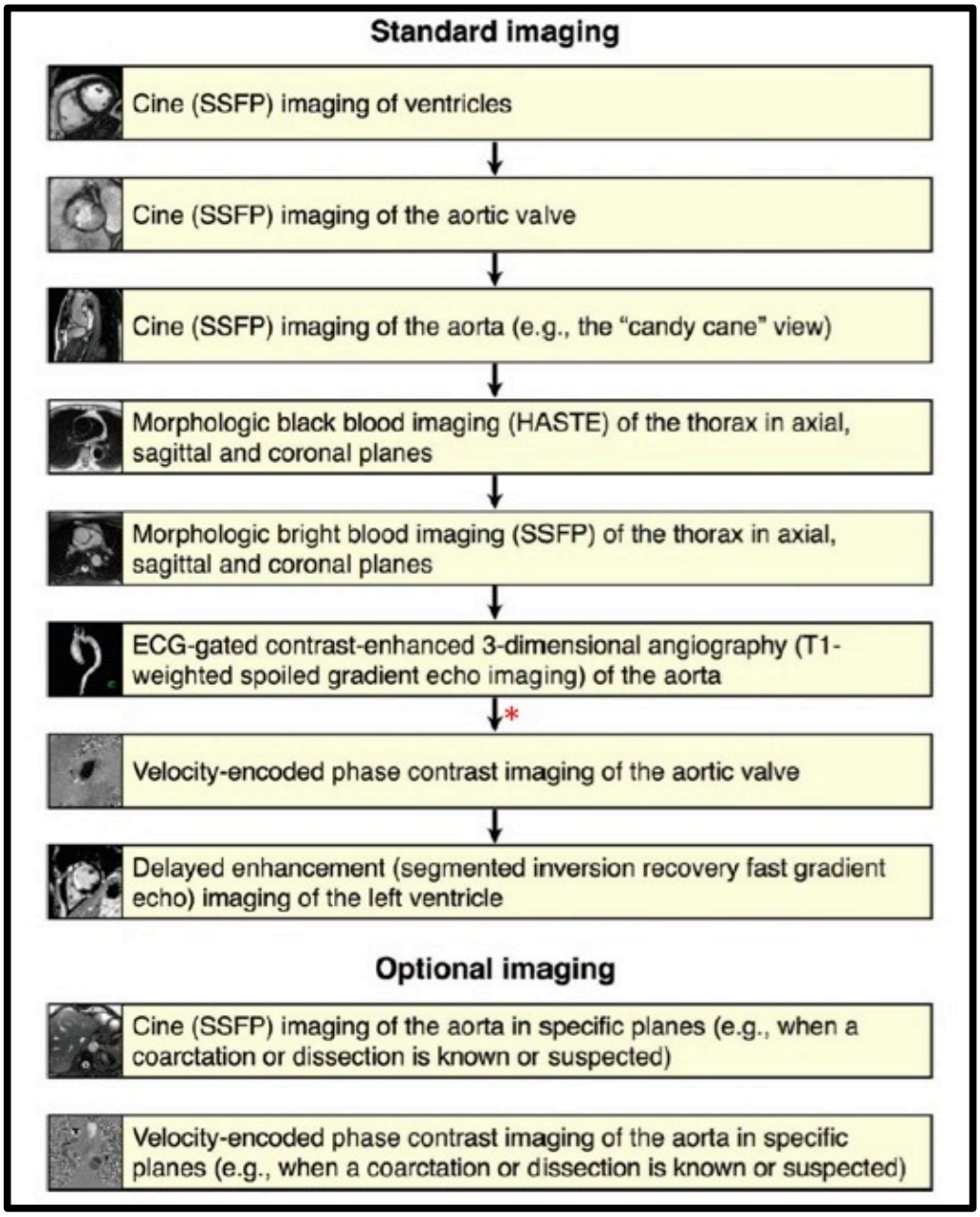

Figure 1. 14. Outline of CMR protocol for the assessment of BAV syndrome.

Adapted from (Shenoy et al., 2014). *As part of our institutional protocol, a 3D isotropic whole-heart image acquisition is routinely performed following the 3D contrast-enhanced MRA imaging. The entire study is typically performed in under an hour. SSFP, steady-state free precession; HASTE, half-Fourier acquisition single-shot turbo spin-echo; ECG, electrocardiogram.

1.5. HYPOTHESES AND AIMS

Despite being the commonest form of congenital cardiac disorder with significant clinical implications and health burden, the underlying genetic basis of BAV disease is mostly undetermined.

1.5.1. Hypotheses

There are two hypotheses being addressed in this thesis.

Hypothesis 1: In a significant proportion of patients with BAV disease, there is an underlying genetic cause of the disorder. Identification of the genetic and molecular basis of BAV disease has major implications in our understanding of disease pathogenesis as well as in creating great opportunities for the development of novel pharmacological treatment and prevention strategies.

Hypothesis 2: There is an inherent structural abnormality within the ascending aortic wall of patients with BAV, which predispose them to develop ascending aortic dilatation in response to life-long haemodynamic stress. This structural abnormality can be detected clinically using non-invasive exercise CMR imaging by evaluating various measures of aortic stiffness or elasticity.

1.5.2. Aims of the project

Based on the above hypotheses, there are two main aims:

1. To perform genetic studies to identify causative and modifier genes as well as molecular pathways responsible for BAV disease development and progression.
    - Specifically, a **candidate gene approach** will be used in sporadic cases of BAV and a **whole-exome sequencing approach** in familial cases of BAV. Furthermore, **transcriptome analysis of aortic valve** tissues will be performed to evaluate the differential pattern of gene expression underlying structural valve degeneration in BAV versus TAV.
    - When a positive genetic study is obtained, a genotype-phenotype correlation study is to be performed.

2. To evaluate the differential aortic wall mechanical properties between those with BAV and TAV, using **real-time exercise CMR imaging**, in order to identify predictors of adverse clinical outcome in those with BAV-related aortopathy.

A summary of the research plan is shown in Figure 1.15.

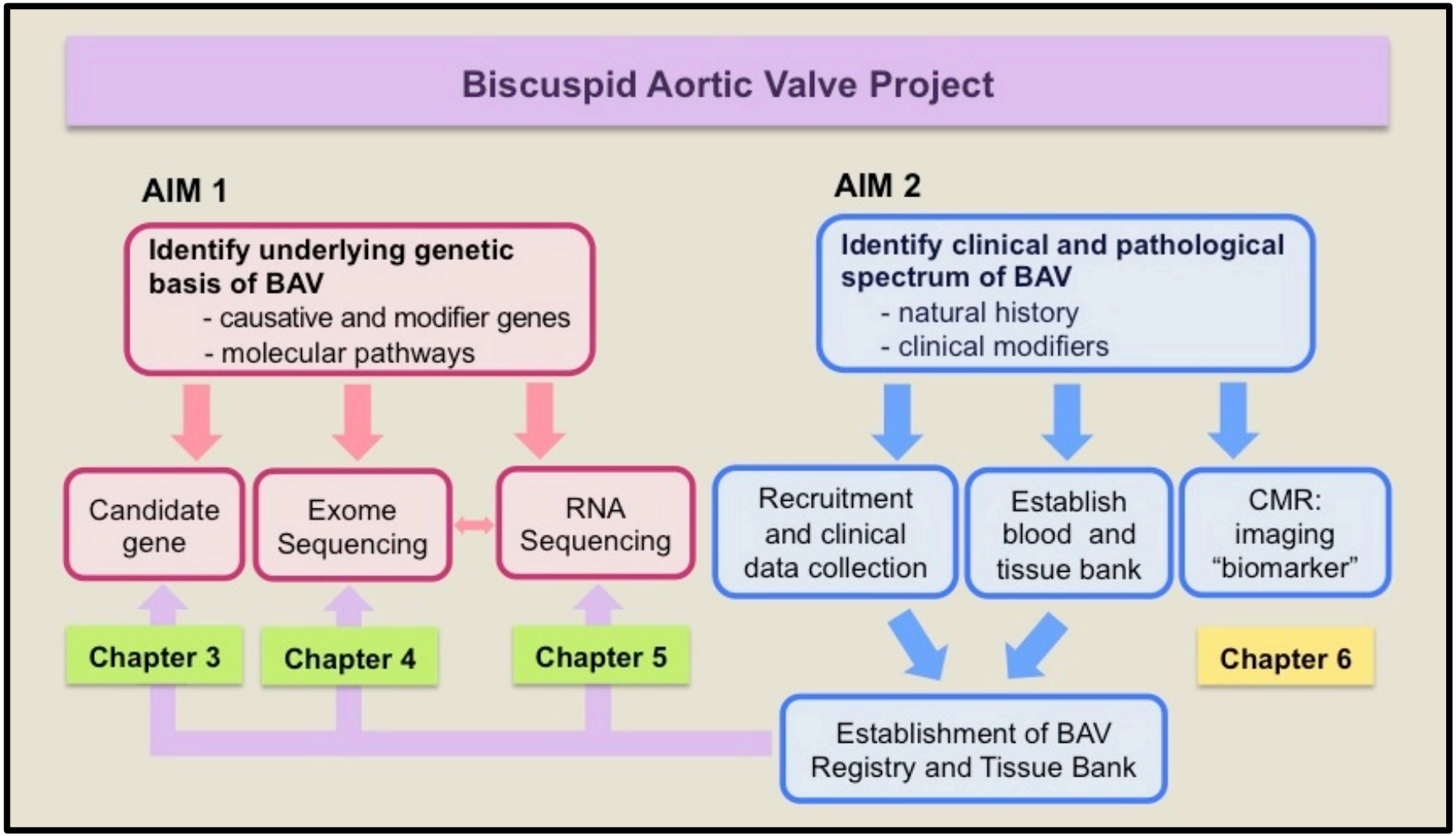

Figure 1. 15. Thesis overview.

CHAPTER 2: MATERIALS AND METHODS

2.1. MATERIALS

Table 2. 1. General materials, chemicals and molecular biology reagents.

Reagent	Source / Supplier
DNA extraction procedure	
QIAamp DNA Blood Mini Kit	Qiagen (Germantown, MD, USA)
PCR reagents	
GoTaq® Flexi Buffer	Promega (Maddison, WI, USA)
$MgCl_2$	Promega (Maddison, WI, USA)
GoTaq® Flexi DNA polymerase	Promega (Maddison, WI, USA)
dNTPs	Roche Diagnostics GmbH (Mannheim, Germany)
Dimethly sulfoxide (DMSO)	Sigma-Aldrich (St. Louis, MO, USA)
Primers	Geneworks (Hindmarsh, SA, Australia)
PCR product purification	
Exonuclease I	Amersham Biosciences (Piscataway, NJ, USA)
Antarctic phosphatase	New England BioLabs (Ipswich, MA, USA)
Agarose gel electrophoresis	
Agarose	Amresco (Solon, OH, USA)
EDTA	Sigma Aldrich (St. Louis, MO, USA)
Tris base	Sigma Aldrich (St. Louis, MO, USA)
Glacial acetic acid	Crown Scientific (Moorebank, NSW, Australia)
TAE, 25x Ready-Pack	Amresco (Solon, OH, USA)
Orange G Sodium salt	Sigma Aldrich (St. Louis, MO, USA)
Gel red	Biotium (Hayward, CA, USA)
DNA Molecular Weight Marker IX	Roche Diagnostics GmbH (Mannheim, Germany)
RNA preservation	
RNA*later*®	Ambion, Life Technologies (CA, USA)
RNA extraction	
100% ethanol	Chem-Supply (Gillman, SA, Australia)
Isopropyl alcohol	Sigma Aldrich (St. Louis, MO, USA)
Triple distilled water (TDW)	Centenary Institute (Sydney, NSW, Australia)
TRIzol® Reagent	Invitrogen, Life Technologies (CA, USA)
Chloroform	Chem-Supply (Gillman, SA, Australia)
DEPC-treated water	Ambion, Life Technologies (CA, USA)
cDNA synthesis and reverse transcription quantitative PCR (RT-qPCR)	
SuperScript® VILO	Invitrogen, Life Technologies (CA, USA)
Express SYBR® GreenER qPCR SuperMix Universal	Invitrogen, Life Technologies (CA, USA)

2.2. ONLINE TOOLS AND DATABASES

Table 2. 2. Online tools, software and databases used in the project.

Tool or Database	Website
1000 Genomes Project	http://www.1000genomes.org/home
Bowtie	http://bowtie-bio.sourceforge.net/index.shtml
Burrows-Wheeler Aligner (BWA)	http://bio-bwa.sourceforge.net/
dbSNP (build 137)	http://www.ncbi.nlm.nih.gov/projects/SNP/
Database for Annotation, Visualisation and Integrated Discovery (DAVID) version 6.7	http://david.abcc.ncifcrf.gov
Ensembl	http://www.ensembl.org/index.html
Genome Analysis Toolkit (GATK, version 2.7.2)	http://www.broadinstitute.org/gsa/wiki/index.php/The_Genome_Analysis_Toolkit
Human genome reference (GRCh37/hg19)	http://genome.ucsc.edu
Integrative Genome Viewer (IGV)	http://broadinstitute.org/igv/
Ingenuity Pathway Analysis (IPA)	http://www.ingenuity.com/products/ipa
National Centre for Biotechnology Information (NCBI)	http://www.ncbi.nlm.nih.gov/guide/
NetPrimer (Premier Biosoft)	http://www.premierbiosoft.com/NetPrimer/AnalyzePrimer.jsp
NHLBI Exome variant server (EVS)	http://evs.gs.washington.edu/EVS/
PANTHER Classification System	http://www.pantherdb.org
Primer3 version 0.4.0	http://bioinfo.ut.ee/primer3-0.4.0/
Primer3Plus©	http://www.bioinformatics.nl/cgi-bin/primer3plus/primer3plus.cgi
Primer-BLAST	http://www.ncbi.nlm.nih.gov/tools/primer-blast/
Polyphen2	http://genetics.bwh.harvard.edu/pph2/
SamTools version 0.1.19	http://samtools.sourceforge.net/
Seattle Seq Annotation tool	http://snp.gs.washington.edu/SeattleSeqAnnotation131/index.jsp
TopHat2 version 2.0.6	http://tophat.cbcb.umd.edu
OligoEvaluator DNA calculator	http://www.sigmaaldrich.com/life-science/custom-oligos.html
SeqMonk (Babraham Bioinformatics)	http://www.bioinformatics.babraham.ac.uk/projects/seqmonk/
Uniprot	http://www.uniprot.org/

2.3. STUDY POPULATIONS AND TISSUE BANK

Patient recruitment and all human sample collection were done following informed consent. The study protocol was approved by the Sydney South West Area Health Service Ethics Committee.

2.3.1. BAV populations

Patients attending specialised cardiology clinics and those who were scheduled to have aortic valve replacement (AVR) surgery at the Royal Prince Alfred Hospital (RPAH), Sydney, Australia, were prospectively recruited from February 2011 to January 2013. Following informed consent, clinical information and 20mls of peripheral blood were collected from each patient. All patients underwent clinical evaluation that included family history, physical examination, and 2D-echocardiography. In each case, aortic valve morphology was confirmed by imaging and/or during cardiac surgery and their functional state was determined according to the American Heart Association and the American College of Cardiology guidelines (Bonow et al., 2008).

Aortic valve was categorised as structurally normal when the valve had 3 completely separate leaflets, i.e. tricuspid/tri-leaflet aortic valve (TAV), and was bicuspid when it had only 2 leaflets. BAV morphology was classified as anatomically bicuspid when there were 2 approximately symmetrical leaflets without a raphe; functionally bicuspid when the 2 leaflets were unequal in size with the larger leaflet having a central raphe due to commissural fusion; or

indeterminate when the morphology was unrecognisable, e.g. due to heavy calcification.

2.3.2. Control population

The control DNA population used in the candidate gene study consisted of 160 predominantly Caucasian individuals, 51% females, from Sydney, Australia, who did not suffer from any cardiac-related health problems at the time of blood collection. Routine clinical and/or formal echocardiographic evaluations however were not performed amongst the majority of the control subjects at the time of recruitment.

2.3.3. Tissue banking

Aortic valve tissue of BAV or TAV morphology were prospectively collected from all consenting participants undergoing aortic valve or aortic root surgery at the RPAH between February 2011 to December 2013. The valve tissues obtained between February 2011 to February 2012 were immediately snap-frozen in dry ice upon surgical removal and stored at -80°C fridge until genetic materials were extracted. Since March 2012, all harvested leaflet tissues were immersed in RNA*later* solution (Ambion Inc, Austin, TX) overnight and stored at -80°C to allow better RNA preservation, prior to extraction.

2.4. MOLECULAR GENETIC METHODS

2.4.1. Methods of DNA analysis

2.4.1.1. DNA extraction

Genomic DNA was extracted from the peripheral blood leukocytes of all adult cohorts using the QIAamp DNA Blood Mini Kit according to the standard manufacturer's protocol. For young cohorts, aged 12 or below, the Oragene DNA Self-Collection Kit (either OG-300 or OG-250; DNA Genotek Inc, Kanata, Ontario, Canada) was used to collect and extract participants' genomic DNA from their saliva, in accordance to the manufacturer's instructions. The concentration and purity of all stock genomic DNA samples were assessed using the Nanodrop 2000 spectrophotometer (Thermo Scientific, MA, USA). Aliquots of stock genomic DNA samples were diluted with TDW to 15ng/μL working concentration and stored at 4°C until their use in subsequent downstream applications.

2.4.1.2. Standard DNA Polymerase Chain Reaction amplification

Polymerase chain reaction (PCR) was used to amplify DNA sequences of interest. Primers were designed with Primer3Plus software, using reference sequences obtained from the Ensembl Genome Browsers. Specific primer sequences and their optimal reaction conditions used in the different sections of this project are listed in Appendix I.

The PCR mixture consisted of 2.5µL of template DNA (15ng/µL), 5µL of 5x GoTaq® Flexi Buffer (pH 8.5), 1.2µL of dNTPs (0.4mM), 1.2µL of $MgCl_2$ (2.0mM), 1µL of each forward and reverse primer (0.6µM), and 0.08µL of GoTaq Flexi DNA polymerase (5U/µL), with or without DMSO (2.5µL), made up to a final volume of 25µL per reaction with TDW. A negative control of DNA replaced by TDW was used to verify the absence of DNA contaminations in reactions. The PCR was carried out in a PTC-100 or the PTC-200 Peltier Thermal Cycler (MJ Research Inc., Waltham, MA, USA). Thermal cycling was performed at 95°C for 2 minutes, followed by 35 cycles of 95°C for 30 seconds, primer specific annealing temperature (Ta) for 30 seconds and 72°C for 1 minute, followed by a final extension of 72°C for 5 minutes. PCR products were stored at 4°C.

2.4.1.3. Agarose gel electrophoresis

The size of PCR products, RNA and DNA were resolved using agarose gel electrophoresis. Five µL of samples were mixed with 5µL Orange G loading dye and electrophoresed in either a 1% (for PCR products or DNA) or 2% (for RNA) agarose gel containing 1:10,000 parts of Gel Red. DNA molecular weight marker (Marker IX, in a 1 in 5 dilution with Orange G loading dye) was run simultaneously next to samples to determine approximate size of nucleic acid. Electrophoresis was performed in 1x TAE buffer (100 mM Tris base, 50 mM glacial acetic acid, 3 mM EDTA, pH 8.0) at 190 Volts for 50-60 minutes. The gel was then visualised under UV light using Syngene Image Analyser G:Box.

2.4.1.4. PCR product purification

PCR products were purified prior to sequencing to remove excess PCR primers and dNTPs, which may interfere with DNA sequencing. Five U/µL Exonuclease I and 1 U/µL Antarctic Phosphatase, made up to 4 µL with 0.1 mM Tris buffer, was added to 20 µL PCR product and incubated at 37°C for 30 minutes, followed by 80°C for 30 minutes to heat inactivate the enzymes.

2.4.1.5. Direct sequencing of PCR products

Sanger sequencing of the PCR products was performed in the forward and/or reverse direction at the Macrogen Ltd Facility (Gasan-Dong, Geumchun-Gu, Seoul, Korea). Sequencing data were analysed for variants using Sequencher Version 4.8 (Gene Codes Corporation, Ann Arbor, MI, USA). This method is used during candidate gene screening.

2.4.2. Methods of RNA analysis

2.4.2.1. RNA extraction

Total RNA was isolated from approximately 75-100mg of leaflet tissue following immediate homogenisation directly in the TRIzol Reagent with Polytron sonication (Polytron pt-MR2100 homogenizer, Kinematica AG, Lucerne, Switzerland). The RNA extraction procedure was performed using a modified TRIzol protocol that includes two RNA-DNA-protein phase separations to maximise RNA yield while minimising degradation and contamination. A similar two-phase separation method had recently been validated as an effective method for RNA extraction from cartilaginous tissue (Ali and Alman, 2012),

which had low cellularity and high proteoglycan content as seen in human aortic valve. Briefly and specific to our protocol, following the addition of isopropyl alcohol, incubation and centrifugation, a thin transparent layer of RNA will collect at the bottom half of the tube. The upper aqueous isopropyl alcohol phase was carefully removed, without disrupting the RNA layer, and discarded. One ml of TRIzol was then added to the residual solution containing the RNA layer and the extraction procedure was continued as per the standard protocol. The precipitated RNA was later re-suspended in DEPC-treated water and stored at the -80°C freezer until further use.

RNA quality was assessed for integrity (lack of degradation) and purity (absence of contaminants). The RNA purity and concentration was measured with a Nanodrop 2000 spectrophotometer (Thermo Scientific, MA, USA). The RNA integrity was assessed by 2% gel electrophoresis (as outlined in Chapter 2.4.1.3) and/or the Agilent 2100 Bioanalyzer (RNA6000 Nano LabChip, Agilent Technologies, Santa Clara, CA, USA). RNA samples with clear 28S and 18S rRNA bands on gel electrophoresis, where the intensity of the 28S band was approximately twice that of the 18S band, indicate good quality RNA. An RNA integrity number (RIN) of ≥ 7 on the Bioanalyzer indicates acceptable RNA quality for transcriptome analysis.

2.4.2.2. Reverse Transcription quantitative PCR (RT-qPCR)

RT-qPCR was used to quantitatively study gene expression levels in specific tissue or organ of interest through the creation of complementary DNA (cDNA)

transcripts. Here, two-step RT-qPCR was used, as previously described in our group (Bagnall et al., 2012). The RNA template is first converted into a cDNA using a reverse transcriptase. The cDNA is then used as a template for exponential amplification using PCR.

2.4.2.2.1. cDNA synthesis

RNA was reverse transcribed in duplicate using SuperScript® VILO cDNA synthesis kit and master mix to make cDNA. The reaction mixture includes 2 µL of 5x VILO buffer (containing random primers, $MgCl_2$ and dNTPs), 1 µL of 10x SuperScript® III RT Enzyme Mix (containing SuperScript® III RT, RNase OUT Recombinant Ribonuclease Inhibitor and a proprietary helper protein), 3µL of RNA (at 100 ng/µL) and 4 µL of DEPC-treated water. Two negative controls, without reverse transcriptase and without RNA template, were included to evaluate for the presence of contamination with DNA and contamination with RNA or cDNA, respectively. The final reaction mixture was incubated in the PTC-100 or the PTC-200 Peltier Thermal Cycler under the following conditions: 25°C for 10 minutes, 42°C for 60 minutes, followed by 85°C for 5 minutes. The resultant cDNA sample was diluted with DEPC-treated water to a concentration of 1.5 ng/µL and stored at -80°C until PCR can be performed.

2.4.2.2.2. RT-qPCR preparation and analysis

Primers were designed with Primer3 (version 0.4.0) software, using reference sequences obtained from the Ensembl Genome Browser. The quality and specificity of each set of primers were then assessed using NetPrimer, NCBI

Primer-BLAST and OligoEvaluator DNA calculator, to avoid the presence of dimers, cross-dimers, primer dimer, hairpins and secondary structures. Specific RT-qPCR primer sequences and their optimal reaction conditions are described in Chapter 5.

The RT-qPCR mixture consisted of 5 µL of Express SYBR® GreenER qPCR SuperMix Universal, 0.15 µL of forward primer, 0.23 µL of reverse primer and 4 µL of cDNA, made up to a final volume of 10 µL per reaction with DEPC-treated water. Two negative controls (ie. no RT control and no RNA template control) were used to verify the absence of contaminations in reactions, as described on the previous section. RT-qPCR was carried out in a Mx3000P qPCR System (Agilent Technologies, Santa Clara, CA, USA). Thermal cycling was performed at 95°C for 2 minutes, followed by 40 cycles of 95°C for 5 seconds and primer specific annealing temperature (Ta, °C) for 20 seconds, and a final incubation of 95°C for 1 minute, primer specific Ta for 30 seconds, followed by 95°C for 30 seconds. Data was analysed using MxPro qPCR software version 2.0 (Stratagene, La Jolla, CA, USA). Two reference genes were used to calculate the normalisation factor by geNorm version 3.4 algorithms. The relative amount of each gene-of-interest expression was normalised to the reference genes expression. Microsoft® Excel® version 14.0.1 software was used for delta-delta Ct analysis. Statistical analysis was performed using the Prism software package (GraphPad Software Inc., La Jolla, CA, USA).

2.4.3. Whole Exome Sequencing

Whole exome sequencing is an efficient strategy used to selectively enrich and sequence the protein-coding regions of the genome. As previously described in our group (Bagnall et al., 2014), the steps involved are detailed as follows.

2.4.3.1. Exome sequencing library construction and sequencing

Exome sequencing (library construction, capture and sequencing) was carried out at the Macrogen Facility, South Korea. Briefly, approximately 5 µg of genomic DNA with a concentration of >100ng/µL was prepared for each sample and sent for sequencing. After passing the initial quality control, the genomic DNA was fragmented by nebulization to achieve a mean size of ~200bp. The fragmented DNA ends were repaired by way of 5' phosphorylation using the enzyme Klenow polymerase. Adenine bases were added to the 3' end of the phosphorylated fragment and ligated to Illumina paired-end adapters that have a T-base overhang at their 3'ends. Following ligation, the adapter-ligated products were assessed for size distribution on the Agilent Bioanalyzer and then PCR amplified. The amplified DNA library was subsequently hybridised and enriched using the Illumina TruSeq Exome Enrichment protocol, and the exome selected using streptavidin-coated magnetic beads. The exome-enriched library was then eluted from the beads and PCR amplified. Appropriate amount of library were afterwards loaded onto the Illumina flowcell and following cluster generation, the captured library was sequenced using the Illumina HiSeq2000 Sequencer. This yielded the raw exome data for processing within the exome bioinformatics pipeline, which has been compiled in the

Molecular Cardiology Laboratory, Centenary Institute, by Dr. Richard Bagnall, as described in the following section.

2.4.3.2. Exome sequencing bioinformatics and variant analysis

Sequence alignment and variant calling was performed against the reference human genome (GRCh37/hg19). The raw 101 bp sequencing data were aligned using Burrows-Wheeler Alignment Tool (BWA, version 0.7.4) alignment program. The software package SAMtools were then used to convert and merged the aligned sequence reads to sorted and indexed BAM files with reference to their chromosome position. Duplicate reads were removed using Picard tools version 1.81. These BAM files were then analysed using a sequence variant calling software, called the Genome Analysis Toolkit (GATK) program (version 2.7.2), which recalibrated base quality scores, called and filtered variants, and then compiled all gene variants from each individual sample into a single variant call format (VCF) file. Insertions and deletions (Indels) were identified based on the reads mapped with BWA, with its ability to align reads that contain gaps to the reference genome. Functional annotations of the genetic variants were performed using the SeattleSeq Annotation tool version 8.07, with respect to locations (exonic, intronic, splice site, 5' UTR, 3' UTR, upstream, downstream, or intergenic) and exonic functions (non-synonymous, synonymous, stop, frameshift insertion or deletion). Allele frequencies were generated for known variants in the 1000 Genomes Project, dbSNP (build 134), and the National Heart, Lung, and Blood Institute (NHLBI) Exome Variant Server (EVS) (6,503 sequenced exome to date). To predict

deleterious effects of non-synonymous variants, functional annotation algorithms (e.g. SIFT and PolyPhen2), GERP score, which identified evolutionarily constrained elements in multiple sequence alignments across species, and Gratham score, which categorised codon replacement into classes of increasing chemical dissimilarity, were utilised. To eliminate common variants and sequencing artifacts, the sample data were also filtered to exclude variants present in the in-house exome datasets from unrelated individuals with normal trileaflet aortic valve. A visualisation tool, Integrative Genome Viewer (IGV), was used to examine aligned sequence reads and genome annotation files, as well as to assess coverage and the overall quality of the aligned sequence reads.

With the principal assumption that BAV has an autosomal dominant pattern of inheritance, where a single mutation is both sufficient and necessary to cause disease, the variant will affect a protein sequence and that the causative mutation will occur at a frequency of no more than 1%, the following criteria are used to prioritise variants identified by exome sequencing: (i) the presence of variants in all exome sequencing samples from affected members within the studied family; (ii) the novelty of the variants by excluding those found in the in-house exome dataset of unrelated individuals with different phenotype and those with minor allele frequency (MAF) of >1% in the 1000Genome Project, the dbSNP, and the EVS database; (iii) the putative pathogenic effect of the gene variants by excluding synonymous, intronic or intergenic variants and by including those with non-synonymous missense, nonsense, splice-site gain- or loss-of-function variants and frame-shift insertion or deletion mutations; (iv) a positive GERP conservation score; (v) the presence of cardiac expression of

the genes which harboured the variants. The variants that fulfilled these criteria were then considered for downstream validation analysis.

2.4.3.3. Validation of variants identified by exome sequencing

Following identification of putative disease-causing variants by exome sequencing, confirmation on the presence of each variant in the exome-sequenced family members and assessment of the pattern of variant segregation in other family members (affected and non-affected relatives) were performed using standard Sanger sequencing of PCR amplicons from genomic DNA, in similar manner as described in Chapter 2.4.1.2 to 2.4.1.5.

2.4.4. RNA Sequencing

Similar to exome sequencing, RNA sequencing uses massive parallel sequencing technologies to reveal a comprehensive snapshot of all messenger RNA (the "transcriptome") present in a specific tissue type in a given moment in time. Data obtained from RNA sequencing provides information on both gene expression and genetic polymorphisms.

2.4.4.1. RNA sequencing library construction and sequencing

RNA sequencing (library construction, capture and sequencing) was carried out at the BGI Facility, Hong Kong. RNA sequencing library was prepared using the Illumina TruSeq RNA Sample Preparation Kit (Illumina, San Diego, CA, USA) from 5μg of total RNA, with a RNA integrity number (RIN) ≥ 7, according to the manufacturer's protocol. Briefly, following DNAse I treatment, magnetic beads

with Oligo (dT) are used to isolate mRNA from the total RNA. After mixing with the fragmentation buffer, the mRNA is fragmented into short fragments (~100bp in size), which are then used as templates to synthesise cDNA. The short cDNA fragments are purified, resolved with EB buffer for end reparation and single nucleotide A (adenine) addition, and subsequently connected with adapters. After agarose gel electrophoresis, the suitable fragments are selected as templates for PCR amplification and later sequenced on a HiSeq2000 (Illumina). The resultant raw RNA sequencing data (in Illumina FASTQ format) are then processed within the in-house bioinformatics pipeline, which has been compiled in the Molecular Cardiology Laboratory, Centenary Institute, by Dr. Richard Bagnall.

2.4.4.2. RNA sequencing bioinformatics pipeline and analysis

A number of publically available packages, including Bowtie and TopHat, were used to map the raw sequence reads data to the reference genome. Initially, the FASTQ files were aligned to the human reference sequence (NCBI GRCh37/hg19) using Bowtie. However, as Bowtie cannot align reads that span introns, TopHat2 version 2.0.6 (Kim et al., 2013) with a transcriptome-index was used to guide mapping of splice junction-spanning reads. Aligned reads in BAM format were then annotated against the protein-coding mRNA regions and analysed using SeqMonk version 0.24.1 platform (Babraham Bioinformatics, Cambridge UK), where visualisation of mapped read, data quantification (using corrected $\log_2$ transformed Reads Per Million Values of non-strand specific, unmerged isoform) and percentile normalisation were performed. Differentially

expressed genes (DEGs) were identified on the normalised quantification data using an intensity difference analysis method.(Brien et al., 2013) A gene was classified as up- or downregulated using a cutoff value of more or less than 1.5-fold expression difference, respectively, between BAV versus TAV, with an adjusted p-value <0.05, following post-hoc Bonferroni correction. A small number of unannotated genes with uncharacterised protein were excluded from subsequent analysis.

Ingenuity Pathway Analysis (IPA) and PANTHER online tools were used to assess biological networks and pathways connected to the DEGs. Gene Ontology (GO)-based enrichment and KEGG pathway analysis of DEGs were performed against a background list of global aortic valve protein-coding mRNAs expression, using the Database for Annotation, Visualisation and Integrated Discovery (DAVID) bioinformatics resources (version 6.7; NIH). Enrichment score of ≥ 1.3 and Benjamini-Hochberg corrected p-value <0.05 were used as a cut-off for significance. SeqMonk was also utilised to perform hierarchical clustering and heat map analysis of DEGs.

2.4.4.3. Validation of differential gene expression observed from RNA-sequencing data

Validation of RNA sequencing data was performed on a subset of DEGs-of-interest. This was performed on total aortic valve RNA from unrelated individuals by RT-qPCR, as described in Chapter 2.4.2.2.

2.5. CMR ASSESSMENT OF THE THORACIC AORTA IN BAV DISEASE

CMR imaging was performed using 1.5 Tesla Phillips Achieva MR scanner (Phillips Medical System, Best, Netherland). The study was performed without gadolinium contrast administration and consisted of 3 imaging stages, namely the resting phase (baseline), exercise (Stage 1 and Stage 2) and recovery phase. Exercise was performed using a pneumatic MRI-compatible pedal ergometer, which was attached at the foot of the MRI table. A free-breathing real-time phase-contrast CMR imaging was employed with sufficient spatiotemporal resolution to acquire beat-to-beat hemodynamic information to characterize transient blood flow phenomenon and to study aortic wall pulsatility associated with each heartbeat, at rest and during exercise. The study was performed in approximately 50-60 minutes for each patient. The specifics of the study protocol will be discussed in greater details in Chapter 6.2.

CHAPTER 3: CANDIDATE GENE INVESTIGATION OF SPORADIC BAV

3.1. INTRODUCTION

Positive family history for aortic valve disease has been reported in up to 14% of patients with BAV, supporting the need for routine echocardiographic screening of first-degree relatives (Panayotova et al., 2013). Indeed, familial clustering and genetic studies have established that BAV is a highly heritable trait and it likely exhibits genetic heterogeneity with variable modes of inheritance (Huntington et al., 1997, Cripe et al., 2004).

To date, only mutations in the *NOTCH1* gene at chromosome 9q34.3 have been linked to the development and progression of BAV in a limited number of familial cases and in less than 5% of sporadic cases (Garg et al., 2005, McKellar et al., 2007, Mohamed et al., 2006). However, the molecular mechanisms by which *NOTCH1* missense mutations, or frameshift mutations leading to haploinsufficiency result in BAV development in humans remain to be elucidated. In mice, deficiency of endothelial nitric oxide synthase (*Nos3*) and *Nkx2-5* haploinsufficiency are associated with a higher incidence of BAV (Biben et al., 2000, Lee et al., 2000). Again, the mechanisms by which *Nos3* and *Nkx2-5* mutations contribute to BAV formation in these mice are presently not well understood. Nevertheless, neither of these genes have shown an association with human cases of BAV (Lincoln and Yutzey, 2011, Majumdar et al., 2006, Schott et al., 1998).

A homeobox-containing transcription factor, *NKX2-5* is an attractive candidate gene for BAV, given its important role in cardiac development in many

organisms, including the zebrafish, frog, chick, mouse and human (Srivastava and Olson, 2000, Harvey, 1996). Heterozygote *NKX2-5* mutations are associated with a diverse range of cardiac malformations in humans (Figure 3.1), including atrial septal defects with or without atrioventricular conduction block, ventricular septal defects, Tetralogy of Fallot, double-outlet right ventricle, tricuspid valve abnormalities, and subvalvular aortic stenosis (Benson, 2010, Schott et al., 1998). This suggests an essential role of *NKX2-5* in atrial, ventricular, and conotruncal septation, maintenance of atrioventricular conduction, and heart valve formation (Benson, 2010). Located on chromosome 5q34, *NKX2-5* is also known to modulate the extracellular matrix of the aorta during embryonic development (Ponticos et al., 2004). This is an interesting observation given the frequent presence of aortic abnormalities in patients with BAV, which is seen in over 50% of cases (Fedak et al., 2002). Whilst a previous study has failed to demonstrate an association between BAV and *NKX2-5* mutation, the study was limited by a small population size (n=19) (Majumdar et al., 2006). Therefore, mutations in *NKX2-5* cannot yet be excluded as a possible cause of BAV based on this study alone and further evaluation in a larger cohort is warranted.

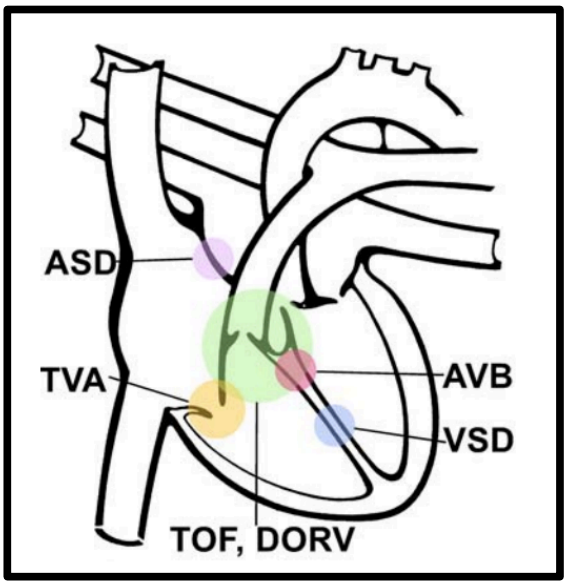

Figure 3. 1. Diverse cardiac malformations associated with *NKX2-5* mutations.
Adapted from (Benson, 2010). ASD, atrial septal defect; AVB, atrioventricular block; DORV, double-outlet right ventricle; TOF, Tetralogy of Fallot; TVA, tricuspid valve abnormality; VSD, ventricular septal defect.

Recently, *GATA5* was reported to have an essential role in cardiac morphogenesis and aortic valve development (Laforest et al., 2011, Laforest and Nemer, 2011), and targeted deletion of *Gata5* in mice leads to partially penetrant BAV with right and noncoronary leaflet fusion morphology (Laforest et al., 2011). Located at chromosome locus 20q13.33, *GATA5* is a transcription factor that belongs to a sub-group of the GATA family of zinc finger proteins, which, together with *GATA4* and *GATA6*, is expressed in an overlapping but distinct spatial and temporal pattern in the developing heart (Charron and Nemer, 1999, Peterkin et al., 2005). The GATA-4, -5 and -6 proteins share 2 evolutionarily conserved N-terminal transcriptional activation domains and 2 C-terminal DNA binding and nuclear localisation zinc-finger domains (Morrisey et al., 1997). Unlike *GATA4* and *GATA6* however, the expression of *GATA5* is restricted to endocardial cells and endocardial cushions of the outflow tract and

atrioventricular canal during cardiogenesis (Laforest and Nemer, 2011) and is not maintained in adult cardiovascular structures (Molkentin, 2000). Studies in developing murine heart have implicated the important function of GATA4/5/6 subfamily, which acts cooperatively, in the regulation of endocardial cushion development and/or outflow tract morphogenesis (Charron and Nemer, 1999, Peterkin et al., 2005, Laforest and Nemer, 2011). Of note, aortic valve hypertrophy and stenosis were observed amongst the surviving adult mice with *Gata4/Gata5* compound mutations (Laforest and Nemer, 2011). *Gata5/Gata6* compound heterozygous mice die during the embryonic or perinatal period due to the development of highly penetrant double-outlet right ventricle, suggesting disrupted valvulogenesis in $Gata5^{+/-}Gata6^{+/-}$ embryos (Laforest and Nemer, 2011). Overall, these observations provide support for the essential role of *GATA5* in the aortic valve and outflow tract morphogenesis in mice. Nevertheless, the role of *GATA5* in human cases of BAV is not yet clear.

Therefore, this chapter describes the study that sought to investigate the relationship between *Nkx2-5* and *GATA5* mutations and the development of non-syndromic BAV with its associated aortopathy in 100 prospectively recruited BAV patients.

3.2. METHODS

3.2.1. Study populations

The study used the BAV cohort and the healthy control population described in Chapter 2.3. Clinical evaluation of the BAV cohort included family history, physical examination, and 2D-echocardiography. In each case, BAV was confirmed by imaging and/or during aortic valve replacement surgery. BAV morphology was classified as anatomically bicuspid when there were 2 approximately symmetrical leaflets without a raphe; functionally bicuspid when the 2 leaflets were unequal in size with the larger leaflet having a central raphe due to commissural fusion; or indeterminate when the morphology was unrecognisable, e.g. due to heavy calcification. Following informed consent, 20 mls of peripheral blood and clinical information were collected from each patient. The study protocol was approved by the Sydney South West Area Health Service ethics committee.

3.2.2. Genetic analysis

BAV cohort was screened for the presence of disease-causing mutations in the 2 candidate genes of interest, namely *GATA5* and *Nkx2-5,* by means of direct Sanger sequencing. Upon identification, the putative disease-causing variants were then checked for their presence amongst the control population, using a similar method. Genomic DNA was obtained from peripheral blood leukocytes, using method described in Chapter 2.4.1.1.

3.2.2.1. Primers design, PCR optimisation and troubleshooting

Primers flanking the protein coding exons and splice signal sequences of the *GATA5* and *Nkx2-5* genes were designed using the on-line tool Primer3Plus©, to produce a product size of approximately 423-850bp, using custom settings (Appendix I, Table I-1). Each primer pair was tested across an annealing temperature gradient, ranging from 50°C to 65°C, in standard PCR conditions (Chapter 2.4.1.2) to determine the temperature at which the primers efficiently and specifically amplify the target sequence (Figure 3.2). PCR products were visualised using standard gel electrophoresis to determine the optimum primer annealing temperature, indicated by a clear, bright, single band of the correct product size. For non-specific primer binding, 10% DMSO was added to obtain specific primer binding. If this troubleshooting method failed to produce specific priming, primers for the region were redesigned and the new set of primers re-tested for its optimal annealing temperature. The optimal condition and PCR annealing temperature to amplify the specific target sequences for different primer pairs used in this study are listed in Appendix I, Table I-1.

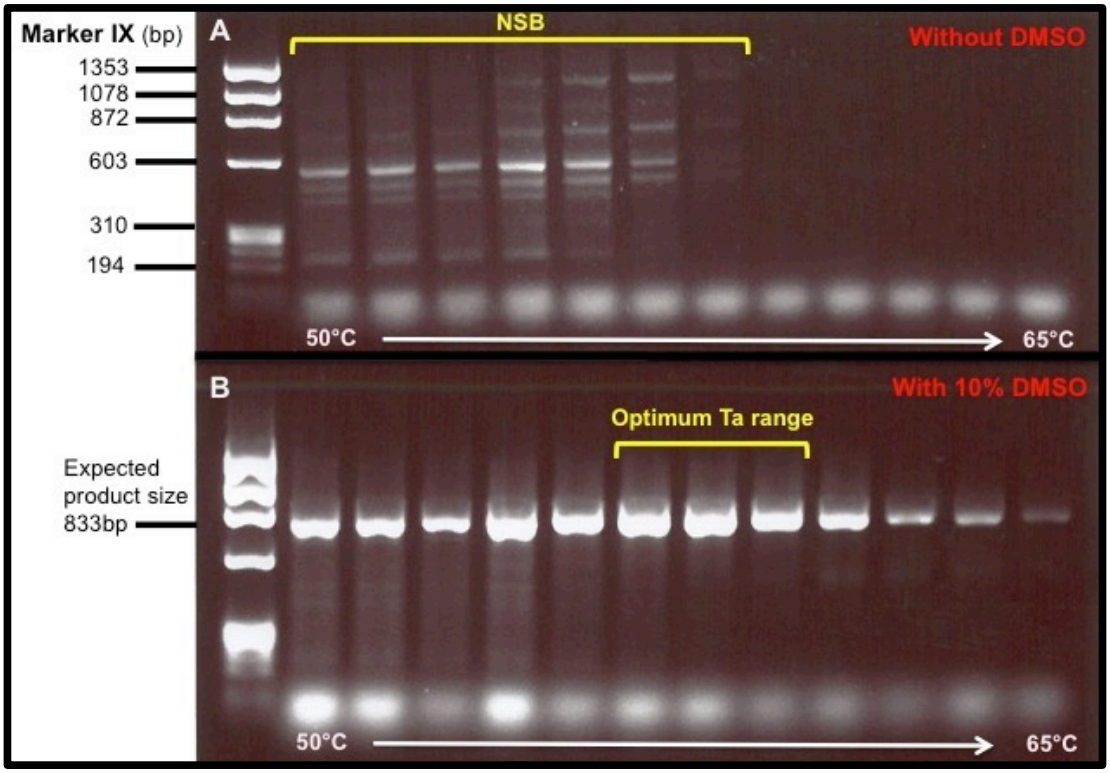

Figure 3. 2. Example of PCR optimisation, using primers designed for *GATA5* exon 1 to produce an 833bp PCR product size.

A) Primer temperature optimisation using a temperature gradient ranging from 50°C to 65°C, in standard PCR conditions. This panel showed an example of an unsuccessful temperature gradient optimisation where non-specific binding (NSB) appeared at lower temperatures and no band appeared at the expected product size. B) The addition of 10% DMSO to the PCR reaction resulted in a more specific binding, producing a single product at the expected PCR product size. In this case, the optimum annealing temperature (Ta) range was regarded to be between 56.4°C to 61°C.

3.2.2.2. Sanger sequencing and variant analyses

The two and six exons of the coding region of *NKX2-5* and *GATA5*, respectively, were sequenced via direct Sanger Sequencing (Chapters 2.4.1.2 to 2.4.1.5). Briefly, PCR products were amplified using genomic DNAs of the study cohort on a DNA Engine Peltier Thermal Cycler. Following PCR product

purification process, they were DNA sequenced at the Macrogen Facility, South Korea, and analysed for sequence variants using Sequencher version 4.8 (Gene Codes Corp, Ann Arbor, MI, USA). Upon identification, rare non-synonymous variants were genotyped in our Control population, utilising the same method as described for the study cohort. Reference populations from the National Heart, Lung, and Blood Institute Exome Variant Server (NHLBI EVS) and 1000 Genomes project were used as additional controls.

The following criteria were investigated for each non-synonymous variant to determine pathogenicity: (i) frequency of the variant in control alleles, in the NHLBI EVS and in the 1000 Genomes project; (ii) conservation level of the amino acid residue amongst protein orthologues and paralogues; (iii) *in-silico* prediction of pathogenicity using the on-line resource SIFT and/or PolyPhen2, which predict the possible impact of an amino acid substitution on the structure and function of a human protein on the basis of three dimensional structure and multiple alignment of homologous sequences.

3.3. RESULTS

3.3.1. Study population characteristics

Table 3.1 describes the clinical and valvular characteristics of the 100 unrelated patients with BAV who participated in the *GATA5* and *Nkx2-5* candidate genes screening. The group comprised 77% males with a mean age at diagnosis of 29 ± 22 years (range 0-63 years). BAV morphology was functionally bicuspid in 53%, anatomically bicuspid in 17% and indeterminate in 30%. Of the functionally bicuspid group, 79.2% (n=42), 18.9% (n=10) and 1.9% (n=1) had non-separation of left and right (L-R), right and noncoronary (R-N), and left and noncoronary (L-N) leaflets, respectively. BAV was present in a first-degree relative in 13% of the cohort. Coexistent cardiovascular anomalies occurred in 21%, and this was predominantly coarctation of the aorta.

Table 3. 1. Patient clinical and valvular characteristics.

	Anatomically bicuspid	Functionally bicuspid	Indeterminate morphology	Total
n	17	53	30	100
Male gender (%)	12 (70.6)	41 (77.4)	24 (80.0)	77 (77)
Caucasian background (%)	14 (82.4)	45 (84.9)	26 (86.7)	85 (85)
Mean age at diagnosis	32 ± 18	31 ± 22	25 ± 24	29 ± 22
Abnormal valve function* (%)	10 (58.8)	28 (52.8)	13 (43.3)	51 (51)
Concomitant aortopathy[#] (%)	12 (70.5)	32 (60.4)	15 (50.0)	59 (59)
Concurrent CHD^ (%)	1 (5.9)	9 (17)	11 (36.7)	21 (21)
Positive family history (%)	2 (11.8)	5 (9.4)	6 (20.0)	13 (13)

*Aortic regurgitation of at least 2/4 in severity and/or aortic stenosis of at least moderate severity (defined as mean aortic gradient of ≥ 30mmHg and/or peak aortic velocity of ≥ 3.0 m/sec).

[#]Aortic dilatation ≥ 40 mm, affecting any part of the aorta from sinus of Valsalva to proximal descending aorta.

^Anatomically bicuspid group, 1 patient with coarctation of the aorta (CoA); Functionally bicuspid group, 5 patients with CoA, 1 patient with CoA and mild tricuspid valve dysplasia, 1 with supra-aortic ridge and supravalvular aortic stenosis, 1 with anomalous left coronary artery, 1 with Shone complex (including CoA) and inferior wall left ventricular non compaction; Indeterminate group, 6 patients with CoA, 1 with a small ventricular septal defect (VSD), 1 with aberrant right subclavian artery origin, 1 with a small patent foramen ovale, 1 with CoA and primum atrial septal defect and 1 with CoA and muscular VSD.

3.3.2. *GATA5* screening

PCR amplification and Sanger sequencing for the *GATA5* gene screening was successfully performed on the DNA of the entire study cohort (Figure 3.3).

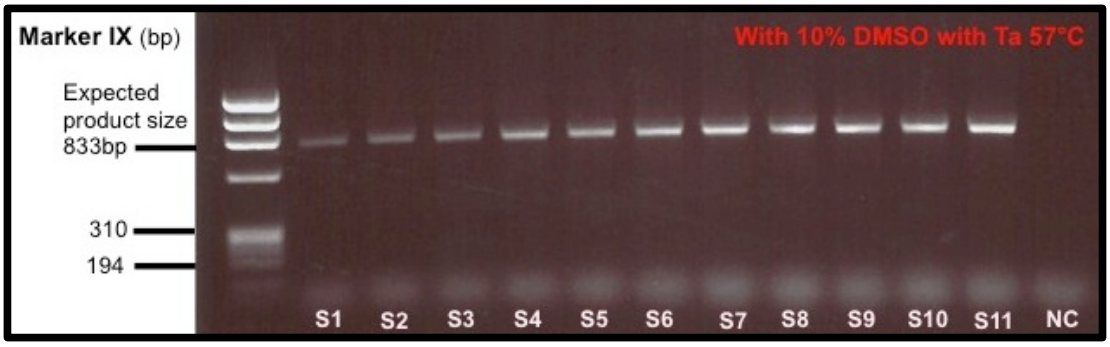

Figure 3. 3. Example of a successful PCR amplification.
Gel electrophoresis of *GATA5* exon 1 PCR product in 11 out of the 100 study cohorts (S1-S11) showed the presence of a single bright and clean band at the expected product size (833bp), indicating a successful PCR amplification. PCR reaction was performed using 10% DMSO at 57°C annealing temperature (Ta). NC indicates negative control (no DNA template).

The findings from the genetic analysis of *GATA5* are summarised in Table 3.2. Sequencing of all 6 coding exons and splice signal sequences of *GATA5* in the study cohort revealed 5 non-synonymous, 4 synonymous and 2 intronic variants. Of note, 4 non-synonymous variants, Gln3Arg, Ser19Trp, Tyr142His and Gly166Ser, were identified in one patient each (MAF = 0.005), and all were located in the transcriptional activator domains encoded by exon 1 of *GATA5* (Figure 3.4.A, 3.4.C). The clinical characteristics of the individuals harbouring these rare non-synonymous *GATA5* variants are summarised in Table 3.3. These 4 variants were all found in male patients. Furthermore, genotyping

revealed that the c424T>C variation (rs111554140) causing the Tyr142His replacement and the c496G>A variation (rs141950357) causing the Gly166Ser were absent in 320 control alleles (Table 3.2). The c8A>G nucleotide variant (rs113068438) causing the Gln3Arg replacement, and the novel c56C>G variant causing the Ser19Trp replacement, were present in 2 out of 320 control alleles (MAF = 0.006).

Table 3. 2. *GATA5* DNA variations identified in the patient cohort.

Reference SNP ID	Exon	Nucleotide change	Amino acid change	MAF				
				BAV (n=100)	Controls (n=160)	dbSNP European Control	1k Genomes Project	EVS European population
rs113068438	1	c8A>G	Gln3Arg	0.005	0.00625	n/a	n/a	0.0047
-	1	c56C>G	Ser19Trp	0.005	0.00625	n/a	n/a	0.001
rs6142775	1	c199A>C	Thr67Pro	0.18	-	n/a	0.129	0.098
rs111554140	1	c424T>C	Tyr142His	0.005	0	n/a	n/a	0.00045
rs141950357	1	c496G>A	Gly166Ser	0.005	0	n/a	n/a	0.00016
rs41305803	2	c609C>T	Asp203Asp	0.48		0.417-0.458	0.418	0.438
rs78235297	-	IVS 2-27C>T	-	0.025		n/a	0.059	-
rs6587239	4	c852G>A	Lys284Lys	0.46		0.466-0.478	0.488	0.481
rs6061244	-	IVS 4-46C>G	-	0.394		0.408	0.357	-
rs6061243	5	c981G>C	Ser327Ser	0.455		0.465-0.492	0.479	0.486
rs6061550	6	c1128A>G	Pro376Pro	0.445		0.467	0.452	0.488

Rare non-synonymous variants are shaded grey. EVS, the National Heart, Lung, and Blood Institute Exome Variant Server; n/a, not available.

Table 3. 3. Clinical characteristics of the individuals with the rare non-synonymous *GATA5* variants.

Variants identified	Gender	Genetic background	Current age (years)	Age at diagnosis (years)	BAV morphology	Aortic valve function	Associated aortopathy	Family History of BAV
Gln3Arg	Male	Caucasian	62	56	Indeterminate	Mild AS	Yes	No
Ser19Trp	Male	Caucasian	28	18	Indeterminate	Trivial AR	No	No
Tyr142His	Male	Caucasian	58	15	L-R	Severe AS	Yes	No
Gly166Ser	Male	Asian	27	3	L-R	Normal	Yes	Yes

L-R, functional BAV due to left and right coronary cusps non-separation; AS, aortic stenosis; AR, aortic regurgitation.

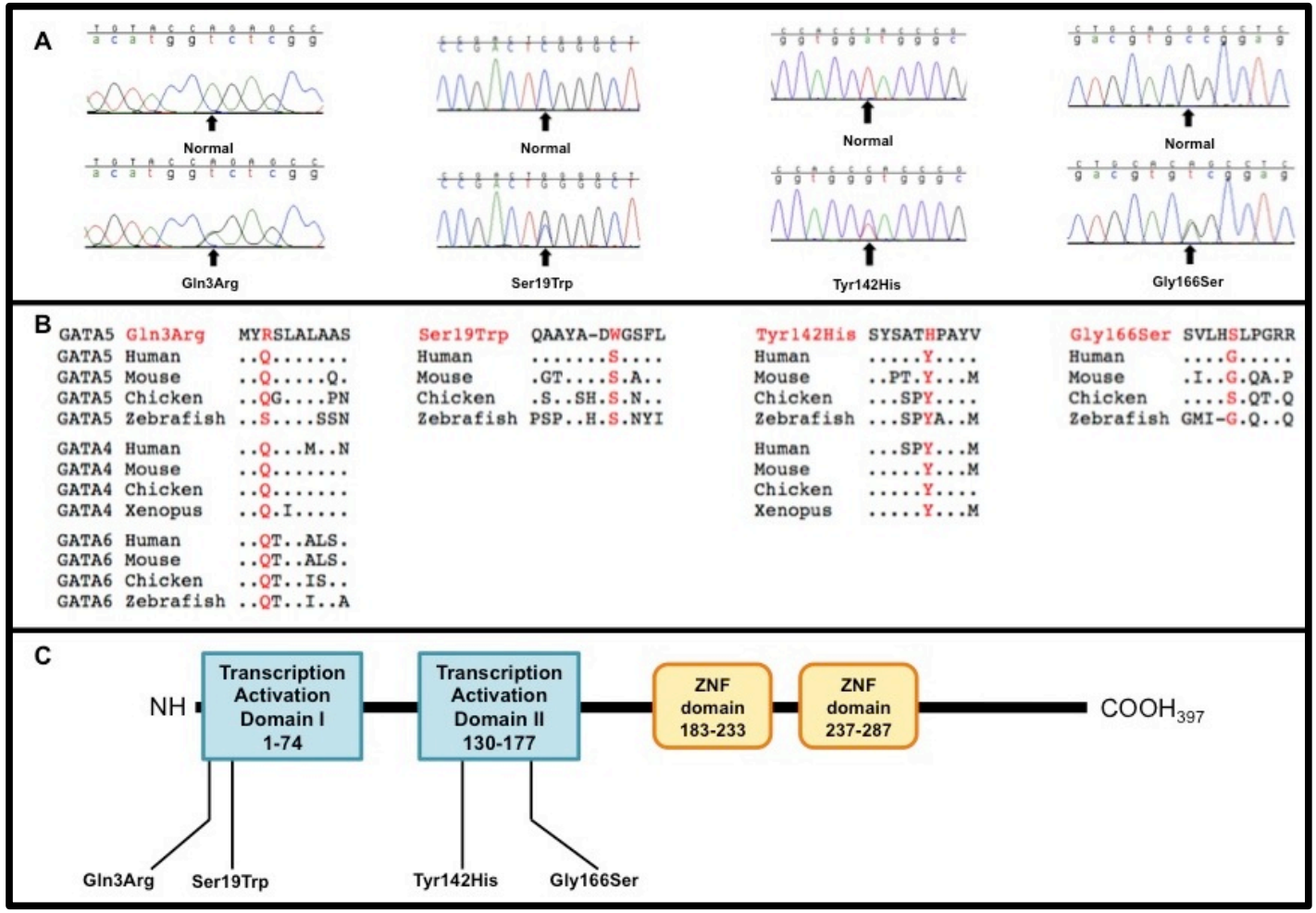

Figure 3. 4. Rare non-synonymous variations identified in *GATA5*.

A) DNA sequence electropherogram of rare non-synonymous variants. B) GATA protein conservation. C) Location of domains and non-synonymous variations in GATA5 protein.

3.3.3. *Nkx2-5* screening

PCR amplification and Sanger sequencing of the *Nkx2-5* gene screening was also successfully performed on the DNA of the entire study cohort. Table 3.4 summarised the result of the *Nkx2-5* gene screening.

Sequencing of the 2 coding exons and splice signal sequences of *Nkx2-5* in the study cohort revealed 4 synonymous and 2 novel non-synonymous (missense) variants. The missense variants, namely c169G>T and c727G>T substitutions, resulted in Ala57Ser and Val243Leu replacements, respectively, and they were identified in one male patient each (MAF=0.005). These variants were located outside the homeobox-containing domain encoded by exon 2 of *NKX2-5* (Figure 3.5A, 3.5C).

Table 3. 4. *Nkx2-5* DNA variations identified in patient cohort.

Reference SNP ID	Exon	Nucleotide change	Amino acid change	MAF			
				BAV (n=100)	dbSNP European control	1000 Genomes Project	EVS
rs2277923	1	c63A>G	Glu21Glu	0.302	0.489	0.489	0.281
-	1	c169G>T	Ala57Ser	0.005	n/a	n/a	n/a
rs72554028	2	c543G>A	Gln181Gln	0.0099	0.0055	0.006	0.008
rs3729753	2	c606G>C	Leu202Leu	0.005	0.02	0.021	0.0001
-	2	c727G>T	Val243Leu	0.005	n/a	n/a	n/a
rs77612903	2	c861C>T	Ala287Ala	0.005	0.008	0.008	0.0002

Non-synonymous variant was shaded in grey. n/a, not available

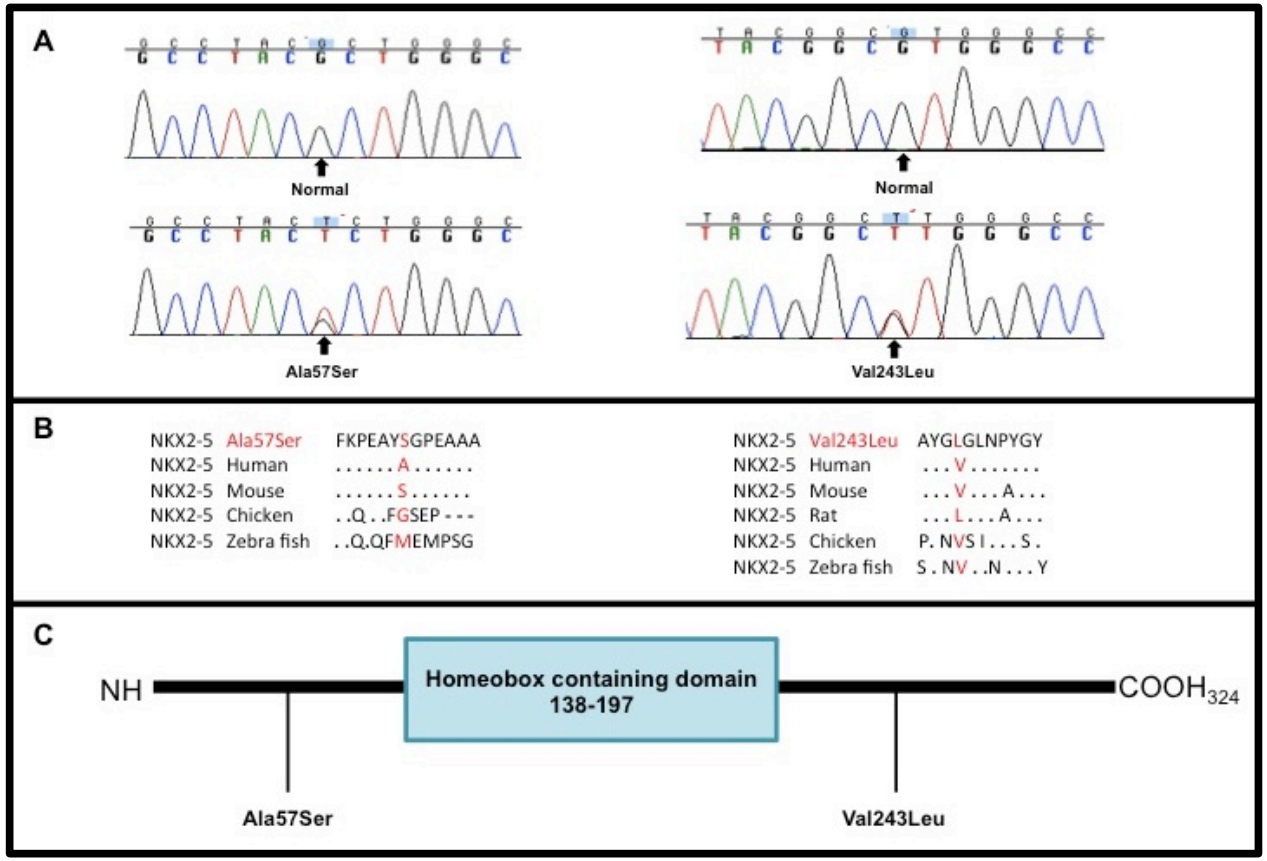

Figure 3. 5. Novel non-synonymous variations identified in *NKX2-5.*

A) DNA sequence electropherogram of novel non-synonymous variants. B) *NKX2-5* protein conservation. C) Location of homeobox containing domain in NKX2-5 protein.

3.4. DISCUSSION

The present study investigated, for the first time, the relationship between *GATA5* gene variations and BAV disease in 100 unrelated, non-syndromic, sporadic and familial cases of BAV, with or without its associated aortopathy. The study also investigated the correlation between *Nkx2-5* gene variations and BAV disease within the same patient cohort. Whilst screening of *Nkx2-5* failed to identify disease-causing mutations in the study cohort, analysis of the *GATA5* gene screening identified the presence of 4 rare non-synonymous variants located in the transcriptional activator domains I and II of *GATA5*, of which 3 affected highly evolutionarily conserved amino acid residues. These non-synonymous variants may alter the transcriptional activity of *GATA5*, and therefore may be important in the pathogenesis of BAV disease in humans.

Specifically, the *GATA5* Gln3Arg replacement was found in a Caucasian male patient aged 62 years with no family history of BAV, who was diagnosed with the condition at the age of 56 years, following detection of cardiac murmur during routine clinical screening. He had indeterminate BAV morphology that was mildly stenotic and associated with mild ascending aortic dilatation. The Gln3Arg replacement is present in 23 of 4894 EVS alleles and 2 of 320 control alleles. The Gln3 residue occurs within a highly conserved subdomain of transcriptional activation domain I of *GATA5* gene, and is highly conserved amongst the *GATA4/5/6* subfamily of vertebrates (Figure 3.4.B). Functional importance of the Gln3 residue, at least for *GATA4*, was demonstrated by its replacement with arginine in a construct containing *GATA4* activation domain I,

which resulted in an 80% reduction in transcriptional activity of a reporter gene construct, supporting its pathogenic role (Morrisey et al., 1997). Further, the Gln3Arg variant is predicted to be damaging by in-silico analysis using both PolyPhen2 (score 0.891) and SIFT algorithms (score 0.001).

The *GATA5* Tyr142His replacement was found in a Caucasian male aged 58 years with sporadic BAV that was due to non-separation of the left and right coronary cusps. He had an aortic valve replacement at age 28 years for severe aortic stenosis and, subsequently, ascending aortic replacement at age 58 years for progressive ascending aortic aneurysm. The Tyr142His replacement is extremely rare, being present in only 3 out of 6596 EVS alleles (MAF 0.00045) and is predicted to be 'possibly damaging' by PolyPhen2, with a Grantham score of 83. The Tyr142 residue is located in a conserved subdomain of transcription activation domain II and is highly conserved between *GATA4* and *GATA5* of vertebrates (Figure 3.4.B, 3.4.C). Replacement of the equivalent tyrosine residue in *GATA4* with alanine (Tyr162Ala), in a construct containing *GATA4* activation domain II, resulted in a 60% reduction in transcriptional activity of a reporter gene construct (Morrisey et al., 1997). Together, the demonstration of a functional importance of Gln3 and Tyr162 of *GATA4* strongly suggests that the rare non-synonymous variations at equivalent evolutionarily conserved positions in *GATA5* (Gln3 and Tyr142) likely impact on transcriptional activation of *GATA5* target regions and may well contribute to BAV development.

The novel *GATA5* Ser19Trp variation causing the replacement of serine at residue 19 for tryptophan (Grantham Score 144) was found in a Caucasian male patient aged 28 years without a family history of BAV or other congenital heart disease and he had an indeterminate BAV morphology with only trivial regurgitation, and without associated aortopathy. The Ser19 residue is conserved amongst vertebrate *GATA5* proteins, was present in 2 out of 320 control alleles and 5 out of 4934 EVS alleles, and is predicted to be 'probably damaging' by PolyPhen2.

The *GATA5* Gly166Ser replacement was found in a male patient aged 27 years of South Asian background with a positive family history for BAV and associated aortopathy. He had a functional BAV due to non-separation of the left and right coronary cusps with normal hemodynamics and associated mild to moderate dilatation of his aortic root at 42mm. His 59-year old mother also had BAV with a left and right coronary cusps non-separation morphology, which was associated with mild aortic stenosis and mild to moderate dilatation of her mid ascending aorta of 43mm. Interestingly, she also shared the *GATA5* Gly166Ser variant (Figure 3.6). Unfortunately, no other family members were available for testing at the time when this study was conducted. The Gly166Ser replacement was only present in 1 out of 6332 EVS alleles, however, the equivalent amino acid residue in *Gata5* of chicken is also a serine (Figure 3.4.B).

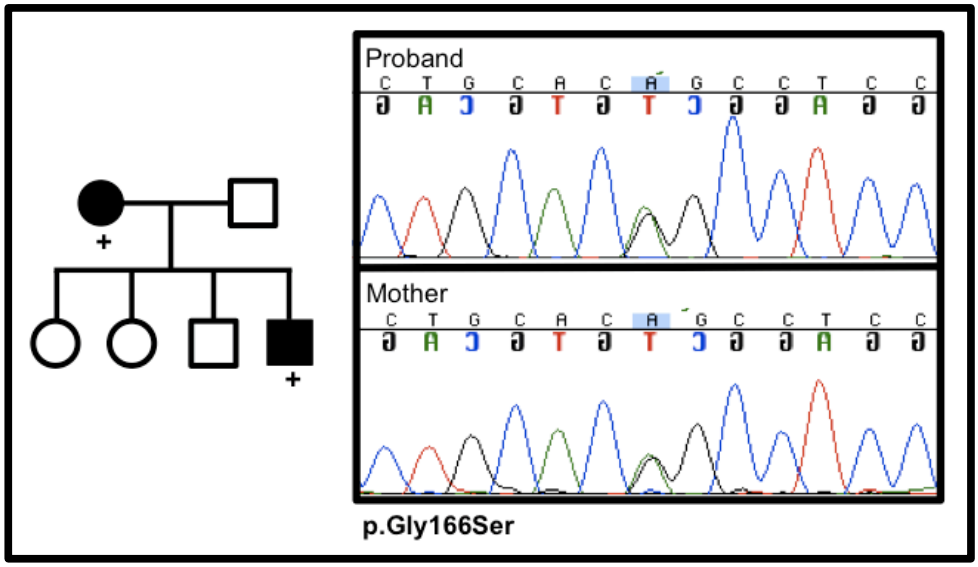

Figure 3. 6. Family pedigree of the individual with *GATA5* Gly166Ser variant with DNA sequence electropherograms showing that the variant was inherited from his affected mother.

Meanwhile, screening of *Nkx2-5* in this patient cohort revealed the presence of 2 novel non-synonymous variants, namely Ala57Ser and Val243Leu. The *Nkx2-5* Ala57Ser variant was present in a 26 years old man, who had murmur detected at birth, and diagnosed with non-familial case of BAV at the age of 1. He subsequently had an aortic valve and ascending aortic replacement at 24 years of age for moderately severe mixed aortic valve disease and a 50mm ascending aortic aneurysm. Inspection of the aortic valve at time of surgery revealed a true (anatomical) BAV with a right to left configuration. The Ala57 residue is conserved amongst human, cattle, rhesus monkey and dog, however the equivalent amino acid residue in *Nkx2-5* of mouse is also a serine (Figure 3.5B). The Ala57Ser variant is predicted to be 'benign' by Polyphen2 and 'tolerated' by SIFT, with a Grantham score of 99.

The *NKX2-5* Val243Leu variation (Grantham score 32) was found in a 54 year old man, who at the age of 42 was diagnosed with a sporadic case of functional BAV, due to fusion of the right and left coronary leaflets, following an investigation of a murmur. He subsequently progressed to develop severe aortic stenosis, requiring an isolated aortic valve replacement at 53 years of age. He was noted to have mild dilatation of his ascending aorta at time of surgery and was placed on a yearly surveillance program post-operatively. The Val243 residue is a moderately conserved amino acid, although interestingly, the equivalent amino acid residue in *Nkx2-5* of rat is also a leucine (Figure 3.5B). The Val243Leu variant is predicted to be 'benign' by Polyphen2 and 'tolerated' by SIFT.

Of note, no other cardiovascular malformation was found in these 2 patients with the novel *Nkx2-5* variants; specifically, there were no septal defects, conduction block or Tetralogy of Fallot. Both of these variants were located outside the homeobox-containing domain of *NKX2-5.* Therefore, the 2 non-synonymous *NKX2-5* variants found in the study are unlikely to be the disease-causing variant in this patient cohort. However, study on *Nkx2-5* heterozygous mutant mice model had shown that the presence of BAV in the *Nkx2-5* haploinsufficient mice was strictly dependent on genetic background, being exclusively found in the C57B1/6 strain (Biben et al., 2000). This suggested the presence of another genetic modifier to influence BAV development. Therefore, it is entirely plausible that *NKX2-5* may still play a role as a modifying factor that can induce BAV development in certain genetically susceptible individuals.

During this candidate gene study, the *NOTCH1* (34 exons, coding a protein of 2,555 amino acids) and *GATA4* genes (6 exons, coding a protein of 442 amino acids) were also screened within a small subgroup of these patients (n=14-15). However, no disease-causing variants were found during the screening process (data not shown).

Overall, there is substantial evidence for a genetic basis to BAV, representing anomalies in cardiac development (Cripe et al., 2004, Hinton and Yutzey, 2011). Yet, the exact mechanisms underlying the pathogenesis of BAV remain unclear. Recently, Laforest et al. reported that targeted deletion of *Gata5* in mice leads to partially penetrant BAV formation, particularly of the R-N morphology, thus implicating *GATA5* in aortic valve formation (Laforest et al., 2011). In contrast to *GATA4* and *GATA6*, which are expressed in cardiac myocytes and other regions of the heart, *GATA5* transcripts in the heart are largely restricted to transient expression during embryogenesis in endocardial cells and endocardial cushions of the outflow tract and atrioventricular canal (Laforest et al., 2011, Laforest and Nemer, 2011). Nevertheless, evidence suggests that *GATA5* and the 2 other cardiac GATA factors interact during endocardial cushion formation and outflow tract remodelling, and together with other families of cofactors, work synergistically to regulate gene expression during cardiac morphogenesis (Laforest and Nemer, 2011, Peterkin et al., 2005, Holtzinger and Evans, 2007). Importantly, *GATA5* regulates several pathways involved in endocardial cell differentiation, including those directed by *Bmp4*, *Tbx20*, and, notably, *NOS3* and *NOTCH1* (Laforest et al., 2011). Of interest, deficiency of *NOS3* and mutation of *NOTCH1* genes have been associated with

BAV development in mice and human, respectively (Garg et al., 2005, Lee et al., 2000, Mohamed et al., 2006).

In this study, 3 out of the 4 patients with the rare non-synonymous *GATA5* variants (Gln3Arg, Ser19Trp and Gly166Ser) have rather modest clinical pathology. Moreover, there is an observed discrepancy between the severity of the clinical manifestation of BAV disease in patients with the Gln3Arg and Tyr142His variants and the degree of transcriptional down-regulation in the related *GATA4* reporter gene construct. Specifically, Tyr142His variant was associated with a more severe clinical phenotype albeit less marked reduction of *GATA4* reporter gene construct transcriptional activity and the vice versa was noted with Gln3Arg variant. These observations can probably be explained by the presence of genetic heterogeneity in BAV disease, where involvement of mutations in diverse genes encoding transcription factors, extracellular matrix proteins and various cellular signalling pathways likely to play a contributory role in disease development and manifestations (Garg, 2006, Martin et al., 2007, Ward, 2000). Epigenetic factors, such as micro-RNAs (Nigam et al., 2010), and environmental influences, such as mechanical shear stress, blood pressure and cholesterol level, are also likely to be important in modulating BAV disease phenotype, hence contributing to the wide spectrum of disease expression. Another explanation for the discrepancy observed between the clinical phenotype and the transcriptional activity of GATA4 reporter gene construct was that the later study was performed within a cell culture system. Therefore, although these findings are suggestive and important, they may not be directly translatable to the changes found *in-vivo*.

Following our report (Padang et al., 2012a), the role for GATA5 in human BAV disease was further supported by 2 more recent studies. During the screening of 110 unrelated BAV cohorts, Shi *et al*. identified 2 novel heterozygous *GATA5* loss-of-function mutations, Tyr16Asp and Thr252Pro, each occurring in a familial case of BAV (Shi et al., 2014). Functional assays revealed that these 2 mutations significantly reduced the transcriptional activity of *GATA5*, compared with their wild-type counterpart, hence supporting their pathogenic role (Shi et al., 2014). Very recently, Bonachea *et al.* also reported the presence of 2 rare heterozygous non-synonymous *GATA5* variants during screening of their 78 BAV cohort, namely Leu233Pro and, notably, Gln3Arg variant (Bonachea et al., 2014 [Epub ahead of print]). The Gln3Arg variant was found in a male patient with BAV and coarctation of the aorta. Providing further support to our findings, the pathogenicity of the Gln3Arg variant was strengthened by their *in-vitro* transfection assay, where Gln3Arg variant resulted in a 10-fold reduction of the transcriptional activity of *GATA5 (Bonachea et al., 2014 [Epub ahead of print])*. Overall, these studies support our finding on the potential pathogenic role of rare non-synonymous *GATA5* mutations in human BAV development.

The current study included a group of BAV patients with a mixed morphology, with only 10% having a R-N BAV morphology. Since *Gata5* deletion in mice resulted in R-N BAV, the role of *GATA5* may be greater in a cohort of BAV patients with a higher proportion of R-N BAV morphology. Further, while the control cohort used in the study consisted of individuals without any reported heart disease, many have not had echocardiographic examination to exclude

BAV, including those control subjects with the Gln3Arg and Ser19Trp. This highlights the importance of well-defined control populations, particularly for common disorders such as BAV, and especially in the current era of next generation sequencing of very large cohorts lacking phenotypic data, such as the 1000 Genomes project and EVS, where the discovery of rare sequence variations of unknown significance confounds efforts to determine pathogenicity.

In conclusion, this candidate gene study supports a role for rare non-synonymous variations within the highly conserved and functionally important *GATA5* transcriptional activation domains in the pathogenesis of BAV disease in humans. It remains uncertain however if these variants are directly causal or serving as critical genetic modifiers where additional genetic or environmental factors are required to produce the disease phenotype. Further studies to assess the functional consequences of rare non-synonymous *GATA5* variants in patients with BAV and its associated aortopathy are therefore warranted.

CHAPTER 4: EXOME SEQUENCING ANALYSIS OF FAMILIAL BAV

4.1. INTRODUCTION

The impetus for a candidate gene approach, as described in chapter 3, is a prior knowledge of potential involvement of the candidate gene(s) in the pathogenesis of disease of interest (Marian, 2012). Over the past few decades, this technique has been used successfully in identifying a number of single gene defects in patients with isolated or nonsyndromic congenital heart disease (CHD). For example, identification of *GATA4* mutations in families with isolated atrial septal defects (Garg et al., 2003), *GATA6* mutations in patients with truncus arteriosus (Kodo et al., 2009), and the discovery of the relationship between *TBX5* and *TBX20* gene variants in those with septal and valve defects (Reamon-Buettner and Borlak, 2004, Kirk et al., 2007). These studies highlight that screening high-risk kindred from a large family with multiple affected family members can lead to the discovery of pathogenic gene variants (Arrington et al., 2012).

However, whilst candidate gene screening has identified causative mutations in a number of conditions, this technique has had limited success for many other types of CHD (Arrington et al., 2012), including bicuspid aortic valve (BAV) disease. The plausible explanations include knowledge that many genes are involved in cardiac development (genetic heterogeneity) and each represents a candidate for disease; causative mutation(s) may be found in introns or regulatory regions that are not typically screened in a candidate gene study; and a wide spectrum of disease phenotypes is seen in BAV, even within the same family, suggesting BAV may result from the cumulative effect of many

partially penetrant variations, i.e. a complex genetic trait, as well as the likely presence of genetic modifier loci. Adding to the complexity, at the epigenetic level, histone modifications and chromatin remodelling may have substantial roles in BAV development by activating or silencing gene expression, whilst microRNAs might promote development of BAV by post-transcriptional regulation of gene expression. Therefore, alternative approaches may be more fruitful to identify causative genetic variants that are responsible for BAV development. One successful example is linkage analysis in a large multi-generation family affected by congenital heart disease and valve calcification that led to the identification of mutations in *NOTCH1* as a cause of aortic valve disease.

Relatively recently, whole genome sequencing has emerged as a method to interrogate every nucleotide variation in the genome, however, this is currently cost-prohibitive and poses a significant bioinformatics challenge for many laboratories. Presently, an alternative and more preferable method is whole-exome sequencing, which targets a small proportion of the genome at a significantly lower cost and simpler bioinformatics burden. Exome sequencing offers a powerful unbiased strategy to survey the entire protein-coding region (i.e. exons) of the human genome, without consideration for existing data to implicate any particular gene in the disease pathogenesis. Although exons constitute only ~1% of the human genome, approximately 85% of highly penetrant mutations in Mendelian disorders reside within these functional regions (Choi et al., 2009). Therefore, exome sequencing has the great potential to identify novel, unanticipated pathogenic gene variants in BAV

disease. Application of the whole-exome sequencing approach on a well-characterised multi-generation family with multiple affected family members with BAV may be very useful in delineating the genetic basis of BAV disease, where the pathogenicity of a putative mutation can be robustly validated by demonstrating co-segregation with disease.

Another approach to identify genes that are involved in the development of BAV is comparative analysis of mRNA expression levels in normal and diseased tissue, either using microarray hybridisation analysis, or more recently, analysis of RNA transcripts using next generation sequencing, i.e. RNASeq, as described in Chapter 5.

This chapter describes whole-exome sequencing analyses of 2 large families of Caucasian background with preponderance for BAV and its associated aortopathy.

4.2. METHODS

4.2.1. Study population

4.2.1.1. Familial cases of BAV (Families A and B)

Between July 2011 and October 2012, two large families with highly penetrant cases of BAV were identified (Family A and Family B). All members of the families were invited to participate in the exome sequencing study. Following informed consent, participating family members underwent clinical evaluation that included 2D-echocardiography and had their blood samples, or, in cases of young children (less than 5 years old), saliva collected for DNA isolation. Medical records, when available, were reviewed for demographic, clinical and surgical data.

4.2.1.2. BAV validation cohort

Patients with sporadic and nonsyndromic cases of BAV were recruited in parallel, as described in Chapter 2.3.1. The study protocol was approved by the Sydney South West Area Health Service ethics committee.

4.2.2. Exome sequencing

4.2.2.1. Library construction and sequencing

Exome sequencing (library construction, capture and sequencing) was carried out at the Macrogen Facility, South Korea, on 3 related DNA samples from each family. These belonged to affected family members III:2, IV:3 and IV:5 from Family A (Figure 4.1) and affected family members III:3, III:8 and V:10 from Family B (Figure 4.2). The process of library construction, capture and sequencing are detailed in Chapter 2.4.3.1.

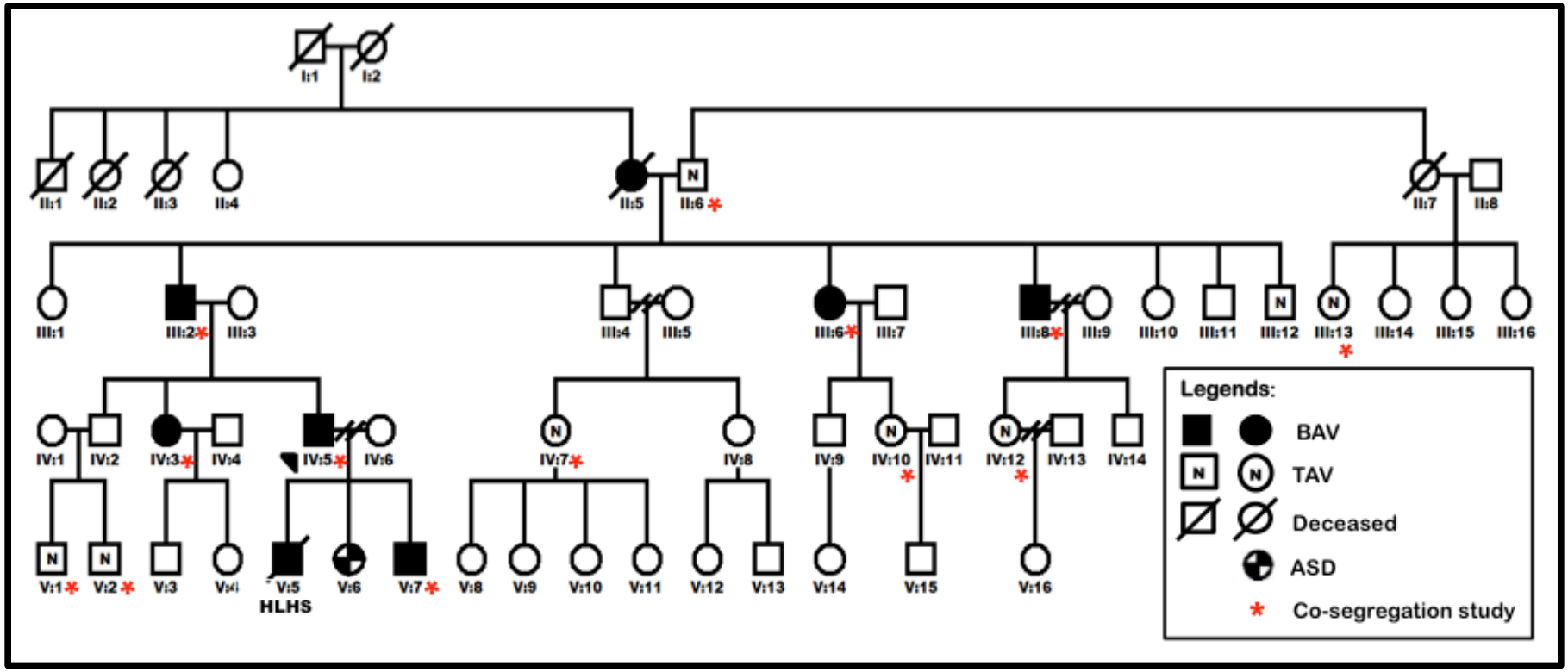

Figure 4. 1. Pedigree of Family A.

Variant co-segregation study was performed on 13 participating family members; they included those with BAV and/or the associated aortopathy [III:2, III:6, III:8, IV:3, IV:5 (proband) and V:7] and those with normal tri-leaflet aortic valve (II:6, III:13, IV:7, IV:10, IV:12, V:1 and V:2). Individual V:5 died within 3 weeks of life and the subsequent autopsy study demonstrated hypoplastic left heart syndrome (HLHS) and the presence of BAV. ASD, atrial septal defect; TAV, tri-leaflet aortic valve.

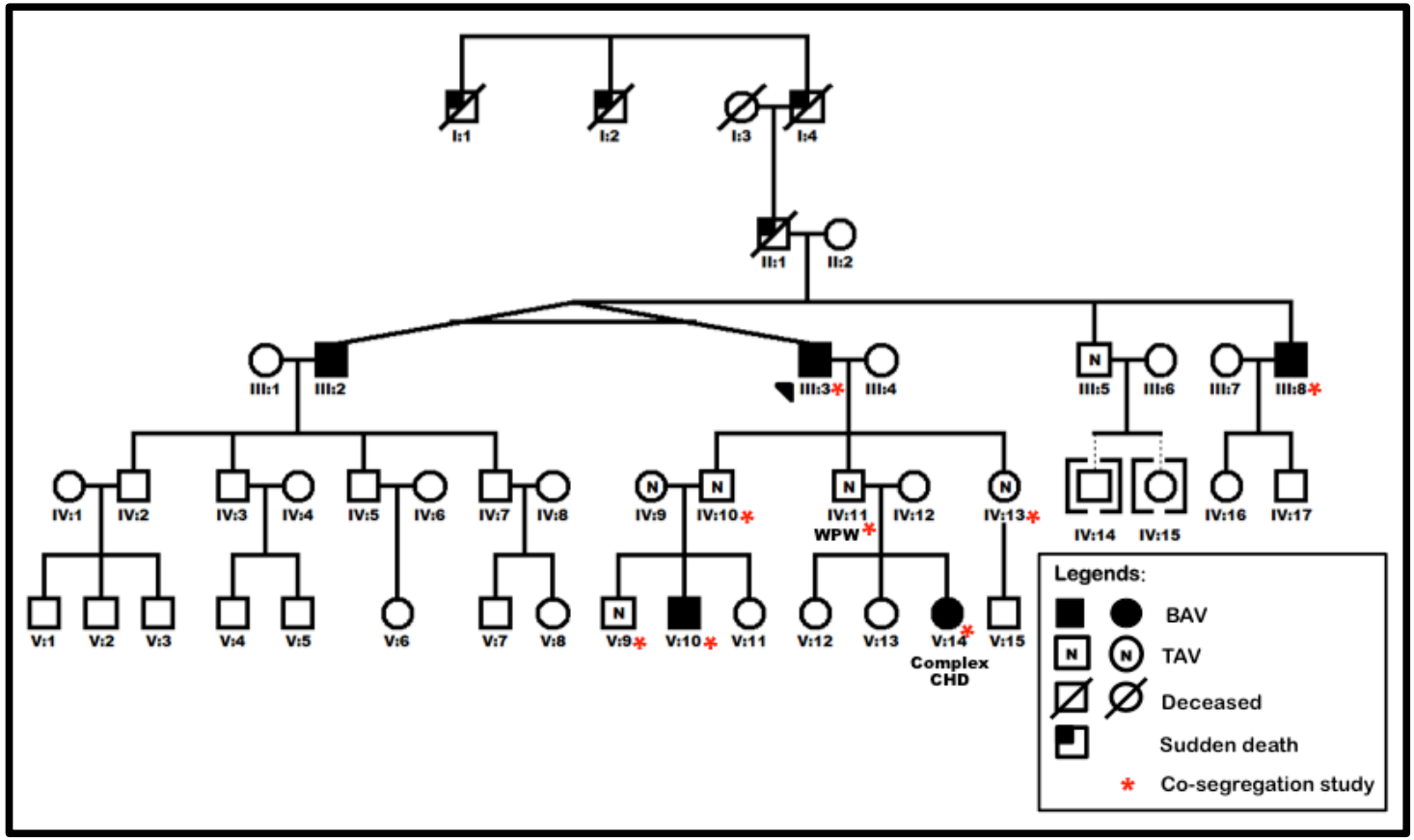

Figure 4. 2. Pedigree of Family B.

Variant co-segregation was performed on 9 participating family members. They included those with BAV and/or the associated aortopathy [III:3 (proband), III:8, V:10 and V:14] and those with normal tri-leaflet aortic valve (IV:9, IV:10, IV:11, IV:13 and V:9). TAV, tri-leaflet aortic valve; WPW, Wolf Parkinson White syndrome.

While exome sequencing was always attempted on 3 most distantly related affected individuals in the family, selection of these individuals (Individuals III:2, IV:3 and IV:5 from Family A and Individuals III:3, III:8 and V:10 from Family B) was made based on the available list of enrolled family members at the time of exome sequencing and the availability of high quality DNA that was suitable for sequencing.

4.2.2.2. Bioinformatics and variants analysis

Raw exome sequencing data were processed using a bioinformatics pipeline developed by Dr Richard Bagnall of the Molecular Cardiology Program, Centenary Institute, as described in Section 2.4.3.2. This pipeline deposits single nucleotide variants (SNV) and insertions/deletions (InDels) for each individual patient in a database, with annotations against various genomic features. These annotations included chromosome position, gene description, dbSNP rsIDs number, genomic evolutionary rate profiling (GERP) score, variant location (i.e. exonic, intronic, splice site, 5' UTR, 3' UTR, intergenic), consequence (i.e. missense, synonymous, stop, frameshift, insertion/deletion, etc), several protein annotations (i.e. amino acid substitution and protein domain), predicted physiochemical dissimilarities of the replaced codons (Grantham score), predictions of possible pathogenicity of an amino acid substitution (by Polyphen (Family A) or PolyPhen2 (Family B)), and minor allele frequency (MAF) in the 1000 Genomes data and 6500 exomes of the NHLBI Exome Sequencing Project (EVS).

Variant analysis was performed by retrieving variations from the database with the principal assumptions that:

1. BAV is caused by an autosomal dominant mutation that is both sufficient and necessary to cause disease
2. The causal variant will affect a protein-coding DNA sequence or canonical splice signal sequence
3. The causative mutation will occur at a frequency of no more than 1% in publically available data of control populations.

Based on these postulations, the subsequent variant prioritisation was carried out using the following criteria: (i) heterozygous variants present in all 3 exome sequencing samples of affected individuals within each family; (ii) the novelty of the variants by excluding those that were present in the in-house exome dataset of unrelated individuals with different phenotype (4 samples during Family A study and subsequently 96 samples during Family B study) and those with MAF of >1% in the 1000Genome Project, the dbSNP, and the EVS database; (iii) the putative pathogenic effect of the gene variants by excluding synonymous, intronic or intergenic variants and by including those with non-synonymous missense, nonsense, splice-site gain- or loss-of-function variants and frame-shift insertion or deletion mutations; (iv) a positive GERP conservation score; (v) the presence of aortic valve expression of the genes which harboured the variants. These putative disease-causing variants were inspected manually using the Integrative Genome Viewer (IGV) visualisation tool to examine the overall quality and coverage of the aligned sequence reads at the variant site (Figure 4.3). Variants that fulfilled these criteria were then considered for validation and co-segregation analysis.

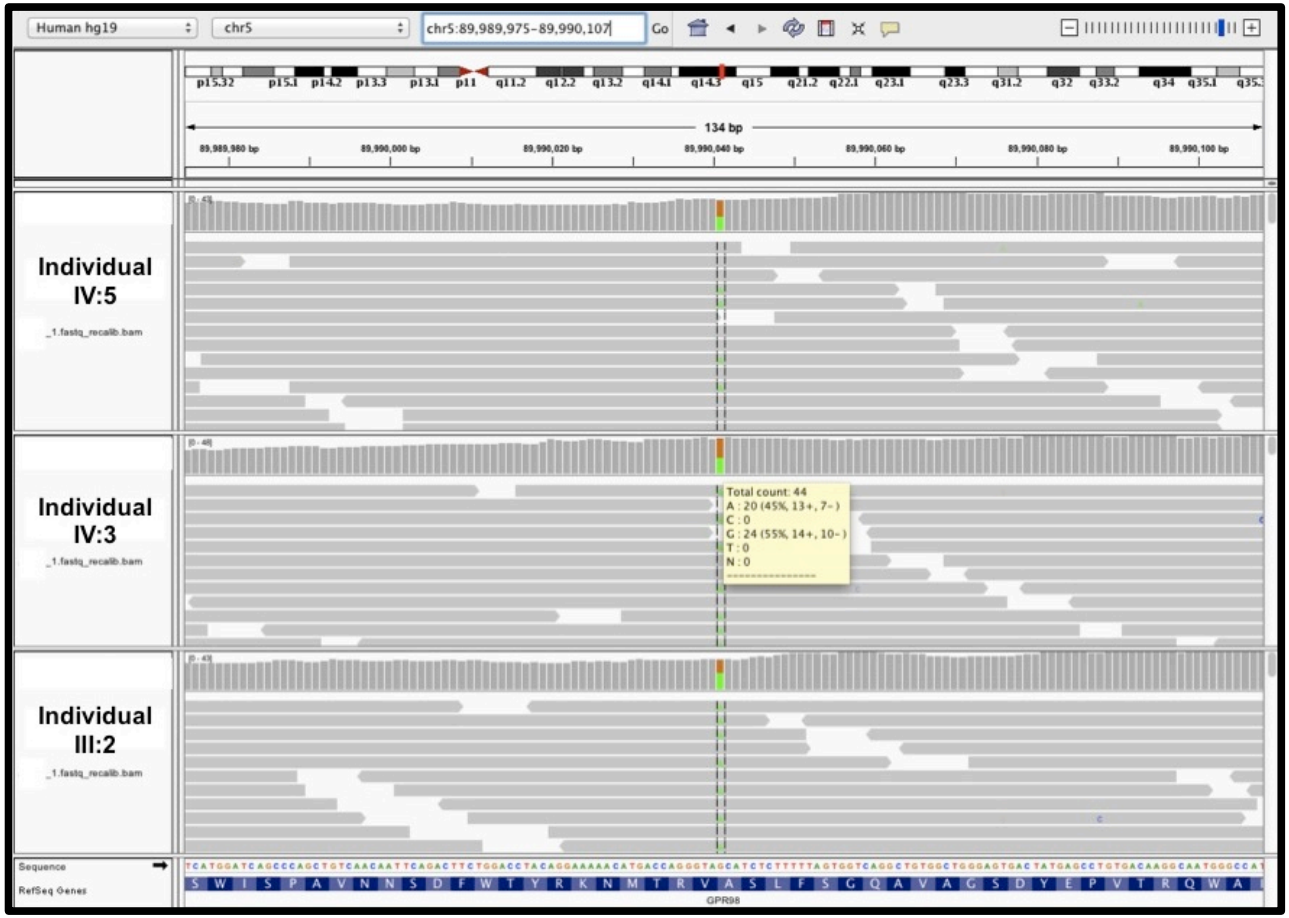

Figure 4. 3. Example of a direct SNV visualisation in IGV browser.

The inspected variant occurred in a well-covered region, had a good mean read-depths (>40 reads per sample), and the non-reference base (A) distributed in both forward and reverse reads.

4.2.3. Co-segregation study

Once a variant that fulfilled quality filters was identified, all participating family members were genotyped to determine the pattern of variant segregation by means of standard Sanger sequencing, as described in Chapters 2.4.1.2 to 2.4.1.5. Appendix 1, Table I-2 and I-3, listed the primer sequence and PCR conditions used in variant segregation analysis for Family A and Family B, respectively. Assistance was obtained from Miss Annie Evans, research assistant in The Molecular Cardiology Program, Centenary Institute, in screening the last 20 variants from Family A, as listed on Appendix 1, Table I-2. Validated variations obtained from screening of family members were considered as a candidate mutation if the non-reference allele co-segregated completely with the disease phenotype and was excluded if it was not observed to co-segregate with BAV.

As enrolment of family members in Family A and B occurred sporadically over 2 to 2.5 years, some individuals were recruited only after the initial co-segregation analysis. If a family member was recruited after a variant had been excluded from the initial co-segregation study (based on the absence of variant in an affected family member recruited earlier who were not exome sequenced), then determination of the status of the variant in the later recruited individual was deemed unnecessary. Similarly, in the case of sequencing failure, should a variant be excluded due to its absence in an affected family member, then the failed sequencing attempt was not repeated. In both scenarios, the status of the individual was marked “not determined (ND)”.

4.2.4. Candidate mutation gene screening in unrelated sporadic BAV cohort

Remaining variants that fulfilled the criteria as candidate mutations were reviewed for the available literature, associated gene pathways and molecular regulation, levels of gene expression on aortic valve RNA-sequencing data (Chapter 5), and existing animal models. The primary candidate gene was then selected for direct gene screening in a cohort of 130 unrelated sporadic BAV, using method described in Chapters 2.3.1.2 to 2.4.1.5. The aim was to evaluate whether there was a higher rate of rare non-synonymous variants within the gene of interest amongst the BAV cohort compared to the background sequence variation rate amongst the NHLBI EVS European American 'control' population, which consists of sequence variation data on 4298 exomes. A higher rate of rare non-synonymous sequence variation amongst the BAV cohort supports the likely importance of the candidate genes in the pathogenesis of BAV.

4.2.5. Linkage analysis and screening of poorly covered region in exome sequencing

Genome-wide linkage analysis was performed in Family A, with the assistance of Dr Richard Bagnall. Briefly, a genome-wide SNP genotyping array was performed at the Australian Genome Research Facility (AGRF, Victoria, Australia) utilising the Illumina Cyto-12 BeadChip panel (Illumina, San Diego, CA, USA), which consisted of over 200,000 SNP markers. Twelve individuals from Family A (II:6, III:2, III:6, III:8, III:12, IV:3, IV:5, IV:10, IV:12, V:1, V:2 and

V:7) were genotyped regardless of their clinical status. Linkdatagen was used to generate linkage analysis input files for MERLIN using the raw genotype calls from the Illumina SNP arrays. Multipoint nonparametric linkage analysis was then performed using MERLIN (version 1.1.2). Logarithm of odd ratio (LOD) scores were calculated for each marker assuming an autosomal dominant mode of inheritance with 70% disease penetrance, a disease allele frequency of 0.01 and absence of phenocopies. Haplotypes were constructed assuming a minimum number of recombination and viewed using Haplopainter.

Identified regions with suggestive linkage (LOD scores ≥ 1.5) were then manually inspected using IGV browser to look for regions with poor coverage on exome sequencing (i.e. exon regions with less than 10 read-depths). These regions were then manually sequenced by means of Sanger sequencing, as described in Chapters 2.4.1.2 to 2.4.1.5, and analysed for the presence of plausible disease-causing variants, using the same criteria detailed in Chapter 4.2.2.2.

4.2.6. Statistical analysis

All data are expressed as mean ± standard deviation (SD). Statistical analysis to determine non-random associations between 2 categorical variables was performed with Fisher's exact test. A two-tailed p-value ≤ 0.05 was considered statistically significant. Statistical analyses were performed using GraphPad Prism Version 6.0b (GraphPad Software, La Jolla, California, USA).

4.3. RESULTS

4.3.1. FAMILY A

4.3.1.1. Family A Pedigree and individual characteristics

The family was of Caucasian background and the pertinent clinical information of participating family members are summarised in Figure 4.1 and Table 4.1. The proband (Individual IV:5) was a 41 years old man from rural NSW, who was diagnosed with a moderately stenotic BAV at the age of 34 years following investigation of a murmur. He was also detected to have enlargement of his ascending aorta at the time of BAV diagnosis. Over the subsequent 7 years, he developed progressive enlargement of his aorta, which was associated with intermittent chest pains, triggering a surgical evaluation for his condition and subsequent operative intervention. Of note, proband has 3 offspring, all of whom were born with congenital cardiac defect(s). This included simple atrial septal defect (Individual V:6), BAV (Individual V:7) and hypoplastic left heart syndrome, which resulted in the untimely death of Individual V:5 at 3 weeks of age. DNA was available for 13 of these individuals and used in the co-segregation study.

Table 4. 1. Clinical characteristics of recruited family members of Family A.

Pedigree position	Gender	Current age (years)	Valve Type	Age at diagnosis (years)	BAV Function	Comments
II:6	Male	90	TAV	-	-	Clinically unaffected
III:2	Male	69	BAV	57	Severe AS	Dilated ascending aorta; AVR age 60
III:6	Female	65	BAV	20	Moderate AS	Mild ascending aorta and aortic root dilatation
III:8	Male	63	BAV (R-L)	52	Mild to Moderate AR	No associated aortopathy
III:12	Male	55	TAV	-	-	Clinically unaffected
III:13	Female	64	TAV	-	-	Clinically unaffected
IV:3	Female	44	BAV	19	Severe AS	Dilated ascending aorta; AVR age 29
IV:5	Male	41	BAV (R-N)	34	Moderate AS	Moderate to severely dilated ascending aorta; AVR and aortic replacement age 41
IV:7	Female	43	TAV	-	-	Clinically unaffected
IV:10	Female	49	TAV	-	-	Clinically unaffected
IV:12	Female	41	TAV	-	-	Previous infective endocarditis with subsequent AVR age 31
V:1	Male	20	TAV	-	-	Clinically unaffected
V:2	Male	12	TAV	-	-	Clinically unaffected
V:5	Male	Deceased	BAV	3 weeks of age	Unknown	HLHS; died 3 weeks of age
V:6	Female	7	TAV	At birth	-	Small ASD diagnosed at birth; conservative management
V:7	Male	5	BAV	At birth	Trivial AR	No associated aortopathy

n/a, not applicable; AVR, aortic valve replacement; TAV, tricuspid (tri-leaflet) aortic valve; BAV, bicuspid aortic valve; AS, aortic stenosis; AR, aortic regurgitation; R-N, right and non coronary cusps fusion BAV morphology; R-L, right and left coronary cusps fusion BAV morphology; HLHS, hypoplastic left heart syndrome; ASD, atrial septal defect.

4.3.1.2. Exome sequencing analysis and plausible variants list

Exome sequencing was performed on DNA samples from Individuals III:2, IV:3 and IV:5 from the pedigree depicted in Figure 4.1. An average of 59,370,400 reads were generated for each individual sample and an average of 52,780,300 reads (89.9%) were mapped uniquely to the genome. Approximately 86.5% of target exome regions received more than 10 sequence reads and an average of 48 reads per target base pair was achieved for each exome. Following base identification and variant calling, each individual had an average of 67,200 SNVs. After multiple filtering steps (Figure 4.4), 90 plausible disease-causing variants were shared amongst the 3 individuals. Moreover, there was an average of 489 coding InDels for each individual, 278 of which were shared. After similar filtration steps, removal of duplicate variant calls of InDels with multiple accessions ID numbers, and direct visualisation on IGV, 3 InDels were included for further analysis. Appendix II, Table II-1 described the 90 prioritised and filtered variants and the 3 InDels, which were included in the co-segregation analysis.

4.3.1.3. Co-segregation study of Family A

All these prioritised variants and InDels were subsequently analysed for their pattern of co-segregation with BAV disease amongst 13 participating family members. Apart from those who were exome sequenced, they included those who also had BAV and/or the associated aortopathy (III:6, III:8, and V:7) and those with normal trileaflet aortic valve (II:6, III:13, IV:7, IV:10, IV:12, V:1 and V:2). The result of the segregation analysis of variants performed is

summarised in Table 4.2. There were 13 variants that co-segregated with BAV disease phenotype within the family. However, based on the aortic valve RNA sequencing study (Chapter 5), *UGT3A1, GPR98, LMOD2* and *B7H6* genes are either not expressed or have extremely low level of expressions within the aortic valve (FKPM <0.03) and therefore they were filtered out from subsequent analysis. The 9 remaining putative disease-causing missense variants (i.e. candidate gene mutations) are listed in Table 4.3

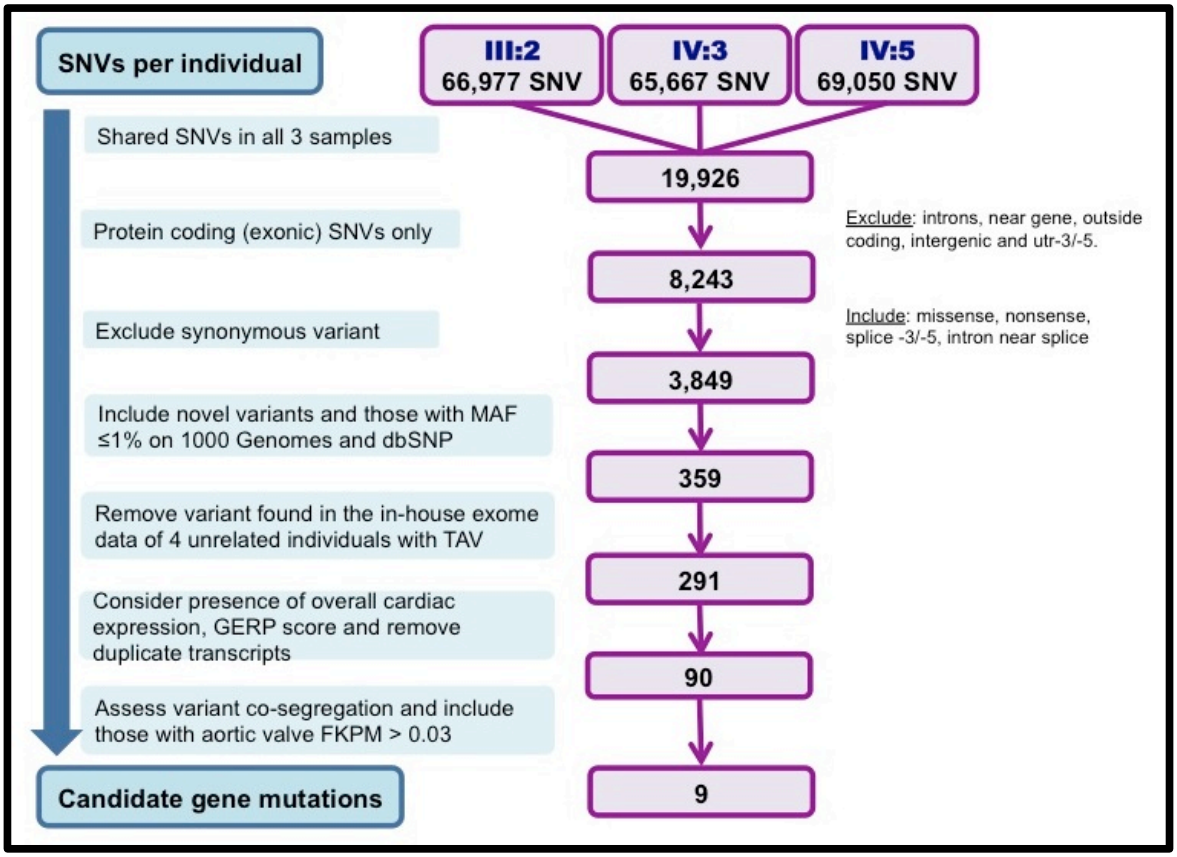

Figure 4. 4. Filtering steps used to analyse the SNVs obtained from Family A exome sequencing result.

SNV, single nucleotide variations; FKPM, Fragments per Kilobase of transcript Per Million mapped reads (of RNA sequencing data), which is proportional to the level of expression of the gene of interest within the tissue sample studied.

Table 4. 2. Variant co-segregation analysis of Family A.

		BAV						TAV						
GENE	**Variant**	**III:2**	**III:6**	**III:8**	**IV:3**	**IV:5**	**V:7**	**II:6**	**III:13**	**IV:7**	**IV:10**	**IV:12**	**V:1**	**V:2**
GTF3C5	**Phe474Leu**	HET	HET	HET	HET	HET	HET	WT	WT	WT	HET	WT	WT	WT
ITGA10	**Arg1161Gly**	HET	HET	HET	HET	HET	HET	WT	WT	WT	HET	HET	WT	WT
RTP4	**Gln44Lys**	HET	HET	HET	HET	HET	HET	WT	WT	WT	WT	HET	WT	WT
PDE4DIP	**Ala1245Thr**	HET	HET	HET	HET	HET	HET	WT	WT	WT	HET	HET	WT	WT
MATN1	**Arg343Gln**	HET	HET	HET	HET	HET	HET	WT	WT	WT	HET	HET	WT	WT
PTGES2	**Gly206Ala**	HET	HET	HET	HET	HET	HET	WT	WT	WT	HET	WT	WT	WT
SLC4A2	**Arg107Gln**	HET	HET	HET	HET	HET	HET	WT	WT	WT	WT	HET	HET	HET
GPR98^	**Ala1490Thr**	HET	HET	HET	HET	HET	HET	WT	WT	WT	WT	WT	HET	WT
LMOD2^	**Ile221Thr**	HET	HET	HET	HET	HET	HET	WT	WT	WT	WT	HET	HET	HET
UGT3A1^	**Asn250Tyr**	HET	HET	HET	HET	HET	HET	WT	WT	WT	WT	WT	HET	WT
ABCA13	**Thr4550Ala**	HET	HET	HET	HET	HET	HET	WT	WT	WT	WT	HET	HET	HET
GDNF	**Arg93Trp**	HET	HET	HET	HET	HET	HET	WT	WT	WT	WT	WT	HET	WT
B7H6^	**His264Asn**	HET	HET	HET	HET	HET	HET	HET	WT	WT	HET	HET	WT	HET
BCLAF1	Leu461His	HET	HET	HET	HET	HET	HET	HET	HET	HET	HET	HET	HET	HET
BCLAF1	Tyr459His	HET	HET	HET	HET	HET	HET	HET	HET	HET	HET	HET	HET	HET
GPRIN2	Trp91Arg	HET	HET	HET	HET	HET	HET	HET	HET	HET	HET	HET	HET	HET
ADRB2	Tyr326Cys	HET	HET	WT	HET	HET	HET	WT	WT	WT	HET	WT	WT	WT
HPS3	Arg220Ser	HET	HET	WT	HET	HET	HET	WT	WT	WT	HET	WT	WT	WT
KCNMB3	Thr166Ala	HET	HET	WT	HET	HET	HET	WT	WT	WT	ND	WT	WT	WT
MAP2	Glu55Lys	HET	WT	WT	HET	HET	HET	WT	WT	WT	WT	WT	WT	HET
HGF	Gly648Arg	HET	WT	WT	HET	HET	HET	WT	WT	WT	WT	WT	HET	WT
FAM160A2	Arg862Cys	HET	WT	HET	HET	HET	HET	HET	WT	WT	WT	HET	WT	HET
ADAMTS6	His155Gln	HET	HET	WT	HET	HET	HET	WT	WT	WT	HET	WT	HET	WT
PLCL1	Thr274Ala	HET	WT	WT	HET	HET	HET	WT	WT	WT	WT	WT	WT	HET
HS1BP3	Thr137Ala	HET	HET	WT	HET	HET	HET	HET	HET	WT	HET	WT	WT	WT
ABCB4	Leu73Val	HET	HET	WT	HET	HET	HET	WT	WT	WT	WT	WT	HET	WT

Table 4.2. Family A co-segregation analysis continued

		BAV						TAV						
GENE	Variant	III:2	III:6	III:8	IV:3	IV:5	V:7	II:6	III:13	IV:7	IV:10	IV:12	V:1	V:2
MED16	Arg876Pro	HET	WT	HET	HET	HET	HET	HET	HET	WT	WT	WT	WT	WT
PMPCB	Ala3Val	HET	HET	WT	HET	HET	HET	WT	WT	WT	WT	WT	HET	WT
ECEL1	Arg702Leu	HET	HET	WT	HET	HET	ND	HET	WT	HET	WT	WT	WT	HET
CYP7A1	Pro398Ala	HET	WT	HET	HET	HET	WT	HET	WT	WT	WT	WT	HET	WT
ABOBEC1	Trp21stop	ND	ND	ND	ND	ND	ND	ND	ND	ND	ND	ND	ND	ND
COL11A1	Tyr233Cys	HET	WT	ND	HET	HET	HET	WT	WT	ND	ND	ND	WT	WT
ARAP2	Arg1626Gln	HET	ND	ND	HET	HET	WT	ND	ND	ND	ND	ND	WT	WT
RFC1	Ser1042Gly	HET	ND	ND	HET	HET	WT	ND	ND	ND	ND	ND	WT	WT
PKD2	Arg872Gln	HET	ND	ND	HET	HET	WT	ND	ND	ND	ND	ND	WT	WT
AHRR	Pro580Ala	HET	ND	ND	HET	HET	WT	ND	ND	ND	ND	ND	WT	WT
FNDC1	Asp60Asn	HET	ND	ND	HET	HET	WT	ND	ND	ND	ND	ND	WT	WT
MMP17	Leu78Met	HET	ND	ND	HET	HET	WT	ND	ND	ND	ND	ND	WT	ND
GAS6	Thr259Pro	WT	ND	ND	WT	WT	WT	ND	ND	ND	ND	ND	WT	WT
NCOR1	Glu191Lys	WT	ND	ND	WT	WT	WT	WT	WT	ND	ND	ND	WT	WT
BCLAF1	Gly66Ala	WT	ND	ND	WT	WT	WT	WT	WT	ND	ND	ND	WT	WT
BCLAF1	Splice variant	WT	ND	ND	WT	WT	WT	WT	WT	ND	ND	ND	ND	WT
TIGD6	Ser481Ala	HET	WT	ND	HET	HET	HET	WT	WT	ND	ND	ND	WT	WT
TTC18	Arg1029Lys	HET	ND	ND	HET	HET	WT	WT	WT	ND	ND	ND	WT	HOMO*
ACACB	Val1996Met	HET	ND	ND	HET	HET	WT	HET	WT	ND	ND	ND	HET	HET
HGSNAT	Ala615Thr	HET	ND	ND	HET	HET	WT	HET	WT	ND	ND	ND	HET	WT
ULK1	Ser317Phe	HET	ND	ND	HET	HET	WT	HET	HET	ND	ND	ND	WT	WT
SLC6A3	Arg515Trp	HET	ND	ND	HET	HET	WT	HET	WT	ND	ND	ND	WT	WT
FASN	Gly2052Ala	WT	ND	ND	ND	ND	ND	ND	ND	ND	ND	ND	WT	WT
MAP2K3	Arg96Trp	WT	ND	ND	WT	ND	ND	WT	WT	ND	ND	ND	WT	WT

Table 4.2. Family A co-segregation analysis continued

		BAV						TAV						
GENE	**Variant**	**III:2**	**III:6**	**III:8**	**IV:3**	**IV:5**	**V:7**	**II:6**	**III:13**	**IV:7**	**IV:10**	**IV:12**	**V:1**	**V:2**
MAP2K3	Arg94Leu	WT	ND	ND	WT	ND	ND	WT	WT	ND	ND	ND	WT	WT
MAP2K3	Pro40Thr	WT	ND	ND	WT	ND	ND	WT	WT	ND	ND	ND	WT	WT
MAP2K3	Gln102stop	WT	WT	ND	WT	WT	WT	WT	WT	ND	ND	ND	WT	WT
SH3RF3	Ser700Phe	HET	WT	ND	HET	HET	HET	WT	WT	ND	ND	ND	WT	WT
KDM1B	Ser252Pro	ND	ND	ND	ND	HET	WT	ND	HET	ND	ND	ND	HET	ND
ACTR3C	Gln121stop	WT	ND	ND	WT	WT	WT	ND	WT	ND	ND	ND	WT	WT
AFMID	Arg35Gln	HET	WT	ND	HET	HET	WT	WT	WT	ND	ND	ND	WT	WT
TH1L	Ala257Thr	HET	ND	ND	HET	HET	WT	HET	HET	ND	ND	ND	WT	WT
URB1	Arg1601Gln	ND	ND	ND	ND	HET	WT	ND	ND	ND	ND	ND	WT	ND
SASH1	Ser387Phe	HET	HET	ND	HET	HET	WT	WT	WT	ND	ND	ND	WT	WT
ANKAR	Arg1272His	HET	WT	ND	HET	HET	ND	WT	WT	ND	ND	ND	WT	HET
BST1	Val85Met	HET	HET	ND	HET	HET	WT	HET	WT	ND	ND	ND	WT	HET
BTBD16	Gly242Glu	HET	WT	ND	HET	ND	ND	WT	WT	ND	ND	ND	WT	ND
C1ORF168	Glu522Lys	HET	ND	ND	HET	HET	WT	WT	WT	ND	ND	ND	ND	WT
DDX51	Thr193Ile	HET	WT	ND	HET	HET	HET	HET	HET	ND	ND	ND	WT	WT
DNAH10	Lys2132Glu	HET	WT	ND	HET	HET	WT	HET	WT	ND	ND	ND	HET	HET
DNALI	Gln259Arg	HET	HET	ND	HET	HET	WT	WT	WT	ND	ND	ND	WT	WT
GJB6	Ser199Thr	HET	WT	ND	HET	HET	WT	HET	WT	ND	ND	ND	WT	WT
HKDC1	Arg178Gln	HET	HET	ND	HET	HET	WT	WT	WT	ND	ND	ND	WT	HET
LRRN4	Tyr549Asn	HET	WT	ND	HET	HET	WT	HET	WT	ND	ND	ND	WT	HET
NOS3	Val845Gly	WT	WT	ND	WT	WT	WT	WT	WT	ND	ND	ND	WT	WT
ULBP1	Gly26Glu	HET	HET	ND	HET	HET	WT	WT	WT	ND	ND	ND	WT	WT
TACC3	Pro612Ala	HET	HET	ND	HET	HET	WT	HET	HET	ND	ND	ND	WT	WT
PRH2	Ser38Phe	HET	WT	ND	HET	ND	ND	ND	WT	ND	ND	ND	HET	ND

Table 4.2. Family A co-segregation analysis continued

		BAV						TAV						
GENE	**Variant**	**III:2**	**III:6**	**III:8**	**IV:3**	**IV:5**	**V:7**	**II:6**	**III:13**	**IV:7**	**IV:10**	**IV:12**	**V:1**	**V:2**
NUP43	His65Tyr	HET	HET	ND	HET	HET	WT	WT	WT	ND	ND	ND	WT	WT
MICALCL	Arg453His	WT	WT	ND	HET	HET	WT	WT	WT	ND	ND	ND	HET	WT
MUSK	Gly107Glu	HET	HET	ND	HET	HET	WT	WT	WT	ND	ND	ND	WT	WT
PCDHB7	Pro575Leu	WT	WT	ND	WT	WT	WT	WT	WT	ND	ND	ND	WT	WT
TGM2	Val665Leu	HET	ND	ND	HET	HET	WT	HET	HET	ND	ND	ND	WT	HET
SVEP1	Arg492Gln	HET	ND	ND	HET	HET	WT	HET	WT	ND	ND	ND	WT	WT
WDR47	Arg661His	HET	WT	ND	HET	HET	HET	WT	WT	ND	ND	ND	WT	WT
ZNF831	Asp861Asn	HET	ND	ND	HET	HET	WT	HET	HET	ND	ND	ND	WT	WT
TYRO3	Splice variant	WT	ND	ND	WT	WT	WT	WT	WT	ND	ND	ND	WT	WT
TYRO3	Splice variant	WT	ND	ND	WT	WT	WT	WT	WT	ND	ND	ND	WT	WT
BRSK1	Pro764Ala	HET	WT	ND	HET	HET	HET	ND	WT	ND	ND	ND	WT	ND
CST4	Val87Ile	HET	WT	ND	HET	HET	WT	HET	HET	ND	ND	ND	WT	HET
SI	Tyr975His	ND	HET	ND	HET	HET	WT	WT	WT	ND	ND	ND	WT	WT
SDSL	Ala236Thr	HET	WT	ND	HET	HET	WT	HET	WT	ND	ND	ND	HET	HET
PUS1	Asp133Asn	HET	WT	ND	HET	HET	HET	HET	ND	ND	ND	ND	WT	WT
MTHFR	Cys519Ser	HET	WT	ND	HET	HET	HET	WT	WT	ND	ND	ND	WT	WT
NEURL2	frameshift	INS	WT	ND	INS	INS	WT	INS	INS	ND	ND	ND	WT	WT
OXA1L	frameshift	INS	WT	ND	INS	INS	INS	ND	ND	ND	ND	ND	WT	WT
GNAS	frameshift	WT	WT	ND	WT	WT	WT	WT	WT	ND	ND	ND	WT	WT

Typed in bold are the plausible candidate gene mutations that co-segregate with disease. ^However, based on the aortic valve transcriptome study (Chapter 5), *UGT3A1, GPR98, LMOD2* and *B7H6* genes have either zero or very low expression within the aortic valve (FKPM <0.03) and therefore they were filtered out from subsequent analysis; *HOMO, Homozygous for alternate allele; HET, heterozygous; WT, wild type; ND, not determined.

Table 4. 3. Summary of the remaining candidate genes for Family A.

Variant	Gene description	FKPM		Chr	No. of Exon	Amino acid length	MAF		B/G rNSV noise	Grantham	GERP	Polyphen
		TAV	BAV				EVS	1KGP				
PDE4DIP Ala1245Thr	phosphodiesterase 4D interacting protein	70.3	52.3	1	47	2482	0.60%	0.89%	High*	58	5.97	unknown
SLC4A2 Arg107Gln	solute carrier family 4, anion exchanger	33.8	28.2	7	23	1241	0.33%	novel	3.3%	43	4.4	probably damaging
ITGA10 Arg1161Gly	integrin alpha 10	16.1	22.1	1	30	1167	0.70%	0.55%	9.3%	125	3.11	unknown
GTF3C5 Phe474Leu	general transcription factor IIIC polypeptide 5	12.3	18.1	9	12	526	0.27%	0.18%	1.95%	22	5.13	benign
PTGES2 Gly206Ala	prostaglandin E synthase 2	8.3	11.4	9	7	377	0.74%	0.3%	1.9%	60	4.94	benign
RTP4 Gln44Lys	receptor (chemosensory) transporter protein 4	2.8	5.1	3	2	246	0.07%	0.09%	2.0%	53	3.2	probably damaging
GDNF Arg93Trp	glial cell line-derived neurotrophic factor	1	1.2	5	3	228	0.28%	0.3%	1.3%	101	4.96	probably damaging
ABCA13 Thr4550Ala	ATP-binding cassette, sub-family A (ABC1), member 13; associations with bipolar/mood disorder	0.05	0.06	7	62	5058	0.51%	0.63%	High*	58	5.35	possibly damaging
MATN1 Arg343Gln	matrilin 1 cartilage matrix protein	0.04	0.08	1	8	496	0.13%	novel	1.1%	43	3.23	possibly damaging

*Greater than 10% background noise of rNSV; ND, not detected; FKPM, Fragments per Kilobase of transcript per Million mapped reads. As a reference: FKPM of NOTCH1 in human AV is ~8; Nkx 2-5 of ~1; GATA5 of ~2.3; GATA4 of ~20; B/G rNSV noise, the prevalence rate of all rare nonsynonymous variants (MAF <1%) within a gene of interest amongst the 4298 exomes data of NHLBI EVS European American 'control' population (i.e. "the background noise of rare nonsynonymous sequence variants for a particular gene").

As shown in Table 4.2, candidate gene variants appeared to segregate in an autosomal dominant pattern with incomplete penetrance in Family A.

4.3.1.4. Linkage analysis and regions with poor coverage

As mentioned previously, an average of 13.5% of target exome had inadequate coverage amongst the 3 exome sequencing samples, with less than 10 reads per target base pair. Meanwhile, genome wide linkage analysis of Family A identified 3 regions of suggestive linkage (LOD > 1.5), 2 on chromosome 5 and 1 on chromosome 9 (Figure 4.5).

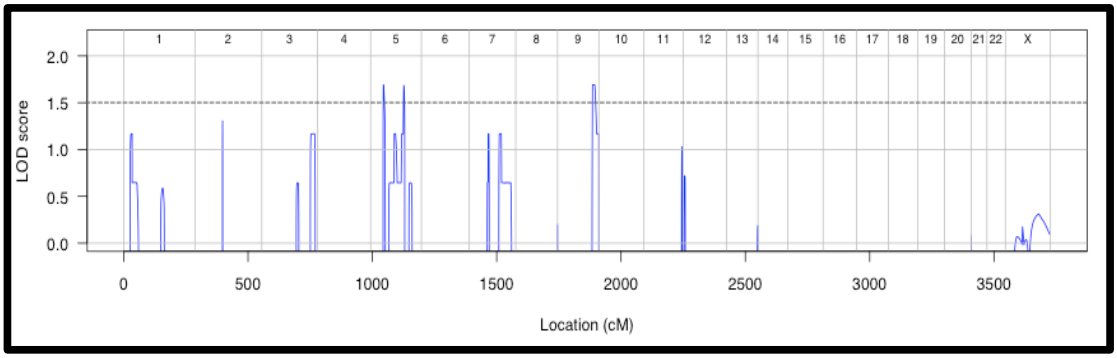

Figure 4. 5. Multipoint LOD scores from linkage analyses of Family A.

Concentrating on these 3 areas with the highest linkage peaks and the regions with poor coverage, a total of 507 exonic regions were identified to have inadequate coverage in at least 1 exome sequencing sample. Manual inspection of these regions using IGV browser confirmed 24 regions with either incomplete or absence of coverage in all 3 exome samples. These regions were later directly screened by Sanger sequencing, using proband's DNA, to look for the presence of plausible causative gene variants and the results are summarised in Table 4.4.

Table 4. 4. Screening results of the poorly covered exome sequencing regions.

Chr	Nucleotide regions		Gene	FKPM	Annotation	Variants found	IV:5	Nucleotide change	Protein change	MAF
	From	To								
5	122359080	122359698	*PPIC*	39.3	peptidylprolyl isomerase C (cyclophilin C)	rs451195	A/G	c569A>G	Asn190Ser	C=0.16
5	122425695	122426301	*PRDM6*	0.6	PR domain containing 6	None	-	n/a	n/a	n/a
5	128796795	128797450	*ADAMTS19*	0.2	ADAM metallopeptidase with thrombospondin type 1 motif, 19	None	-	n/a	n/a	n/a
5	129240523	129241324	*CHSY3*	6.2	chondroitin sulfate synthase 3	rs33917	G/C	c450G>C	Pro150=	C=0.479
5	130759616	130762984	*RAPGEF6*	2.9	Rap guanine nucleotide exchange factor (GEF) 6	None	-	n/a	n/a	n/a
5	130766552	130767042	*RAPGEF6*	2.9	Rap guanine nucleotide exchange factor (GEF) 6	None	-	n/a	n/a	n/a
5	132112800	132113067	*SEPT8*	44.4	Septin-8	None	-	n/a	n/a	n/a
5	132158012	132158805	*SHROOM1*	16.6	shroom family member 1	None	-	n/a	n/a	n/a
5	132160855	132162002	*SHROOM1*	16.6	shroom family member 1	rs2292030	C/T	c539C>T	Pro180Leu	A=0.100
9	130889718	130890474	*PTGES2*	8.4	prostaglandin E synthase 2	None	-	n/a	n/a	n/a
9	131013004	131013219	*DNM1*	18.6	dynamin 1	None	-	n/a	n/a	n/a
9	131182759	131183353	*CERCAM*	72.6	cerebral endothelial cell adhesion molecule	None	-	n/a	n/a	n/a
9	131418820	131419129	*WDR34*	15.9	WD repeat domain 34	rs4837292	G/G	c178T>G	Trp60Gly	A=0.006
9	131445934	131446286	*SET*	75.4	SET nuclear oncogene	None	-	n/a	n/a	n/a

Table 4.4 continued

Chr	Nucleotide regions		Gene	FKPM	Annotation	Variants found	IV:5	Nucleotide change	Protein change	MAF
	From	To								
9	131492067	131493673	*ZER1*	15.5	zyg-11 related, cell cycle regulator	None	-	n/a	n/a	n/a
9	131580779	131581464	*ENDOG*	2.7	endonuclease G	rs2293969	T/T	c35C>T	Ser12Leu	C=0.335
9	131909666	131911223	*PPP2R4*	48.6	protein phosphatase 2A activator, regulatory subunit 4	rs2480452	C/T	c965C>T	Ser322Leu	T=0.081
9	131937831	131940540	*IER5L*	27.3	immediate early response 5-like	rs184457	T/T	c313C>T	Pro105Ser	A=0.205
9	132397880	132400736	*ASB6*	4.9	ankyrin repeat and SOCS box containing 6	None	-	n/a	n/a	n/a
9	132427920	132428405	*PRRX2*	19.2	paired related homeobox 2	None	-	n/a	n/a	n/a
9	132510934	132511016	*PTGES*	7.1	prostaglandin E synthase	None	-	n/a	n/a	n/a
9	133884504	133884974	*LAMC3*	9.7	laminin, gamma 3	rs13286358	C/T	c75C>T	Cys25=	T=0.078
9	133884504	133884974	*LAMC3*	9.7	laminin, gamma 3	rs3739512	T/G	c219T>G	His73Gln	T=0.363
9	136419479	136419815	*ADAMTSL2*	12.8	ADAMTS-like 2	rs35767802	G/A	c1090G>A	Val364Ile	Unknown

Chr, chromosome; FKPM, Fragments per Kilobase of transcript per Million mapped reads; n/a, not applicable.

Screening of these 24 poorly covered exome sequenced regions on the proband (Individual IV:5) revealed the presence of 2 rare non-synonymous SNVs (MAF < 1%), namely *WDR34* Trp60Gly and *ADAMTSL2* Val364Ile. Genotyping of the *WDR34* variant, which resulted from c178T>G variation (rs4837292) on the proband revealed that the proband was in fact homozygous for the alternate allele. Further, *WDR34* c178T nucleotide is a poorly conserved nucleotide, which codes for a poorly conserved amino acid Tryptophan at position 60, and this substitution is predicted to be functionally tolerated by SIFT. Similarly, *ADAMTSL2* Val364Ile variant resulted from c1090G>A substitution (rs35767802) which was a poorly conserved nucleotide. Further, Valine at position 364 were found to be weakly conserved amino acid and its substitution to Isoleucine resulted in small physiochemical difference and was also predicted to be functionally tolerated by SIFT. Therefore, both variants were unlikely to be the causative variants in this family and they were excluded from further analysis.

4.3.1.5. Plausible candidate gene (GDNF) screening in unrelated sporadic BAV cohort

Following review of the literature on the candidate genes listed in Table 4.3, the gene *GDNF* (glial cell line-derived neurotrophic factor) was high on the list of possible causal variants in this family with BAV as it appeared to have functional relevance to BAV pathogenesis. It was therefore selected for screening amongst an unrelated sporadic BAV cohort. The clinical characteristics of the 130 individuals, which made up this cohort, are described

in Table 4.5. The group comprised of 81% males of predominantly Caucasian background, with a mean age of 42 ± 14 years. Most (84%) were diagnosed with BAV by the age of 40 years or earlier. BAV was present in a first-degree relative in 16% of cohort and BAV-related aortopathy was present in nearly three-quarters of the cohort.

Table 4. 5. Clinical characteristics of 130 unrelated BAV cohort.

n = 130 unrelated BAV cohort	
Male gender	105 (81%)
Current age, mean (range)	42 ± 14 (20-68) years 67% aged ≤ 50 years
Age at diagnosis	Range: 0-55 years 84% diagnosed ≤40 years old
Genetic background	90% Caucasian
Positive family history of BAV	21 (16%)
Associated aortopathy	73%
Coexisting CHD	26% - majority were CoA (79%)
Cardiovascular events	71% of patients had at least 1 surgery for BAV, the related aortopathy and/or associated CHD

CHD, congenital heart disease; CoA, coarctation of the aorta

Appendix I, Table I-4 listed the primers sequences and corresponding PCR conditions used during *GDNF* gene screening. Table 4.6 summarises the combined findings from the genetic analysis of the *GDNF* gene in this cohort and Family A. Sequencing of all the 5 exons and splice signal sequences of *GDNF*, which made up all of its 7 transcripts, revealed 2 non-synonymous (missense) variants, 1 synonymous variants, 2 intronic variants and 3 variants

in the 5'UTR (Figure 4.6). The Arg93Trp variant was identified exclusively in Family A. Meanwhile, the novel Gly105Arg variant was found in a 39 year-old unrelated male patient, who was diagnosed with BAV with a right and left coronary cusp fusion morphology at the age of 2, following investigation of a childhood murmur, and had an associated mild ascending aortic dilatation.

Therefore, *GDNF* screening in the 130 unrelated patient cohort revealed an overall 0.8% rate for the presence of rare non-synonymous (missense) *GDNF* variants in BAV. This rate was comparable to the 1.3% background noise of rare non-synonymous variants that are present in the European American EVS control cohort (*p*-value = 0.378 by Fisher's exact test).

Table 4. 6. Summary of variants found during GDNF screening in the 130 unrelated BAV cohort and Family A.

Exon no	Transcript	rsID	cDNA position	Amino acid change	Mutation type	MAF in BAV	MAF 1kGP	MAF EVS EA	Polyphen2	SIFT	GERP
5'UTR	GDNF-001	rs2973033	c.-51A>G	n/a	-	C=0.327	C=0.363	n/a	-	-	-
5'UTR	GDNF-201	rs45455796	c.-26-664A>G	n/a	-	C=0.023	C=0.014	n/a	-	-	-
5'UTR	GDNF-201	rs138709472	c.-26-591G>C	n/a	-	C=0.008	C=0.006	n/a	-	-	-
intronic	-	rs143142348	c.-26-555G>A	n/a	-	T=0.019	T=0.011	n/a	-	-	-
4	GDNF-001	rs146337283	c.72C>G	p.Ala24=	synonymous	C=0.004	n/a	C=0.000	-	-	4.79
intronic	GDNF-001	rs149499929	c.26-93A>G	n/a	-	C=0.021	C=0.008	n/a	-	-	-
5	GDNF-001	rs36119840	c.277C>T	p.Arg93Trp	missense	A=0.004	A=0.002	A=0.003	probably damaging	deleterious	4.96
5	GDNF-001	novel	c.313G>A	p.Gly105Arg	missense	T=0.004	novel	n/a	benign	tolerated	2.29

Shaded in grey is the variant found exclusively in Family A. 1kGP, 1000 Genomes Project; EVS EA, NHLBI Exome Variant Server European American population.

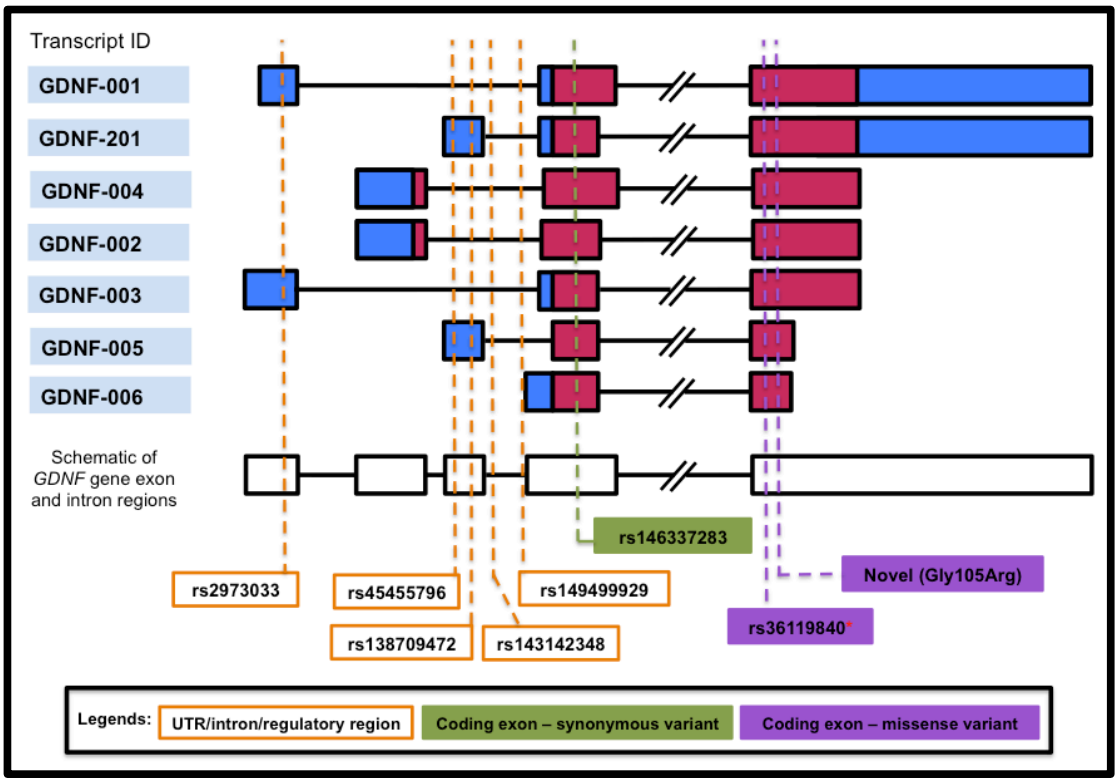

Figure 4. 6. Diagrammatic representation of all the GDNF variants found during screening of the 130 unrelated BAV cohort and Family A.

GDNF has 7 transcripts or splice variants (GDNF-001, -201, -004, -002, -003, -005 and -006) and 5 exonic regions as depicted in the figure above. The exon box shaded in blue represented the 5'- and 3'-UTR and the box shaded in maroon colour represent the coding exon regions. The positions of the variants found during the screening process were marked with dotted lines. Red asterisk marked the rare non-synonymous *GDNF* variant found in Family A (rs36119840).

4.3.2. FAMILY B

4.3.2.1. Family B Pedigree and individual characteristics

The family was of Caucasian background and the pertinent clinical information of participating family members are summarised in Figure 4.2 and Table 4.7. Of note, the proband (Individual III:3) has an identical twin brother (Individual III:2) who also has been diagnosed with BAV and ascending aortic aneurysms following family screening. Unfortunately, he declined participation into the study and no contact could be made to allow screening of his offspring. Alarmingly, the family has a strong history of sudden unexpected death affecting males in the earlier 2 generations, mostly occurring in their late 40s or early 50s. Unfortunately, due to the geographical remoteness at the time of their deaths, no autopsies were ever performed to clarify the exact cause of their deaths. Further, based on Family B's pedigree, heritability of BAV appeared to run in autosomal dominant condition with incomplete penetrance, with Individuals IV:10 and IV:11 acting as an obligate carrier for the condition. The second offspring of Individual IV:10 (i.e. V:10) was born with critical aortic stenosis at birth secondary to BAV. He required a percutaneous balloon aortic valvuloplasty to relief the critical obstruction immediately after birth, followed by a Ross procedure at 6 weeks of life to treat his condition. Of interest, Individual IV:11 reported a history of WPW syndrome and his third offspring (V:14) was born with complex CHD, which included septal defects, BAV, coarctation of the aorta and patent ductus arteriosus.

Table 4. 7. Clinical characteristics of recruited family members of Family B.

Pedigree position	Gender	Current age (years)	Valve Type	Age at diagnosis (years)	BAV Function	Comments
III:3	Male	52	BAV (R-L)	51	Mild AS	Severe ascending aortic aneurysm; AVR and aortic replacement age 52
III:8	Male	44	BAV (R-L)	33	Mild AR	Mild aortic root dilatation
IV:9	Female	31	TAV	-	-	Clinically unaffected
IV:10	Male	31	TAV	-	-	Clinically unaffected
IV:11	Male	29	TAV	-	-	History of WPW syndrome
IV:13	Female	27	TAV	-	-	Clinically unaffected
V:9	Male	6	TAV	-	-	Clinically unaffected
V:10	Male	4	BAV	At birth	Critical AS	Critical AS at birth; had PBAV followed by Ross procedure at 6 weeks
V:14	Female	2	BAV	At birth	Mild AS	Complex CHD (ASD, VSD, BAV, CoA, PDA)

n/a, not applicable; AVR, aortic valve replacement; TAV, tricuspid (tri-leaflet) aortic valve; BAV, bicuspid aortic valve; AS, aortic stenosis; AR, aortic regurgitation; R-N, right and non coronary cusps fusion BAV morphology; R-L, right and left coronary cusps fusion BAV morphology; CHD, congenital heart disease; ASD, atrial septal defect; VSD, ventricular septal defect; CoA, coarctation of the aorta; PDA, patent ductus arteriosus; PBAV, percutaneous balloon aortic valvuloplasty; WPW, Wolf-Parkinson-White syndrome.

4.3.2.2. Exome sequencing result and variants list

Exome sequencing was performed on DNA samples from Individuals III:3, III:8 and V:10 from the pedigree depicted in Figure 4.2. An average of 62,062,000 reads were generated for each individual sample and an average of 59,538,100 reads (95.9%) were mapped uniquely to the genome. Approximately 90.6% of target exome regions received more than 10 sequence reads and an average of

57 reads per target base pair was achieved for each exome. Following base identification and variant calling, each individual was identified to have an average of 75,315 SNVs. After multiple filtering steps (Figure 4.7), 32 plausible disease-causing variants were shared amongst the 3 individuals. Appendix II, Table II-2 described the 32 prioritised and filtered variants, which were included in the co-segregation analysis.

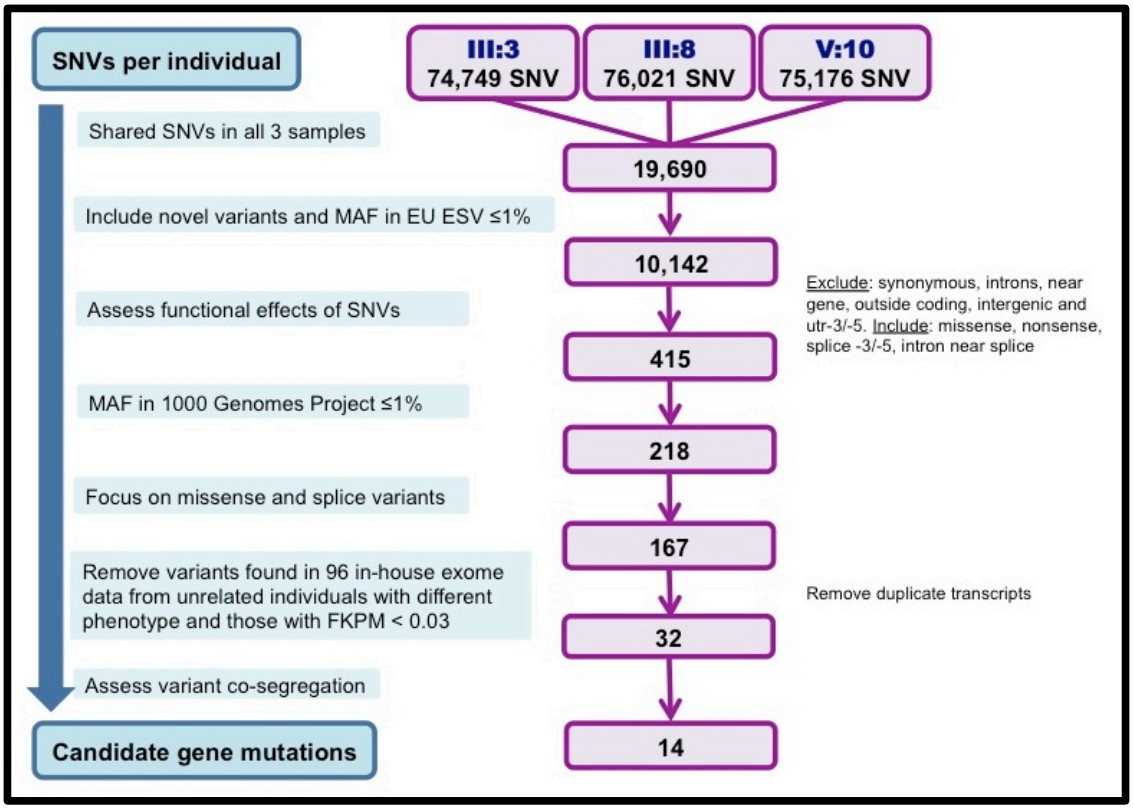

Figure 4. 7. Filtering steps used to analyse the SNVs obtained from Family B exome sequencing result.

SNV, single nucleotide variations.

4.3.2.3. Co-segregation study of Family B

Prioritised variants were subsequently analysed for their pattern of co-segregation with BAV disease amongst 8 participating family members. Apart from those who were exome sequenced, they included the child with BAV and other complex CHD (V:14) and those with phenotypically normal tri-leaflet aortic valve (IV:10, IV:11, IV:13 and V:9). The result of the segregation analysis of variants performed is summarised in Table 4.8. Table 4.9 lists the 14 remaining plausible missense variants (i.e. candidate gene mutations), which co-segregated with BAV disease amongst the 8 family members studied.

Table 4. 8. Variant co-segregation analysis of Family B.

Gene Name	Variant	BAV				TAV OBLIGATE CARRIER		TAV "NORMAL"	
		III:3	III:8	V:10	V:14	IV:10	IV:11	IV:13	V:9
ZNF226	**Thr358Met**	HET	HET	HET	HET	HET	HET	WT	HET
ZNF226	**Val83Glu**	HET	HET	HET	HET	HET	HET	WT	HET
TTF2	**Arg838His**	HET	HET	HET	HET	ND	ND	WT	WT
DENND2C	**Ser687Phe**	HET	HET	HET	HET	HET	HET	WT	WT
DMKN	**Val135Leu**	HET	HET	HET	HET	HET	HET	WT	HET
DMKN	**Thr230Met**	HET	HET	HET	HET	HET	ND	WT	HET
SMG5	**His100Gln**	HET	HET	HET	HET	HET	HET	WT	WT
RAB3A	**Tyr65Cys**	HET	HET	HET	HET	HET	HET	WT	HET
ZDHHC19	**Arg224Gly**	HET	HET	HET	HET	HET	HET	WT	HET
ETV4	**Ala426Val**	HET	HET	HET	HET	HET	HET	WT	WT
ZNF234	**Gly602Glu**	HET	HET	HET	HET	HET	ND	WT	HET
BZRAP1	**Glu1154Asp**	HET	HET	HET	HET	HET	HET	WT	WT
ERBB2	**Arg4Trp**	HET	HET	HET	HET	HET	HET	WT	WT
BRIP1	**Asn955His**	HET	HET	HET	HET	HET	HET	WT	WT
COL6A6	Gly1075Ala	HET	HET	HET	WT	HET	ND	WT	HET
SVIL	Ala765Val	HET	HET	HET	WT	HET	ND	HET	HET
RBM45	Arg137Trp	HET	HET	HET	WT	HET	WT	WT	WT

Table 4.8. continued

Gene Name	Variant	BAV				TAV OBLIGATE CARRIER		TAV "NORMAL"	
		III:3	III:8	V:10	V:14	IV:10	IV:11	IV:13	V:9
SERINC3	Val249Ile	HET	HET	HET	WT	HET	WT	ND	HET
KIAA1257	Asp68Tyr	HET	HET	HET	WT	HET	WT	HET	HET
ACVR1C	Asn100His	HET	HET	HET	WT	HET	WT	WT	WT
DEFB124	Glu71Lys	HET	HET	HET	WT	HET	WT	WT	HET
BRD7	Lys328Arg	HET	HET	HET	WT	HET	WT	HET	WT
FAM198B	Gly141Glu	HET	HET	HET	WT	HET	HET	HET	ND
POLE4	Asp117Gly	HET	HET	HET	WT	HET	ND	ND	WT
FUK	Pro392Arg	HET	HET	HET	WT	HET	HET	HET	WT
SEMA5B	Gly699Glu	HET	HET	HET	WT	HET	WT	HET	HET
MYH7B	Glu372Gly	HET	HET	HET	WT	HET	WT	WT	HET
MLKL	Leu10Arg	HET	HET	HET	WT	HET	HET	HET	WT
TIAM2	Gly595Ala	HET	HET	HET	WT	HET	ND	WT	HET
WTAP	His360Arg	HET	HET	HET	WT	HET	WT	WT	HET
ASPG	Ala442Thr	HET	HET	HET	WT	HET	ND	ND	HET

Note: Primers could not be designed to screen for the *ZNF43* Ser740Phe variant due to tandem repeats sequence. Typed in bold are the remaining candidate variants.

Table 4. 9. Summary of the remaining candidate genes for Family B.

Gene	Gene description	FKPM AV	Chr	No. of exons	Amino acid length	MAF		Grantham	GERP	PolyPhen2
						EVS	1kGP			
SMG5 His100Gln	smg-5 homolog, nonsense mediated mRNA decay factor (C. elegans)	24.8	1	22	1017	0	0	24	1.67	0.168
DMKN Thr230Met	dermokine	18.3	19	16	466	0.2%	0.13%	81	3.27	1
DMKN Val135Leu	dermokine	18.3	19	16	466	0.19%	0.13%	32	-4.62	0.566
ERBB2 Arg4Trp	v-erb-b2 erythroblastic leukemia viral oncogene homolog 2 (avian)	12.5	17	29	1226	0.02%	0	101	5.23	1
ZNF226 Val83Glu	zinc finger protein 226	6.5	19	7	95	0.64%	1.0%	121	0.59	0.005
ZNF226 Thr358Met	zinc finger protein 226	6.5	19	7	804	0.62%	1.0%	81	3.23	0.885
TTF2 Arg838His	transcription termination factor, RNA polymerase II	2.7	1	23	1163	0.59%	1.0%	29	5.1	1
ZNF234 Gly602Glu	zinc finger protein 234	2.5	19	6	701	0.62%	1.0%	98	1.89	0.999
DENND2C Ser687Phe	DENN/MADD domain containing 2C	1.6	1	21	929	0.79%	1.0%	155	5.74	1
BZRAP1 Glu1154Asp	benzodiazapine receptor (peripheral) associated protein 1	1.5	17	32	1849	0	0	45	3.41	0.461
ETV4 Ala426Val	ets variant 4	1.4	17	13	485	0.14%	0.13%	64	6.02	0.991
RAB3A Tyr65Cys	RAB3A, member RAS oncogene family	0.8	19	5	221	0	0	194	4.23	0.996
ZDHHC19 Arg224Gly	zinc finger, DHHC-type containing 19	0.4	3	8	310	0.20%	0	125	4.09	0.975
BRIP1 Asn955His	BRCA1 interacting protein C-terminal helicase 1	0.2	17	20	1250	0	0	68	2.99	0.001

AV, aortic valve; FKPM, Fragments per Kilobase of transcript per Million mapped reads, which is proportional to the level of expression of the gene of interest within the tissue sample studied.

4.4. DISCUSSION

This study sought to investigate the underlying genetic basis of BAV disease in 2 large families of Caucasian background with preponderance for BAV and its associated aortopathy by means of exome sequencing. In both families, a modest number of novel and rare non-synonymous variants were shared in the affected family members, although none of the likely pathogenetic variants segregated exclusively with the BAV phenotype. Instead, in both families, BAV heritability appeared to run in an autosomal dominant pattern with incomplete penetrance. Further, both families had a completely different list of shared candidate gene variants. While the composition of the lists of shared candidate gene variants within the 2 families, apart from the causative variant itself, was mostly determined by chance, the fact that the lists were completely different between the 2 families, and assuming that the causative variant was within the lists, implied that the causative variant responsible for BAV development in Family A and B would be different and unique to each family. These factors highlighted the complexity of BAV genetics and the likely presence of genetic modifiers or other regulatory control during BAV development.

Co-segregation analysis from the whole exome sequencing approach of Family A identified 9 heterozygous missense candidate gene variants. Although each of these mutations may have a possible role in the pathogenesis of BAV disease within the family, high on the list of possible causative genes are *GDNF*, *ITGA10* (integrin alpha 10) and *MATN1* (matrilin 1 cartilage matrix protein). A modulator of collagen fibrillogenesis in cartilaginous tissue, *MTN1*

mutations have been associated with inherited chondrodysplasias and idiopathic scoliosis (Segat et al., 2000, Montanaro et al., 2006). Located on chromosome 1p35 and mainly expressed in the cartilage, *MTN1* expression within the heart is transient, occurring solely during embryological heart development, where it has been suggested to play a role in regulating cardiac collagen fibril formation and assembly (Segat et al., 2000). Consistent with this, it is found at a very low level of expression within the adult aortic valves (FKPM <0.1, Table 4.3). The *MATN1* Arg343Gln variant is a rare variant, which has been reported at a MAF of 0.13% on the EVS database and is predicted to be possibly damaging by Polyphen. The variant is shared amongst all affected individuals of Family A and in 2 unaffected family members (IV:10 and IV:12).

Meanwhile, integrin is an integral membrane protein that is known to participate in cell adhesions and cell-surface mediated signalling. *ITGA10* gene is located on chromosome 1q21 and is primarily expressed in the cartilage, cardiac valves and fascia of skeletal muscle (Camper et al., 2001). In humans, deletion of *ITGA10* occurred as part of TAR syndrome (thrombocytopenia with absent radius), a rare autosomal recessive disorder resulting from 200-kb regions deletion at chromosome band 1q21.1 (Albers et al., 2013). Of interest, up to 30% of patients with TAR syndrome have cardiac manifestations, usually in form of atrial septal defects and Tetralogy of Fallot (Hall, 1987). The *ITGA10* Arg116Gly variant is a rare variant that has been previously reported with a MAF of 0.7% on the EVS database and is of unknown pathogenicity as predicted by Polyphen. Like the *MATN1* variant, *ITGA10* Arg116Gly is shared amongst all affected individuals of Family A and in 2 family members with

normal aortic valve (IV:10 and IV:12). It has a modest level of expression within adult aortic valve (FKPM ~19, Table 4.3).

Top on the list of putative candidate gene mutation in Family A is the *GDNF* gene. Distantly related to the transforming growth factor- β (TGF-β) superfamily, *GDNF* is a gene that encodes a highly conserved neurotrophic factor, playing an important role in promoting the survival and differentiation of midbrain dopaminergic neurons, as well as being important in kidney morphogenesis and spermatogenesis (Airaksinen and Saarma, 2002, Hiltunen et al., 2000). Mice with *Gdnf* deficiency (*Gdnf*$^{-/-}$) were observed to have total renal agenesis, pyloric stenosis, duodenal dilatation and congenital megacolon (Bahuau et al., 2001); these findings highly resembled that of *Ret* deficient mice (*Ret*$^{-/-}$), thus supporting GDNF as a ligand of *RET* (Bahuau et al., 2001). *GDNF* is expressed in adult aortic valve at a similar level of expression with Nkx2-5 (FKPM ~1, Table 4.3). This is of significance as Nkx2-5 haploinsufficiency is associated with a higher incidence of BAV in mice (Biben et al., 2000). Interestingly, a crosstalk between GDNF and NOTCH pathway had been reported where *GDNF*, through its *Ret/GFRα1* receptor activity can activate NOTCH signalling, by upregulating *Jag1* (a NOTCH ligand) expression (Kuure et al., 2005). Of note, Notch signalling pathway plays an important role during aortic valve development and mutations in *NOTCH1* has been linked to the development and calcific progression of non-syndromic BAV in humans (Garg et al., 2005, Niessen and Karsan, 2008). Additionally, previous study in developing rodent heart has revealed the presence of mRNA expression of various members of the GDNF family receptors (particularly Gfrα1 and Gfrα2) within the endocardial

cushion mesenchyme, in the developing and mature valves, and in the walls of the aorta and the pulmonary trunk (Hiltunen et al., 2000), suggesting the potential role of GDNF signalling in cardiac development. Interestingly, morphological examinations of either Gfrα1$^{-/-}$ and Gfrα2$^{-/-}$ mice hearts did not reveal any gross structural abnormalities of the atrioventricular and semilunar valves or the great vessels (Hiltunen et al., 2000). This indicates that the expression of Gfrα receptors mRNAs in valvuloseptal regions may not be essential for their proper development and that there may be compensatory or redundant mechanisms by other TGF-β superfamily members (Hiltunen et al., 2000). It is however still highly plausible that GDNF, particularly through *GFRα1* signalling, to have a modulatory role in endocardial cushion and valve development in humans. With these in mind, *GDNF* becomes an attractive candidate gene in this study.

The *GDNF* Arg93Trp variant (rs36119840) found in Family A is a rare variant that has also been previously reported with a MAF of 0.28% on the EVS database. The Arg residue at position 93 is a highly conserved amino acid amongst 14 species, down to the level of zebra fish. Its substitution to the amino acid tryptophan results in a moderate physiochemical difference (Grantham score of 101) and is predicted to be deleterious by SIFT and probably damaging by Polyphen. The *GDNF* Arg93Trp variant is shared amongst all affected individuals of Family A and is also present in 1 unaffected family member (V:1). Interestingly, the *GDNF* Arg93Trp variant has been reported to have an important modifier role on a number of human disease susceptibility, albeit in a minority of cases, including congenital central

hypoventilation syndrome, Hirschsprung disease and pheochromocytoma (Bahuau et al., 2001, Amiel et al., 2003, Woodward et al., 1997, Angrist et al., 1996). However, none of these diseases were observed amongst individuals from Family A. Further, *GDNF* screening amongst the 130 unrelated sporadic BAV cohorts showed a comparable frequency of rare missense variants amongst those with BAV and the EVS control population. This later finding thus suggests that GDNF mutations do not appear to have a major causative role in the pathogenesis of BAV in this sporadic BAV cohort. Nevertheless, it remains possible that allelic variation at the GDNF locus may still play an important role as a genetic modifier for BAV susceptibility, including in Family A.

On the other hand, co-segregation analysis of the whole exome sequencing result of Family B identified 14 missense variants amongst 12 candidate genes. Of these genes, high on the list of causative genes are *ETV4* (ETS variant 4; also known as PEA3 or polyomavirus enhancer activator 3) and *ERBB2* (v-erb-b2 avian erythroblastic leukemia viral oncogene homolog 2) variants.

A transcription factor from the ETS (E26 transformation-specific) subfamily, *ETV4* plays a role in neuronal, spermatogonial, limb and kidney development and is overexpressed in metastatic breast cancers (Clementz et al., 2011, Lu et al., 2009). Of interest, in a mouse model investigating kidney morphogenesis, *Etv4* was shown to be primarily and positively regulated by *GDNF* and normal expression of *Etv4* depends strongly on *GDNF-Ret* signalling (Lu et al., 2009). Therefore, these combined exome sequencing findings on the presence of rare nonsynonymous variants in *GDNF* gene in Family A and in ETV4 gene in

Family B might provide further support on the role of GDNF signalling in influencing BAV susceptibility, where disruptions anywhere along the pathway may promote disease development. Furthermore, recent study in human breast cancer has demonstrated a link between ETV4 and NOTCH signalling where *ETV4* (*PEA3*) can act as a transcriptional activator for both *NOTCH1* and *NOTCH4*, which are critical in breast tumorigenesis (Clementz et al., 2011). *ETV4* can also partner with other activators to regulate genes such as *MMP-1/-3/-7/-9* and, notably, *ERBB2* (Clementz et al., 2011), the second candidate gene in Family B. The *ETV4* Ala426Val variant is found at a MAF of 0.14% in the EVS database with a low level of expression in the aortic valve (FKPM 1.4, Table 4.9). Alanine at position 426 is a highly conserved amino acid and its substitution to Valine is predicted to be probably damaging by PolyPhen2 (score of 0.991). The variant is present in all affected members of Family B and in the obligate carriers, but are absent in Individual IV:13 and V:9 (Figure 4.5).

Finally, the *ERBB2* Arg4Trp is found extremely rarely amongst the EVS cohort (MAF 0.02%). The Arg residue at position 4 is a highly conserved amino acid. Its substitution to the amino acid tryptophan results in a moderate physiochemical difference (Grantham score of 101) and is predicted to be damaging by Polyphen2 (score of 1). Similar to the ETV4 variant, the ERBB2 variant is present in all affected members of Family B and in the obligate carriers, but are absent in Individuals IV:13 and V:9 (Figure 4.5). The receptor *ERBB2* is a member of the epidermal growth factor receptor family and its overexpression correlates with a worse prognosis for breast cancer patients (Lee et al., 1995). *ERBB2* has also been shown to be important in cardiac

development and its absence resulted in embryonic lethality of the mutant *erbB2* null mice, associated with a lack of cardiac trabeculation and maturation (Lee et al., 1995). Additionally, a significant decrease (30%) in *Erbb2* mRNA expression has been observed amongst the *Tie2-cre*$^{+}$*Gata5*$^{fl/fl}$ transgenic mouse model, which has a 7x higher incidence of BAV development compared to the wild-type littermates (Laforest et al., 2011). This places *ERBB2* as an attractive gene candidate for BAV development in Family B.

The high preponderance for BAV observed in Families A and B provides support for a genetic basis of BAV disease. Whilst whole exome sequencing analysis from both families produces a different list of candidate gene variants, GDNF-related pathway appeared to be mutually affected in both families. This provides a clue towards its potential regulatory role in BAV development, which warrants further investigation.

This study has a number of limitations that need to be acknowledged. As discussed in Chapter 1.4.3, exome sequencing approach can present a technical or analytical bioinformatics challenge. The true causative mutation might be missed if the variant was located outside the target definition (e.g. unannotated genes or non-coding/regulatory variants) or in regions with inadequate coverage. The criteria imposed for variant prioritisation and for a variant to be classified as putative pathogenic mutation in this study may be too stringent and thus the causal variant may have been excluded in the process; for example, the GERP cut off or the aortic valve expression level (i.e. FKPM value of < 0.03) could be too high. Further, genes that are active during

cardiogenesis may not necessarily be expressed in adult cardiovascular structures. Therefore, using aortic valve RNA expression level to guide variant prioritisation, albeit being set at a very low level, may result in unintentional exclusion of pathogenic variant. Additionally, recent study has reported the role of rare copy number variants (CNV) in the development of congenital left sided heart disease, including BAV (Hitz et al., 2012). CNV analysis however was not done as part of this study. Thus, transmission of a copy number variant cannot be ruled out as an underlying contributor to BAV in these 2 families. Furthermore, the co-segregation studies in both families have been unsuccessful in identifying a single causative mutation. This is contributed by the lack of additional family members in the pedigree to further filter out the non-causative variants. Therefore, this is an ongoing study that needs to be continued upon further recruitment of additional family members into the study.

Overall, this study highlights the fact that, even in familial cases of BAV with multiple affected family members, identification of the underlying genetic aetiology can be very challenging. Whilst whole exome sequencing provides a powerful and unbiased approach to study BAV genetics, it is associated with significant bioinformatics challenges, including that which relates to the assessment of the functional significance and causality of novel or rare sequence candidate gene variants, identified by exome sequencing, on disease pathogenesis. Nevertheless, the rapid pace of change in sequencing technologies will continue to transform clinical medicine, and cardiovascular disease is no exception. As exome sequencing becomes the method of choice for identifying the genetic causes of heritable cardiovascular disorder, such as

BAV, ongoing incorporation of clinical information provided by family screening and development of robust approaches to interpret the significance and define pathogenicity of segregating rare variants will continue to be very important.

CHAPTER 5: RNA SEQUENCING IN THE INVESTIGATION OF PHENOTYPE HETEROGENEITY OF STRUCTURAL VALVE DEGENERATION IN HUMAN BAV DISEASE

5.1. INTRODUCTION

Bicuspid aortic valve (BAV) is the most common congenital cardiovascular malformation, affecting 1.3% of the general population (Michelena et al., 2011, Siu and Silversides, 2010). BAV is an important risk factor for aortic valve disease and ascending aortic aneurysm (Michelena et al., 2011, Padang et al., 2012b, Cripe et al., 2004). Structural aortic valve degeneration (SVD), and consequent valve dysfunction, is the most common complication of BAV disease, which often occurs prematurely and is responsible for up to one-thirds of aortic valve replacement in the Western world (McKellar et al., 2010, Michelena et al., 2011, Michelena et al., 2008). Valve dysfunction in BAV ranges from predominantly stenotic lesions with heavy valve calcification and/or fibrosis to predominantly regurgitant lesions with leaflet prolapse, fibrotic retraction, malcoaptation from aortic root dilatation, or leaflet destruction from infective endocarditis. Furthermore, whilst BAV underlies 70%-85% of stenotic aortic valve in children and over 50% of aortic stenosis in adults (Cripe et al., 2004), different pathological processes appear to be present. In newborn infants or young children, BAV-related stenosis is a consequence of thickened leaflets with severe restriction in valve orifice opening (Siu and Silversides, 2010, Tutar et al., 2005), probably signifying a more severe disorder of aortic valvulogenesis. Meanwhile, premature leaflet sclerosis and calcific degeneration from the abnormal hemodynamic shear stress likely to be responsible for BAV-related stenosis during adulthood (Siu and Silversides, 2010, Tutar et al., 2005). In contrast, although any degree of aortic regurgitation can be detected in up to 59% of community cohort with BAV during

echocardiography, intervention for isolated severe aortic incompetence is relatively uncommon in BAV, affecting only 3-7% of patients (Michelena et al., 2011, Tzemos et al., 2008, McKellar et al., 2010). These facts highlight the wide spectrum of clinical manifestation and outcome of SVD and valve dysfunction in BAV. Detection of BAV-related SVD is important, as it is an independent predictor of long-term cardiovascular events, including aortic valve surgery and cardiac death, even in patients with normally functioning BAV at baseline (Michelena et al., 2008).

High heritability rate and familial clustering strongly imply that BAV has an underlying genetic basis (Cripe et al., 2004). In humans, mutations of the transcription factor *NOTCH1* gene are associated with limited cases of familial and sporadic BAV, as well as aortic valve calcification, possibly as a result of derepression of *RUNX2*, a downstream transcriptional regulator of osteoblast cell fate (Garg et al., 2005). Recently, the presence of rare non-synonymous variations within the conserved transcriptional activator domains of *GATA5*, a transcription factor essential to cardiac and aortic valve development, were reported in patients with BAV (Chapter 3) (Padang et al., 2012a). Additionally, orchestrated regulation of gene transcription is essential during cardiac development and valvulogenesis, and disruption to this process likely contributes to various cardiac pathologies, including BAV. Microarray profiling of microRNA regulators of gene expression highlighted reduced expression of miR-26a, miR-30b, and miR-195 in stenotic BAV associated with calcification, compared with a regurgitant BAV phenotype (Nigam et al., 2010). These microRNAs were shown to modulate the mRNA levels of several calcification-

related genes in-vitro (Nigam et al., 2010). Further, exon microarray profiling has revealed altered gene expression and mRNA splicing in the myocardium of patients with hypoplastic left heart syndrome, a condition that is genetically related to BAV disease (Hinton et al., 2009, Ricci et al., 2012). Despite these recent insights, the molecular mechanism underlying the development of phenotype heterogeneity of SVD in BAV disease however remains incompletely understood. Further, clinical risk prediction of individual patient's outcome is imprecise and there are currently no treatments to slow or prevent aortic valve degeneration.

The tissue transcriptome contains the entire repertoire of all transcripts expressed in a given tissue of an organism. Presently, transcriptome analysis using next generation sequencing technologies (RNA-seq) is becoming a preferred method of choice over hybridisation-based microarray profiling (Kogenaru et al., 2012). Advantages of RNA-seq include a large dynamic range of expression levels that is not affected by on-chip sequence biases, low background signal due to perfect matching of sequencing reads, single base resolution of transcription boundaries, and the relatively small amount of total RNA required for quantification when compared to microarray (Kogenaru et al., 2012). This current study utilised RNA-seq to profile and compare the transcriptomes of non-calcified, primarily regurgitant BAV and calcified, primarily stenotic BAV subtypes with calcified stenotic (degenerative) tricuspid aortic valves (TAV), and highlight molecular pathways that are disrupted following valve degeneration in BAV disease.

5.2. METHODS

5.2.1. Study population and aortic valve collection

Patients with BAV or TAV, referred for aortic valve or aortic root surgery at the Royal Prince Alfred Hospital, Sydney, Australia, were prospectively recruited from May to December 2012. Patients with a history of rheumatic heart disease, infective endocarditis or connective tissue disorders were excluded. All patients underwent clinical evaluation that included family history and pre-operative 2D-echocardiography where the morphology and functional state of the aortic valve was determined according to the American Heart Association and the American College of Cardiology guidelines (Bonow et al., 2008). The aortic valve morphology and the presence of SVD, as signified by the extent of leaflet calcification, thickening, prolapse and/or redundancy, were documented at surgery. Calcification was graded mild (<1/3 leaflet area affected) or severe (>2/3 leaflet area affected). Immediately following surgical removal, a portion of the aortic valve leaflet was immersed in RNA*later* solution (Ambion Inc, Austin, TX) overnight and stored at -80°C.

All patients gave written informed consent and the study was approved by the Sydney South West Area Health Service Ethics Committee.

5.2.2. RNA isolation

Total valve RNA was isolated from the non-calcified portion of the leaflets using TRIzol Reagent (Invitrogen, Life Technologies, CA, USA), using methods described in Chapter 2.4.2.1. RNA purity, concentration and integrity were

evaluated using a combination of Nanodrop 2000 spectrophotometer (Thermo Scientific, MA, USA), 2100 Bioanalyzer (RNA6000 Nano LabChip, Agilent Technologies, Santa Clara, CA, USA), and/or agarose gel electrophoresis.

5.2.3. RNA sequencing and gene expression analysis

RNA-seq was performed on 8 male, DNAse I treated RNA samples having RNA integrity number (RIN) ≥ 7 (3 TAV, 5 BAV) (BGI Facility, Hong Kong). The specific steps involved in RNA-seq, including library construction, sequencing and bioinformatics analyses, were detailed in Chapter 2.4.4.

Briefly, Illumina TruSeq RNA-seq library (Illumina, San Diego, CA, USA) was prepared on 5μg total RNA according to the manufacturer's instructions, and 100 base paired-end sequenced on a HiSeq2000 (Illumina). FASTQ files were aligned to the human reference sequence (NCBI GRCh37/hg19) using Bowtie and TopHat2 v2.0.6 (Kim et al., 2013) with a transcriptome-index to guide mapping of splice junction-spanning reads (ftp://ftp.ensembl.org/pub/release-73/gtf/homo_ sapiens/Homo_sapiens.GRCh37.73.gtf.gz). Aligned reads in BAM format were then annotated against the protein-coding mRNA regions. SeqMonk v.0.24.1 platform (Babraham Bioinformatics, Cambridge UK) were utilised to visualise the annotated/mapped read (Figure 5.1), quantify data (using corrected $\log_2$ transformed Reads Per Million Values of non-strand specific, unmerged isoform) and perform percentile normalisation. An intensity difference analysis method (Brien et al., 2013) were used to identify differentially expressed genes (DEGs) on the normalised quantification data. A gene was classified as up- or downregulated using a cut-off value of more or

less than 1.5-fold expression difference, respectively, between BAV versus TAV, with an adjusted p-value <0.05, following post-hoc Bonferroni correction. A small number of unannotated genes with uncharacterised protein were excluded from subsequent analysis.

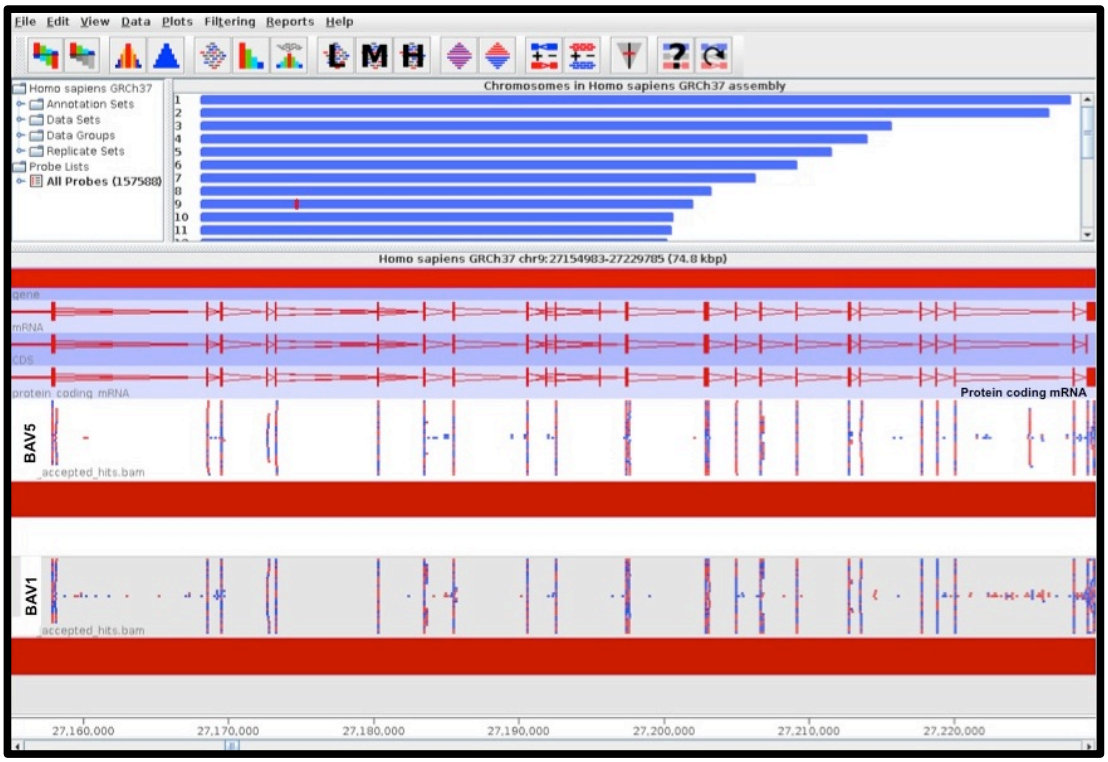

Figure 5. 1. Example of visualisation of mapped reads in SeqMonk platform over a well-covered region of a gene in Chromosome 9 in 2 BAV samples.

SeqMonk was also utilised to perform hierarchical clustering and heat map analysis of DEGs. Ingenuity Pathway Analysis (IPA) and PANTHER (www.pantherdb.org) were used to assess biological networks and pathways connected to the DEGs. Gene Ontology (GO)-based enrichment and KEGG pathway analysis of DEGs were performed against a background list of global

aortic valve protein-coding mRNAs expression, using the Database for Annotation, Visualisation and Integrated Discovery (DAVID) bioinformatics resources (version 6.7; NIH). Enrichment score of ≥ 1.3 and Benjamini-Hochberg corrected p-value <0.05 were used as a cut-off for significance.

5.2.4. Reverse transcription quantitative PCR (RT-qPCR)

As described in Chapter 2.4.2.2, RT-qPCR was performed using EXPRESS SYBR® GreenER qPCR SuperMix (Invitrogen, Life Technologies, CA, USA) on a Mx3000P and data analysed using MxPro qPCR software v.2.0 (Stratagene, La Jolla, CA, USA). Two reference genes (*GAPDH* and *TFRC*) were used to calculate the normalisation factor by geNorm v.3.4 algorithm (Vandesompele et al., 2002). Relative amounts gene-of-interest expression were normalised to the reference genes expression. RT-qPCR primer sequences were listed in Appendix 1, Table I-5.

5.2.5. Statistical analysis

Normally distributed data were reported as mean ± standard deviation (SD). Statistical evaluation of parametric data was performed with a two-tailed unpaired Student's t-test using Welch's correction for data with unequal variance. Statistical analysis of RT-qPCR data was performed on the normalised relative expression level using the Kruskal-Wallis test with *post-hoc* Dunn's test for 3 groups comparison and a Mann-Whitney unpaired t-test for 2 groups comparison. A $p < 0.05$ was considered statistically significant. Statistical analyses were performed using GraphPad Prism v.6.0b (GraphPad Software, La Jolla, California, USA).

5.3. RESULTS

Between May 2012 to December 2012, aortic valve leaflets from 36 unrelated patients were collected and their RNAs extracted. Nine of these RNAs were excluded due to poor quality (i.e. degraded RNAs), thus leaving total RNAs from the remaining 27 suitable samples (21 BAV and 6 TAV samples) for RT-qPCR analysis (Figure 5.2). Of these, 5 BAV and 3 TAV RNA samples with a RIN >7.0 underwent RNA-seq analysis. Clinical characteristics of the 8 patients comprising the RNA-seq cohort were described in Table 5.1; all were males and predominantly Caucasian. The three TAV patients had severe calcific (degenerative) aortic stenosis and were significantly older at surgery (71±8 years vs. 53±12 years, p=0.038) compared to the BAV patients, of which two had severe calcific aortic stenosis, one had mild aortic stenosis and two had moderate or severe aortic regurgitation.

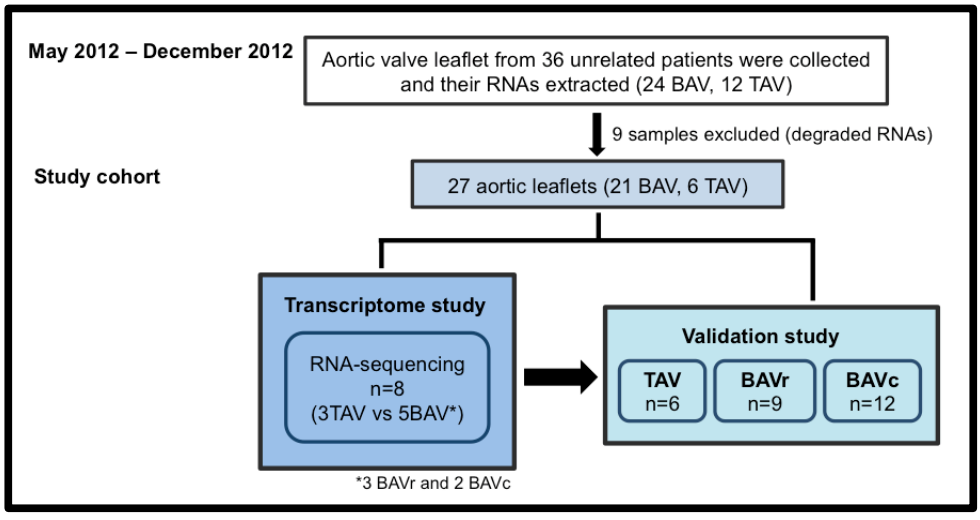

Figure 5. 2. Study outline: aortic valve collection and allocations.
BAV = bicuspid aortic valve; TAV = tricuspid aortic valve; BAVr = BAV with leaflet redundancy and either none or no more than mild calcification; BAVc = BAV with heavy leaflet calcifications.

Table 5. 1. Characteristics of patients in RNA sequencing cohort.

Patient	Background	Sex	Age at surgery	Age at diagnosis	Family History	BAV subtype	Predominant AV function	Leaflet calcification*	Ascending aorta dimension#
TAV1	Caucasian	M	71	-	-	n/a	Severe AS	+++	Normal
TAV2	Caucasian	M	64	-	-	n/a	Severe AS	+++	Mildly dilated
TAV3	Caucasian	M	79	-	-	n/a	Severe AS	+++	Mildly dilated
BAV1	Asian	M	55	27	No	R-L cusps fusion	Severe AR	-	Severely dilated
BAV2	Caucasian	M	63	62	No	R-L cusps fusion	Moderate AR	+	Severely dilated
BAV3	Caucasian	M	33	33	No	R-L cusps fusion	Mild AS	+	Severely dilated
BAV4	Caucasian	M	56	55	Yes	True bicuspid	Severe AS	+++	Moderately dilated
BAV5	Caucasian	M	59	41	No	R-N cusps fusion	Severe AS	+++	Moderately dilated

*denotes the degree of leaflet calcification, ranging from '+++' for heavily calcified leaflets (>2/3 leaflet area affected), '+' for very mild calcification (<1/3 area affected) to '–' for no calcification; #ascending aortic size was graded as normal (<38mm), mildly (38mm to <45mm), moderately (45mm to <50mm) or severely (≥50mm) dilated; AV, aortic valve; TAV, tricuspid aortic valve; BAV, bicuspid aortic valve; M, male gender; R-L, right and left; AS, aortic stenosis; AR, aortic regurgitation; n/a, not applicable.

5.3.1. Differential gene expression profiling in BAV and TAV

Global gene expression levels of BAV (n=5) and TAV (n=3) demonstrated significant correlation (Pearson's R=0.992; Figure 5.3). Intensity difference analysis revealed differential expression of 1,102 probe sets, corresponded to 59 and 177 genes, that were significantly up- or downregulated, respectively, in BAV (Table 5.2; full list in Appendix III, Table III-1). Notably, 7 of the 10 most significantly up- and downregulated genes were involved in extracellular matrix production and degradation, namely matrix metalloproteinases 13 and 9 (*MMP13, MMP9)*, *LAMC3* (laminin, gamma 3)*, CHAD* (chondroadherin), *IBSP* (integrin-binding sialoprotein), *COL11A1* (collagen, type 11α1) and *SPP1* (osteopontin).

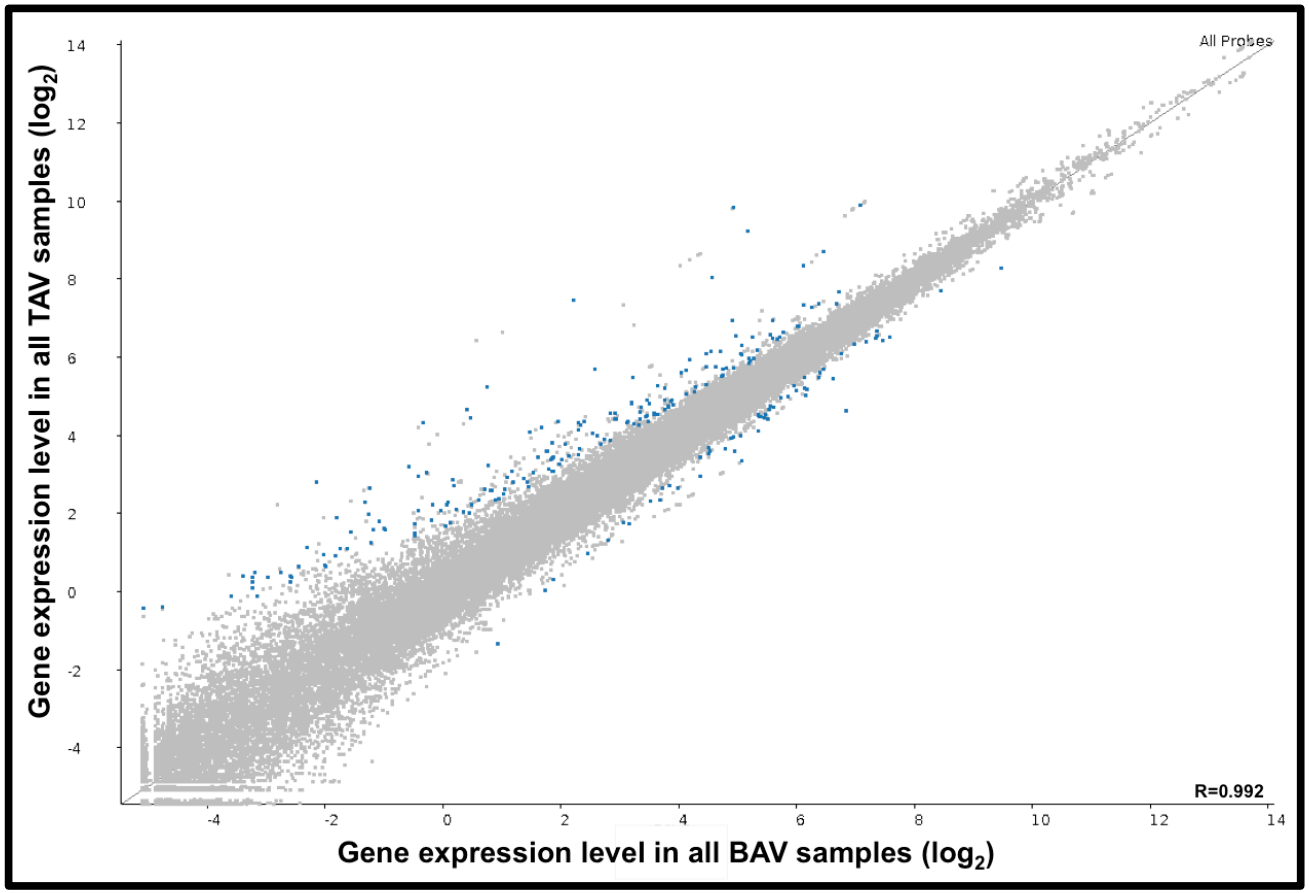

Figure 5. 3. Intensity difference of expressed genes in BAV versus TAV samples.

Gene expression levels were presented in log_2 scale. Each dot represents a probe set present for every gene analysed on SeqMonk. The blue coloured dots represent differentially expressed genes in the BAV versus the TAV samples.

Table 5. 2. Top 10 genes up- and downregulated in BAV versus TAV group, based on statistical significance.

UPREGULATED GENES				DOWNREGULATED GENES			
Gene symbol	**Gene annotation**	**Fold change**	**Adjusted p-value**	**Gene symbol**	**Gene annotation**	**Fold change**	**Adjusted p-value**
HLA-DRB5	major histocompatibility complex, class II, DR beta 5	4.68	0	*HBB*	haemoglobin, beta	-4.11	0
SPOCK3	sparc/osteonectin, cwcv and kazal-like domains proteoglycan (testican) 3	3.35	5.37E-09	*HBA2*	haemoglobin, alpha 2	-4.75	0
LAMC3	laminin, gamma 3	2.11	8.32E-06	*COL11A1*	collagen, type XI, alpha 1	-4.84	0
IGSF10	immunoglobulin superfamily, member 10	2.19	1.18E-05	*SPP1*	secreted phosphoprotein 1	-7.07	0
NR1D1	nuclear receptor subfamily 1, group D, member 1	2.24	3.40E-05	*IBSP*	integrin-binding sialoprotein	-8.65	0
HLA-DQB1	major histocompatibility complex, class II, DQ beta 1	2.56	4.81E-05	*MMP9*	matrix metallopeptidase 9 (gelatinase B, 92kDa type IV collagenase)	-11.08	0
CHAD	chondroadherin	2.06	1.28E-04	*CD79A*	CD79a molecule, immunoglobulin-associated alpha	-15.80	0
MUC20	mucin 20, cell surface associated	2.67	4.44E-04	*IGJ*	immunoglobulin J polypeptide	-16.73	0
CLU	clusterin	2.28	5.15E-04	*MMP13*	matrix metallopeptidase 13 (collagenase 3)	-19.06	0
POLR2J2	polymerase (RNA) II (DNA directed) polypeptide J2	2.15	5.95E-04	*RP11-1280I22.1*	Plasma cell-induced resident endoplasmic reticulum protein	-25.56	0

p-value adjusted for Bonferroni correction.

Amongst these 236 differentially expressed genes (DEGs), IPA identified 4 major biological networks whose functions were broadly involved in connective tissue disorders, tissue morphology, cardiovascular system development and function, immune cell trafficking and cell-to-cell signalling and interaction (Table 5.3). Exploration of GO-related terms similarly revealed overrepresentation of extracellular matrix component and biological processes involving inflammatory response, ossification, homeostatic and collagen metabolic process (Table 5.4). Specific biological functions most significant to the DEGs and considered to be pertinent to BAV development and aortic valve degeneration, including calcium signalling, connective tissue development, fibrosis and proteolysis, were presented in Appendix III, Table III-2.

Hierarchical clustering and heat mapping of the DEGs indicated differences in the overall gene expression between BAV and TAV (Figure 5.4). Furthermore, heterogeneity within the BAV group was apparent as distinct expression patterns separated BAV patients with leaflet redundancy/prolapse and no more than mild leaflet calcifications (BAVr) from patients with heavily calcified BAV leaflets (BAVc). Expression pattern of BAVc group appeared to be an “intermediate pattern” that more resembled the TAV group (particularly sample BAV5) and in some contrast to BAVr. Closer inspection of quantitative data of DEGs expression within each individual samples further supported this observation (data not shown).

Table 5. 3. Gene network functions of DEGs between BAV vs TAV samples as determined by IPA.

	Associated network functions	No. of genes in network	IPA score*	Upregulated genes	Downregulated genes
Network 1	Connective tissue disorders, inflammatory disease, skeletal and muscular disorders	87	144	*CLU, COL13A1, COL6A6, CPAMD8, ERAP2, GATA4, HLA-DQB1, HLA-DRB5, HNRNPD, LTBP4, MAPT, PTN, RIMS4, TNXB*	*A2M, ACAN, ACP5, ADCYAP1, ADRA2A, APOC1, APOC2, APOC4, BGLAP, CCL3, CCL4, CCL7, CCL14, CCL19, CCL21, CCL3L1/CCL3L3, CD53, CD3E, CD79A, COL10A1, COL11A1, COL2A1, CTSG, CXCL5, CXCL9, CXCL13, DPP4, EMR1, F3, FCGR1A, FCRL3, FGR, FLT4, GPR68, GZMA, GZMB, GZMK, HBA1/HBA2, HBB, HDC, HLA-DOB, HLA-DQB2, IBSP, IGJ, IGLL1/IGLL5, IL1RN, IRF4, ITGA7, ITGAL, ITGAX, KIT, KRT18, MATK, MMP1, MMP7, MMP9, MMP13, MMRN1, MS4A1, NR5A2, PAX5, PLAU, POU2AF1, PPBP, SDC1, SP7, SPIB, SPP1, SRGN, TM4SF18, TPSAB1/TPSB2, VCAM1, ZAP70*
Network 2	Haematological system development and function, tissue morphology, cellular function and maintenance	64	98	*ARHGDIG, EYA1, GBP3, GSTM1, HAND2, LAMC3, PLCH1, POLR2J2/POLR2J3, RASA4B, SYNM, TCEAL2, UPK3BL*	*ACP5, APLN, BHLHA15, CD79A, CHI3L1, CHI3L2, CHIT1, CHST1, COL11A1, CPA3, CRHBP, CST7, CXCL5, DACH1, DDX39B, DEFA1, DLL4, EGFLAM, GLRX, GREM1, HDC, HMOX1, IGLL1/IGLL5, IKZF3, IL21R, ITGAL, LTB, MAT1A, MFAP5, MMP13, MS4A7, NDUFA4L2, NELL2, NFASC, NUP210, PAX5, PCDH18, PIM2, PLVAP, PNP, RASSF6, RGS16, SLC7A2, SMOC2, SP7, STMN2, TMEM119, TP53I11, TPSD1, TSPAN10, ZFAT, ZNF266*
Network 3	Connective tissue disorders, cellular movement, cardiovascular system development and function	59	86	*ATOH8, CHAD, CHST9, DBP, DSP, HLF, MAPK4, MASP1, MATN4, MUC20, NR1D1, NR1D2, NSG1, PER1, PIK3IP1, PKP2, SLC14A1, SPOCK3, TEF*	*ACAN, AQP9, ATP6VOD2, CBLN4, CCL3, CCL4, CCL7, CMA1, COL11A1, COL2A1, DNASE1L3, EBF2, FAIM3, FMO3, GPHA2, GREM1, IFI30, IGLL1/IGLL5, IKZF3, KLK4, LBH, LRRC15, MMP7, MMP13, PCDH17, PILRA, PLA2G2D, PRND, SCUBE1, SDS, SGCA, SLC11A1, SLPI, SMOC1, SP7, TDO2, TINAGL1, TMC8, UCP2, WNT7A*
Network 4	Cellular movement, cell-to-cell signalling and interaction, immune cell trafficking	38	46	*C1orf51, CLU, CNTFR, GFAP, IGSF10, KIRREL3, MYH10, PDZRN4, S100B, SLC6A1, TMEM56*	*A2M, ACP5, AMPD1, AOAH, APOC2, BMP3, CLEC5A, DERL3, FCRL5, GPIHBP1, GZMA, HBA1/HBA2, ITK, KCNK2, KIT, MMP9, PNOC, SLAMF6, SLAMF7, SLC2A3, SLC2A5, THNSL2, TM4SF19, TREM1, TREM2, TSPAN13, ZAP70*

*IPA score is based on a p-value calculation, representing the likelihood that the differentially expressed genes are part of a network therein by random chance alone. Mathematically, the score is the negative exponent of the right-tailed Fisher's exact test. DEGs, differentially expressed genes.

Table 5. 4. Enrichment clusters of up- and downregulated genes in BAV (BAV1-BAV5) vs TAV based on GO terms.

	GO classification	Specific GO term	Number of genes	Benjamini-Hochberg*	Enrichment score
Upregulated genes	**Cellular constituent**	Extracellular region	16	4.3E-3	4.24
		Extracellular matrix	7	1.2E-2	3.12
	Molecular function	Glycosaminoglycan binding	5	6.6E-3	3.12
		Protein dimerization activity	7	3.2E-2	2.27
		Structural constituent of cytoskeleton	4	6.0E-3	1.32
Downregulated genes	**Biological process**	Inflammatory response	20	16.1E-12	15
		Homeostatic process	16	1.8E-2	5.92
		Biological adhesion	18	1.9E-4	4.12
		Extracellular matrix organisation	8	5.2E-4	3.48
		Ossification	7	9.3E-3	3.32
		Collagen metabolic process	4	2.7E-2	2.53
		Leucocyte activation	11	3.1E-4	2.49
		Regulation of response to external stimulus	7	2.4E-2	2.09
		Positive regulation of cell proliferation	11	1.3E-2	1.99
	Cellular constituent	Extracellular region	76	1.7E-26	34.92
		Plasma membrane	52	3.8E-3	4.68
		Integral to plasma membrane	16	3.0E-2	4.23
		Proteinaceous extracellular matrix	14	2.1E-3	3.48
		Extracellular matrix part	8	4.2E-3	2.04
		High-density lipoprotein particle	4	2.8E-2	1.6
		Secretory granule	7	4.6E-2	1.42
	Molecular function	Chemokine activity	11	1.4E-9	5.92
		Serine-type endopeptidase activity	10	6.4E-3	4.64
		Extracellular matrix structural constituent	6	1.0E-3	3.48
		Polysaccharide binding	6	4.5E-2	2.25
		Protein dimerization activity	12	4.2E-2	2.17
		Calcium ion binding	20	9.1E-4	1.91

*Benjamini-Hochberg globally corrected enrichment p-value <0.05 was considered statistically significant; GO = gene ontology.

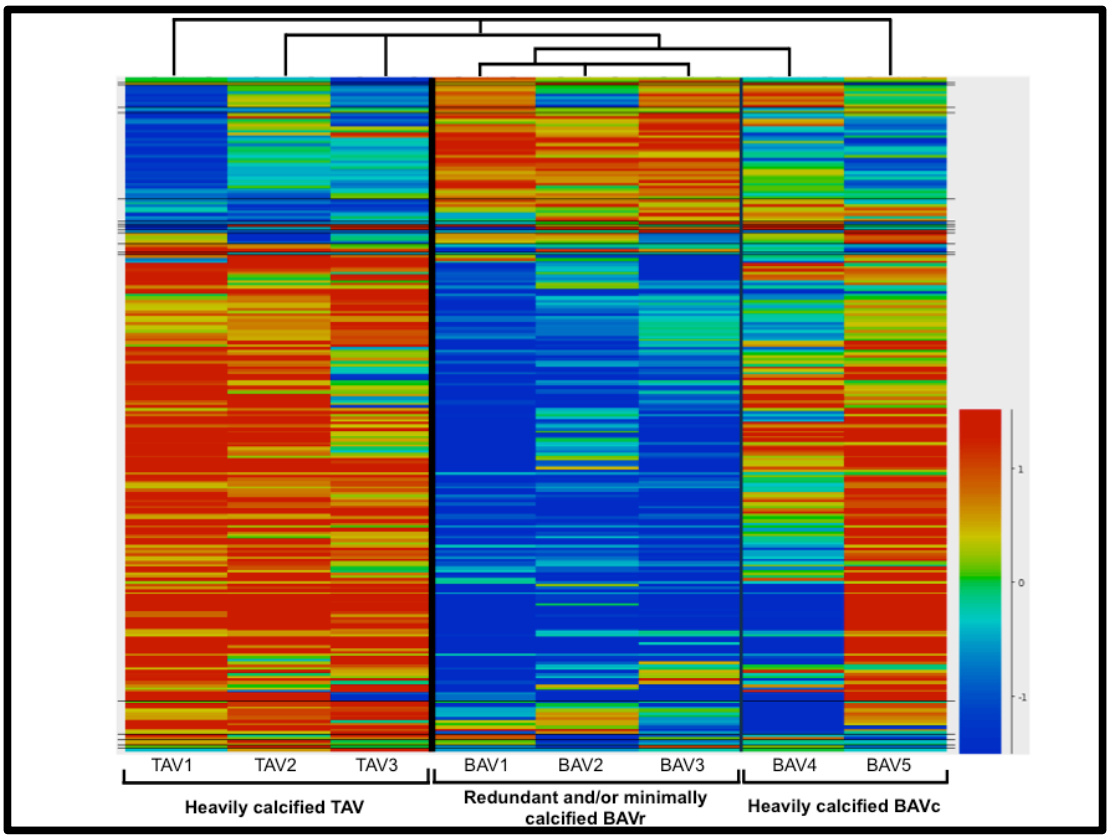

Figure 5. 4. Hierarchical clustering and heat map in BAV and TAV.
Hierarchical clustering indicated heterogeneity within the BAV group, separating those with heavy calcification (BAVc; BAV4-BAV5) from those with redundant leaflets and no more than mild calcification (BAVr; BAV1-BAV3). The expression pattern of BAVc represented an intermediate group, with more resemblance to the TAV group (particularly sample BAV5).

5.3.2. Comparative analyses of DEGs in subgroups

Given the heterogeneity observed within the BAV group during hierarchical clustering and heat map analysis, DEGs were evaluated between the different combinations of subgroup pair, i.e. BAVr versus TAV; BAVr versus BAVc; and BAVc versus TAV. Overall, BAVc versus TAV group analyses yielded the smallest number of DEGs (Figure 5.5) with a narrower range in the degree of

fold-change in gene expressions, compared to the other 2 subgroup pairs. Eighty out of 193 DEGs (41%) in BAVc versus TAV group had <2-fold change in their mRNA expression level, whilst none of the 265 DEGs in BAVr versus BAVc group and only 1 out of 224 DEGs (0.4%) in BAVr versus TAV group had a similar degree of alteration (Appendix III, Table III-3, III-4 and III-5). Further, side-by-side comparison of selected extracellular matrix and cardiac-related genes-of-interest revealed similar trend in the direction of change (up- or downregulation) and the degree of fold change in BAVr versus BAVc and BAVr versus TAV group. Dysregulation of these genes were however less notable in BAVc versus TAV group (Appendix III, Table III-6). These observations suggested that BAVc expression pattern was more similar to the TAV rather than the BAVr group.

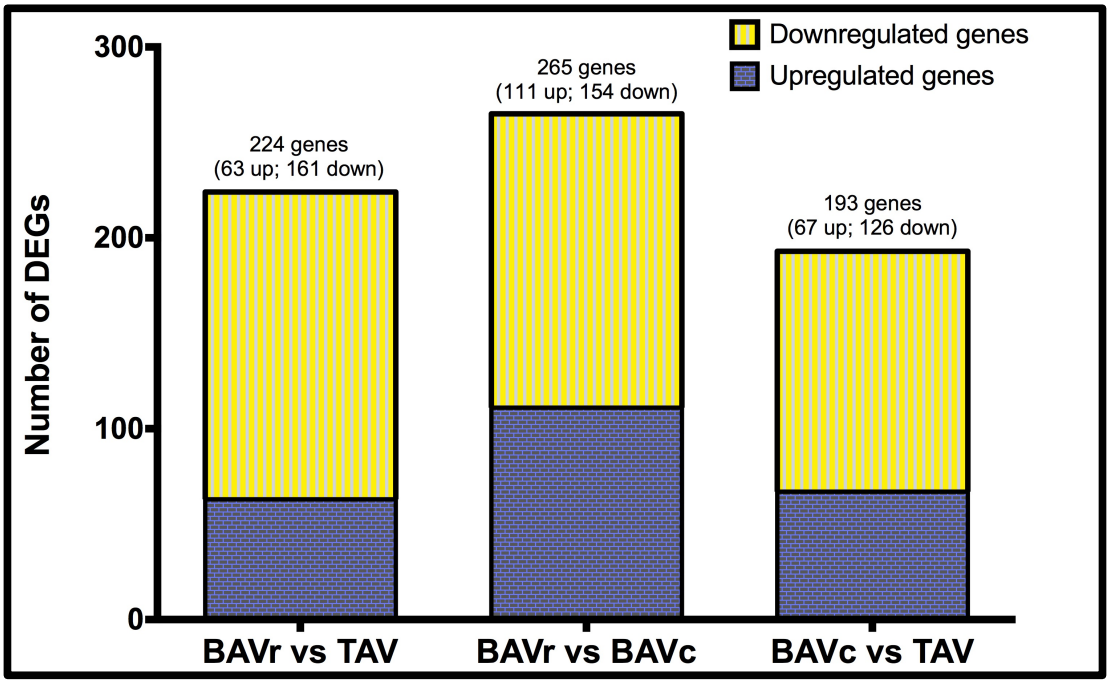

Figure 5. 5. Bar graph comparing the number of DEGs amongst the different subgroup pairs.

Analyses of GO-related terms enrichment clusters from the different comparative subgroup analyses revealed that dysregulation of extracellular matrix genes and focal adhesion-related genes to be a common feature of SVD amongst the 3 comparative subgroups (Appendix III, Table III-7A, III-7B and III-7C). Meanwhile, ossification and inflammatory response gene clusters overexpression were notable in both BAVc and TAV when compared to the BAVr.

5.3.3. Validation of RNA-seq data

Total RNA isolated from 31 aortic valve leaflet preparations obtained from 27 unrelated patients, including the 8 samples used in the RNA-seq experiment, were included to in the RT-qPCR validation study and analysed simultaneously with 2 overarching aims. First, to provide technical validation of the RNA-seq findings by validating a subset of DEGs-of-interest by RT-qPCR using the same RNAs used in the RNA-seq experiments. Second, to provide biological validation of the RNA-seq findings by performing RT-qPCR on the same selection of genes-of-interest using RNAs from different patients. The results obtained from the validation experiments were then extrapolated to the remaining non-validated genes. RT-qPCR validation data were analysed by comparing the gene expression level amongst the TAV, BAVr and BAVc subgroups.

Clinical characteristics of the validation groups are summarised in Appendix III, Table III-8. The validation groups consisted of 8, 10 and 13 total valve RNA samples obtained from 6 TAV, 9 BAVr and 12 BAVc patients, respectively, majority of whom were male and of Caucasian background. In 2 BAV and 2 TAV patients in whom excess aortic valve leaflet tissues were available, 2 total RNA preparations were made from each patient, extracted from different part of the leaflets and treated as separate samples to maximise the number of total RNA available for statistical analysis.

Nine DEGs-of-interest from the overall BAV versus TAV comparative analysis were selected for RT-qPCR analyses, namely *ACAN* (aggrecan), *CHI3L1* (cartilage glycoprotein-39), *COL6A6 (collagen, type 6α6), IBSP, LAMC3, MMP13, MMP7, MMP9* and *SPP1.*

Overall, RT-qPCR analyses validated the differential expression between BAVr versus TAV on all of the selected genes-of-interest (Figure 5.6). RT-qPCR also validated the differential expression of 5 of these genes (*ACAN, COL6A6, LAMC3, MMP13* and *MMP7*) in the BAVr compared to BAVc group. RNA-seq however found no significant difference in the expressions of *CHI3L1, COL6A6, IBSP, LAMC3* and *MMP13* in the BAVc versus TAV group and these too were verified by the RT-qPCR analysis. This indicated a relatively good agreement between the RNA-seq and the RT-qPCR results.

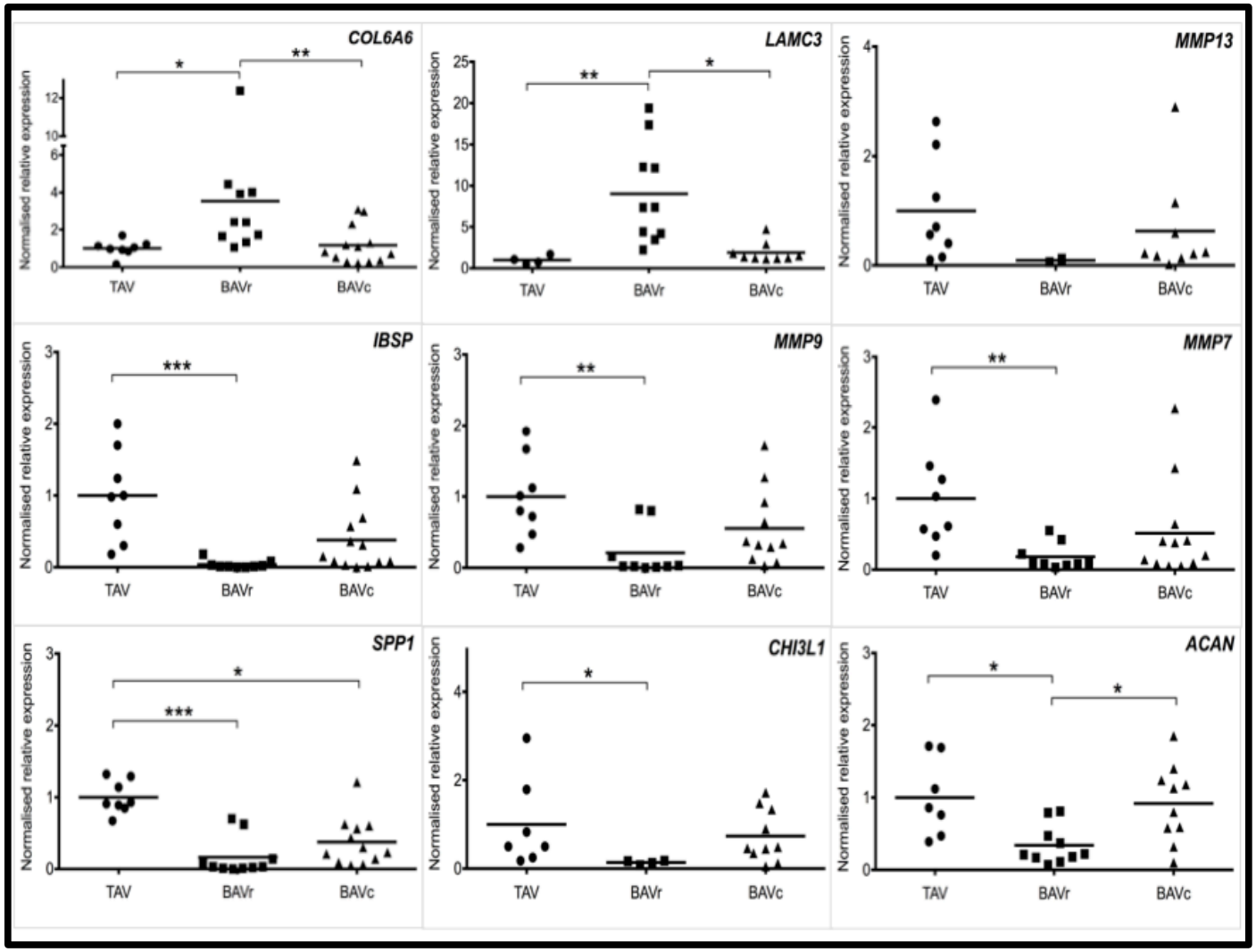

Figure 5. 6. RT-qPCR validation of selected DEGs-of-interest amongst TAV, BAVr and BAVc.

*p<0.05; **p<0.005; ***p<0.0005, ^p-value assessed using Mann Whitney two-tailed test. Note on *MMP13*: In 7 out of 9 BAVr samples, amplicon of correct size had failed to be amplified in two independent experiments, suggesting negligible expression of *MMP13* in these samples and supporting the RNA-seq findings.

5.3.4. Identification of shared and unique pathways

To identify unique and common genes that were important in the pathogenesis of SVD amongst subgroups, a Venn diagram was constructed using the DEGs gene list specific to different subgroup pairs (Figure 5.7; full gene list on Appendix III, Table III-9). The rationale was that DEGs between the BAVr versus TAV group would consist of genes that were not only responsible for BAV leaflet redundancy/prolapse or calcification in TAV but also BAV development; whilst BAVr versus BAVc comparison would highlight genes responsible for the different form of SVD in BAV leaflets and possibly, genes determining distinct BAV morphology. Similarly, BAVc versus TAV comparison could give insights to the shared versus differential calcification-related pathways and possibly, also BAV origin.

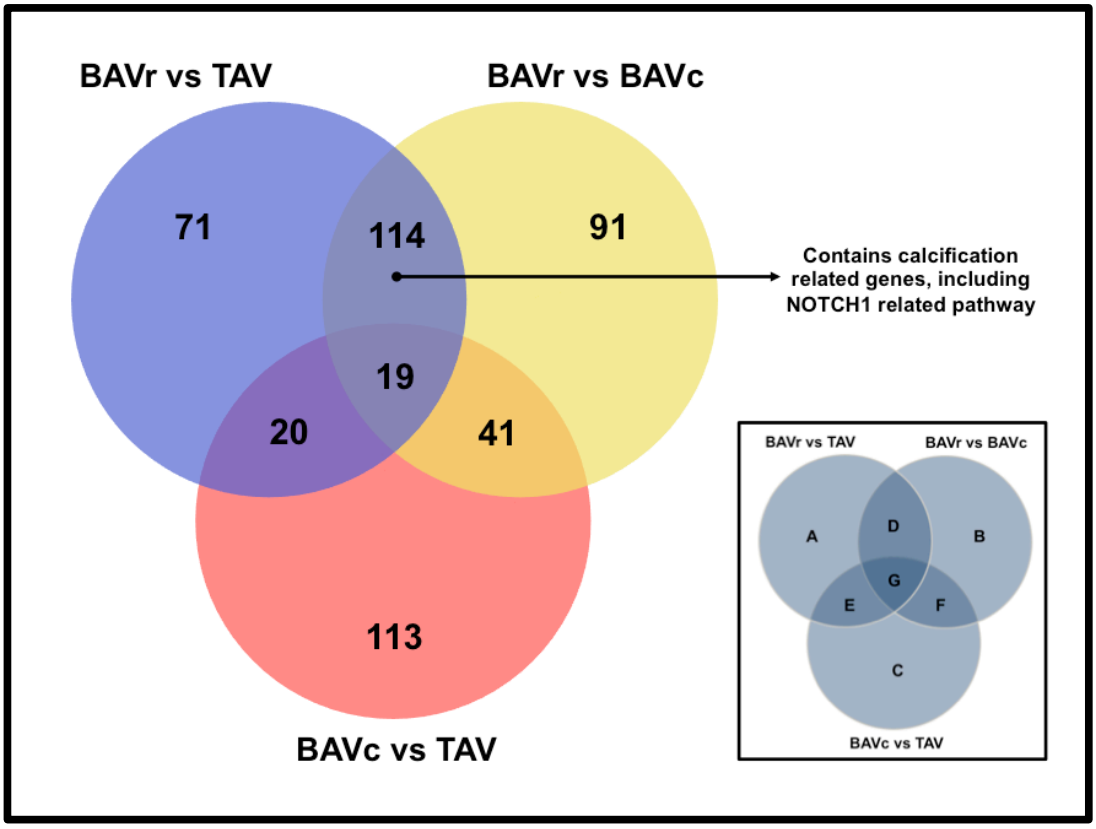

Figure 5. 7. Venn diagram showing overlap in the number of differentially expressed genes between analysed subgroups.

Gene lists of compartments A-G (insert) were summarised in Appendix III, Table III-9.

Nineteen DEGs were shared amongst all the subgroup pair comparisons, which included genes regulating cell adhesion (*ACAN, TIMD4* (T-cell immunoglobulin and mucin domain containing 4) and *FCRL5* (Fc receptor-like protein 5)), developmental process (*IGLL5* (immunoglobulin lambda-like polypeptide 5), *CNTFR* (ciliary neurotrophic factor receptor), *MYOC* (myocilin) and *ACAN*) and matrix protease *MMP9* (gelatinase B). Within the 114 overlapping genes between BAVr versus TAV and BAVr versus BAVc intersect (i.e. compartment D on Figure 5.6 insert), there was a common pattern of extracellular matrix-related genes dysregulation, including significant upregulation of inflammatory

response genes, serpin protease inhibitors (*SERPINA1*, *SERPINE1*), and calcification-related genes (*BGLAP* (osteocalcin)*, DLL4* (delta-like 4, NOTCH ligand)*, GFAP* (glial fibrillary acidic protein)*, HBA1/HBA2* (haemoglobin, alpha)*, MMP1* and *SPP1)* in the BAVc and TAV, compared to the BAVr group. Interestingly, IPA identified these calcification-related genes as downstream affecters of *NOTCH1* signalling pathway. Moreover, downregulation of metalloprotease *ADAMTS9* (a disintegrin and metallopeptidase with thrombospondin type 1 motif 9) was uniquely observed in BAVr versus TAV subgroup pair.

Unique pattern of DEGs regulating cardiogenesis and/or heart valve development was also noted between different subgroup pairs. Namely, within 71 DEGs unique to BAVr versus TAV there were developmental factors *HAND2* (heart and neural crest derivatives expressed 2), *EYA1* (eyes absent homolog 1 (Drosophila))*, GREM1* (gremlins1), *SEMA6B* (semaphorin 6B) and cardiac transcription factor *GATA4*. Upregulation of transcription factor *TBX20* (T-box 20) was observed uniquely within BAVr versus BAVc, whilst upregulation of *COL13A1* and downregulation of *WNT7A* (wingless-type MMTV integration site family, member 7A) were unique to BAVc versus TAV. Further, increased expression of valve progenitor markers *COL2A1, COL11A1, ACAN* and *MMP13* (collagenase-3) were observed in both BAVc and TAV compared to BAVr.

5.4. DISCUSSION

The present study described genome-wide differential transcriptome profiling behind SVD in human BAV and TAV using RNA-seq for the first time. The data obtained from the study provides new insight into the molecular basis of phenotype heterogeneity seen in this complex disorder. Differential gene expression profiles were observed amongst BAV patients, dividing them into two subgroups: those with calcification predominant disease (BAVc) and those with primarily redundant leaflet degeneration (BAVr). The gene expression pattern of BAVc was found to be more similar to the TAV rather than the BAVr group. Comparative functional analysis of the DEGs revealed the presence of shared and unique genes/pathways between the different subgroup pairs. Dysregulation of extracellular matrix genes and genes regulating cellular adhesions appeared to be a common feature of SVD in both BAV and TAV. Meanwhile, significant overexpression of ossification and inflammatory response genes were seen in both BAVc and TAV with notable downregulation of the *NOTCH1* signalling pathway. This implied the presence of a common terminal pathway in genes regulating valvular calcification in both BAV and TAV. A unique pattern of differential expression of genes controlling cardiac and/or heart valve development was also identified amongst the subgroups. In particular, downregulation of *ADAMTS9* and ACAN were observed in the BAVr compared to the TAV. Furthermore, there was notable downregulation of semaphorins signalling through *SEMA6B* and *SEMA3F* in BAVr and BAVc, respectively, compared to the TAV group. Taken together, these findings indicated the presence of distinct gene expression signatures that marked the

different type of SVD in BAV, compared to TAV, supporting the emerging theory that BAV is heterogeneous with respect to molecular events in disease progression (Figure 5.8).

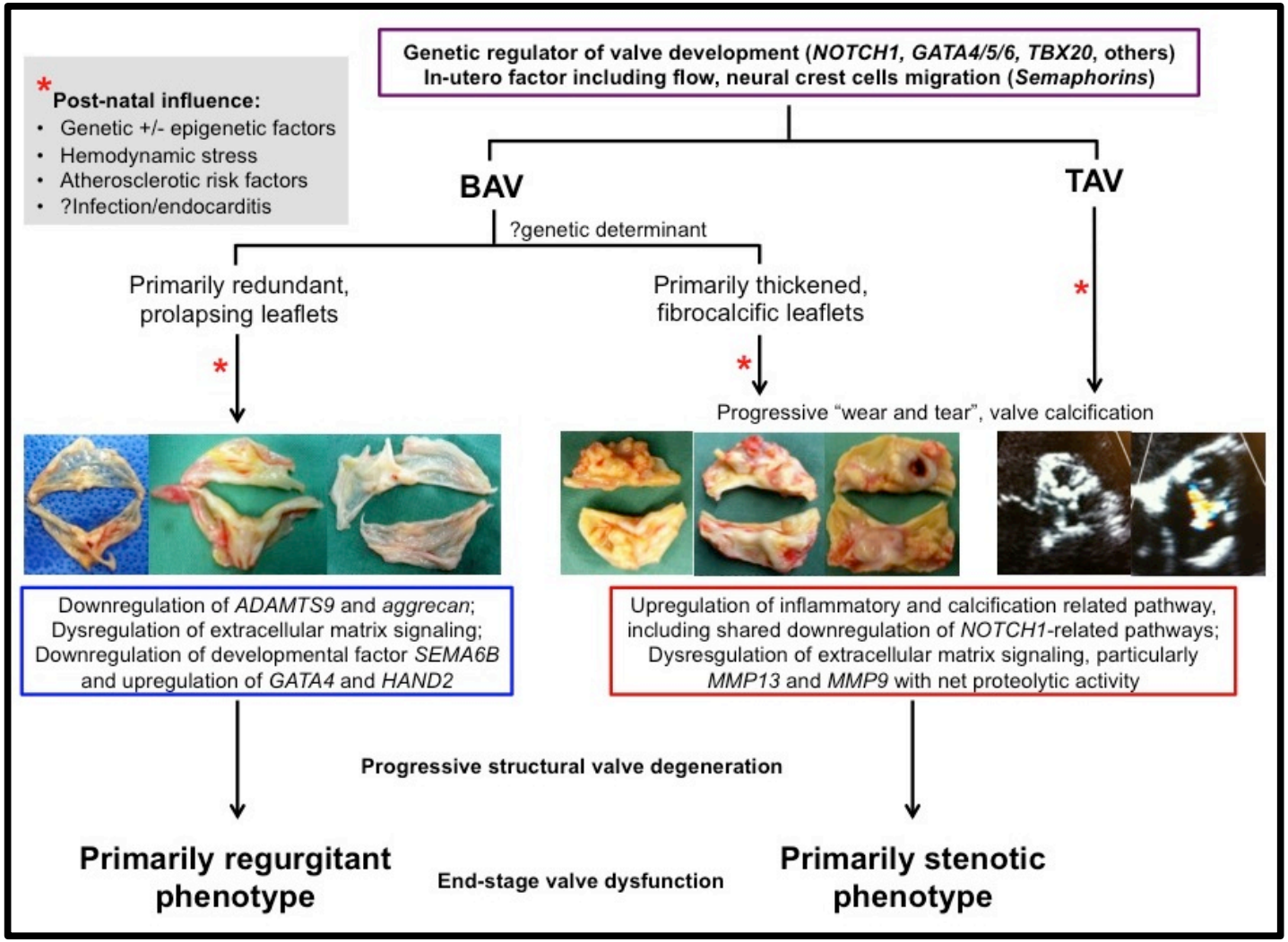

Figure 5. 8. Proposed mechanism leading to the development structural valvular degeneration in BAV versus TAV.

Central to the pathogenesis of human heart valve disease is the disruption of the normal valve homeostatic process, which leads to abnormal leaflet architectural organisation and disproportionate alteration of extracellular matrix constituents (Padang et al., 2012b). Imbalance of proteases MMPs and ADAMTS expression can accelerate leaflet degradation process, by changing the structural composition of the valve matrix, leading to pathological remodelling, SVD and subsequent valve dysfunction. In this study, 4 MMPs were differentially expressed, namely *MMP1, MMP7*, and, notably, *MMP9* and *MMP13*, but not *MMP2*. The matrix remodelling enzyme gene *MMP13* was found to be the most highly upregulated gene in the degenerative TAV and BAVc groups, compared to the extremely low expression in BAVr, suggesting its importance in valvular calcification.

MMP13 is a major collagenase that plays an important role during cardiogenesis and heart valve development, with catalytic activity predominantly on type II collagen and aggrecan matrix constituents (Borzi et al., 2010, Cheek et al., 2012). In degenerative bone disease model, such as osteoarthritis, *MMP13* facilitates chondrocyte terminal differentiation by ensuring concerted upregulation of *RUNX2* (runt-related transcription factor 2), *VEGF* (vascular endothelial growth factor), and active β-catenin signalling pathways, which induce osteoblastogenesis and new bone formation (Borzi et al., 2010). Given the presence of a shared molecular mechanism regulating heart valve, cartilage, and bone development, which can be reactivated in adult valve disease (Lincoln et al., 2006), it is conceivable that *MMP13* induces calcific valve phenotype in either BAV or TAV through similar mechanism.

Meanwhile, significant dysregulation of *MMP9* was commonly observed amongst all 3 subgroups comparison. Normally involved in type IV collagen and elastin degradation, increase in *MMP9* activity had been detected in vascular pathologies, such as abdominal aortic aneurysms, and in diseased BAV compared to diseased or normal TAV leaflets (Koullias et al., 2004). In some contrast, this study showed that significant increase in *MMP9* activity can be observed in heavily calcified leaflets of either TAV (highest activity) or BAV origin (BAVc), compared to the lower expression in the minimally calcified BAVr (lowest activity) group. Nevertheless, in concordance to other previous studies (Edep et al., 2000, Fondard et al., 2005), this indicated the presence of enhanced proteolytic/elatolytic activity of *MMP9* in calcified leaflets, in both BAV and TAV. As inflammatory cells (e.g. macrophages and neutrophils), but not valvular interstitial cells, are prevalent MMP9 producers, this indirectly implied a higher degree of inflammation in heavily calcified and stenotic leaflets, compared with redundant and regurgitant leaflets, which is in support of previous study (Fondard et al., 2005). Indeed, inflammatory infiltration of activated macrophages and T-cells has been reported in human stenotic aortic valve (Moreno et al., 2011, Nagy et al., 2011). Notably, no significant differential expression of tissue inhibitor of MMPs (TIMPs) was observed within the dataset, suggesting the presence of net proteolytic activity of MMPs in valve disease pathogenesis.

This study provided further evidence that BAV-related calcification occurred in a similar fashion to that seen in patients with calcific TAV, where it is an active biological process involving inflammation, oxidation, angiogenesis, extracellular

matrix remodelling/fibrosis, and atherosclerosis-like ectopic calcification, with bone-like mineralisation of the aortic side of the valve leaflet (Bosse et al., 2009). Indeed, shared upregulation of osteogenic gene programs were observed between the BAVc and TAV groups, which included upregulation of bone-specific transcription factor *SP7* (osterix), bone differentiation marker *IBSP* and *BGLAP*, NOTCH ligand *DLL4*, *MMP1* and *MMP9* proteases, and bone biomineralisation marker *SPP1* (osteopontin); many of which interact with or known as part of the downstream signalling pathway of the transcription factor *NOTCH1* (Engin et al., 2008, Rusanescu et al., 2008). In fact, the NOTCH1 signalling pathway appeared to be downregulated in these calcific leaflets, probably mediated through the reduction in NOTCH1-mediated repression of *Runx2* activity (Rusanescu et al., 2008), a central transcriptional regulator of osteoblast cell fate, which resulted in the observed upregulation of *SP7* and *SPP1* activities. This is an interesting finding as missense and frameshift mutations of *NOTCH1* gene, leading to haploinsufficiency, are associated with human BAV, as well as calcific aortic stenosis in both BAV and TAV patients (Ducharme et al., 2013, Garg et al., 2005). This suggested that *NOTCH1* signalling pathway may be a common terminal pathway in aortic valve calcification, although further study is required to elucidate the initial molecular event that may have triggered the initiation of calcification process in both BAV and TAV. Such events are likely to be multifactorial in origin, involving complex interplay between genetic, epigenetic, environmental, and hemodynamic factors.

Whilst many pathways regulating calcific aortic stenosis have been described, genetic and molecular factors leading to intrinsic BAV leaflet redundancy, prolapse and subsequent development of aortic regurgitation remain mostly unknown. Recently, adult murine models with *Adamts9* haploinsufficiency have been shown to develop aortic valve thickening, enlargement (redundancy) and even malformation, as well as ascending aortic wall anomalies (Kern et al., 2010). Important in cardiovascular development and/or allostasis, the proteoglycanase ADAMTS9 is involved in cleavage of large proteoglycan aggrecan (ACAN) and versican, two important components of human valve matrix. Interestingly, downregulation of *ADAMTS9* and *ACAN* were observed in the BAVr compared to the TAV. It is hypothesised that reduced *ADAMTS9* expression in the BAVr group likely resulted in reduced ACAN processing, its pathological accumulation and consequent downregulation at gene expression level. Hence, this might contributed to redundant leaflet phenotype in the BAVr group.

Further, the study observed lower expression of valve progenitor markers *COL2A1* and *COL11A1* in the BAVr compared to the BAVc and TAV groups. This implied that synthesis of collagen, a structural protein, might be downregulated in the BAVr group, giving the aortic valve a lower tensile strength. Over time, this structural abnormality likely contributes to progressive leaflet laxity, redundancy and chronic valvular dysfunction (i.e. regurgitation), as seen in end-stage disease amongst those with regurgitant BAV.

Human genetic studies are beginning to provide evidence that developmental pathways important in valvulogenesis also contribute to adult valve disease (Lincoln et al., 2006). This is supported by the current RNA-seq study, which demonstrated unique pattern of dysregulation of foetal genes important in cardiac and heart valve development amongst the study subgroups. Of particular interest were unique upregulation of *TBX20* in BAVr compared to the BAVc group; as well as unique downregulation of *SEMA6B* and *SEMA3F* in BAVr versus TAV and BAVc versus TAV groups, respectively.

Transcription factor *TBX20* is a member of a highly conserved T-box gene family that is implicated in cardiac muscle maturation and is strongly expressed in the endocardial cushion mesenchyme during heart development (Kirk et al., 2007). Human *TBX20* mutations, including a gain-of-function mutation, are associated with adult-onset cardiomyopathy, septal defects, and interestingly, coarctation of the aorta, mitral and aortic valve abnormalities (Kirk et al., 2007, Posch et al., 2010). Mouse embryos with a partial RNAi-mediated knockdown of *Tbx20* expression show severe hypoplasia of atrioventricular (aortic and pulmonary) valve, further supporting its critical role in valve development (Takeuchi et al., 2005). Interestingly, *TBX20* interacts with other cardiac developmental transcriptional factors, including *TBX5, GATA4, GATA5* and *Nkx2*-5 (Kirk et al., 2007, Posch et al., 2010). Notably, *Nkx2*-5 haploinsufficiency and targeted deletion of *Gata5* in mice had been associated with BAV development. Therefore, the observed upregulation of *TBX20* in BAVr versus BAVc group was indeed hypothesis stimulating with regard to its contribution to human BAV development, which was probably mediated through

its interaction with the cardiac GATA factors and *Nkx2*-5 (Laforest et al., 2011, Biben et al., 2000).

Semaphorins comprise a diverse family of secreted, transmembrane and GPI-linked proteins that shared a conserved cysteine-rich sema domain (Kruger et al., 2005). Semaphorins are major regulators of morphogenesis, involved in a variety of processes ranging from neural connectivity, angiogenesis, immune-regulation, cardiac and bone development, to cancer biology (Kruger et al., 2005). In particular, class 3 and 6 semaphorins, as well as semaphorin receptor Plexins, signalling are important in cardiogenesis and outflow tracts formation, which in part are mediated by their regulatory role in neural crest cells (NCC) migration (Kruger et al., 2005, Toyofuku et al., 2008). Necessary for normal outflow tract septation and formation/remodelling of the semilunar valves, abnormal NCC migration and condensation within the outflow endocardial cushion during cardiogenesis in mice has been linked to the development of BAV and abnormalities of the aortic root and ascending aortic wall (Jain et al., 2011, Phillips et al., 2013). The perceived downregulation of *SEMA6B* and *SEMA3F* in BAVr and BAVc, compared to TAV, respectively were therefore exciting finding as this may give the first clue into the role of semaphorins in the development of human BAV. Further, this may also provide the molecular link between the abnormal valve patterning and the predisposition to ascending aortic dilatation within the BAV cohort, in addition to hemodynamic factors.

Even after focusing the present analyses to the protein-coding mRNAs expression profiling, extracting biological meaning from RNA-seq data

continues to pose a major challenge, as the amount of data available is overwhelming and challenging to interpret. To facilitate interpretation, this study relied heavily on the available bioinformatics tools and literature, which may create some limitations, as to date many gene functions and molecular pathways are yet to be elucidated. Further, the current study is limited by the unavailability of structurally normal TAV as the ideal comparative control group and therefore, a number of important genes related to the anomaly itself could probably be missed during the analysis. The lack of an ideal control group has also made analysis for differential stimuli for inflammatory activation and calcification between BAV and TAV highly challenging. The study is also limited by the relatively small sample size of the RNA-seq group. The latter was partly contributed by the difficulty in obtaining sufficient quantity of high quality total valve RNAs, especially from heavily calcified leaflets that would be suitable for RNA-seq purpose. Moreover, wide variability was observed amongst a number of samples within each subgroup on RT-qPCR data. This may reflect the fact that each individual samples, even those within the same subgroups, might be at a different stage of disease process. Also, different posttranslational and/or epigenetic regulation was likely to be present in different individuals, further contributing to heterogeneity in gene expression and subsequently their phenotype. Finally, the current study analysis was limited to the end-stage form of the valve disease process, whilst the initiating factor that drives the disease onset remains to be elucidated. Further studies are therefore required to validate these findings in a larger cohort. Nevertheless, the data obtained in this study provides an invaluable insight into genome-wide differential gene expression patterns within BAV disease compared to TAV.

In conclusion, this study presented the first global comparative transcriptome profiling of human BAV disease compared to TAV using RNA-seq. The study demonstrated the relatively close resemblance of gene expression patterns of calcified human BAV and calcified human TAV leaflets, with shared upregulation of inflammatory pathways and downregulation of *NOTCH1* signalling, suggesting a common mechanism of calcific leaflet degeneration in both BAV and TAV. Dysregulation of *ADAMTS9* and *ACAN* were likely to contribute to leaflet redundancy or prolapse in BAV disease. This study has also identified the unique dysregulation of foetal gene programs, including the potential role of semaphorins in the development of BAV and its related aortopathy. Understanding of genetic pathways leading to SVD is important, as it is a precursor of overt clinical valve dysfunction. The present limitation of pharmacological treatment in delaying or stopping valve disease progression has left surgical therapies as the most effective, but not necessarily the ideal "cure" for end-stage valve dysfunction in both BAV and TAV. Improvement in our understanding of gene and molecular pathways involved in the pathogenesis of SVD in BAV will help to foster the development of new therapies that halt progressive leaflet degeneration, with the ultimate goal of reducing the overall health burden created by this complex, albeit common, human disease.

CHAPTER 6: REAL TIME EXERCISE CMR IMAGING IN THE EVALUATION OF AORTIC BIOMECHANICS IN BAV DISEASE

6.1. INTRODUCTION

As the most common form of congenital heart defects (CHD) in adults, affecting ~1.3% of the population worldwide, BAV is responsible for more deaths and complications than the combined effects of all other CHD (Fedak et al., 2002, Siu and Silversides, 2010). Although valvular dysfunction is the most common complication of a bicuspid aortic valve, dilatation of any segment of the proximal aorta from the aortic root to the aortic arch, the so-called BAV-related aortopathy, is present in over 50% of affected individuals (Verma and Siu, 2014, Fedak et al., 2002), usually occurring at a younger age in BAV than it does in patients with the normal tricuspid aortic valves (TAV). As aortic dilatation has a propensity for dissection and rupture, BAV-related aortopathy is a potentially lethal disease. Thus, it warrants life-long periodic monitoring, with possible early prophylactic surgical intervention to prevent unfavourable outcome.

As an important adjunct to the traditional transthoracic echocardiography assessment of BAV disease, Cardiac Magnetic Resonance (CMR) imaging provides the unique ability to provide comprehensive three-dimensional (3D) data combined with accurate flow imaging in the assessment of BAV-related aortic pathologies (Quenot et al., 2005). Not only does CMR imaging allow for detailed assessment of the left ventricle, the aortic valve and the aorta in one examination, it also provides highly reproducible and accurate measurements. One may argue that CMR currently has the potential to serve as a 'one-stop shop' for many patients with BAV disease (Shenoy et al., 2014), although the lack of institutional access, limited local expertise, high cost and individual

patient-related factors (i.e. presence of metallic device, claustrophobia, etc.) may limit its widespread adoption at the present time. Nevertheless, given the need for life-long routine serial arch imaging and the lack of radiation exposure that is associated with CT angiography, MR imaging appears to be the imaging modality of choice in the long-term follow-up of aortic pathologies in this group of often relatively young patients.

It is well-established that individuals with BAV disease have larger aortic annulus, sinus and proximal ascending aorta compared to those with TAV (Cecconi et al., 2005, Nkomo et al., 2003) and progressive aortic dilatation occurs more commonly in those with larger aortas at baseline (Holmes et al., 2007, Michelena et al., 2011). Further, accumulating evidence suggests that BAV-related aortopathy has a highly heterogeneous phenotypic expression, even amongst patients with specific valve fusion pattern and similar level of valve dysfunction (Barker et al., 2012, Girdauskas et al., 2011a, Hope et al., 2012, Schaefer et al., 2008). This likely reflects the diversity in genetic, molecular, rheologic, and clinical features underlying aortic abnormalities in BAV (Verma and Siu, 2014). Whilst studies have linked genetics to the development of BAV-related aortopathy, the important role of valve-related alterations in aortic hemodynamic and their impact in the underlying aortopathy have been increasingly recognised (Girdauskas et al., 2011a). Recently, studies based on flow-sensitive 4D CMR have provided irrefutable evidence that the modified hemodynamic environments associated with BAV, even a 'normally functioning one', can cause altered wall shear stress in the ascending aorta, which may trigger maladaptive vascular remodelling (Hope et al., 2011, Hope et

al., 2012, Mahadevia et al., 2014). Indeed, intrinsic aortic wall abnormalities from accelerated degeneration of the aortic media have been reported in thoracic aortic tissue of BAV patients, including decreased fibrillin, elastin fragmentation, matrix disruption and apoptosis (Fedak et al., 2002). These intrinsic wall abnormalities are likely to have negative impacts on aortic biomechanical properties, such as aortic wall elasticity and compliance, which may in turn impact on aortic aneurysm development and growth rate.

However, not every individual with BAV develops aortic dilatation (Michelena et al., 2011, Tadros et al., 2009). In those who do, many (up to 43%) may not progress (Detaint et al., 2014); and in those who do progress, the rate of progression varies significantly between individual patients, independent of baseline aortic diameter, BAV morphology or valve dysfunction (except in a smaller subset of those with aortic regurgitation and sinus of Valsalva dilatation) (Detaint et al., 2014). This suggests the presence of inherent differences in how each individual aorta of BAV patients responds to hemodynamic shear stress associated with activities of daily living. This inherent variability in aortic mechanical properties may explain the generally higher growth rate of ascending aortic dilatation in patients with BAV compared to TAV and may be used to categorise those BAV patients who are ‘progressor’ or ‘non-progressor’ in terms of aortic dilatation. Therefore, the hypothesis behind this study is that the increased hemodynamic shear stress produced by exercise can be used to identify the differential aortic wall mechanical properties between BAV patients with predisposition for BAV-related aortopathy and those with TAV, and thus allowing identification of those at risk for adverse events.

CMR imaging has previously been established as an accurate non-invasive tool for assessment of aortic stiffness, compliance and distensibility (Melina et al., 2002, Metafratzi et al., 2002). Conventionally, this is performed using a combination of ECG-gated spin echo, retrospectively gated bSSFP (balanced steady state free precession) cine sequences and standard phase-contrast CMR imaging (Metafratzi et al., 2002). This approach requires breath-holding and regular cardiac rhythm, rendering it impractical for exercising individuals. Recently, a free-breathing high-resolution real-time phase-contrast cine CMR imaging technique has been developed and successfully used to detail physiological blood flow changes in the ascending aorta, even during Valsalva and Mueller manoeuvres, with high reliability and sufficient spatiotemporal resolution (Sohns et al., 2013, Lin et al., 2012c).

To the best of our knowledge, real-time CMR imaging has not previously been used to study the impact of exercise on the differential aortic wall mechanical properties, namely aortic distensibility, compliance and stiffness index, between patients with BAV and TAV. Accordingly, the current pilot study sought to use real-time CMR imaging to identify the differential aortic wall mechanical properties in response to hemodynamic stress, at rest and during exercise, between BAV patients and those with TAV, in the absence of significant valve dysfunction or overt aortic dilatation.

6.2. PATIENTS AND METHODS

6.2.1. Study populations

Between September 2013 and January 2014, 6 patients with BAV and 6 age- and gender-matched healthy subjects were prospectively studied with CMR imaging at the Royal Prince Alfred Hospital, Sydney, Australia. The patients with BAV were identified and recruited from our institutional BAV disease database. Inclusion criterion was the presence of BAV as diagnosed by echocardiography. Exclusion criteria were evidence of more than mild aortic stenosis (peak aortic velocity of ≥3.0 m/sec on echocardiography) and/or regurgitation as per the American Heart Association and the American College of Cardiology guidelines (Bonow et al., 2008), more than mild ascending aortic dilatation (≥4.5cm), co-existing aortic coarctation or other forms of congenital heart disease, Marfan syndrome or other connective tissue disorders, previous surgery or intervention of the aorta or aortic valve, usage of beta blockers or non-dihydropyridines calcium channel blockers, and general contraindications to CMR imaging. Clinical characteristics and functional status as expressed as New York Heart Association class of the patients were obtained from the medical records and/or clinical direct assessment.

Age- and gender-matched healthy volunteers consisted of PhD students or employees at the Centenary Institute, Sydney, Australia, in whom BAV or other congenital cardiac pathology had been excluded by clinical history, physical examination and echocardiography. The study protocol was approved by the Sydney South West Area Health Service Human Research Ethics Committee and all subjects gave informed consent at the time of the CMR scan.

6.2.2. CMR imaging

CMR imaging was performed using 1.5 Tesla Phillips Achieva MR scanner (Phillips Medical System, Best, Netherland). The study protocol is summarised in Table 6.1. Dr. Rajesh Puranik and/or Dr. Madhusudan Ganigara provided co-supervision during all CMR studies.

Table 6. 1. CMR imaging protocol used in the study.

CMR Imaging Protocol		
BP and BSA measurement		☐
Routine resting image (baseline)	**1. T1-scout scan (planning)**	☐
	2. 3-point plan cine across aortic arch	☐
	3. LVOT cine	☐
	4. Aortic flow	☐
	5. Sagittal oblique NAVIGATOR	☐
Free breathing, real time (RT) phase contrast flow and cine CMR imaging 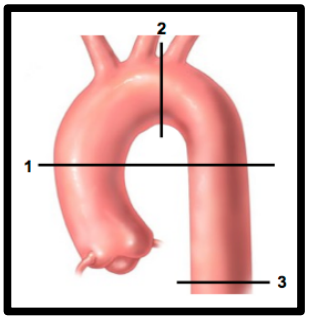	**1. Baseline RT flow** • **RT-flow*** • **RT-cine***	☐
	2-3 minutes exercise	
	2. Exercise Stage 1 RT flow • **RT-flow*** • **RT-cine***	☐
	Rest followed by 2-3 minutes exercise	
	3. Exercise Stage 2 RT flow • **RT-flow*** • **RT-cine***	☐
	Rest 3 minutes	
	4. Recovery RT flow • **RT-flow*** • **RT-cine***	☐

*All real time (RT)-flow and RT-cine assessment were performed at 4 different levels, as depicted by the figure insert, namely: (1) Pulmonary artery level, to obtain proximal ascending aorta and proximal descending aorta diameters; (2) transverse arch level; and (3) right hemidiaphragm level to obtain diaphragmatic aorta diameter. BP, blood pressure; BSA, body surface area; LVOT, left ventricular outflow tract. Image adopted from www.ucaorta.org/aortic-arch.html with modification.

6.2.2.1. Baseline (resting) CMR data

6.2.2.1.1. Aortic cine imaging

Evaluation of the dynamic changes across the aortic arch and LVOT morphology was assessed using cine CMR imaging. Retrospectively gated steady-state free precession (bTFE, balanced turbo field echo) cine CMR images of the aortic long axis, along the ascending, transverse, arch and descending aorta were routinely undertaken. The LVOT was examined in two perpendicular views. The following imaging parameters were used: repetition time [TR] = 2.9 - 3.5 ms; echo time [TE] = 1.4 - 1.6 ms; flip angle = 60°; slice thickness = 10 mm; matrix = 256 x 192; field of view = 340 mm; and temporal resolution ≤ 40 ms; acquired during a single breath-hold.

6.2.2.1.2. Aortic dimensions: 3-D sagittal oblique NAVIGATOR

Measurements were acquired with a non-contrast, free breathing NAVIGATOR-gated 3D balanced fast field echo (FFE) CMR sequence, where the data was acquired in mid-diastole and during expiration (Figure 6.1). Slices were obtained in the sagittal plane in several contiguous locations to ensure complete coverage of the thoracic aorta. Imaging parameters were TR = 4.7 ms; TE = 2.3 ms; flip angle = 90°; slice thickness = 1.0 mm; matrix = 192 x 512; field of view = 400 mm. Aortic measurements were made systematically at the level of the proximal ascending aorta, transverse aortic arch, proximal descending aorta and distal descending aorta at the level of the diaphragm.

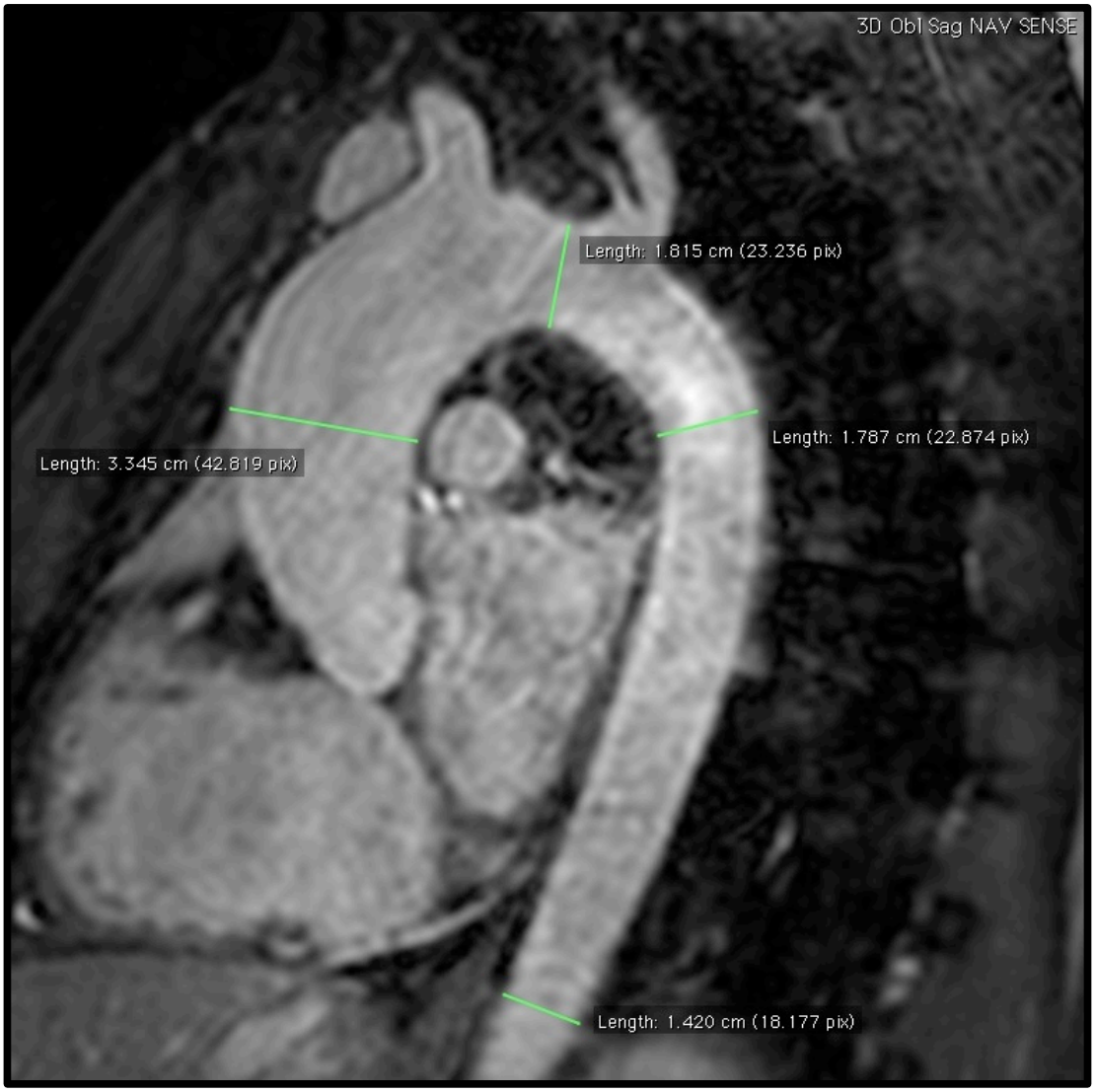

Figure 6. 1. Example of aortic dimension measurements using images obtained using 3D Sagital Oblique NAVIGATOR sequence in a patient with BAV.

6.2.2.1.3. Aortic flow quantification: Phase Contrast Data

Assessment of aortic blood flow was acquired by use of a flow-sensitive 2D T1 fast field echo sequence (T1-FFE; TR = 4.4 ms; TE= 2.8 ms; flip angle = 15°; slice thickness = 10 mm; field of view = 360 mm; matrix = 176 x 256; 40 heart phases; phase contrast velocity encoding of 200 cm/sec) acquired during a breath-hold. Imaging plane was located at the midpoint of the ascending aorta (at the level of main pulmonary artery bifurcation), where through-plane flow data was acquired by use of retrospective cardiac gating. Arterial blood flow was calculated from phase contrast images by use of a semiautomatic vessel edge-detection algorithm (Reportcard, GE) with manual operator correction. Net forward flow within the proximal ascending aorta (ml) and aortic regurgitation fraction (%) was calculated as total aortic flow minus backward aortic flow and percent backward aortic flow over total aortic flow, respectively.

6.2.2.2. Exercise-based free breathing real-time CMR data

6.2.2.2.1. Exercise protocol during CMR imaging

Participants performed progressive resistance exercise using a custom built pneumatic MRI-compatible pedal ergometer, which was attached to the foot of the MRI table. The exercise study consisted of 2 stages; Stage 1 was achieved when participants achieved at least 30% of their maximum predicted heart rate (MPHR) and Stage 2 when at least 60% of MPHR was reached. A higher intensity exercise was not included in the protocol as excessive movements may degrade the quality of the data. The MPHR was calculated adding either 30% or 60% of the participant's heart rate reserve (HRR), depending on the

stage of exercise performed, to the resting heart rate. The HRR was obtained by subtracting the resting heart rate from the maximum predicted heart rate (i.e. 220 minus participant's age at the time of the study).

Participants were monitored while pedalling in a recumbent position against a low to moderate level of resistance and at a moderate level of cadence for a period of 3-5 minutes. Regular prompts were provided during the test to progressively increase the level of exercise until the predetermined target heart rate was achieved, following which data acquisition was commenced (using free breathing real-time CMR imaging; Chapter 6.2.2.2.2). Participants continued to exercise during the scanning. The total scan time during each stage of exercise was less than 2 minutes. Periodic automated left brachial blood pressure and continual oxygen saturation measurements (Medrad® Veris® MR Vital Signs Monitor, Bayer Health Care, Pennsylvania, USA) were obtained throughout the testing procedure. Participants were given a 3-minute rest period between the 2 exercise stages. At the completion of 2nd stage of exercise, participants were given a 3- to 5-minute period of recovery, following which the final real-time data acquisition was obtained.

6.2.2.2.2. Free breathing real-time flow and cine CMR imaging

Imaging slices for real-time CMR imaging were obtained in the axial plane of 3 locations of interest, specifically: (1) at the main pulmonary artery level, to obtain proximal ascending aorta and proximal descending aorta diameters; (2) at the transverse arch level, at the mid point between the origin of left common

carotid and left subclavian artery; (3) at the right hemidiaphragm level to obtain diaphragmatic aorta diameter. Real-time cine and flow measurements were performed on these imaging planes at 4 study phases: at rest (baseline), during stage 1 and stage 2 of exercise when the targeted MPHR was reached, and finally, during recovery. Each flow data set consisted of 100 consecutive dynamic scan, free breathing, real-time (no ECG-triggering), 2D T1-FFE sequence, 60 seconds acquisition (TR =11.0 ms; TE = 4.9 ms; flip angle = 15°; slice thickness = 10 mm; matrix = 112 x 144; field of view = 400 mm; flow encoding velocity 200 cm/sec). Each cine data set consisted of 40 consecutive, free breathing, real-time (no ECG-triggering), balance turbo field echo (bTFE) sequence with sensitivity encoding (SENSE) acquisition (TR = 2.7 – 3.5 ms; TE = 1.3 – 1.5 ms; flip angle = 50°; slice thickness = 10 mm; matrix = 192 x 224; field of view = 400 mm).

6.2.3. Analysis of aortic mechanical properties

Analyses of aortic biomechanical properties, including aortic regional compliance, distensibility and aortic stiffness index (β), were performed at the proximal ascending aorta and diaphragmatic aorta at rest (baseline) and during exercise, using the real-time cine CMR data.

Arterial compliance is defined as the absolute change in area for a given pressure step at a fixed vessel length and is the reciprocal of arterial stiffness (Antonini-Canterin et al., 2009). Aortic compliance (in mm^2/mmHg) is calculated as $(A_{max} – A_{min})/(SBP – DBP)$ (Antonini-Canterin et al., 2009), with A_{max} and A_{min}

as maximal and minimal cross-sectional lumen area (in mm^2) of the aortic segment studied, and SBP and DBP as systolic and diastolic brachial blood pressure (in mmHg), respectively.

In contrast, aortic distensibility is defined as the relative compliance, or the relative change in area for a given pressure step increase (Antonini-Canterin et al., 2009). Aortic wall distensibility assessment (in $cm^2dyne^{-1}10^{-6}$) by CMR imaging is calculated according to the following formula (Cavalcante et al., 2011): $(A_{max} – A_{min})/(A_{min} \times [SBP – DBP] \times 1{,}000)$. Meanwhile, aortic stiffness index (β) is a surrogate marker of the stiffness of the vascular wall and is calculated as $\ln(SBP/DBP)/([A_{max} – A_{min}]/A_{min})$ (Shibata and Levine, 2011, Tian and Chesler, 2012).

6.2.4. Statistical analysis

All data are presented as mean ± standard deviation (SD). The means of quantitative data involving 2 independent groups were analysed using a 2-tailed unpaired Student's t-test. A 2-tailed paired-samples Student's t-test was used to compare various measures of aortic mechanical properties at rest and during exercise amongst subjects within a group. Fisher's exact test was used to assess relationship between groups with dichotomous variables. A 2-tailed p-value ≤ 0.05 was considered statistically significant. Statistical analyses were performed using GraphPad Prism Version 6.0b (GraphPad Software, La Jolla, California, USA).

6.3. RESULTS

6.3.1. Study population

Between September 2013 and January 2014, 12 individuals (6 BAV and 6 age- and gender-matched healthy control) participated in the exercise CMR study. The baseline characteristics of the study participants are summarised in Table 6.2. The BAV group comprised of 3 males (50%) with a mean age of 33 ± 6 years at time of CMR imaging, which by study design, was similar to the control group. There were no significant differences between the BAV and the control group in terms of body mass index (BMI), body surface area (BSA), history of hypertension, or resting blood pressures. All patients were free from any cardiac symptoms at the time of CMR imaging with New York Heart Association functional class 1 and had normal LV function by resting echocardiography. Two-thirds of the BAV group had echocardiographic evidence of no more than mild valvular dysfunction (aortic stenosis and/or regurgitation). Further, whilst not overtly dilated, individuals with BAV had a significantly larger proximal ascending aorta compared to the control group (3.29 ± 0.31 cm vs 2.56 ± 0.24 cm, p=0.001). There was no significant difference between the 2 groups in terms of transverse arch, proximal descending or diaphragmatic aortic dimensions.

Table 6. 2. Study cohort characteristics.

Characteristics	BAV (n=6)	Control (n=6)	*p*-value
Age at CMR imaging (years)	33 ± 6	33 ± 7	0.965
Male gender (%)	3 (50)	3 (50)	1.000
Height (m)	1.64 ± 0.12	1.72 ± 0.07	0.177
Weight (kg)	67 ± 19	64 ± 9	0.703
BMI (kg/m^2)	24.6 ± 4.8	21.4 ± 1.8	0.161
BSA* (m^2)	1.72 ± 0.29	1.75 ± 0.15	0.8330
Hypertension (%)	1 (17)$^{\wedge}$	0 (0)	1.000
NYHA functional class I	6 (100)	6 (100)	1.000
Normal LV function, EF>55% (%)	6 (100)	6 (100)	1.000
Valvular function			
Normal	2	6	-
Mild AS and/or AR	4$^{\$}$	0	-
Resting blood pressure (mmHg)			
Resting SBP	109 ± 12	112 ± 7	0.609
Resting DBP	71 ± 11	68 ± 8	0.577
Maximum aortic dimension (cm)$^{\#}$			
Proximal ascending aorta	3.29 ± 0.31	2.56 ± 0.24	**0.001**
Transverse arch	2.00 ± 0.26	2.01 ± 0.14	0.924
Proximal descending aorta	2.04 ± 0.36	2.02 ± 0.23	0.925
Diaphragmatic aorta	1.75 ± 0.23	1.75 ± 0.24	0.991

*Body surface area (BSA) is calculated using DuBois & DuBois formula (BSA = 0.20247 x height (m)$^{0.725}$ x weight (kg)$^{0.425}$); $^{\$}$One patient has a mixed mild AS and AR, 1 has trivial AR and 2 has mild AS; $^{\wedge}$One BAV patient has a history of mild hypertension, which was well controlled with a low dose angiotensin-II receptor blocker; $^{\#}$Measurements taken from 3D sagittal oblique NAVIGATOR CMR images. AS, aortic stenosis; AR, aortic regurgitation; SBP, systolic blood pressure; DBP, diastolic blood pressure; PP, pulse pressure; NYHA, New York Heart Association.

6.3.2. Exercise data

Table 6.3 summarises the exercise haemodynamic data amongst the 2 groups. Complete resting haemodynamic parameters were obtained from all patients. Compared to the BAV group, the control group had a lower resting heart rate (58 ± 5 vs 69 ± 10 beats per minute (bpm), p=0.036) and a slightly wider resting pulse pressure (44 ± 2 vs 38 ± 6 mmHg, p=0.039), despite having similar systolic and diastolic blood pressure levels.

All patients in the BAV group achieved the target MPHR for stage 1 exercise whilst only 2 (33%) achieved the heart rate target for stage 2 exercise. Meanwhile, only 4 (67%) and 1 (17%) participants from the control group achieved the target MPHR for stage 1 and 2 exercise, respectively. Although all patients tolerated the exercise regime and no adverse events occurred during the test, calf muscle fatigue was commonly reported by participants who did not achieve the exercise target, which prevented them from performing a higher level of exercise. This resulted in an overall lower heart rate level observed in the control group compared to the BAV group during stage 1 of exercise (98 ± 2 vs 111 ± 8 bpm, p=0.005).

Table 6. 3. Exercise haemodynamic data.

Characteristics	BAV	Control	*p*-value
Number of patients, n (%)	6 (100)	6 (100)	-
Resting haemodynamic			
Heart rate (bpm)	69 ± 10	58 ± 5	**0.036**
SBP (mmHg)	109 ± 12	112 ± 7	0.609
DBP (mmHg)	71 ± 11	68 ± 8	0.577
Pulse pressure (mmHg)	38 ± 6	44 ± 2	**0.039**
Stage 1 exercise haemodynamic			
Heart rate (bpm)	111 ± 8	98 ± 2	**0.005**
SBP (mmHg)	124 ± 17	131 ± 9*	0.425
DBP (mmHg)	76 ± 19	78 ± 8*	0.828
Pulse pressure (mmHg)	48 ± 5	53 ± 8*	0.254
Patients achieving target MPHR for S1 exercise, n (%)	6 (100)	4 (67)	-
Patients achieving target MPHR for S2 exercise, n (%)	2 (33)	1 (17)	-

*These values were obtained from 5 out of the 6 participants in the control group due to sphygmomanometer failure occurring in 1 control participant at time of exercise. S1, stage 1 exercise; S2, stage 2 exercise; MPHR, maximum predicted heart rate; SBP, systolic blood pressure; DBP, diastolic blood pressure.

As three-quarters of the study population did not achieve the predetermined heart rate target for stage 2 exercise, from this point forward, analyses were performed only on participants with complete data sets available from stage 1 exercise. This included data from 6 BAV patients (100%) and 3 healthy controls (50%). Three control participants were excluded from the exercise analysis due to failure to reach the exercise target for stage 1 (n=2) and sphygmomanometer malfunction at time of exercise (n=1), which precluded the necessary blood pressure assessment.

6.3.3. Real time exercise CMR imaging

In general, real time measurements for dynamic evaluation of aortic dimensions were feasible in all patients, both at rest and during moderate level of exercise (Figure 6.2), provided that the same upper body position was maintained on the MRI table whilst exercising. Of note, alteration of the aortic imaging plane occurred in one-third of the study participants as they inadvertently moved up the MRI table whilst exercising at a higher intensity (particularly during stage 2 of exercise), thus precluding comparative measurements to be made in these patients. Nevertheless, good spatiotemporal resolution was observed from the free-breathing real-time exercise CMR images, even when image acquisitions were performed with a heart rate of 150 bpm at the time of exercise.

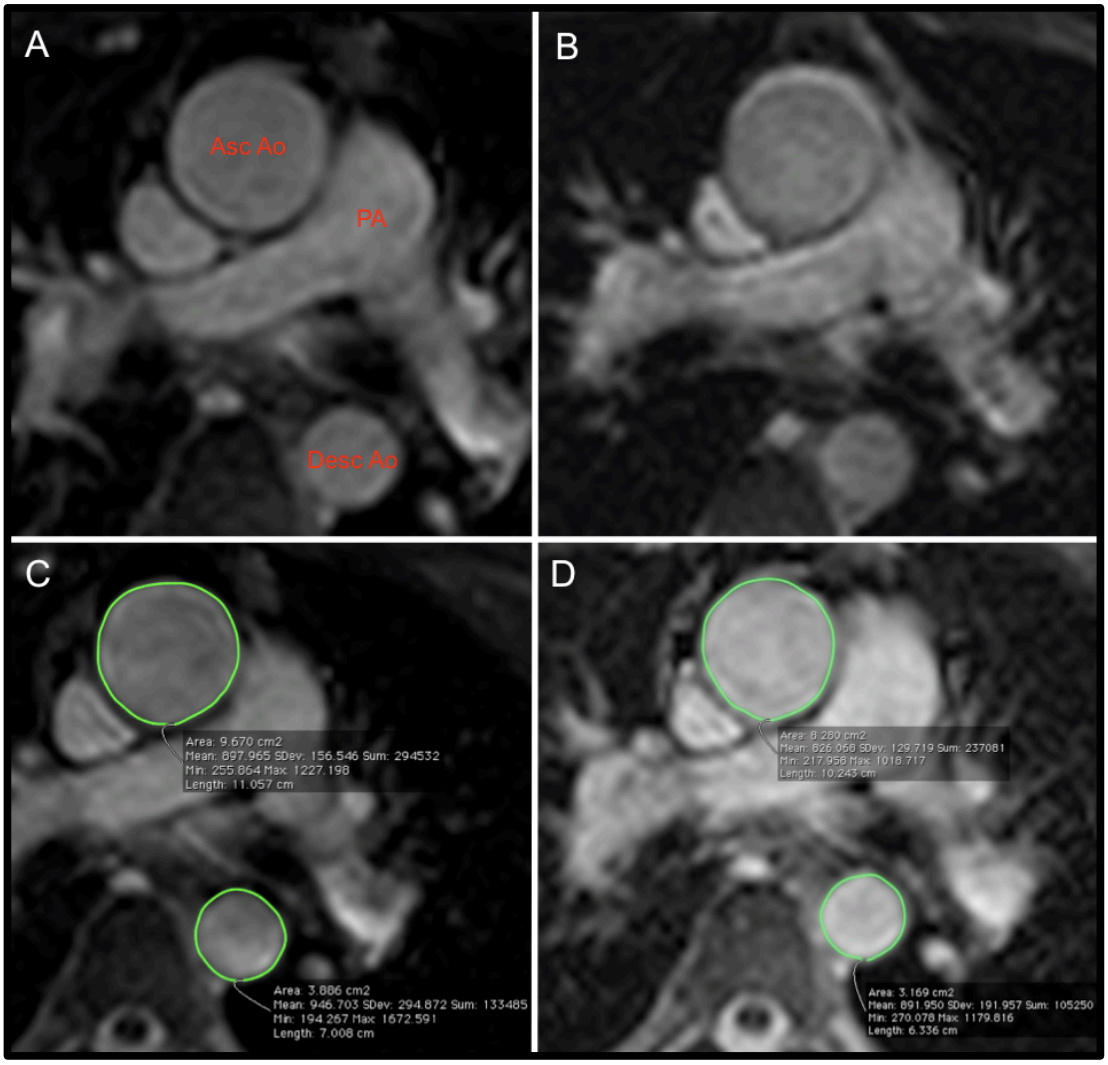

Figure 6. 2. Real time (RT) CMR images of thoracic aorta at the level of main pulmonary artery bifurcation in a patient with BAV.

Images were taken at rest (A, C and D) and during stage 2 of exercise (B), with heart rates of 70 bpm and 135 bpm, respectively. The images at the top panel (A, B) showed good spatiotemporal resolution of RT CMR imaging even during exercise. This allowed accurate assessments of the dynamic change in aortic area with each cardiac cycle as depicted by the lower panel, during maximal (C) and minimal aortic flow (D). PA, pulmonary artery; Asc Ao, ascending aorta; Desc Ao, descending aorta.

The biomechanical properties of the proximal ascending aorta and diaphragmatic aorta are compared between the BAV and the control groups in Table 6.4. Overall, no significant differences were observed in aortic distensiblity, compliance or stiffness between the 2 study groups, at rest or during low-level exercise, either at the level of proximal ascending aorta or diaphragmatic aorta. However, an immediate reduction of the proximal ascending aortic compliance was seen amongst subjects with BAV following a short period of resistance exercise using pedal ergometer (3.87 ± 1.25 and 2.89 ± 1.79 mm^2/mmHg at rest and exercise, respectively, p=0.035), albeit a low intensity one (Stage 1 exercise) (Table 6.5). Furthermore, exercise resulted in a significant reduction of aortic distensibility at the level of proximal ascending aorta (5.84 ± 2.61 vs 3.89 ± 2.89 $cm^2dyne^{-1}10^{-6}$ at rest vs exercise, respectively, p=0.019) and diaphragmatic aorta (8.24 ± 2.08 vs 6.66 ± 1.68 $cm^2dyne^{-1}10^{-6}$ at rest vs exercise, respectively, p=0.030) amongst the BAV cohort (Table 6.5). Whilst similar trends for reduction in aortic compliance and distensibility in response to exercise were also observed amongst the control group, they did not reach statistical significance.

Table 6. 4. Comparative aortic mechanical properties between BAV and healthy controls at rest and during low-level resistance exercise using pedal ergometer.

Parameters	Rest			Exercise (Stage 1)		
	BAV	Control	*p*-value	BAV	Control	*p*-value
No of patients for analysis (%)*	6 (100)	6 (100)	-	6 (100)	3 (50)	-
Distensibility ($cm^2dyne^{-1}10^{-6}$)						
Proximal ascending aorta	5.84 ± 2.61	7.15 ± 2.20	0.368	3.89 ± 2.89	3.45 ± 1.56	0.819
Diaphragmatic aorta	8.24 ± 2.08	9.17 ± 2.88	0.536	6.66 ± 1.68	6.96 ± 3.03	0.849
Compliance (mm^2/mmHg)						
Proximal ascending aorta	3.87 ± 1.25	3.35 ± 1.02	0.444	2.89 ± 1.79	1.88 ± 0.65	0.390
Diaphragmatic aorta	2.31 ± 0.88	2.10 ± 0.64	0.649	1.84 ± 0.39	1.99 ± 0.68	0.681
Stiffness index (β)						
Proximal ascending aorta	2.19 ± 0.69	1.73 ± 0.59	0.250	3.57 ± 1.86	3.28 ± 1.52	0.827
Diaphragmatic aorta	1.47 ± 0.44	1.36 ±0.45	0.661	1.70 ± 0.67	1.63 ± 0.79	0.885

*Only participants with complete data sets were included in the analysis. Three healthy control participants were excluded from the exercise analysis due to participants not reaching the exercise target (n=2) and sphygmomanometer malfunction at time of exercise (n=1), which precluded the necessary blood pressure assessment.

Table 6. 5. Acute impacts of low dose resistance exercise to aortic mechanical properties.

	Compliance (mm^2/mmHg)			Distensibility ($cm^2 dyne^{-1} 10^{-6}$)			Stiffness index (β)		
	Rest	**Exercise S1**	***p*-value**	**Rest**	**Exercise S1**	***p*-value**	**Rest**	**Exercise S1**	***p*-value**
Proximal ascending aorta									
BAV (n=6)	3.87 ± 1.25	2.89 ± 1.79	**0.035**	5.84 ± 2.61	3.89 ± 2.89	**0.019**	2.19 ± 0.69	3.57 ± 1.86	0.073
Control (n=3*)	3.08 ± 1.06	1.88 ± 0.65	0.177	5.80 ± 1.86	3.45 ± 1.56	0.175	2.13 ± 0.60	3.28 ± 1.52	0.236
Diaphragmatic aorta									
BAV (n=6)	2.31 ± 0.88	1.84 ± 0.39	0.075	8.24 ± 2.08	6.66 ± 1.68	**0.030**	1.47 ± 0.44	1.70 ± 0.67	0.136
Control (n=3*)	2.59 ± 0.42	1.99 ± 0.68	0.084	9.77 ± 1.85	6.96 ± 3.03	0.076	1.21 ± 0.16	1.63 ± 0.79	0.404

*Only participants with complete data sets were included in the analysis. Three healthy control participants were excluded from the analysis due to participants not reaching the exercise target (n=2) and sphygmomanometer malfunction at time of exercise (n=1), which precluded the necessary blood pressure assessment.

6.4. DISCUSSION

The purpose of the current pilot study was to use free-breathing real-time CMR imaging to evaluate the differential aortic wall mechanical properties in response to hemodynamic stress at rest and during exercise between patients with BAV and TAV, in the absence of significant valve dysfunction or overt aortic dilatation. This study showed that free-breathing real-time CMR imaging was able to provide adequate spatial and temporal resolutions to allow dynamic structural assessment of the aorta, at rest and during exercise, even with a rapid heart rate response of up to 150 bpm. In addition, whilst this study did not detect differential aortic mechanical properties between the BAV and control groups, immediate reduction in a number of measures of aortic elastic properties were observed amongst the BAV cohort in response to a brief period of low level resistance exercise. This included reduction in proximal ascending aortic compliance and distensibility, and interestingly, a decrease in aortic distensibility beyond the aortic arch, at the level of diaphragmatic aorta. This pilot study therefore provided an important foundation for further evaluation in a larger cohort to validate these findings.

Previous studies have established CMR imaging as a valuable noninvasive, accurate and reproducible tool to evaluate aortic wall function (Melina et al., 2002, Metafratzi et al., 2002). Unlike the standard applanation tonometry, which gives an average measure of the overall arterial stiffness, CMR imaging enables the detection of more subtle changes in regional stiffness of the aortic segment of interest (Cavalcante et al., 2011). Further, CMR ability to provide a

full 3-dimensional visualization of the aorta enables the imaging plane to be placed perpendicular to the vessel wall in a reproducible location, thus allowing accurate assessment of aortic distensibility and compliance (Cavalcante et al., 2011). These assessments are traditionally performed at rest and during breath holds, as high CMR image quality requires regular heart rhythm and constant cardiac position. Exercise therefore poses a significant challenge for standard CMR image acquisition, as a reliable ECG signal is difficult to obtain (due to magneto-hydrodynamic turbulence) and vigorous respiration causes cardiac translation, resulting in blurring or ghosting of images collated across cardiac cycles and spatial planes (La Gerche et al., 2013). To overcome this challenge, a free-breathing real-time CMR imaging technique has recently been developed and successfully used to evaluate biventricular volumes quantification during high-intensity exercise with high reproducibility and accuracy (La Gerche et al., 2013). In response to this finding, the present study evaluated the feasibility of real-time CMR imaging in evaluating the arterial mechanics in patients with BAV during moderate intensity exercise. Here, our study showed that free-breathing real time CMR imaging was indeed able to provide adequate spatial and temporal resolutions to allow dynamic structural assessment of the aorta, both at rest and during exercise. This likely has important implications for the development of future imaging protocols and other large vessels researches.

However, the present study did not detect a significant difference in measures of aortic elastic properties between the BAV and control groups, either at rest or exercise. This result is unexpected and is in contrast to previous studies that have shown the presence of significantly reduced resting aortic elasticity in

patients with BAV, even at the non-dilated stage, which not only affects the proximal part of the aorta but also extends into the entire aorta (Nistri et al., 2008, Grotenhuis et al., 2007, de Wit et al., 2013, Forsell et al., 2014). It is highly likely that the inherent limitation created by a small sample size used in this pilot study has resulted in insufficient power to detect a significant difference. Hence, further evaluation in a larger cohort is required.

Nevertheless, this study was able to detect an immediate alteration in aortic biomechanical properties amongst patients with BAV in response to a brief period of low-level resistance exercise, using a pneumatic pedal ergometer. The reductions in aortic distensibility and/or compliance were noted in both the ascending thoracic aorta and diaphragmatic aorta. While this finding is in agreement with a previous study which has shown that one bout of resistance exercise can acutely and transiently decreases central arterial compliance in healthy individuals (DeVan et al., 2005), this study is the first to investigate the impact of resistance exercise on arterial mechanics in individuals with BAV. As intense physical exertion, such as weight lifting, have been causally linked as an inciting event leading to aortic dissection (Hatzaras et al., 2007), this finding is important as it provides additional mechanistic insights into this potentially fatal event. Indeed, a combined effect of the inherent weakness in the mechanical properties of the aortic wall of BAV patients, a further reduction in aortic elasticity (or increasing aortic stiffness) occurring acutely during resistance exercise, and exercise-induced rise in central arterial blood pressures likely results in critically high wall tension that exceeds the tensile strength of the aortic wall, hence predisposing them to tearing at time of intense

exercise. Notably, the risk of aortic dissection in patients with BAV was approximately 8 times higher than the general population (Michelena et al., 2011).

However, the reason behind the acute reduction in aortic elasticity, or increased in aortic stiffness, during resistance exercise is not entirely clear. It had been suggested that an increase in sympathetic adrenergic vasoconstrictor tone and impaired endothelial function could be responsible for this phenomenon (DeVan et al., 2005, Pratley et al., 1994, Raastad et al., 2001). Interestingly, aerobic exercise, such as running, had been shown to give the opposite effect where an increased in arterial compliance was observed immediately following the exercise. Similarly, the mechanism behind this observation is unclear and could be related to sympathoinhibition after aerobic exercise (Seo et al., 2013). Therefore, given the contrasting effect of the different type of exercises on aortic mechanical properties, further study using a larger cohort that compares the impact of aerobic and resistance exercise on BAV aortas, in those with and without aortic dilatation, would be important. This has significant clinical implications whilst recommending an individualised exercise prescription in patients with BAV.

Further, although not overtly dilated, the presence of BAV in the study cohort was associated with significantly larger ascending aortic dimension, compared to the healthy controls with TAV, which is consistent with previous reports (Puranik et al., 2009, Padang et al., 2014). Given the common occurrence of ascending aortic dilatation and/or aneurysm in BAV and the presence of

inherent structural wall abnormality in the ascending aorta of BAV patients, irrespective of the underlying valve haemodynamic, a meticulous life-long surveillance protocol is clearly warranted in this group of patients, in case of progressive aortic enlargement over time (Padang et al., 2014).

This study has a number of limitations to be acknowledged. As a pilot study, this study was conducted in a small sample size and thus has inadequate power to conclusively address the research question. A larger study is therefore needed. All MRI-based measurements in the present study were made solely by the author of this thesis. Therefore, inter-observer variability and reproducibility need to be evaluated prior to its future application. Further, whilst real-time CMR imaging can achieve good spatiotemporal resolution for measurements of dynamic changes within the vascular wall, a constant position on the MRI table during image acquisition whilst exercising remains important. Alteration in imaging plane as subjects shifted their position upwards on the MRI table was observed in one-third of the study during stage 2 of exercise, precluding further analysis. In the future, this could be avoided by providing a fixed shoulder harness, attached to the table, to prevent upwards shifting during intense exercise. Additionally, three-quarters of the study participants failed to reach the heart rate target for stage 2 exercise, as calf muscle fatigue prevented more vigorous exercise, thus limiting the heart rate response when patients cadence on the pedal ergometer gradually decreased. Different types of exercise during CMR imaging should therefore be considered, such as using programmable cycle ergometer. Also, as previously mentioned, a comparative

study on the impact of the different type of exercises on BAV aortas should be undertaken.

In conclusion, this pilot study supports the use of free-breathing real time CMR imaging in the assessment of dynamic structural alteration of the aorta in response to haemodynamic variations at rest and during exercise. Further study with a larger cohort is required to conclusively evaluate the differential impact of exercise on aortic wall mechanical properties between patients with BAV and TAV. A clinical correlation to evaluate the relationship between the degree of alteration in their aortic elastic properties and long-term outcomes in terms of aortic events would be equally important. Identification of different aortic mechanical properties between patients with BAV and TAV, or even amongst the BAV patients themselves (i.e. between those with and without aortic dilatation), during episodes of increased haemodynamic stress is important as it could potentially be used as imaging biomarker to identify patients with a more 'malignant' disease course. For this purpose, CMR imaging is indeed an invaluable non-invasive imaging tool for the assessment and follow-up of patients with this relatively common syndrome.

CHAPTER 7: SUMMARY AND CONCLUSIONS

7.1. SUMMARY AND FUTURE RESEARCH

Whilst the familial clustering and heritability of BAV disease have been increasingly recognised in the past 4 decades, the underlying genetic basis of BAV in humans remains mostly undetermined. And although clinical heterogeneity seen in BAV possibly reflects complex and variable interplay between specific gene mutations, modifier loci, epigenetic control and environmental influences (particularly haemodynamic basis), the gene and molecular pathways that drive specific phenotypic expression and determine disease progression / outcome are not well understood. Moreover, identification of individuals with BAV who are at the highest risk for related complications presents a highly challenging task for most clinicians today. The work carried out in this thesis aimed to address these gaps in our present knowledge of BAV disease. The work focused on many aspects of BAV disease, from the investigation of genetics underlying BAV development using candidate gene approach (Chapter 3) and whole exome sequencing (Chapter 4), elucidation of genes and molecular pathways that determine valve degeneration in adult patients with BAV by means of RNA sequencing (Chapter 5), to efforts in identifying novel imaging biomarkers that can potentially be used to predict those with the highest risk for adverse aortic complications using state-of-the-art real-time exercise CMR imaging (Chapter 6). An overview of the studies completed in this project is presented in Figure 7.1. Much of the work carried out in this thesis will form a foundation for future research, building on the genetic data obtained from exome and RNA sequencing studies, as well as clinical and imaging data obtained from the CMR study.

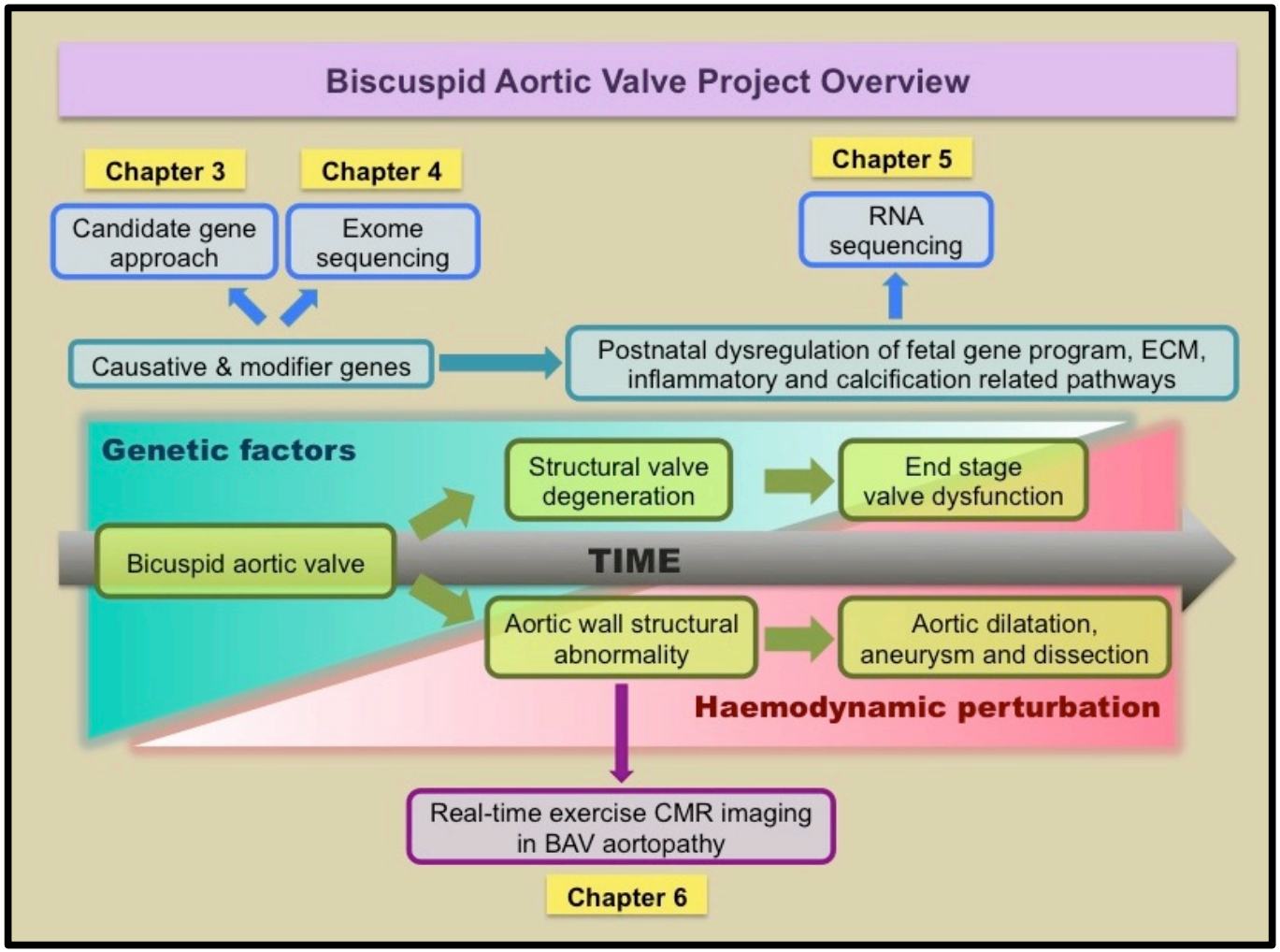

Figure 7. 1. Overview of this PhD study in the investigation of clinical and pathogenetic basis of BAV disease in humans.

7.1.1. Identification of causative and modifier genes in BAV disease

BAV is a clinically heterogeneous disorder with valve dysfunction and related aortopathy being the major complications. However, despite it being the most common congenital heart defect in adults that is accountable for more deaths and complications than the combined effects of all the other congenital heart defects, the underlying genetic basis of BAV is mostly unknown (Padang et al., 2012b, Siu and Silversides, 2010). Genetic studies and familial clustering demonstrate that BAV is a highly heritable disease (Cripe et al., 2004, Garg et al., 2005, Siu and Silversides, 2010). Until recently, only mutations in the transcriptional regulator *NOTCH1* gene have been linked to the development and calcific progression of non-syndromic BAV in humans, in a limited number of familial cases and ~4% of sporadic cases (Garg et al., 2005, McKellar et al., 2007, Mohamed et al., 2006). For the remaining majority, the underlying genetic basis of BAV is undetermined.

Recently, studies in animal models have demonstrated the essential role of *GATA5* in cardiac morphogenesis and aortic valve development (Laforest et al., 2011, Laforest and Nemer, 2011). Further, in 2011, Laforest *et al.* reported that targeted deletion of *Gata5* in mice led to partially penetrant BAV (Laforest et al., 2011). At the time of commencement of this PhD, there had been no study that evaluated the role of *GATA5* mutation in human BAV disease.

Following Laforest *et al.* work on *Gata5*$^{-/-}$ murine model, this project first evaluated the role of *GATA5* mutation in human BAV disease. The results are

presented in Chapter 3, which reported the presence of rare non-synonymous variants within the transcriptional activator domains I and II of the *GATA5* gene, affecting 4 out of the 100 prospectively recruited BAV cohort. These variants may alter the transcriptional activity of *GATA5* and thus may contribute to BAV development. This study was first to provide support for the potential role of *GATA5* in the development of human BAV disease. This finding was subsequently reinforced by 2 more recent studies, using 2 independent BAV cohorts, and the pathogenicity of the variants found were supported by *in-vitro* assays (Bonachea et al., 2014 [Epub ahead of print], Shi et al., 2014). However, it remains uncertain if rare non-synonymous *GATA5* variants are directly causative or serve as critical genetic modifiers and future studies that explore this relationship are warranted.

Further, while this finding is important, - like the *NOTCH1* gene and similar to findings from the other studies -, *GATA5* variants are not responsible for the majority of cases of BAV. Hence, the project also explored a number of other candidate genes, including investigating the relationship between *NKX2-5* mutations and BAV in the same patient cohort, as well as screening the *NOTCH1* and *GATA4* genes in a small subset of the study cohort. However, no potentially pathogenic variants were identified during screening of these candidate genes. Therefore, further investigation to explore new candidate genes for BAV disease is needed.

Meanwhile, advancements in sequencing-based technologies over the past decade have resulted in the emergence of massively parallel sequencing

technologies, such as whole exome sequencing. Whole exome sequencing is a powerful tool in the study of complex diseases, such as BAV, as it provides an unbiased, cost-effective, and comprehensive genetic screening strategy (Bamshad et al., 2011, Towne et al., 2013), which allows discovery of novel, unanticipated pathogenic gene variants that play a role in disease development.

Given the limitation and the relatively low success rate of candidate gene approach in the study of BAV genetics, whole exome sequencing studies were then adopted to investigate the genetics underlying familial cases of BAV (Chapter 4). Exome sequencing data was obtained on 6 affected individuals originating from 2 large families with preponderance for BAV and the related aortopathy (i.e. 3 individuals per family). There were 3 key findings resulting from the subsequent co-segregation analyses in this study. Firstly, heritability of familial cases of BAV appeared to be autosomal dominant with incomplete penetrance and highly variable clinical manifestations. Secondly, the 2 families had a completely different list of shared candidate gene variants. Assuming that the causative variant was present within the lists, this implied that different genetic mutations to be responsible for the development of BAV in Family A and B. While this finding is not completely unexpected, it supported a previous observation that suggested the presence of mutations in diverse genes (i.e. genetic heterogeneity) to be responsible for the development of BAV in different families (Cripe et al., 2004). Finally, this study identified mutations in the GDNF-related pathway to be mutually occurring in both families, thus providing some clues toward its potential regulatory role in BAV development, which warrants further investigation.

Overall, findings from the candidate gene approach and exome sequencing studies highlighted the complex and heterogeneous nature of BAV genetics and the likely presence of genetic modifiers or other regulatory control during BAV development. Whilst the genetic basis of BAV in the majority of cases remains to be elucidated, this project has given new insights into the underlying genetic basis of BAV in humans. It also has provided a platform for future research, in particular studies that continue to build on the genetic analyses performed to date, including the completion of co-segregation studies in both families upon further recruitment of additional family members and performing rare copy number variant analysis on the available exome data.

7.1.2. Molecular pathways underlying structural valve degeneration in BAV

The work in this thesis subsequently focused on the molecular pathogenesis behind structural valve degeneration in human BAV disease. Structural valve degeneration (SVD) and consequent valve dysfunction is the most common complication of BAV disease, which is highly heterogeneous in its clinical manifestation. It is believed that aberrant and variable modulation of both qualitative and, to a larger extent, quantitative level of gene expression at the level of the aortic valve, e.g. through splice site variation, 3'-untranslated regulatory regions, noncoding RNAs and the direct interactions of transcription factors, likely contribute to the marked phenotypic heterogeneity observed in

SVD in BAV disease. To investigate this further, transcriptome interrogation was performed using RNA sequencing.

RNA sequencing is particularly useful in providing a snapshot assessment on the present state of gene expression for a given cell or tissue, which ultimately is the product of interaction between genetic factors, environmental influences and even the effect of the disease state itself on the transcriptome (Churko et al., 2013, Schnabel et al., 2012). Elucidation of distinct gene expression signatures in different BAV disease states can therefore provide insight into perturbed molecular pathways contributing to a specific valve disease phenotype, such as a predominantly calcific BAV with stenosis or a predominantly regurgitant BAV with leaflet redundancy. In turn, this may lead to the identification of novel therapeutic target that aims at delaying or stopping valve disease progression.

Findings in Chapter 5 described, for the first time, the result of genome-wide differential transcriptome profiling underlying SVD in human BAV compared to TAV using RNA sequencing. The study identified that differential gene expression profiles existed even within the BAV group themselves, dividing them into those with calcification predominant disease and those with primarily redundant leaflet degeneration. Further, it demonstrated the relatively close resemblance of gene expression patterns of calcified human BAV and TAV leaflets, with shared upregulation of inflammatory pathways and downregulation of *NOTCH1* signalling, indicating a common mechanism of calcific leaflet degeneration in both BAV and TAV. This finding on the importance of NOTCH1

signalling in the development of calcific aortic valve stenosis in both BAV and TAV supported results from previous studies that showed the presence of rare functional DNA variants at the *NOTCH1* locus in patients with severe aortic stenosis in the context of BAV and TAV (Garg et al., 2005, Ducharme et al., 2013). Moreover, a unique pattern of dysregulation of foetal gene programs was also identified amongst the different study subgroups. This provides further support to a growing body of evidence, which suggests that developmental pathways important in valvulogenesis also contribute to adult valve disease (Lincoln et al., 2006). Taken together, these findings indicated the presence of distinct gene expression signatures that marked the different type of SVD in BAV, compared to TAV, supporting the emerging theory that BAV is heterogeneous with respect to molecular events in disease progression (Fedak, 2008). Further research however is necessary to confirm these findings and determine if these differential gene expression patterns and molecular mechanisms can be exploited for new clinical therapies.

7.1.3. Utility of real-time exercise CMR imaging in BAV-related aortopathy

In the final part of this thesis, my work concentrated on the identification of new clinical markers to improve risk stratification of BAV patients who are at risk for developing adverse aortic complications. Here, the project investigated the role of state-of-the-art real-time CMR imaging in the evaluation of differential aortic wall mechanical properties between patients with BAV and TAV in response to hemodynamic stress at rest and during exercise, which can potentially be used

as an imaging biomarker to predict those with a more aggressive disease phenotype (Chapter 6).

BAV-related aortopathy, another common complication of BAV disease that affects over 50% of patients (Fedak et al., 2002), is a potentially lethal condition due to the propensity for dissection or rupture. Similar to the valvular manifestation, BAV-related aortopathy has a highly heterogeneous phenotypic expression and both genetic and haemodynamic factors contribute to its development (Padang et al., 2013). Further, the rate of progression and clinical outcome of those with BAV-related aortopathy varies significantly between individual patients (Detaint et al., 2014). This suggests the presence of inherent differences in how each individual aorta responds to haemodynamic shear stress associated with activities of daily living. Presently, making a clinical prediction regarding which patient has a more 'malignant' disease phenotype, and thus would benefit from an earlier and/or more extensive intervention, is a highly challenging task for most clinicians, and yet, it has important surgical implications. There is therefore a pressing need for the identification of novel, non-invasive imaging biomarker that can predict for the development of adverse outcome in those with predispositions for BAV-related aortopathy.

This awareness had led to a pilot study utilising free-breathing real-time CMR imaging to evaluate the differential aortic mechanical properties between patients with BAV and TAV in response to exercise, as described in Chapter 6. The hypothesis behind this study was that the increased hemodynamic shear stress produced by exercise could exaggerate the differential aortic wall

mechanical properties between BAV patients with predisposition for BAV-related aortopathy and those with TAV, thus identifying those at risk for adverse events.

This study had 2 key findings. Firstly, it demonstrated that free-breathing real-time CMR imaging was able to provide the necessary spatial and temporal resolution to allow accurate dynamic structural assessment of the aorta, both at rest and during exercise, even with a heart rate response as high as 150 bpm. This finding has important implications for the development of future imaging protocols and other large vessel research. Secondly, whilst this study did not detect a statistically significant difference on aortic mechanical properties between patients with BAV and TAV, presumably a result of the inherent limitation created by a small sample size, the study identified an immediate reduction of aortic elastic properties amongst patients with BAV in response to a brief period of resistance exercise. While this finding is in agreement with a previous study which shows that one bout of resistance exercise can acutely and transiently decreases central arterial compliance in healthy individuals (DeVan et al., 2005), this study is the first to investigate the impact of resistance exercise on arterial mechanics in individuals with BAV. As intense physical exertion, particularly resistance exercise such as weight lifting, have been causally linked as an inciting event leading to aortic dissection (Hatzaras et al., 2007), this finding is important as it provides additional mechanistic insights into this potentially fatal event, especially since the risk of aortic dissection in patients with BAV was approximately 8 times higher than the general population (Michelena et al., 2011).

This study therefore provided an important foundation for further evaluation in a larger cohort to validate these findings, as well as to conclusively evaluate the impact of exercise on the differential aortic wall mechanical properties between patients with BAV and TAV. Data obtained from such studies have important clinical implications in areas where evidence-based medicine is presently lacking. Indeed, they can potentially be used as imaging biomarkers to identify high-risk patients with rapidly progressing aortic dilatations or even as a guide whilst recommending an individualised exercise prescription for patients with BAV, who are often relatively young but at a higher risk of adverse aortic events.

7.1.4. Clinical significance of research

The findings presented in this thesis, coupled with previous studies, provide mounting evidence on the complex and heterogeneous nature of BAV genetics and the likely presence of genetic modifiers or other regulatory control during BAV disease development and progression. While the results from the genetic studies presented in this thesis may not be directly or immediately be applicable to the present day-to-day clinical management of BAV disease, they have added new insights into the current understanding of the genetic and molecular basis underlying BAV development and subsequent valve degeneration and dysfunction. These findings are therefore important given the present limitation of available therapeutic armamentarium in delaying or halting BAV-related valve disease progression, which has left surgical therapies as the most effective, but

not necessarily the ideal 'cure'. Indeed, results obtained from this thesis have provided an important step forward in our understanding of gene and molecular pathways involved in the pathogenesis of human BAV disease, which will help foster the development of new therapies that halt disease progression.

Finally, while the present attempt to identify novel imaging biomarkers in BAV-related aortopathy using CMR imaging is inconclusive, the study has laid a foundation for future research in a larger cohort and established the feasibility and the potential application of real-time free-breathing exercise CMR imaging for other large vessel researches. Further, the result of this study indicated the need for a comparative study that evaluates the impact of different type of exercise on aortas of patients with BAV, as our preliminary data, together with others, hinted that they could be different. Such a study will have significant implications on the clinical management of patients with BAV, as it will allow clinicians to make personalised exercise prescriptions that have been tailored to each individual's risk for adverse aortic complications. In turn, this will likely translate to improved quality of life and outcomes of patients with BAV.

7.2. CONCLUDING REMARKS

In conclusion, the studies presented in this thesis have contributed to the present understanding of the underlying genetic and molecular basis of BAV disease development and progression in humans. While much work remains, the studies in this thesis have identified important questions, which will form the basis for future research aimed at identification of molecular targets for potential therapies to halt or even stop valve disease progression. The project also has laid an important foundation for future real-time exercise CMR imaging-based work in efforts to identify novel imaging biomarkers that can be used to better risk stratify those with BAV-related aortopathy. Overall, the work in this thesis have provided an important step forward in our efforts to gain greater understanding on the pathogenetic basis of BAV disease and one step closer towards our ultimate goal in reducing the overall health burden created by this complex, albeit common, human disease.

APPENDICES

Appendix I. Primer sequences and corresponding PCR or RT-qPCR conditions

Table I- 1. *Nkx2-5* and *GATA5* candidate genes primer sequences and corresponding PCR conditions.

Exon	Forward primer	Reverse primer	Product size (bp)	Ta (°C)	10% DMSO used
Nkx2-5x1	CTTGTGCTCAGCGCTACCT	TTCCTCTGAACCTCCGATTG	676	60	No
Nkx2-5x2	CACAGTGGCCTCCACGAG	CAAAATCCAGGGGACTCAGG	850	66	No
*GATA5*x1	GTTCCTCTCCCTCGGGTTC	CTGCTGGTGTCGCTCCTG	833	57	Yes
*GATA5*x2	CACAAGATTTGTGCCTTAAGTTT	GCGCTCTCAAAGAAGACCTG	491	60	No
*GATA5*x3	GAGCGTGTCCAGGCAGAG	GTGCCGTGAGTGTAACAGGA	489	65	No
*GATA5*x4	GCCAGACAAGGACACTGCTC	AGGTCACCACAGGGCAGA	496	65	No
*GATA5*x5	GGTGGTGACAGCATGTGG	AGAGCCAGCTCTAGGGGAAG	490	65	No
*GATA5*x6	TCCCTAAGGGCAAATACCG	GCCTCCCCACCACTGTGT	423	57	No

PCR reactions were performed in a 25µL final volume; Ta, annealing temperature; *25% deazaNTP was used in PCR reaction mix, rather than using the standard dNTP. The 25% deazaNTP mixture was made by mixing 10 mM (5 µL) dATP, 10 mM (5 µL) dCTP, 10 mM (5 µL) dTTP, 7.5 mM (3.75 µL) dGTP, 2.5 mM (12.5 µL) deazaGTP and 68.75 µL of TDW, making up at total volume of 100 µL.

Table I- 2. Primer sequences and corresponding PCR conditions used for validating variants identified through exome sequencing in Family A.

Variant gene name	Forward primer	Reverse primer	Product size (bp)	Ta (°C)	10% DMSO used
GTF3C5	GCCCTTGAAGCTGCTCAT	CTCCTCGTCTTCCCCAGAC	299	55	No
COL11A1	AAGTAGGTCATTTTTCTTCTTCAAAT	CACAGTATACAAGTGAAGCACCA	489	55	No
MAP2	CAGTTGCAGGAGAAATAACAAGG	GGGGAAATGTCAAGTTAGTTGC	471	55	No
ARAP2	CGGCTCAGTGAAAAGTGTGA	CCAAAGTAGCTTTGCTATTCCTG	238	55	No
RFC1	AAACATGGATTATCTGTCGCTTC	CAAACCTGGTAATAGAAAGTGACG	240	62	No
PKD2	TGACAAGCACTTTGTCCCTCT	TTTTCATTAATAACACCATGCTCA	244	50	No
AHRR	CCATCAAGATGGAGAAGGACTC	AGGGTGGAAAGGGGTCAG	245	64	No
FNDC1	TGAGTTGATAGTTGCGCTGTTT	CAGCTCTCCATTCCCAAAGA	359	55	No
HGF	TGTCTTTGTTTCTTACTTTTCTCACC	CACTAAGCTATGAATCACATACTCCTT	248	55	No
SLC4A2	GGGTCCTAGTGGGAGGAGTG	ATGGGCAGGAGTGACCAG	395	65	No
MMP17	AGACAAGAGGTGCCTTGTGG	AGCTACACCAGGCCAGGAC	399	65	No
GAS6	CCCCGTTAGAATCTGCATGT	TTCTCATCCCAAACCTCCAC	398	55	No
ADRB2	CCCTCAAGACGTTAGGCATC	CCACGTGATATCCACTCTGC	294	54	No
BCLAF1A	GAAGGGGATGACACAGAGGA	TCGTGCATCCAGATTCTTGT	375	54	No
BCLAF1B	TTTAGAATGGTAGCATGGAATACTT	ACTCCTGGAACGTGAACGAC	298	54	No

Table I-2 continued

Variant gene name	Forward primer	Reverse primer	Product size (bp)	Ta (°C)	10% DMSO used
BCLAF1Sp	TGACGACAGAGATGATGGTGT	ATGCGGAGAGTGAAAAGGAA	324	54	No
FAM160A2	GCTGCTCAGAAATGTCACGA	TTCTGTCCCCTGACCAGAAG	360	54	No
GPR98	CCCACTTTGGAGAACTTGGA	TGGCTGAAATGTTCATGAGG	398	54	No
NCOR1	ATTCGGAGGCAAACATGAAG	CAAGTCCGAATATATAAGGCATGA	298	54	No
TIGD6	TGATCTCATTATCTCTCAGGACACA	TGCATTATTTTGTTTGGAGGAA	296	54	No
TTC18	TCCTCTCACCAATCTTCTTGC	ACAGCCCTGATTGCTATTCC	378	54	No
ACACB	GCCTGAGCATCAGGATTTGT	AGGAGGTGACAGGGACAGAA	362	53	Yes
HGSNAT	TGTGACTCATCTGTGAGAAACAT	CAAAGGCTGCTTCAGTCCTC	300	53	Yes
LMOD2	CAGCAATGGGAGGAACACA	CGACGTTTACGTTGGTGATG	293	53	Yes
ULK1	CGGAGCACAGGAAGAAAGAC	CACACTGTGCATCCAACACA	380	53	Yes
ADAMTS6	CGTGTTTTAACCCTGTAAATGGA	CGCTTTGTAAAAGCTGCACA	314	54	No
PLCL1	ATCTGGGTGTCTGGGTTACG	AGCATGAGATCATTGGCATC	374	53	Yes
SLC6A3	CTTGGGAGTCAGCGAGGA	GACTCCAGCCACAGTGACAA	299	57	Yes
FASN	TGCCCTGAGCTGGACTACTT	TCATCGTCTCCACCAAAATG	358	64	No
HS1BP3	ACTCCACTCCAGGCTTCCTT	CCTCTTCTGCCACTTGGTCT	392	65	No
ITGA10	TCCATTTTTGGAAACAGAACAA	GCTTCTTGTCCCATCTGAGC	269	50	No
MAP2K3A	TACCGAGGCTAGGCTTTTTG	GACTGATGGGTGGGAGGTG	294	64	No
MAP2K3B	CAGCAGCCAGTGAGAGGAG	CTCGTCAGGTGAAGTGAGAGG	250	65	No
SH3RF3	GCATGGCAAGTTGCAAACTAA	CTTGGAGCCCACATTCTAGC	491	65	No

Table I-2 continued

Variant gene name	Forward primer	Reverse primer	Product size (bp)	Ta (°C)	10% DMSO used
UGT3A1	AGTTTCTCCAGGAGCCAATG	TCCCAAACTGAATGCTGAGG	249	57	No
KDM1B	TGCCACCACATTCTTTAGGA	TTGGACCAAAAGGAGCAGTC	277	50	No
ABCA13	TGTAGGATTCAGTAATATCTGCATTT	GCATAATGGTTATGAGCATGG	250	50	No
ACTR3C	TGGGCTTCCTGGTTATTTGT	CCATCCCACACTTGAGCAC	295	57	No
ABCB4	TTATGGAAGAGGAGAAATTCCA	GGTAATGAATAGCAAAATCAACTCC	296	57	No
AFMID	TTGGAGACCCTGGGATACTG	CCCCAGCATTCTGAATCAC	290	50	No
TH1L	GGAGGCTTGGCTCTCGTC	GAGCTAGCAGCTTTGGCTGT	299	65	No
URB1	GGGCTCTGTGACCAGTCTCT	GAAGCTGAGGGTGCAGATG	287	65	No
SASH1	CTCACCACGTCTCCATCCTC	TGAAACTCCTCCAGGGACAC	293	65	No
MED16	CTGCAGGGCTGTTGAAGG	AGAGGGCGTTTATTGGACCT	288	57	Yes
RTP4	TCCTGAGAAACGAGCAAACC	CCTTCAACAAGCTCTCAGAGGA	300	65	No
ANKAR	ACACTGCCATTTGTTTGCAT	TCCTTTAAAAATGCTGGGTTAAT	300	54	No
BST1	GACAAATGGGCATACTTCACAA	ATGCAGGGGACAGCTAATGT	294	54	No
BTBD16	TGTCGTCTCAGGCCAGCA	AGCCTCCATCAGAGCACCT	293	63	No
C1orf168	AAAAACATGTGGGTGAGTTTCA	AAAAGATGATGATGGGAGTCG	344	60	No
DDX51	CCTCCCCTAGCTTTTTCCAC	CAGGGAGGTGTTCCCTCAG	276	63	No
DNAH10	CAGCTGCCATTGTTTGTCC	AAACACGCTGAGTCGAAAGG	289	60	No
DNALI1	GGCATTCTCTCCTCAGATCG	CAGTGCATGTGGACAAACAT	293	54	No
GDNF	ACAGCAAATATGCCAGAGGA	GCAAGAGCCGCTGCAGTA	300	63	No

Table I-2 continued

Variant gene name	Forward primer	Reverse primer	Product size (bp)	Ta (°C)	10% DMSO used
GJB6	CTGCCCTGGGTGTTGAAAT	GCTTGGGAAACCTGTGATTG	297	60	No
HKDC1	GCACGTAGGCATGAAGTTTCT	CTCTGATTCTCCCTCCATGC	300	63	No
HPS3	TTCTCACTATTGGACTTTGAACG	CCGGGCACCATATATACCAC	299	60	No
KCNMB3	TTCAAAAGGAATGGCAAAAGA	CATTTGACACAGCAAGATGC	300	54	No
LRRN4	CAGAGGACACACGCCACA	GTCCGTGGTCTCCGTCAC	279	65	No
NOS3	GGCTCTCTAACAGTCACCAAAA	CTAGCCCCTGTGCCTCATT	300	60	No
ULBP1	TAGGATCCCGCCCAGTGTAT	CCAGAAGCCTCCCCTCCT	298	63	No
TACC3	GCTTGTCCACATGGTCCTCT	CAAAACCAAAGGCTCAGACC	272	63	No
PRH2	TTCACCACCCTAATGTGGATT	AGGGCCATCATTCTGGTTC	287	54	No
NUP43	TGTTTTGGAGCAACATTTCC	CAACTTTTATGATGCTCTGCTTG	297	60	No
PDE4DIP	GCCCCTTTCACAGTTGGATA	GCTCAATAACCACGTTATGTCG	297	60	No
MICALCL	GCCTCCAAAGAAAAGAATCTCA	GGGCAGACATTTATCAGGACA	295	63	No
MUSK	TCATTAACAAGTCATCGGTTTGA	AGGTTGCAGTGAACCGAGAT	392	51	No
PCDHB7	TCAGGTCCCTGGACTACGAG	CCATTGTCCTTGACCAGCA	397	54	No
NEURL2	ACATCTGCGTCTCGGTCTG	CTGGTCCAAGAGATGGCTGT	286	63	No
MATN1	CCACTGACCTGGTCTTCCTC	AGTTGGGCTATACCCGTGTG	458	61	No
PTGES2	GTTGGTCCTGGCTCCACTCT	TCTACTGAAATCCGGCATGG	395	61	No
TGM2	TAGGAGGGCAGATTGTCCAG	GAAGGGGCATATTTTGCTCA	396	53	Yes
PMPCB	CTGCAGACTCCCCAATTCAT	CGACCCACTGTTCGGATCT	384	53	No
SVEP1	TGCAGGCATTGCTAAACTTG	TGGAGAGGAGTAAGACAACACATC	438	53	No

Table I-2 continued

Variant gene name	Forward primer	Reverse primer	Product size (bp)	Ta (°C)	10% DMSO used
WDR47	TTAATAAGCTGTTGTCTGACACG	CAGAAATACAACATGGAGAAAACATAA	365	56	No
ECEL1	CTCCAGATGAGGGACAGAGC	CACAGGACCATCACCTCTGA	456	63	No
ZNF831	CCTGTGGGCCCAGACTGT	GGGCAGAGAGCACTCTAGGA	398	63	No
TYRO3	TCCAGTGATTCTGGGGACA	CTCACCACGTCACTCTGCAC	580	63	No
B7H6	GGAGGTGTATGTGATAGGAATGG	TGGTGAAGAGGGACTGACAA	399	61	No
BRSK1	TGGTAATGGGAACCCCAAC	GGGCCTTATTTACAGATTCACA	300	61	No
CST4	TGCCAGCTGACAGGAAGAG	ATACACGGCTCCCCACATAC	399	61	No
CYP7A1	AACATCCGGACAGCTAAGGA	CAAAGACTGTGTGATGGCAAA	342	61	No
GPRIN2	CCACTCCCTCCCTTTCTCTC	TGCATAGCAGCAGCACTAGG	387	61	No
SI	CATACAATGTGTGACTAAACGTCAG	TTTCACCTCCACACGAAGAG	271	61	Yes
SDSL	TAATGCTGAGCTCCAACCAG	GACTTCGTGGGTCTCTGAGC	296	61	No
PUS1	ATGTCGGGTCCTCACAATTC	GCTCCTGGACGTCTCACCTA	290	61	No
MTHFR,LOC10	AGAGAGGGCCCAGCTGTAG	TGACTCAACTCCCCTTTCCA	291	61	No
OXA1L	CCCTCAGGTCCTTTACGACA	TCTCTGTGTGCCACAGTTCC	245	56	No
GNAS	AAGCAGCAGAGATGGAAGGA	TGAGATGGATCTTGCGTCTG	516	56	No

PCR reactions were performed in a 25µL final volume. Reaction condition was one cycle of 95°C for 2 minutes, followed by 35 cycles of 95°C for 30 seconds, primer specific annealing temperature (Ta) for 30 seconds and 72°C for 1 minute, followed by a final extension of 72°C for 5 minutes. Ta, annealing temperature.

Table I- 3. Primer sequences and corresponding PCR conditions used for validating variants identified through exome sequencing in Family B.

Variant gene name	Forward primer	Reverse primer	Product size (bp)	Ta (°C)	10% DMSO used
COL6A6	TGAAGGAATTTCTGGCATCTG	GGACTGGCCATCTGTAAGGA	287	53	No
MYH7B	GGAGAATAGCCGGTAAGCAC	GCGAGTTCAGAGAGGTCTGG	299	63	No
MLKL	CATGAAAATGCTGGGGAGAC	ACGCTCCTCTTTCCTTGGTC	284	64	No
ZNF226p358	TGGGAGAAAAACTTAAGTGTGATG	TGAGCTACAAATGAAGCCCTTA	389	61	No
TFF2	TTGGAGCAGTCCTGTGTCTAAG	TCACTCCCAAGAAAAGACAGG	299	61	No
ZNF234	GGAGTGCACACCTTCAAGC	CCCAGTGTGAACTCGCCTAT	293	64	No
SVIL	TGCTTTTGAAGTTCTTTCGTGA	CACGGCATTGACTTGTTTGT	373	53	No
DMKNp230	AGGAGGCAGATGGGAAGG	CCATGATGCCCAGTCTAAGG	284	64	No
ERBB2	TGGCATGACTTGGAGTGAGT	TCACCTGCAGGAAGGACAG	247	63	No
POLE4	CCTAACTGCCCACCATCTGT	TGGAAGACCTTGCAGAGAAGA	387	65	No
ACVR1C	ATCACCAAATGCCCCAAAA	TGGTAACATACCAGAGCCAGA	250	61	No
ETV4	ACCAGCATGGGAGAGAAATG	GTAGGCGGGGCTCTCATC	298	65	No
BZRAP1	CAAGCCCTTCCAGAGAGATG	CTCTCCTGCAGTCCACTCG	278	64	No
DENND2C	GATCCATAGCGTTGGCACTA	GGAACAAATAAAACACCAGTGTGA	269	61	No
RBM45	TTAAGAAATGGGAAAATAGTTGACA	ATGTAATTCCCCAAGACTACTCTATT	300	53	No
FUK	CTGTCCAGCTGGGTCCTG	AATGCAGGGTGACTGCCTAC	347	65	No
ZNF226p83	CAGTGCATAGGTCTTCATGCTT	CATAGTCACTCAAGGAATGTATGC	300	61	No
TIAM2	ATGCACGCTGCTGTTTTATG	CAAGTTTTGCCTTTTCTGTTCC	250	64	No

Table I-3 continued

Variant gene name	Forward primer	Reverse primer	Product size (bp)	Ta (°C)	10% DMSO used
DEFB124	TGACCTGTGGTTTTCCTCTG	CCATTTCTCCCACATCCTAGA	300	61	No
DMKNp135	AGGCTTTGGCGTAGCAGAT	TCCATCCTTTCAACCGTTTC	250	61	No
BRD7	CCCTTAACAGGTCATCAAGGA	TGATGAAGAGCTCTATGGCAGA	391	61	No
SMG5	TGGAAAGATCAGAGAGTTAGAGC	ATGGGTCCAGTCGATGCAG	300	61	No
FAM198B	GGCAATGGGTCCACTCTG	TAACCAGGTTTGCTCCCTGA	232	61	No
WTAP	GTCCTCCAACAGCTCAGAGG	ACACTTGAGTCCAAGCCATT	231	64	No
SERINC3	GCGCCTTTTATATCCTGTCAA	GGCATGAAATAGAATTATGAAGACTTT	300	53	No
SEMA5B	GAGGGGCATCTGTCTCTGTC	AGAATCCAGGCCACTTTCTG	249	65	No
ASPG	CTGGGCCCTACCCTCAGA	TGCAGCCCTAGCTCCATTAC	280	64	No
RAB3A	CCTCGGATCAGAACTTCGAC	TGAATGACTCCAGTCAGGAAAG	289	61	No
ZDHHC19	GCAGCCCGGTTCCTTAAC	CTGGGTCTGGAGGGACCTA	264	61	No
BRIP1	CAGGACAATGAGTCTACACTTGAA	TGCTCTGGTCTCCTGACAAA	386	64	No
KIAA1257	TACCAGTCCACGAGCGAGT	TGCAGAAAGTCATGCACCTC	250	53	No

Primers could not be designed to screen for the *ZNF43* Ser740Phe variant due to tandem repeats sequence. PCR reactions were performed in a 25µL final volume. Reaction condition was one cycle of 95°C for 2 minutes, followed by 35 cycles of 95°C for 30 seconds, primer specific annealing temperature (Ta) for 30 seconds and 72°C for 1 minute, followed by a final extension of 72°C for 5 minutes. Ta, annealing temperature.

Table I- 4. Primer sequences and corresponding PCR conditions used for screening candidate gene *GDNF* in 130 unrelated BAV cohort.

GDNF exons	Forward primer	Reverse primer	Product size (bp)	Ta (°C)	10% DMSO used
GDNFx1	GGATCTCCAGGCAAGACCTC	ACTCTCACCGTTTGCTCTGG	591	61	Yes
GDNFx2-3	CGTGGCCCTCCTTTGTAG	GCTCCTATAGGCCCCTGAAC	699	63	No
GDNFx4	GCCCTGCTTGAAACTCTGAC	AATTCCATCCCCTCTGTGCT	684	65	No
GDNFx5	TTTGCTGTGGGTCCAATTT	CCTTGGTCCTCATCTTCCAT	700	51	Yes

PCR reactions were performed in a 25µL final volume. Reaction condition was one cycle of 95°C for 2 minutes, followed by 35 cycles of 95°C for 30 seconds, primer specific annealing temperature (Ta) for 30 seconds and 72°C for 1 minute, followed by a final extension of 72°C for 5 minutes. Ta, annealing temperature.

Table I- 5. Primers sequences and conditions used in RT-qPCR validation study.

Gene name	Forward primer	Reverse primer	Ta (°C)	Product size (bp)
COL6A6	GAACTGAAGAAGGTCAATAAAAGGA	AGACATCAAATCCCACCACAAC	61	97
LAMC3	GCTGCTACCCTGGCTTCTT	ATGGCACTGGTCCTCCTG	63	92
MMP13	TGGTGGTGATGAAGATGATTTG	GCGAGATTTGTAGGATGGTAGTATG	64	87
IBSP	CCGAAGAAAATGGAGATGACAG	TAGCCCAGTGTTGTAGCAGAAA	61	142
MMP9	GAACCAATCTCACCGACAGG	CGACTCTCCACGCATCTCT	64	86
MMP7	CGTGCTGTGTGCTGTGTG	TTGAGATAGTCCTGAGCCTGTT	63	108
SPP1	GGCTAAACCCTGACCCATCT	GCTTTCGTTGGACTTACTTGGA	64	74
CHI3L1	AGGAAAGCGTCAAAAGCAAG	GGCATTGGTGAGAGGGAAG	65	134
ACAN	GGGAGCAGCAGTCACACC	CTGGTAGTCTTGGGCATTGTT	65	80
GAPDH	AAGGCTGAGAACGGGAAG	ATCGCCCCACTTGATTTTG	63	87
TFRC	CAAAACCAAAAAGGTGTAGTGGA	AGCCCAAGTAGCCAATCATAAA	63	93

bp, base pairs; Ta, annealing temperature.

Appendix II. Exome sequencing in BAV

Table II- 1. List of prioritised variants identified from Family A exome sequencing.

Gene	Gene description	Chr	Nucleotide Position	Nucleotide change	Amino acid change	Protein position	Functional effect	PolyPhen	GERP score
GTF3C5	general transcription factor IIIC polypeptide 5 63kDa	9	135933206	c1420T>C	Phe474Leu	474/527	missense	benign	5.13
COL11A1	collagen type XI alpha 1	1	103496754	c698T>C	Tyr233Cys	233/1819	missense	unknown	5.59
MAP2	microtubule-associated protein 2	2	210518057	C163G>A	Glu55Lys	55/1828	missense	probably-damaging	4.85
ARAP2	ArfGAP with RhoGAP domain ankyrin repeat and PH domain 2	4	36069767	c4877C>T	Arg1626Gln	1626/1705	missense	probably-damaging	5.98
RFC1	replication factor C (activator 1) 1 145kDa	4	39293306	c3124T>C	Ser1042Gly	1042/1149	missense	unknown	4.53
PKD2	polycystic kidney disease 2 (autosomal dominant)	4	88996056	c2615G>A	Arg872Gln	872/969	missense	unknown	3.34
AHRR	aryl-hydrocarbon receptor repressor	5	434581	c1738C>G	Pro580Ala	580/702	missense	possibly-damaging	3.77
FNDC1	fibronectin type III domain containing 1	6	159618531	c178G>A	Asp60Asn	60/1895	missense	unknown	5.26
HGF	hepatocyte growth factor (hepapoietin A; scatter factor)	7	81334774	c1942C>T	Gly648Arg	648/729	missense	probably-damaging	4.96
SLC4A2	solute carrier family 4 anion exchanger member 2 (erythrocyte membrane protein band 3-like 1)	7	150761715	c320G>A	Arg107Gln	107/1242	missense	probably-damaging	4.4
MMP17	matrix metallopeptidase 17 (membrane-inserted)	12	132322812	c232C>A	Leu78Met	78/604	missense	probably-damaging	2.95
GAS6	growth arrest-specific 6	13	114537583	C775T>G	Thr259Pro	259/679	missense	possibly-damaging	2.71
FAM160A2	family with sequence similarity 160 member A2	11	6235656	c2584G>A	Arg862Cys	862/987	missense	probably-damaging	4.26

Table II-1 continued

Gene	Gene description	Chr	Nucleotide Position	Nucleotide change	Amino acid change	Protein position	Functional effect	PolyPhen	GERP score
GPR98	G protein-coupled receptor 98	5	89990041	c7468G>A	Ala1490Thr	2490/6307	missense	probably-damaging	4.16
NCOR1	nuclear receptor corepressor 1	17	16068340	c571C>T	Glu191Lys	191/2441	missense	probably-damaging	4.05
ADRB2	adrenergic beta-2- receptor surface	5	148207371	c977A>G	Tyr326Cys	326/414	missense	unknown	5.15
BCLAF1	BCL2-associated transcription factor 1	6	136597281	c1382A>T	Leu461His	461/921	missense	probably-damaging	4.06
		6	136597288	c1375A>C	Tyr459His	459/921	missense	possibly-damaging	5.21
		6	136599822	c197C>G	Gly66Ala	66/921	missense	unknown	5.64
		6	136582401	NA	none	NA	splice-5	unknown	5.81
TIGD6	tigger transposable element derived 6	5	149374471	c1441A>C	Ser481Ala	481/522	missense	unknown	1.55
TTC18	tetratricopeptide repeat domain 18	10	75032735	c3086C>T	Arg1029Lys	1029/1122	missense	benign	5.03
ACACB	acetyl-CoA carboxylase beta	12	109690904	c5986G>A	Val1996Met	1996/2459	missense	probably-damaging	5.35
HGSNAT	heparan-alpha-glucosaminide N-acetyltransferase	8	43054647	c1843G>A	Ala615Thr	615/636	missense	benign	5.29
LMOD2	leiomodin 2 (cardiac)	7	123302302	c662T>C	Ile221Thr	221/548	missense	probably-damaging	5.04
ULK1	unc-51-like kinase 1 (C. elegans)	12	132396488	c950C>T	Ser317Phe	317/1051	missense-near-splice	unknown	4.87
ADAMTS6	A disintegrin and metalloproteinase with thrombospondin motifs 6	5	64756163	c465A>T	His155Gln	155/1118	missense	unknown	2.36
PLCL1	phospholipase C-like 1	2	198949061	c820A>G	Thr274Ala	274/1096	missense	benign	4.58
SLC6A3	solute carrier family 6 (neurotransmitter transporter dopamine) member 3	5	1406359	c1543G>A	Arg515Trp	515/621	missense	unknown	2.02
FASN	fatty acid synthase	17	80039893	c6155C>G	Gly2052Ala	2052/2512	missense	unknown	4.77

Table II-1 continued

Gene	Gene description	Chr	Nucleotide Position	Nucleotide change	Amino acid change	Protein position	Functional effect	PolyPhen	GERP score
HS1BP3	HCLS1 binding protein 3	2	20838410	c409T>C	Thr137Ala	137/393	missense	unknown	4.59
MAP2K3	mitogen-activated protein kinase kinase 3	17	21204192	c286C>T	Arg96Trp	96/348	missense	probably-damaging	5.08
		17	21204187	c281G>T	Arg94Leu	94/348	missense-near-splice	probably-damaging	5.08
		17	21202191	c118C>A	Pro40Thr	40/348	missense-near-splice	probably-damaging	4.95
		17	21204210	c304C>T	Gln102stop	102/348	stop-gained	unknown	5.08
ITGA10	integrin alpha 10	1	145542255	c3481A>G	Arg1161Gly	1161/1168	missense	unknown	3.11
SH3RF3	SH3 domain containing ring finger 3	2	110065896	c2099C>T	Ser700Phe	700/883	missense	possibly-damaging	3.06
UGT3A1	UDP glycosyltransferase 3 family polypeptide A1	5	35965583	c748T>A	Asn250Tyr	250/524	missense	probably-damaging	3.05
KDM1B	lysine (K)-specific demethylase 1B	6	18197821	c754T>C	Ser252Pro	252/591	missense	probably-damaging	4.58
ABCA13	ATP-binding cassette sub-family A (ABC1) member 13	7	48556328	c13648A>G	Thr4550Ala	4550/5059	missense	possibly-damaging	5.35
ACTR3C	ARP3 actin-related protein 3 homolog C	7	149983566	c361G>A	Gln121stop	121/211	stop-gained	unknown	1.48
ABCB4	ATP-binding cassette sub-family B (MDR/TAP) member 4	7	87092143	c217G>C	Leu73Val	73/1280	missense	benign	3.65
AFMID	arylformamidase	17	76187091	c104G>A	Arg35Gln	35/304	missense	probably-damaging	2.81
TH1L	TH1-like (Drosophila)	20	57564997	c769G>A	Ala257Thr	257/591	missense	unknown	5.61
URB1	URB1 ribosome biogenesis 1 homolog (S. cerevisiae)	21	33706527	c4802C>T	Arg1601Gln	1601/2272	missense	probably-damaging	0.29
SASH1	SAM and SH3 domain containing 1	6	148840980	c1160C>T	Ser387Phe	387/1248	missense	probably-damaging	4.74
MED16	mediator complex subunit 16	19	868108	c2627C>G	Arg876Pro	876/878	missense	possibly-damaging	-1.68
RTP4	receptor (chemosensory) transporter protein 4	3	187086359	c130C>A	Gln44Lys	44/247	missense	probably-damaging	3.2

Table II-1 continued

Gene	Gene description	Chr	Nucleotide Position	Nucleotide change	Amino acid change	Protein position	Functional effect	PolyPhen	GERP score
ANKAR	ankyrin and armadillo repeat containing	2	190608005	c3815G>A	Arg1272His	1272/1435	missense	probably-damaging	5.05
BST1	bone marrow stromal cell antigen 1	4	15707202	c253G>A	Val85Met	85/319	missense	unknown	5.72
BTBD16	BTB (POZ) domain containing 16	10	124058583	c725G>A	Gly242Glu	242/507	missense	unknown	5.66
C1orf168	chromosome 1 open reading frame 168	1	57207874	c1564C>T	Glu522Lys	522/729	missense	probably-damaging	5.25
DDX51	DEAD (Asp-Glu-Ala-Asp) box polypeptide 51	12	132627365	c578G>A	Thr193Ile	193/667	missense	benign	1.49
DNAH10	dynein axonemal heavy chain 10	12	124343814	c6394A>G	Lys2132Glu	2132/4472	missense-near-splice	benign	5.57
DNALI1	dynein axonemal light intermediate chain 1	1	38027815	c776A>G	Gln259Arg	259/281	missense	unknown	5.41
GDNF	glial cell derived neurotrophic factor	5	37816112	c328G>A	Arg93Trp	93/211	missense	probably-damaging	4.96
GJB6	gap junction protein beta 6 30kDa	13	20797025	c595A>T	Ser199Thr	199/262	missense	probably-damaging	5.61
HKDC1	hexokinase domain containing 1	10	70998835	c533G>A	Arg178Gln	178/918	missense	unknown	4.92
HPS3	Hermansky-Pudlak syndrome 3	3	148858233	c660A>T	Arg220Ser	220/1005	missense	unknown	-1.76
KCNMB3	potassium large conductance calcium-activated channel subfamily M beta member 3	3	178957810	c496T>C	Thr166Ala	166/174	missense	unknown	4.35
LRRN4	leucine rich repeat neuronal 4	20	6022246	c1645A>T	Tyr549Asn	549/741	missense	probably-damaging	5.01
NOS3	nitric oxide synthase 3 (endothelial cell)	7	150707224	c2534T>G	Val845Gly	845/1204	missense	unknown	4.52
ULBP1	UL16 binding protein 1	6	150285262	c77G>A	Gly26Glu	26/245	missense	probably-damaging	-0.38

Table II-1 continued

Gene	Gene description	Chr	Nucleotide Position	Nucleotide change	Amino acid change	Protein position	Functional effect	PolyPhen	GERP score
TACC3	transforming acidic coiled-coil containing protein 3	4	1739053	c1834C>G	Pro612Ala	612/839	missense	possibly-damaging	2.65
PRH2	proline-rich protein HaeIII subfamily 2	12	11083273	c113C>T	Ser38Phe	38/167	missense	probably-damaging	0.051
NUP43	nucleoporin 43kDa	6	150067126	c193G>A	His65Tyr	65/381	missense	possibly-damaging	5.22
PDE4DIP	cardiomyopathy-associated protein 2; phosphodiesterase 4D-interacting protein	1	144881463	c3733C>T	Ala1245Thr	1245/2363	missense	unknown	5.97
MICALCL	MICAL C-terminal like	11	12316336	c1358G>A	Arg453His	453/696	missense	unknown	0.153
MUSK	muscle skeletal receptor tyrosine kinase	9	113449510	c320G>A	Gly107Glu	107/784	missense	benign	4.07
MATN1	matrilin 1 cartilage matrix protein	1	31188935	c1028C>T	Arg343Gln	343/497	missense	possibly-damaging	3.23
PTGES2	prostaglandin E synthase 2	9	130886050	c617C>G	Gly206Ala	206/378	missense	benign	4.94
PCDHB7	protocadherin beta 7	5	140554140	c1724C>T	Pro575Leu	575/794	missense	benign	3.12
TGM2	transglutaminase 2 (C polypeptide protein-glutamine-gamma-glutamyltransferase)	20	36758692	c1993C>A	Val665Leu	665/688	missense	benign	5.19
PMPCB	peptidase (mitochondrial processing) beta	7	102937914	c8C>T	Ala3Val	3/490	missense	unknown	2.21
SVEP1	selectin-like osteoblast-derived protein	9	113265326	c1475C>T	Arg492Gln	492/3572	missense	benign	4.62
WDR47	WD repeat domain 47	1	109526041	c1982C>T	Arg661His	661/928	missense	probably-damaging	4.18
ECEL1	endothelin converting enzyme-like 1	2	233345474	c2105C>A	Arg702Leu	702/776	missense	possibly-damaging	4.94
ZNF831	zinc finger protein 831	20	57768655	c2581G>A	Asp861Asn	861/1678	missense	possibly-damaging	3.95
TYRO3	TYRO3 protein tyrosine kinase	15	41865505	NA	none	NA	splice-3	unknown	5.52
		15	41865199	NA	none	NA	splice-3	unknown	4.86

Table II-1 continued

Gene	Gene description	Chr	Nucleotide Position	Nucleotide change	Amino acid change	Protein position	Functional effect	PolyPhen	GERP score
APOBEC1	apolipoprotein B mRNA editing enzyme catalytic polypeptide 1	12	7805414	c62C>T	Trp21stop	21/237	stop-gained	unknown	3.58
BRSK1	BR serine/threonine kinase 1	19	55823389	c2290C>G	Pro764Ala	764/779	missense	benign	2.77
CST4	cystatin S	20	23667808	c259C>T	Val87Ile	87/142	missense	unknown	0.932
CYP7A1	cytochrome P450 family 7 subfamily A polypeptide 1	8	59404935	c1192G>C	Pro398Ala	398/505	missense	probably-damaging	5.18
GPRIN2	G protein regulated inducer of neurite outgrowth 2	10	46999151	c271T>C	Trp91Arg	91/459	missense	benign	1.98
SI	sucrase-isomaltase (alpha-glucosidase)	3	164741534	c2923A>G	Tyr975His	975/1828	missense	probably-damaging	5.23
SDSL	serine dehydratase-like	12	113874590	c706G>A	Ala236Thr	236/330	missense	possibly-damaging	1.71
PUS1	pseudouridylate synthase 1	12	132416813	c397G>A	Asp133Asn	133/428	missense	benign	5.26
B7H6	B7H6	11	17390443	c790C>A	His264Asn	264/455	missense	possibly-damaging	-5.58
MTHFR	methylenetetrahydrofolate reductase (NADPH)	1	11848068	c1556G>C	Cys519Ser	519/698	missense	benign	1.68
NEURL2	neuralized homolog 2	20	44519224	C>CT	NA	NA	frameshift	unknown	4.83
OXA1L	oxidase (cytochrome c) assembly 1-like	14	23240713	T>TAGC	NA	NA	frameshift	unknown	2.25
GNAS	adenylate cyclase-stimulating G alpha protein	20	57429499	G>GGCAG CCCCT	NA	NA	frameshift	unknown	3.24

Chr = chromosome; NA = not applicable

Table II- 2. List of prioritised variants identified from Family B exome sequencing.

Gene	Gene description	Chr	Nucleotide Position	Nucleotide change	Amino acid change	Protein position	Functional effect	PolyPhen2	GERP
SVIL	supervillin	10	29815938	c2294G>A	Ala765Val	765/2215	missense	0.614	4.66
SERINC3	serine incorporator 3	20	43135506	c745C>T	Val249Ile	249/474	missense	0.015	-6.39
WTAP	Wilms tumor 1 associated protein	6	160176531	c1079A>G	His360Arg	360/397	missense	0.256	3.81
FAM198B	family with sequence similarity 198, member B	4	159092106	c422C>T	Gly141Glu	141/528	missense	0.956	-0.115
SMG5	smg-5 homolog, nonsense mediated mRNA decay factor (C. elegans)	1	156247030	c300G>T	His100Gln	100/1017	missense	0.168	1.67
BRD7	bromodomain containing 7	16	50367513	c983T>C	Lys328Arg	328/653	missense	1	5.24
DMKN	dermokine	19	36002711	c689G>A	Thr230Met	230/466	missense	1	3.27
		19	36003975	c403C>A	Val135Leu	135/466	missense	0.566	-4.62
MLKL	mixed lineage kinase domain-like	16	74729627	c29A>C	Leu10Arg	10/264	missense	0.999	2.11
ERBB2	v-erb-b2 erythroblastic leukemia viral oncogene homolog 2, neuro/glioblasto-ma derived oncogene homolog (avian)	17	37863269	c10C>T	Arg4Trp	4/1226	missense	1	5.23
POLE4	polymerase (DNA-directed), epsilon 4, accessory subunit	2	75196545	c350A>G	Asp117Gly	117/118	missense	0.999	4.08
DEFB124	defensin, beta 124	20	30053314	c211C>T	Glu71Lys	71/72	missense	0	-0.726
TIAM2	T-cell lymphoma invasion and metastasis 2	6	155465893	c1784G>C	Gly595Ala	595/1702	missense	1	5.6
ZNF226	zinc finger protein 226	19	44679149	c248T>A	Val83Glu	83/95	missense	0.005	0.59
		19	44680488	c1073C>T	Thr358Met	358/804	missense	0.885	3.23
FUK	fucokinase	16	70505089	c1175C>G	Pro392Arg	392/1085	missense	1	5.48
ZNF43	zinc finger protein 43	19	21990602	c2219G>A	Ser740Phe	740/804	missense	0.046	-2.43
RBM45	RNA binding motif protein 45	2	178981097	c409C>T	Arg137Trp	137/475	missense	0.055	2.93

Table II-2 continued

Gene	Gene description	Chr	Nucleotide Position	Nucleotide change	Amino acid change	Protein position	Functional effect	PolyPhen2	GERP
TTF2	transcription termination factor, RNA polymerase II	1	117633170	c2513G>A	Arg838His	838/1163	missense	1	5.1
ZNF234	zinc finger protein 234	19	44661974	c1805G>A	Gly602Glu	602/701	missense	0.999	1.89
DENND2C	DENN/MADD domain containing 2C	1	115142870	c2060G>A	Ser687Phe	687/929	missense	1	5.74
BZRAP1	benzodiazapine receptor (peripheral) associated protein 1	17	56388110	c3462C>G	Glu1154Asp	1154/1849	missense	0.461	3.41
ETV4	ets variant 4	17	41606065	c1277G>A	Ala426Val	426/485	missense	0.991	6.02
COL6A6	collagen, type VI, alpha 6	3	130293046	c3224G>C	Gly1075Ala	1075/2264	missense	0.996	5.15
MYH7B	myosin, heavy chain 7B, cardiac muscle, beta	20	33574773	c1115A>G	Glu372Gly	372/1984	missense	0.6	3.66
SEMA5B	sema domain, seven thrombospondin repeats (type 1 and type 1-like), trans-membrane domain (TM) and short cytoplasmic domain, (semaphorin) 5B	3	122632741	c2096C>T	Gly699Glu	699/1152	missense	1	4.13
ASPG	asparaginase homolog (S. cerevisiae)	14	104573573	c1324G>A	Ala442Thr	442/574	missense	0.998	3.72
RAB3A	RAB3A, member RAS oncogene family	19	18313357	c194T>C	Tyr65Cys	65/221	missense	0.996	4.23
ACVR1C	activin A receptor, type IC	2	158412701	c298T>G	Asn100His	100/444	missense	0.003	5.73
ZDHHC19	zinc finger, DHHC-type containing 19	3	195934286	c670G>C	Arg224Gly	224/310	missense	0.975	4.09
BRIP1	BRCA1 interacting protein C-terminal helicase 1	17	59763239	c2863T>G	Asn955His	955/1250	missense	0.001	2.99
KIAA1257	KIAA1257	3	128711946	c202C>A	Asp68Tyr	68/410	missense	1	3.48

Chr = chromosome; The PolyPhen score represents the probability that a substitution is damaging. Values nearer 1 are more confidently predicted to be deleterious.

Appendix III. RNA sequencing in BAV

Table III- 1. Complete list of differentially expressed genes between the BAV (BAV1-BAV5) and TAV (TAV1-TAV3) groups (p<0.05 with post-hoc Bonferroni correction).

UPREGULATED GENES IN BAV (BAV1-BAV5) vs. TAV (TAV1-TAV3)			
Gene symbol	**Gene annotation**	**Fold change**	**Adjusted p-value**
FAM149A	family with sequence similarity 149, member A	4.79	0.0330
HLA-DRB5	major histocompatibility complex, class II, DR beta 5	4.68	0
SPOCK3	sparc/osteonectin, cwcv and kazal-like domains proteoglycan (testican) 3	3.35	5.37E-09
CHST9	carbohydrate (N-acetylgalactosamine 4-0) sulfotransferase 9	3.26	0.0308
MATN4	matrilin 4	2.81	0.0270
EYA1	eyes absent homolog 1 (Drosophila)	2.79	0.0025
C1orf51	chromosome 1 open reading frame 51	2.71	0.0046
MUC20	mucin 20, cell surface associated	2.67	4.44E-04
HLA-DQB1	major histocompatibility complex, class II, DQ beta 1	2.56	4.81E-05
MAPK4	mitogen-activated protein kinase 4	2.55	0.0165
C17orf97	chromosome 17 open reading frame 97	2.53	0.0161
GSTM1	glutathione S-transferase mu 1	2.51	0.0082
ARHGDIG	Rho GDP dissociation inhibitor (GDI) gamma	2.43	0.0267
RIMS4	regulating synaptic membrane exocytosis 4	2.36	6.10E-04
KIRREL3	kin of IRRE like 3 (Drosophila)	2.30	0.0320
CLU	clusterin	2.28	5.15E-04
NR1D1	nuclear receptor subfamily 1, group D, member 1	2.24	3.40E-05
IGSF10	immunoglobulin superfamily, member 10	2.19	1.18E-05
TMEM56	transmembrane protein 56	2.19	0.0022
MYH10	myosin, heavy chain 10, non-muscle	2.19	0.0454
POLR2J2	polymerase (RNA) II (DNA directed) polypeptide J2	2.15	5.95E-04
LAMC3	laminin, gamma 3	2.11	8.32E-06
PLCH1	phospholipase C, eta 1	2.11	0.0387
TCEAL2	transcription elongation factor A (SII)-like 2	2.08	0.0040
CHAD	chondroadherin	2.06	1.28E-04
GBP3	guanylate binding protein 3	2.01	0.0026
PKP2	plakophilin 2	2.00	0.0277
HLF	hepatic leukemia factor	1.99	0.0020
MAPT	microtubule-associated protein tau	1.97	0.0061
GFAP	glial fibrillary acidic protein	1.95	0.0080
PDZRN4	PDZ domain containing ring finger 4	1.93	0.0348
TNXB	tenascin XB	1.92	0.0057
PIK3IP1	phosphoinositide-3-kinase interacting protein 1	1.92	0.0244
CNTFR	ciliary neurotrophic factor receptor	1.91	0.0285
SLC6A1	solute carrier family 6 (neurotransmitter transporter, GABA), member 1	1.89	0.0400
DBP	D site of albumin promoter (albumin D-box) binding protein	1.87	0.0080
S100B	S100 calcium binding protein B	1.87	0.0087
DSP	desmoplakin	1.87	0.0140
MASP1	mannan-binding lectin serine peptidase 1 (C4/C2 activating component of Ra-reactive factor)	1.86	0.0029
NSG1	Neuron-specific protein family member 1	1.82	0.0098
PER1	period homolog 1 (Drosophila)	1.81	0.0041
ERAP2	endoplasmic reticulum aminopeptidase 2	1.80	0.0029
COL6A6	collagen, type VI, alpha 6	1.80	0.0129
HNRNPD	heterogeneous nuclear ribonucleoprotein D (AU-rich element RNA binding protein 1, 37kDa)	1.78	0.0230
COL13A1	collagen, type XIII, alpha 1	1.78	0.0483

Table III-1 continued

UPREGULATED GENES IN BAV (BAV1-BAV5) vs. TAV (TAV1-TAV3)			
Gene symbol	**Gene annotation**	**Fold change**	**Adjusted p-value**
CPAMD8	C3 and PZP-like, alpha-2-macroglobulin domain containing 8	1.76	0.0076
UPK3BL	uroplakin 3B-like	1.75	0.0142
SLC14A1	solute carrier family 14 (urea transporter), member 1 (Kidd blood group)	1.75	0.0392
TMEM132E	transmembrane protein 132E	1.73	0.0116
ATOH8	atonal homolog 8 (Drosophila)	1.72	0.0392
TEF	thyrotrophic embryonic factor	1.71	0.0223
HAND2	heart and neural crest derivatives expressed 2	1.71	0.0329
LTBP4	latent transforming growth factor beta binding protein 4	1.68	0.0384
NR1D2	nuclear receptor subfamily 1, group D, member 2	1.62	0.0466
GATA4	GATA binding protein 4	1.60	0.0446
SYNM	synemin, intermediate filament protein	1.60	0.0480
PTN	pleiotrophin	1.58	0.0277
POLR2J3	polymerase (RNA) II (DNA directed) polypeptide J3	1.58	0.0388
RASA4B	RAS p21 protein activator 4B	1.57	0.0413

Table III-1 continued

DOWNREGULATED GENES IN BAV (BAV1-BAV5) vs. TAV (TAV1-TAV3)			
Gene symbol	**Gene annotation**	**Fold change**	**Adjusted p-value**
IGLL5	immunoglobulin lambda-like polypeptide 5	-30.05	0
RP11-1280I22.1	Plasma cell-induced resident endoplasmic reticulum protein	-25.56	0
DEFA1	defensin, alpha 1	-24.99	0.0054
DEFA1B	defensin, alpha 1B	-20.65	0.0080
MMP13	matrix metallopeptidase 13 (collagenase 3)	-19.06	0
IGJ	immunoglobulin J polypeptide, linker protein for immunoglobulin alpha and mu polypeptides	-16.73	0
CD79A	CD79a molecule, immunoglobulin-associated alpha	-15.80	0
MTRNR2L8	MT-RNR2-like 8	-14.69	4.02E-09
PPBP	pro-platelet basic protein (chemokine (C-X-C motif) ligand 7)	-13.76	0.0019
FCRL5	Fc receptor-like 5	-13.49	5.99E-13
GPIHBP1	glycosylphosphatidylinositol anchored high density lipoprotein binding protein 1	-12.92	2.26E-07
MAT1A	methionine adenosyltransferase I, alpha	-12.74	0.0014
MMP7	matrix metallopeptidase 7 (matrilysin, uterine)	-12.21	5.24E-08
BHLHA15	basic helix-loop-helix family, member a15	-11.15	0.0300
MMP9	matrix metallopeptidase 9 (gelatinase B, 92kDa gelatinase, 92kDa type IV collagenase)	-11.08	0
CCL7	chemokine (C-C motif) ligand 7	-11.08	0.0073
AMPD1	adenosine monophosphate deaminase 1	-10.72	0.0019
SP7	Sp7 transcription factor	-10.20	1.38E-10
SPIB	Spi-B transcription factor (Spi-1/PU.1 related)	-10.00	0.0068
TDO2	tryptophan 2,3-dioxygenase	-9.99	6.12E-10
HLA-DOB	major histocompatibility complex, class II, DO beta	-9.96	0.0193
ATP6V0D2	ATPase, H+ transporting, lysosomal 38kDa, V0 subunit d2	-9.34	1.48E-05
KLK4	kallikrein-related peptidase 4	-9.28	0.0157
IBSP	integrin-binding sialoprotein	-8.65	0
RASSF6	Ras association (RalGDS/AF-6) domain family member 6	-8.50	2.46E-04
BTNL9	butyrophilin-like 9	-8.40	0.0288
C1orf130	chromosome 1 open reading frame 130	-8.13	0.0493
IFITM5	interferon induced transmembrane protein 5	-8.01	0.0284
FCRL3	Fc receptor-like 3	-7.78	0.0175
PNOC	prepronociceptin	-7.62	0.0362
DACH1	dachshund homolog 1 (Drosophila)	-7.19	0.0392
BMP3	bone morphogenetic protein 3	-7.10	0.0074
SPP1	secreted phosphoprotein 1	-7.07	0
CXCL13	chemokine (C-X-C motif) ligand 13	-6.73	9.90E-05
PAX5	paired box 5	-6.60	0.0177
CMA1	chymase 1, mast cell	-6.54	1.57E-06
TSPAN10	tetraspanin 10	-6.54	0.0081
NR5A2	nuclear receptor subfamily 5, group A, member 2	-6.42	0.0396
EMR1	egf-like module containing, mucin-like, hormone receptor-like 1	-6.21	0.0439
DERL3	Der1-like domain family, member 3	-6.14	2.21E-11
ADCYAP1	adenylate cyclase activating polypeptide 1 (pituitary)	-6.12	0.0017
PRND	prion protein 2 (dublet)	-5.87	0.0026
MS4A1	membrane-spanning 4-domains, subfamily A, member 1	-5.80	4.15E-06
POU2AF1	POU class 2 associating factor 1	-5.79	2.61E-10
CBLN4	cerebellin 4 precursor	-5.57	0.0070
FLT4	fms-related tyrosine kinase 4	-5.56	1.22E-05
AQP9	aquaporin 9	-5.54	1.42E-04
CXCL5	chemokine (C-X-C motif) ligand 5	-5.27	1.35E-04
CHIT1	chitinase 1 (chitotriosidase)	-5.26	1.06E-11

Table III-1 continued

DOWNREGULATED GENES IN BAV (BAV1-BAV5) vs. TAV (TAV1-TAV3)			
Gene symbol	**Gene annotation**	**Fold change**	**Adjusted p-value**
COL11A1	collagen, type XI, alpha 1	-4.84	0
HBA2	hemoglobin, alpha 2	-4.75	0
HBA1	hemoglobin, alpha 1	-4.68	1.27E-13
APOC2	apolipoprotein C-II	-4.62	0.0127
EBF2	early B-cell factor 2	-4.56	1.64E-04
TM4SF19	transmembrane 4 L six family member 19	-4.44	5.87E-04
COL2A1	collagen, type II, alpha 1	-4.23	0.0024
APOC4	apolipoprotein C-IV	-4.12	0.0074
HBB	hemoglobin, beta	-4.11	0
TIMD4	T-cell immunoglobulin and mucin domain containing 4	-4.07	7.80E-07
SCUBE1	signal peptide, CUB domain, EGF-like 1	-3.95	0.0268
SLAMF7	SLAM family member 7	-3.91	2.28E-07
C10orf81	chromosome 10 open reading frame 81	-3.87	6.28E-06
SGCA	sarcoglycan, alpha (50kDa dystrophin-associated glycoprotein)	-3.82	3.29E-06
MMP1	matrix metallopeptidase 1 (interstitial collagenase)	-3.80	0.0416
HLA-DQB2	major histocompatibility complex, class II, DQ beta 2	-3.77	1.02E-04
GREM1	gremlin 1	-3.72	8.37E-04
SDS	serine dehydratase	-3.66	0.0034
CCL3	chemokine (C-C motif) ligand 3	-3.64	5.85E-07
TM4SF18	transmembrane 4 L six family member 18	-3.56	4.53E-05
CXorf36	chromosome X open reading frame 36	-3.54	4.03E-04
GPHA2	glycoprotein hormone alpha 2	-3.52	3.00E-05
DLL4	delta-like 4 (Drosophila)	-3.51	0.0028
EGFLAM	EGF-like, fibronectin type III and laminin G domains	-3.41	0.0012
IL1RN	interleukin 1 receptor antagonist	-3.38	0.0037
DNASE1L3	deoxyribonuclease I-like 3	-3.37	0.0132
LRRC15	leucine rich repeat containing 15	-3.35	6.49E-08
MMRN1	multimerin 1	-3.31	1.48E-05
PLA2G2D	phospholipase A2, group IID	-3.29	0.0249
VMO1	vitelline membrane outer layer 1 homolog (chicken)	-3.24	2.98E-04
GZMB	granzyme B (granzyme 2, cytotoxic T-lymphocyte-associated serine esterase 1)	-3.24	0.0111
BGLAP	bone gamma-carboxyglutamate (gla) protein	-3.14	1.02E-05
APOC1	apolipoprotein C-I	-3.11	1.52E-06
ADAMDEC1	ADAM-like, decysin 1	-3.09	0.0359
CCL3L1	chemokine (C-C motif) ligand 3-like 1	-3.08	0.0408
PIM2	pim-2 oncogene	-3.05	3.24E-11
CHI3L1	chitinase 3-like 1 (cartilage glycoprotein-39)	-3.05	6.80E-11
SLC11A1	solute carrier family 11 (proton-coupled divalent metal ion transporters), member 1	-3.05	5.80E-09
HDC	histidine decarboxylase	-3.04	0.0317
THNSL2	threonine synthase-like 2 (S. cerevisiae)	-3.03	4.21E-06
FAIM3	Fas apoptotic inhibitory molecule 3	-2.99	8.97E-04
CXCL9	chemokine (C-X-C motif) ligand 9	-2.96	6.19E-05
KCNK2	potassium channel, subfamily K, member 2	-2.96	0.0261
TPSD1	tryptase delta 1	-2.96	0.0363
PLVAP	plasmalemma vesicle associated protein	-2.95	1.40E-09
GZMK	granzyme K (granzyme 3; tryptase II)	-2.94	0.0037
CTSG	cathepsin G	-2.93	0.0034
CCL21	chemokine (C-C motif) ligand 21	-2.89	4.30E-08
TREM1	triggering receptor expressed on myeloid cells 1	-2.87	8.74E-04
LTB	lymphotoxin beta (TNF superfamily, member 3)	-2.87	0.0096
CCL14	chemokine (C-C motif) ligand 14	-2.84	3.94E-04

Table III-1 continued

DOWNREGULATED GENES IN BAV (BAV1-BAV5) vs. TAV (TAV1-TAV3)			
Gene symbol	**Gene annotation**	**Fold change**	**Adjusted p-value**
CCL4	chemokine (C-C motif) ligand 4	-2.80	0.0198
SDC1	syndecan 1	-2.78	4.10E-04
NELL2	NEL-like 2 (chicken)	-2.76	0.0229
COL10A1	collagen, type X, alpha 1	-2.75	9.21E-08
TSPAN13	tetraspanin 13	-2.74	0.0480
CPA3	carboxypeptidase A3 (mast cell)	-2.70	6.94E-05
ITGAX	integrin, alpha X (complement component 3 receptor 4 subunit)	-2.69	2.92E-08
WNT7A	wingless-type MMTV integration site family, member 7A	-2.66	0.0445
MATK	megakaryocyte-associated tyrosine kinase	-2.58	0.0306
TPSAB1	tryptase alpha/beta 1	-2.57	1.49E-05
SLC7A2	solute carrier family 7 (cationic amino acid transporter, y+ system), member 2	-2.57	1.05E-04
SLAMF6	SLAM family member 6	-2.57	0.0048
IL21R	interleukin 21 receptor	-2.56	0.0080
GZMA	granzyme A (granzyme 1, cytotoxic T-lymphocyte-associated serine esterase 3)	-2.54	0.0204
APLN	apelin	-2.51	0.0109
IRF4	interferon regulatory factor 4	-2.50	0.0338
FMO3	flavin containing monooxygenase 3	-2.48	6.13E-05
CST7	cystatin F (leukocystatin)	-2.45	0.0335
GLRX	glutaredoxin (thioltransferase)	-2.42	3.04E-06
NDUFA4L2	NADH dehydrogenase (ubiquinone) 1 alpha subcomplex, 4-like 2	-2.40	1.58E-06
ISM1	isthmin 1 homolog (zebrafish)	-2.38	1.97E-04
CCL19	chemokine (C-C motif) ligand 19	-2.35	1.48E-05
ACP5	acid phosphatase 5, tartrate resistant	-2.34	1.04E-06
TMEM200A	transmembrane protein 200A	-2.34	0.0277
ZAP70	zeta-chain (TCR) associated protein kinase 70kDa	-2.31	0.0387
ITK	IL2-inducible T-cell kinase	-2.30	0.0396
NUP210	nucleoporin 210kDa	-2.28	0.0049
RGS16	regulator of G-protein signalling 16	-2.28	0.0098
SLC2A5	solute carrier family 2 (facilitated glucose/fructose transporter), member 5	-2.28	0.0409
KIT	v-kit Hardy-Zuckerman 4 feline sarcoma viral oncogene homolog	-2.21	0.0444
GPR68	G protein-coupled receptor 68	-2.18	0.0016
ADRA2A	adrenergic, alpha-2A-, receptor	-2.18	0.0024
DPP4	dipeptidyl-peptidase 4	-2.12	0.0364
CHST1	carbohydrate (keratan sulfate Gal-6) sulfotransferase 1	-2.11	0.0091
CLEC5A	C-type lectin domain family 5, member A	-2.08	0.0132
TREM2	triggering receptor expressed on myeloid cells 2	-2.06	0.0055
F3	coagulation factor III (thromboplastin, tissue factor)	-2.06	0.0391
TP53I11	tumor protein p53 inducible protein 11	-2.05	6.18E-05
CD3E	CD3e molecule, epsilon (CD3-TCR complex)	-2.05	0.0053
MFAP5	microfibrillar associated protein 5	-2.04	0.0054
ACAN	aggrecan	-2.03	1.42E-04
A2M	alpha-2-macroglobulin	-2.02	6.99E-04
AOAH	acyloxyacyl hydrolase (neutrophil)	-2.00	0.0132
FCGR1A	Fc fragment of IgG, high affinity Ia, receptor (CD64)	-1.99	1.62E-04
VCAM1	vascular cell adhesion molecule 1	-1.97	3.55E-04
IKZF3	IKAROS family zinc finger 3 (Aiolos)	-1.97	0.0110
PILRA	paired immunoglobin-like type 2 receptor alpha	-1.93	0.0374
NFASC	neurofascin	-1.93	0.0456
IFI30	interferon, gamma-inducible protein 30	-1.92	0.0299
UCP2	uncoupling protein 2 (mitochondrial, proton carrier)	-1.91	0.0285
STMN2	stathmin-like 2	-1.91	0.0312

Table III-1 continued

DOWNREGULATED GENES IN BAV (BAV1-BAV5) vs. TAV (TAV1-TAV3)			
Gene symbol	**Gene annotation**	**Fold change**	**Adjusted p-value**
PCDH17	protocadherin 17	-1.91	0.0489
ITGAL	integrin, alpha L (antigen CD11A (p180), lymphocyte function-associated antigen 1; alpha polypeptide)	-1.90	0.0362
CHI3L2	chitinase 3-like 2	-1.87	0.0034
LBH	limb bud and heart development homolog (mouse)	-1.87	0.0049
SLPI	secretory leukocyte peptidase inhibitor	-1.86	0.0408
FGR	Gardner-Rasheed feline sarcoma viral (v-fgr) oncogene homolog	-1.85	0.0408
NPIPL2	nuclear pore complex interacting protein-like 2	-1.84	0.0368
KRT18	keratin 18	-1.84	0.0416
ZFAT	zinc finger and AT hook domain containing	-1.83	0.0432
TMEM119	transmembrane protein 119	-1.83	0.0460
SMOC2	SPARC related modular calcium binding 2	-1.81	0.0121
TMC8	transmembrane channel-like 8	-1.81	0.0409
SLC2A3	solute carrier family 2 (facilitated glucose transporter), member 3	-1.77	0.0369
SMOC1	SPARC related modular calcium binding 1	-1.74	0.0031
PNP	purine nucleoside phosphorylase	-1.74	0.0100
HMOX1	heme oxygenase (decycling) 1	-1.74	0.0130
DDX39B	DEAD (Asp-Glu-Ala-Asp) box polypeptide 39B	-1.74	0.0228
PLAU	plasminogen activator, urokinase	-1.73	0.0213
CRHBP	corticotropin releasing hormone binding protein	-1.72	0.0109
TINAGL1	tubulointerstitial nephritis antigen-like 1	-1.72	0.0233
ZNF266	zinc finger protein 266	-1.71	0.0361
MS4A7	membrane-spanning 4-domains, subfamily A, member 7	-1.69	0.0060
CD53	CD53 molecule	-1.62	0.0408
ITGA7	integrin, alpha 7	-1.62	0.0480
SRGN	serglycin	-1.61	0.0381
PCDH18	protocadherin 18	-1.60	0.0480

Table III- 2. Pertinent biological processes with relevance to BAV development and aortic valve degeneration as identified by IPA.

Category	Functions Annotation	p-value	No.	Perturbed molecules/genes
Cardiovascular Disease	Aortic disorder	2.03E-05	8	*GATA4,IL1RN,MMP13,MMP7,MMP9,MYH10,PLAU,SDC1*
	Stenosis of aortic valve	2.15E-04	5	*BGLAP,MMP1,MMP9,SPP1,VCAM1*
	Calcification of aortic valve	3.19E-04	3	*BGLAP,IBSP,SPP1*
	Heart Disease	4.65E-04	29	*ADRA2A,APLN,BGLAP,CCL3L1/CCL3L3,CHI3L1,CLU,DPP4,DSP,EYA1,FLT4, GATA4,GSTM1,HAND2,HBA1/HBA2,HMOX1,IBSP,IL1RN,ITGAL,KCNK2,LTBP4, MMP1,MMP7,MMP9,MYH10,PKP2,PLAU,SGCA,SPP1,VCAM1*
	Aneurysm	4.96E-04	6	*MMP13,MMP7,MMP9,PLAU,SDC1,SPP1*
Cardiovascular System Development and Function	Development of cardiovascular system	6.84E-06	35	*ADRA2A,APLN,CCL7,CD3E,CMA1,COL11A1,COL13A1,COL2A1,DLL4,DSP,EYA1, F3,FGR,FLT4,GATA4,GREM1,GSTM1,HAND2,HBA1/HBA2,HBB,HLADQB1,HMOX1 ,ITGA7,KIT,MMP1,MMP13, MMP9,MYH10,PKP2,PLAU,PLVAP,PTN,SMOC2,SPP1, VCAM1*
	Adhesion of endothelial cells	3.55E-04	8	*CCL3,CCL3L1/CCL3L3,CCL4,CTSG,ITGAL,PPBP,SPP1,VCAM1*
	Morphology of cardiovascular system	5.08E-04	22	*APLN,COL10A1,COL2A1,DLL4,EYA1,F3,FLT4,GATA4,GFAP,HAND2,HBA1/HBA2, HBB,HMOX1, IL1RN,MMP9,MYH10,PIM2,PKP2,PLAU,PLVAP,SPP1,VCAM1*
	Morphology of aorta	6.30E-04	5	*EYA1,GATA4,HAND2,MYH10,SPP1*
Cell Death and Survival	Apoptosis	7.83E-07	73	*A2M,ADCYAP1,CCL19,CCL21,CCL3,CCL3L1/CCL3L3,CCL4,CD3E,CD53,CHI3L1,C LEC5A,CLU,CNTFR,COL2A1,CTSG,DACH1,DLL4,DNASE1L3,DPP4,DSP,EYA1,F3, FAIM3,FCGR1A,FGR,FLT4,GATA4,GLRX,GREM1,GZMA,GZMB,HAND2,HBA1/ HBA2,HLF,HMOX1,IKZF3,IL1RN,IRF4,ISM1,ITGA7,ITK,KIT,KRT18,LTB,MAPT, MMP1,MMP7,MMP9,MS4A1,NR1D1,PAX5,PER1,PIK3IP1,PIM2,PKP2,PLAU,PNP, POU2AF1,PTN,RASSF6,S100B,SDC1,SLC2A3,SLPI,SPIB,SPP1,SRGN,TIMD4, TPSAB1/TPSB2,TREM1,UCP2,WNT7A,ZAP70*
Cell Signalling	Flux of Ca2+	1.83E-13	25	*A2M,ADCYAP1,CCL14,CCL19,CCL21,CCL3,CCL3L1/CCL3L3,CCL4,CCL7,CD3E,C D79A,CXCL13, CXCL5,DEFA1* (include others),*F3,FCGR1A,FGR,ITK,KIT,KLK4, MAPT,MMP1,MS4A1,PPBP,ZAP70*
	Mobilisation of Ca2+	2.01E-07	20	*A2M,ADCYAP1,CCL19,CCL21,CCL3,CCL3L1/CCL3L3,CCL4,CCL7,CD3E,CXCL13, CXCL9,DEFA1* (include others),*FCGR1A,FCRL3,ITK,KIT,PILRA,TPSD1,TREM1, ZAP70*
	Quantity of Ca2+	2.40E-07	22	*A2M,ADCYAP1,ADRA2A,CCL19,CCL21,CCL3,CCL3L1/CCL3L3,CCL4,CCL7,CD3E, CXCL13,CXCL9,HBA1/HBA2,IBSP,MAPT,PLAU,PPBP,PRND,SPP1,TPSAB1/TPSB2 ,VCAM1,WNT7A*

Table III-2 continued

Category	Functions Annotation	p-value	No.	Perturbed molecules/genes
Cell signalling (continue)	Signalling of Ca2+	8.76E-05	6	*A2M,ADCYAP1,CD3E,CXCL9,ITGAL,ZAP70*
	Release of Ca2+	1.12E-04	11	*A2M,CCL19,CCL21,CCL3,CCL4,FCGR1A,ITK,PRND,RGS16,SPP1,ZAP70*
	Synthesis of nitric oxide	4.57E-04	12	*ACP5,ADCYAP1,CTSG,HDC,HMOX1,IL1RN,PLAU,S100B,SLC7A2,SPP1,TREM1,UCP2*
Cellular Assembly and Organisation	Organisation of collagen fibrils	5.04E-05	5	*ACAN,COL11A1,COL2A1,GREM1,TNXB*
	Polymerisation of cytoskeleton	1.64E-04	2	*CD3E,ITK*
	Organisation of filaments	1.91E-04	10	*ACAN,COL11A1,COL2A1,DSP,GFAP,GREM1,KRT18,MFAP5,PLAU,TNXB*
Cellular Function and Maintenance	Cellular homeostasis	6.64E-11	56	*A2M,ADCYAP1,ADRA2A,BHLHA15,CCL14,CCL19,CCL21,CCL3,CCL3L1/CCL3L3,CCL4,CCL7, CD3E,CD79A,CTSG,CXCL13,CXCL5,DEFA1* (includes others), *DLL4,F3, FCGR1A,FGR,GATA4, GZMA, GZMB,GZMK,HDC,HLADQB1,HMOX1,IL1RN,IL21R, IRF4,ITGAL,ITK,KCNK2,KIT,KLK4, KRT18,LTB,MAPT,MMP1,MS4A1,PAX5,PIM2, PLAU,PNP,PPBP,PRND,S100B,SGCA,SLAMF6,SLC11A1,SLC14A1,SPIB,SPP1, UCP2,ZAP70*
Cellular Movement	Migration of cells	2.77E-15	73	*A2M,ACAN,ADCYAP1,ADRA2A,AQP9,CCL14,CCL19,CCL21,CCL3,CCL3L1/CCL3L3,CCL4,CCL7,CD3E,CHI3L1,CHST1,CLEC5A,CLU,CMA1,CTSG,CXCL13,CXCL5, CXCL9,DEFA1* (includes others),*DLL4,DPP4,EBF2,F3,FGR,FLT4,GFAP,GLRX, GREM1, GZMB,HDC,HMOX1,IL1RN,IL21R,ITGAL,ITGAX,ITK,KIT,LTB,MAPT, MAT1A,MATK,MMP1,MMP13,MMP7,MMP9,MYH10,NR1D1,PER1,PIK3IP1,PLAU, PNOC,POU2AF1,PPBP,PTN,RGS16,S100B,SDC1,SLPI,SP7,SPOCK3,SPP1,SYNM, TPSAB1/TPSB2,TPSD1,TREM1,TREM2,UCP2,VCAM1,ZAP70*
Connective Tissue Development and Function	Mineralisation of bone	9.65E-05	9	*ACP5,COL2A1,GREM1,IBSP,IFITM5,MMP13,PTN,SPP1,SRGN*
	Condensation of cartilage tissue	1.33E-04	4	*ACAN,COL11A1,COL2A1,WNT7A*
Organismal Injury and Abnormalities	Fibrosis	2.39E-04	19	*ADRA2A,CXCL13,CXCL9,DSP,F3,FLT4,HBB,HMOX1,IL1RN,KIT,LRRC15,MMP1, MMP13,MMP7, MMP9,PLAU,RGS16,SGCA,SPP1*
	Calcinosis	5.78E-04	5	*BGLAP,COL2A1,IBSP,MMP9,SPP1*
Protein Degradation	Proteolysis	1.26E-05	14	*CMA1,CPA3,CTSG,DPP4,GZMA,GZMB,KLK4,LTBP4,MMP1,MMP13,MMP7,MMP9, PLAU,SDC1*
	Degradation of protein	8.27E-05	19	*CLU,CMA1,CPA3,CTSG,DPP4,GPIHBP1,GZMA,GZMB,IFI30,IL1RN,KLK4,LTBP4, MMP1,MMP13, MMP7,MMP9,PIM2,PLAU,SDC1*
	Molecular cleavage of protein fragment	1.37E-04	11	*CMA1,CPA3,CTSG,DPP4,GZMA,GZMB,KLK4,LTBP4,MMP13,MMP9,PLAU*

Table III-2 continued

Category	Functions Annotation	p-value	No.	Perturbed molecules/genes
Tissue Development	Development of connective tissue	7.38E-06	15	*ACAN,CLEC5A,COL10A1,COL11A1,COL2A1,DLL4,HAND2,HBA1/HBA2,HBB,KIT, MMP13,PER1,SLC14A1,VCAM1,WNT7A*
	Organisation of extracellular matrix	3.78E-05	8	*DPP4,EGFLAM,GFAP,IBSP,MMP9,SMOC1,SMOC2,TNXB*
	Cartilage development	3.05E-04	8	*ACAN,COL10A1,COL11A1,COL2A1,HAND2,MMP13,PER1,WNT7A*
	Adhesion of epithelial cells	5.12E-04	7	*CLU,CTSG,F3,ITGAL,LAMC3,PLAU,SLPI*
Tissue Morphology	Degradation of extracellular matrix	2.57E-05	5	*CMA1,MMP1,MMP13,MMP9,PLAU*
	Degradation of connective tissue	8.75E-05	7	*A2M,ACAN,CTSG,FCGR1A,IL1RN,MMP13,SLPI*

Table III- 3. Complete list of differentially expressed genes (DEGs) between the BAVr (BAV1-BAV3) and TAV (TAV1-TAV3) groups (p<0.05 with post-hoc Bonferroni correction), sorted by fold change.

DEGs in BAVr versus TAV			
Gene symbol	**Gene annotation**	**Fold change**	**Adjusted p-value**
HLA-DRB5	major histocompatibility complex, class II, DR beta 5	8.77	0
SLC6A20	solute carrier family 6 (proline IMINO transporter), member 20	6.61	1.70E-04
SPOCK3	sparc/osteonectin, cwcv and kazal-like domains proteoglycan (testican) 3	5.49	5.93E-08
CHST9	carbohydrate (N-acetylgalactosamine 4-0) sulfotransferase 9	5.44	0.0256
NPPC	natriuretic peptide C	5.00	1.45E-04
CNTFR	ciliary neurotrophic factor receptor	4.76	1.19E-06
PLCH1	phospholipase C, eta 1	4.35	8.69E-05
IGSF10	immunoglobulin superfamily, member 10	4.10	1.77E-08
CADM2	cell adhesion molecule 2	3.66	0.0010
SOX10	SRY (sex determining region Y)-box 10	3.63	0.0110
HMGCLL1	3-hydroxymethyl-3-methylglutaryl-CoA lyase-like 1	3.59	0.0227
RIMS4	regulating synaptic membrane exocytosis 4	3.58	5.39E-06
GFAP	glial fibrillary acidic protein	3.57	5.38E-07
EPB41L4B	erythrocyte membrane protein band 4.1 like 4B	3.56	0.0295
EYA1	eyes absent homolog 1 (Drosophila)	3.48	0.0366
COL6A6	collagen, type VI, alpha 6	3.47	1.24E-05
SCN7A	sodium channel, voltage-gated, type VII, alpha	3.46	0.0381
MYH10	myosin, heavy chain 10, non-muscle	3.41	0.0050
LAMC3	laminin, gamma 3	3.38	6.39E-06
MED12L	mediator complex subunit 12-like	3.37	0.0022
CTSE	cathepsin E	3.35	0.0293
KIF1A	kinesin family member 1A	3.35	0.0056
TRHDE	thyrotropin-releasing hormone degrading enzyme	3.23	0.0219
TMEM56	transmembrane protein 56	3.12	0.0012
CLU	clusterin	3.11	2.56E-04
TMEM132C	transmembrane protein 132C	3.08	3.47E-05
ERAP2	endoplasmic reticulum aminopeptidase 2	3.07	3.48E-05
RBP1	retinol binding protein 1, cellular	3.07	0.0144
MAPT	microtubule-associated protein tau	3.01	0.0010
IL1RL1	interleukin 1 receptor-like 1	2.98	0.0147
KIRREL3	kin of IRRE like 3 (Drosophila)	2.98	0.0125
LCNL1	lipocalin-like 1	2.95	0.0148
NWD1	NACHT and WD repeat domain containing 1	2.80	0.0384
PDZRN4	PDZ domain containing ring finger 4	2.76	0.0082
ATP1A2	ATPase, Na+/K+ transporting, alpha 2 polypeptide	2.73	0.0029
MUC20	mucin 20, cell surface associated	2.69	0.0303
MYOC	myocilin, trabecular meshwork inducible glucocorticoid response	2.69	0.0048

Table III-3 continued

DEGs in BAVr versus TAV			
Gene symbol	**Gene annotation**	**Fold change**	**Adjusted p-value**
AKR1C2	aldo-keto reductase family 1, member C2 (dihydrodiol dehydrogenase 2; bile acid binding protein; 3-alpha hydroxysteroid dehydrogenase, type III)	2.68	0.0177
CPAMD8	C3 and PZP-like, alpha-2-macroglobulin domain containing 8	2.63	0.0016
TNXB	tenascin XB	2.61	0.0052
SCARA5	scavenger receptor class A, member 5 (putative)	2.61	0.0026
PKP2	plakophilin 2	2.61	0.0150
CPEB1	cytoplasmic polyadenylation element binding protein 1	2.61	0.0366
S100B	S100 calcium binding protein B	2.56	0.0082
HLF	hepatic leukemia factor	2.54	0.0180
CHAD	chondroadherin	2.52	0.0015
CLDN11	claudin 11	2.51	0.0161
NSG1	Neuron-specific protein family member 1	2.49	0.0033
TCEAL2	transcription elongation factor A (SII)-like 2	2.49	0.0164
SLC6A1	solute carrier family 6 (neurotransmitter transporter, GABA), member 1	2.46	0.0030
COL4A3	collagen, type IV, alpha 3 (Goodpasture antigen)	2.42	0.0298
PTGDS	prostaglandin D2 synthase 21kDa (brain)	2.41	0.0112
PPP1R1B	protein phosphatase 1, regulatory (inhibitor) subunit 1B	2.41	0.0040
GBP3	guanylate binding protein 3	2.38	0.0048
ABCA8	ATP-binding cassette, sub-family A (ABC1), member 8	2.33	0.0294
GATA4	GATA binding protein 4	2.33	0.0079
SFRP1	secreted frizzled-related protein 1	2.23	0.0461
EMILIN3	elastin microfibril interfacer 3	2.19	0.0170
SLC14A1	solute carrier family 14 (urea transporter), member 1 (Kidd blood group)	2.10	0.0461
DHCR24	24-dehydrocholesterol reductase	2.09	0.0351
HAND2	heart and neural crest derivatives expressed 2	2.08	0.0110
NFIA	nuclear factor I/A	2.00	0.0499
NTRK2	neurotrophic tyrosine kinase, receptor, type 2	1.93	0.0490
MMP13	matrix metallopeptidase 13 (collagenase 3)	-186.53	0
IGLL5	immunoglobulin lambda-like polypeptide 5	-101.77	0
RP11-1280I22.1	Plasma cell-induced resident endoplasmic reticulum protein	-78.85	0
IGJ	immunoglobulin J polypeptide, linker protein for immunoglobulin alpha and mu polypeptides	-54.04	0
GPIHBP1	glycosylphosphatidylinositol anchored high density lipoprotein binding protein 1	-42.61	6.06E-05
CCL7	chemokine (C-C motif) ligand 7	-42.05	0.0125
CD79A	CD79a molecule, immunoglobulin-associated alpha	-40.93	0
IBSP	integrin-binding sialoprotein	-39.43	0
SP7	Sp7 transcription factor	-36.34	2.78E-07
FCRL5	Fc receptor-like 5	-33.70	1.18E-09
MMP9	matrix metallopeptidase 9 (gelatinase B, 92kDa gelatinase, 92kDa type IV collagenase)	-32.29	0
TDO2	tryptophan 2,3-dioxygenase	-32.25	1.17E-09

Table III-3 continued

DEGs in BAVr versus TAV			
Gene symbol	**Gene annotation**	**Fold change**	**Adjusted p-value**
MTRNR2L8	MT-RNR2-like 8	-31.05	4.01E-06
MMP7	matrix metallopeptidase 7 (matrilysin, uterine)	-29.87	5.54E-06
PPBP	pro-platelet basic protein (chemokine (C-X-C motif) ligand 7)	-29.06	0.0358
SPIB	Spi-B transcription factor (Spi-1/PU.1 related)	-28.63	0.0379
AMPD1	adenosine monophosphate deaminase 1	-28.15	0.0039
FLT4	fms-related tyrosine kinase 4	-24.65	5.93E-08
KLK4	kallikrein-related peptidase 4	-23.71	0.0191
EMR1	egf-like module containing, mucin-like, hormone receptor-like 1	-21.91	0.0216
CBLN4	cerebellin 4 precursor	-21.68	0.0067
ATP6V0D2	ATPase, H+ transporting, lysosomal 38kDa, V0 subunit d2	-21.37	5.94E-05
MAT1A	methionine adenosyltransferase I, alpha	-21.35	0.0053
PRND	prion protein 2 (dublet)	-20.87	2.08E-04
SPP1	secreted phosphoprotein 1	-20.35	0
BMP3	bone morphogenetic protein 3	-20.01	0.0043
CXCL13	chemokine (C-X-C motif) ligand 13	-18.99	1.80E-04
PNOC	prepronociceptin	-17.52	0.0490
FCRL3	Fc receptor-like 3	-17.14	0.0100
AQP9	aquaporin 9	-16.97	7.47E-04
CXCL5	chemokine (C-X-C motif) ligand 5	-15.09	0.0017
RASSF6	Ras association (RalGDS/AF-6) domain family member 6	-14.79	0.0017
POU2AF1	POU class 2 associating factor 1	-13.46	7.72E-09
DERL3	Der1-like domain family, member 3	-12.75	3.30E-09
MMP1	matrix metallopeptidase 1 (interstitial collagenase)	-11.69	0.0072
COL11A1	collagen, type XI, alpha 1	-10.92	0
MS4A1	membrane-spanning 4-domains, subfamily A, member 1	-10.63	9.63E-05
C10orf81	chromosome 10 open reading frame 81	-10.52	1.02E-08
ADCYAP1	adenylate cyclase activating polypeptide 1 (pituitary)	-10.26	0.0146
APOC2	apolipoprotein C-II	-9.86	0.0196
HBA2	hemoglobin, alpha 2	-9.29	0
COL2A1	collagen, type II, alpha 1	-9.10	1.34E-04
HBA1	hemoglobin, alpha 1	-9.03	0
EBF2	early B-cell factor 2	-8.98	0.0011
GJB2	gap junction protein, beta 2, 26kDa	-8.64	0.0366
CXorf36	chromosome X open reading frame 36	-8.61	2.31E-06
DLL4	delta-like 4 (Drosophila)	-8.53	8.56E-05
SCUBE1	signal peptide, CUB domain, EGF-like 1	-8.25	0.0474
CCL3	chemokine (C-C motif) ligand 3	-8.23	9.08E-09
SLAMF7	SLAM family member 7	-7.92	3.42E-08
CHIT1	chitinase 1 (chitotriosidase)	-7.79	9.26E-08
HBB	hemoglobin, beta	-7.79	2.36E-12

Table III-3 continued

DEGs in BAVr versus TAV			
Gene symbol	**Gene annotation**	**Fold change**	**Adjusted p-value**
TM4SF19	transmembrane 4 L six family member 19	-7.75	0.0020
GZMB	granzyme B (granzyme 2, cytotoxic T-lymphocyte-associated serine esterase 1)	-7.66	0.0068
LRRC15	leucine rich repeat containing 15	-7.64	0
KCNK2	potassium channel, subfamily K, member 2	-7.15	0.0036
TM4SF18	transmembrane 4 L six family member 18	-6.97	7.07E-06
CHI3L1	chitinase 3-like 1 (cartilage glycoprotein-39)	-6.76	1.20E-10
TIMD4	T-cell immunoglobulin and mucin domain containing 4	-6.53	1.50E-06
CMA1	chymase 1, mast cell	-6.51	8.37E-05
COL10A1	collagen, type X, alpha 1	-6.35	2.35E-10
BGLAP	bone gamma-carboxyglutamate (gla) protein	-6.32	5.22E-05
DLX5	distal-less homeobox 5	-6.26	0.0097
SDC1	syndecan 1	-6.08	4.56E-06
TREM1	triggering receptor expressed on myeloid cells 1	-5.75	3.69E-05
PLA2G2D	phospholipase A2, group IID	-5.75	0.0306
HLA-DOB	major histocompatibility complex, class II, DO beta	-5.62	0.0292
SDS	serine dehydratase	-5.61	0.0296
CCL14	chemokine (C-C motif) ligand 14	-5.52	6.55E-04
GREM1	gremlin 1	-5.43	0.0074
PLVAP	plasmalemma vesicle associated protein	-5.37	2.90E-07
IL1RN	interleukin 1 receptor antagonist	-5.25	0.0100
KCNJ15	potassium inwardly-rectifying channel, subfamily J, member 15	-5.22	0.0075
PIM2	pim-2 oncogene	-5.14	2.86E-09
NELL2	NEL-like 2 (chicken)	-5.08	0.0028
SLC11A1	solute carrier family 11 (proton-coupled divalent metal ion transporters), member 1	-4.95	2.25E-06
CCL4	chemokine (C-C motif) ligand 4	-4.95	0.0029
IRF4	interferon regulatory factor 4	-4.88	5.90E-04
APOC1	apolipoprotein C-I	-4.81	2.93E-05
CCL21	chemokine (C-C motif) ligand 21	-4.65	5.94E-06
ACAN	aggrecan	-4.56	5.37E-09
TMEM200A	transmembrane protein 200A	-4.55	0.0011
SLC2A5	solute carrier family 2 (facilitated glucose/fructose transporter), member 5	-4.51	0.0031
SGCA	sarcoglycan, alpha (50kDa dystrophin-associated glycoprotein)	-4.50	0.0032
GALNT3	Polypeptide GalNAc transferase 3	-4.40	0.0073
VMO1	vitelline membrane outer layer 1 homolog (chicken)	-4.26	0.0010
SLAMF6	SLAM family member 6	-4.08	0.0013
FAIM3	Fas apoptotic inhibitory molecule 3	-4.06	0.0022
ISM1	isthmin 1 homolog (zebrafish)	-4.05	1.34E-04
GPHA2	glycoprotein hormone alpha 2	-3.97	0.0060
ADRA2A	adrenergic, alpha-2A-, receptor	-3.95	1.77E-06
LTB	lymphotoxin beta (TNF superfamily, member 3)	-3.91	0.0127

Table III-3 continued

DEGs in BAVr versus TAV			
Gene symbol	**Gene annotation**	**Fold change**	**Adjusted p-value**
MATK	megakaryocyte-associated tyrosine kinase	-3.80	0.0379
NDUFA4L2	NADH dehydrogenase (ubiquinone) 1 alpha subcomplex, 4-like 2	-3.77	4.39E-06
IL21R	interleukin 21 receptor	-3.74	0.0112
RGS16	regulator of G-protein signalling 16	-3.71	0.0013
SLC7A2	solute carrier family 7 (cationic amino acid transporter, y+ system), member 2	-3.71	4.41E-04
GPR68	G protein-coupled receptor 68	-3.64	2.10E-05
FMO3	flavin containing monooxygenase 3	-3.64	1.01E-04
ITGAX	integrin, alpha X (complement component 3 receptor 4 subunit)	-3.63	3.16E-07
GZMK	granzyme K (granzyme 3; tryptase II)	-3.52	0.0224
FCGR1A	Fc fragment of IgG, high affinity Ia, receptor (CD64)	-3.35	3.97E-06
CHST1	carbohydrate (keratan sulfate Gal-6) sulfotransferase 1]	-3.29	0.0085
SEMA6B	sema domain, transmembrane domain (TM), and cytoplasmic domain, (semaphorin) 6B	-3.28	0.0052
ST14	suppression of tumorigenicity 14 (colon carcinoma)	-3.24	0.0221
CLEC5A	C-type lectin domain family 5, member A	-3.23	0.0049
CXCL9	chemokine (C-X-C motif) ligand 9	-3.22	9.41E-05
SLC44A3	solute carrier family 44, member 3	-3.22	0.0457
VCAM1	vascular cell adhesion molecule 1	-3.19	4.46E-07
PTP4A3	protein tyrosine phosphatase type IVA, member 3	-3.17	0.0011
F3	coagulation factor III (thromboplastin, tissue factor)	-3.12	0.0116
CA12	carbonic anhydrase XII	-3.11	0.0203
NUP210	nucleoporin 210kDa	-3.09	0.0186
SLPI	secretory leukocyte peptidase inhibitor	-3.07	0.0039
STMN2	stathmin-like 2	-3.01	7.78E-04
IFI30	interferon, gamma-inducible protein 30	-2.95	2.57E-05
TREM2	triggering receptor expressed on myeloid cells 2	-2.92	0.0296
ACE	angiotensin I converting enzyme (peptidyl-dipeptidase A) 1	-2.92	0.0201
FPR1	formyl peptide receptor 1	-2.91	0.0032
ADAMTS9	ADAM metallopeptidase with thrombospondin type 1 motif, 9	-2.90	0.0490
MMRN1	multimerin 1	-2.88	0.0039
TNC	tenascin C	-2.87	8.98E-05
APLN	apelin	-2.82	0.0366
GLRX	glutaredoxin (thioltransferase)	-2.81	0.0019
CD52	CD52 molecule	-2.79	0.0401
SERPINA1	serpin peptidase inhibitor, clade A (alpha-1 antiproteinase, antitrypsin), member 1	-2.78	0.0046
ACP5	acid phosphatase 5, tartrate resistant	-2.78	1.23E-05
TP53I11	tumor protein p53 inducible protein 11	-2.74	9.28E-05
FCGR1B	Fc fragment of IgG, high affinity Ib, receptor (CD64)	-2.69	0.0461
S100A9	S100 calcium binding protein A9	-2.64	0.0082
CCL19	chemokine (C-C motif) ligand 19	-2.62	0.0244

Table III-3 continued

DEGs in BAVr versus TAV			
Gene symbol	**Gene annotation**	**Fold change**	**Adjusted p-value**
AOAH	acyloxyacyl hydrolase (neutrophil)	-2.59	0.0244
CCL18	chemokine (C-C motif) ligand 18 (pulmonary and activation-regulated)	-2.57	0.0056
ENPP1	ectonucleotide pyrophosphatase/phosphodiesterase 1	-2.55	0.0057
MYO1G	myosin IG	-2.54	0.0378
CD3E	CD3e molecule, epsilon (CD3-TCR complex)	-2.52	0.0165
MFAP5	microfibrillar associated protein 5	-2.48	0.0221
KIAA1199	KIAA1199	-2.46	0.0115
TSPAN11	tetraspanin 11	-2.45	0.0191
ITGAL	integrin, alpha L (antigen CD11A (p180), lymphocyte function-associated antigen 1; alpha polypeptide)	-2.42	0.0195
SMOC2	SPARC related modular calcium binding 2	-2.40	0.0180
TMEM119	transmembrane protein 119	-2.36	0.0043
C1orf162	chromosome 1 open reading frame 162	-2.33	0.0372
CR1	complement component (3b/4b) receptor 1 (Knops blood group)	-2.32	0.0385
A2M	alpha-2-macroglobulin	-2.31	0.0085
CADM1	cell adhesion molecule 1	-2.30	0.0487
KCNN4	potassium intermediate/small conductance calcium-activated channel, subfamily N, member 4	-2.29	0.0425
ALOX5AP	arachidonate 5-lipoxygenase-activating protein	-2.29	0.0330
SERPINE1	serpin peptidase inhibitor, clade E (nexin, plasminogen activator inhibitor type 1), member 1	-2.25	0.0158
LBH	limb bud and heart development homolog (mouse)	-2.25	0.0148
PLAU	plasminogen activator, urokinase	-2.18	0.0192
LAPTM5	lysosomal protein transmembrane 5	-2.17	0.0295
LYZ	lysozyme	-2.15	0.0443
HMOX1	heme oxygenase (decycling) 1	-2.15	0.0105
SMOC1	SPARC related modular calcium binding 1	-2.14	0.0098
CHST15	carbohydrate (N-acetylgalactosamine 4-sulfate 6-O) sulfotransferase 15	-2.13	0.0270
SRGN	serglycin	-2.11	0.0273
PLAUR	plasminogen activator, urokinase receptor	-2.09	0.0384
OGN	osteoglycin	-2.05	0.0341
KIAA1217	KIAA1217	-2.04	0.0481
CHI3L2	chitinase 3-like 2	-2.02	0.0452

Table III- 4. Complete list of differentially expressed genes (DEGs) between the BAVc (BAV4, BAV5) and TAV (TAV1-TAV3) groups (p<0.05 with post-hoc Bonferroni correction), sorted by fold change.

DEGs in BAVc versus TAV			
Gene symbol	**Gene annotation**	**Fold change**	**Adjusted p-value**
CCKAR	cholecystokinin A receptor	14.97	5.73E-05
RNASE3	ribonuclease, RNase A family, 3	9.98	0.0169
FMN2	formin 2	8.79	0.0456
FOSB	FBJ murine osteosarcoma viral oncogene homolog B	7.75	0
GSTT1	glutathione S-transferase theta 1	5.91	0
C1QTNF8	C1q and tumor necrosis factor related protein 8	5.41	3.23E-07
ABP1	amiloride binding protein 1 (amine oxidase (copper-containing))	4.95	2.76E-11
CST1	cystatin SN	4.92	0.0489
ESPNL	espin-like	4.47	2.47E-04
SSTR5	somatostatin receptor 5	4.39	0.0123
MLC1	megalencephalic leukoencephalopathy with subcortical cysts 1	3.75	0.0033
HLA-DQB1	major histocompatibility complex, class II, DQ beta 1	3.66	3.19E-08
DKK1	dickkopf homolog 1 (Xenopus laevis)	3.38	0.0417
C1orf51	chromosome 1 open reading frame 51	3.31	1.80E-05
PAX8	paired box 8	3.21	3.22E-06
MATN4	matrilin 4	3.13	0.0014
NR1D1	nuclear receptor subfamily 1, group D, member 1	3.01	0
POU6F2	POU class 6 homeobox 2	2.99	0.0319
FOS	FBJ murine osteosarcoma viral oncogene homolog	2.94	2.11E-12
MTRNR2L9	MT-RNR2-like 9 (pseudogene)	2.93	0.0012
C17orf97	chromosome 17 open reading frame 97	2.78	2.10E-04
POLR2J2	polymerase (RNA) II (DNA directed) polypeptide J2	2.77	2.82E-12
DPYSL4	dihydropyrimidinase-like 4	2.77	4.03E-04
MUC20	mucin 20, cell surface associated	2.64	3.86E-04
GSTM1	glutathione S-transferase mu 1	2.57	0.0021
OCLN	occludin	2.55	0.0195
RPSAP58	ribosomal protein SA pseudogene 58	2.51	0.0224
RASA4	RAS p21 protein activator 4	2.30	2.45E-06
JUN	jun proto-oncogene	2.28	5.53E-07
DDX11	DEAD/H (Asp-Glu-Ala-Asp/His) box polypeptide 11	2.23	3.85E-05
CHRFAM7A	CHRNA7 (cholinergic receptor, nicotinic, alpha 7, exons 5-10) and FAM7A (family with sequence similarity 7A, exons A-E) fusion	2.23	0.0365
JAKMIP2	janus kinase and microtubule interacting protein 2	2.20	0.0405
RASA4B	RAS p21 protein activator 4B	2.18	3.16E-06
UPK3BL	uroplakin 3B-like	2.09	3.77E-05
HLA-DQA1	major histocompatibility complex, class II, DQ alpha 1	2.06	0.0011
DBP	D site of albumin promoter (albumin D-box) binding protein	2.06	1.27E-04
COL13A1	collagen, type XIII, alpha 1	2.06	6.58E-04

Table III-4 continued

DEGs in BAVc versus TAV			
Gene symbol	**Gene annotation**	**Fold change**	**Adjusted p-value**
SCG2	secretogranin II	2.05	1.88E-05
PER1	period homolog 1 (Drosophila)	2.04	1.06E-05
CDH6	cadherin 6, type 2, K-cadherin (fetal kidney)	2.02	0.0158
GPX7	glutathione peroxidase 7	1.99	0.0015
MASP1	mannan-binding lectin serine peptidase 1 (C4/C2 activating component of Ra-reactive factor)	1.98	1.53E-05
POLR2J3	polymerase (RNA) II (DNA directed) polypeptide J3	1.98	6.06E-06
KIAA1683	KIAA1683	1.98	0.0028
FNDC1	fibronectin type III domain containing 1	1.87	0.0033
ACAN	aggrecan	1.86	0.0059
NTM	neurotrimin	1.85	7.74E-04
TMTC2	transmembrane and tetratricopeptide repeat containing 2	1.84	0.0168
HLA-DRB5	major histocompatibility complex, class II, DR beta 5	1.82	0.0032
HLF	hepatic leukemia factor	1.82	0.0026
HLA-B	major histocompatibility complex, class I, B	1.81	0.0124
COMP	cartilage oligomeric matrix protein	1.80	0.0326
C1QTNF3	C1q and tumor necrosis factor related protein 3	1.80	0.0059
MIR3654	microRNA 3654	1.78	0.0308
PCDHB5	protocadherin beta 5	1.75	0.0191
ADAM12	ADAM metallopeptidase domain 12	1.72	0.0455
TEF	thyrotrophic embryonic factor	1.71	0.0075
LRRC37A2	leucine rich repeat containing 37, member A2	1.71	0.0121
SLC6A4	solute carrier family 6 (neurotransmitter transporter, serotonin), member 4	1.71	0.0437
GAP43	growth associated protein 43	1.69	0.0230
SCO2	SCO cytochrome oxidase deficient homolog 2 (yeast)	1.68	0.0434
NR1D2	nuclear receptor subfamily 1, group D, member 2	1.66	0.0283
CCDC85B	coiled-coil domain containing 85B	1.64	0.0222
ANK3	ankyrin 3, node of Ranvier (ankyrin G)	1.63	0.0355
HMCN1	hemicentin 1	1.62	0.0447
RRP7A	ribosomal RNA processing 7 homolog A (S. cerevisiae)	1.62	0.0251
LTBP2	latent transforming growth factor beta binding protein 2	1.60	0.0209
DEFA1	defensin, alpha 1	-22.30	0.0277
TSPAN10	tetraspanin 10	-16.32	1.28E-04
SIGLEC6	sialic acid binding Ig-like lectin 6	-10.74	0.0189
GPC5	glypican 5	-8.96	0.0311
MS4A2	membrane-spanning 4-domains, subfamily A, member 2 (Fc fragment of IgE, high affinity I, receptor for; beta polypeptide)	-8.44	3.43E-05
ABCC8	ATP-binding cassette, sub-family C (CFTR/MRP), member 8	-8.30	0.0386
DACH1	dachshund homolog 1 (Drosophila)	-8.16	0.0296
CYP4B1	cytochrome P450, family 4, subfamily B, polypeptide 1	-7.40	2.83E-06
HLA-DQB2	major histocompatibility complex, class II, DQ beta 2	-6.87	8.62E-10

Table III-4 continued

DEGs in BAVc versus TAV			
Gene symbol	**Gene annotation**	**Fold change**	**Adjusted p-value**
NOS1	nitric oxide synthase 1 (neuronal)	-6.85	0.0423
CMA1	chymase 1, mast cell	-6.61	3.38E-07
CTSE	cathepsin E	-6.51	0.0096
THNSL2	threonine synthase-like 2 (S. cerevisiae)	-5.90	0
NKAIN2	Na+/K+ transporting ATPase interacting 2	-5.73	8.57E-04
HDC	histidine decarboxylase	-5.58	6.03E-06
TPSD1	tryptase delta 1	-5.51	1.70E-05
TRDN	triadin	-5.48	0.0085
LTF	lactotransferrin	-5.30	0.0365
CPA3	carboxypeptidase A3 (mast cell)	-4.99	0
ACTC1	actin, alpha, cardiac muscle 1	-4.96	9.64E-11
DES	desmin	-4.86	1.05E-12
IGLL5	immunoglobulin lambda-like polypeptide 5	-4.82	0
MTRNR2L8	MT-RNR2-like 8	-4.77	1.14E-04
RP11-1280I22.1	Plasma cell-induced resident endoplasmic reticulum protein	-4.60	2.46E-11
CHL1	cell adhesion molecule with homology to L1CAM	-4.30	1.27E-04
TPSAB1	tryptase alpha/beta 1	-4.20	0
MMRN1	multimerin 1	-4.10	1.32E-10
CTSG	cathepsin G	-3.86	1.51E-05
CD79A	CD79a molecule, immunoglobulin-associated alpha	-3.79	2.73E-12
RASSF6	Ras association (RalGDS/AF-6) domain family member 6	-3.70	0.0162
CCDC163P	coiled-coil domain containing 163, pseudogene	-3.70	0.0028
COCH	coagulation factor C homolog, cochlin (Limulus polyphemus)	-3.69	1.28E-04
FCRL5	Fc receptor-like 5	-3.42	1.14E-04
ADIPOQ	adiponectin, C1Q and collagen domain containing	-3.41	0.0099
EGFLAM	EGF-like, fibronectin type III and laminin G domains	-3.29	0.0065
SGCA	sarcoglycan, alpha (50kDa dystrophin-associated glycoprotein)	-3.29	8.19E-09
IGJ	immunoglobulin J polypeptide, linker protein for immunoglobulin alpha and mu polypeptides	-3.27	0
MMP7	matrix metallopeptidase 7 (matrilysin, uterine)	-3.19	0.0224
FCN3	ficolin (collagen/fibrinogen domain containing) 3 (Hakata antigen)	-3.17	0.0193
WNT7A	wingless-type MMTV integration site family, member 7A	-3.11	0.0410
GFRA1	GDNF family receptor alpha 1	-3.03	1.10E-11
KIT	v-kit Hardy-Zuckerman 4 feline sarcoma viral oncogene homolog	-3.00	0.0019
GPHA2	glycoprotein hormone alpha 2	-2.95	6.93E-05
CHIT1	chitinase 1 (chitotriosidase)	-2.93	1.40E-06
MYOC	myocilin, trabecular meshwork inducible glucocorticoid response	-2.92	4.04E-05
CXCL9	chemokine (C-X-C motif) ligand 9	-2.61	1.33E-07
PI16	peptidase inhibitor 16	-2.57	4.00E-07
PLP1	proteolipid protein 1	-2.42	0.0263
PPP1R1B	protein phosphatase 1, regulatory (inhibitor) subunit 1B	-2.38	5.42E-04

Table III-4 continued

DEGs in BAVc versus TAV			
Gene symbol	**Gene annotation**	**Fold change**	**Adjusted p-value**
LPL	lipoprotein lipase	-2.37	1.81E-05
AQP2	aquaporin 2 (collecting duct)	-2.34	2.50E-06
ALDH1A1	aldehyde dehydrogenase 1 family, member A1	-2.32	0.0039
MMP9	matrix metallopeptidase 9 (gelatinase B, 92kDa gelatinase, 92kDa type IV collagenase)	-2.30	4.66E-08
PLIN4	perilipin 4	-2.26	0.0021
ABCC9	ATP-binding cassette, sub-family C (CFTR/MRP), member 9	-2.25	0.0306
GZMK	granzyme K (granzyme 3; tryptase II)	-2.23	0.0322
PRRT4	proline-rich transmembrane protein 4	-2.21	0.0411
NOS3	nitric oxide synthase 3 (endothelial cell)	-2.16	6.15E-06
RGS5	regulator of G-protein signalling 5	-2.13	0.0191
APLN	apelin	-2.12	0.0330
WNT9B	wingless-type MMTV integration site family, member 9B	-2.11	0.0134
VMO1	vitelline membrane outer layer 1 homolog (chicken)	-2.11	0.0116
SEMA3F	sema domain, immunoglobulin domain (Ig), short basic domain, secreted, (semaphorin) 3F	-2.09	3.90E-05
CHRDL1	chordin-like 1	-2.07	0.0015
TIMD4	T-cell immunoglobulin and mucin domain containing 4	-2.07	0.0018
C7	complement component 7	-2.07	2.54E-04
CNTFR	ciliary neurotrophic factor receptor	-2.05	0.0448
HSPA12B	heat shock 70kD protein 12B	-2.04	0.0019
APOE	apolipoprotein E	-2.02	9.64E-05
ATP1A2	ATPase, Na+/K+ transporting, alpha 2 polypeptide	-2.02	0.0276
CCL19	chemokine (C-C motif) ligand 19	-2.01	1.80E-05
PDPR	pyruvate dehydrogenase phosphatase regulatory subunit	-2.00	2.30E-04
ZFAT	zinc finger and AT hook domain containing	-2.00	0.0011
SCARA5	scavenger receptor class A, member 5 (putative)	-1.99	8.60E-05
SLCO2A1	solute carrier organic anion transporter family, member 2A1	-1.97	9.27E-05
PTHLH	parathyroid hormone-like hormone	-1.97	4.93E-04
DERL3	Der1-like domain family, member 3	-1.96	0.0102
ST6GALNAC1	ST6 euraminyl-2,3-beta-galactosyl-1,3)-N-acetylgalactosaminide alpha-2,6-sialyltransferase 1	-1.96	0.0083
GLRX	glutaredoxin (thioltransferase)	-1.95	4.12E-05
HYAL2	hyaluronoglucosaminidase 2	-1.93	8.21E-04
ESAM	endothelial cell adhesion molecule	-1.92	0.0086
ARHGEF15	Rho guanine nucleotide exchange factor (GEF) 15	-1.91	0.0014
GPR116	G protein-coupled receptor 116	-1.89	6.66E-04
LIFR	leukemia inhibitory factor receptor alpha	-1.89	8.24E-04
DDX39B	DEAD (Asp-Glu-Ala-Asp) box polypeptide 39B	-1.88	0.0011
TIE1	tyrosine kinase with immunoglobulin-like and EGF-like domains 1	-1.88	0.0191
SELE	selectin E	-1.87	0.0054
GOLGA8B	golgin A8 family, member B	-1.87	0.0015

Table III-4 continued

DEGs in BAVc versus TAV			
Gene symbol	**Gene annotation**	**Fold change**	**Adjusted p-value**
NPR1	natriuretic peptide receptor A/guanylate cyclase A (atrionatriuretic peptide receptor A)	-1.86	0.0033
DYNC1LI2	dynein, cytoplasmic 1, light intermediate chain 2	-1.83	0.0150
C4orf48	chromosome 4 open reading frame 48	-1.82	0.0294
HS3ST1	heparan sulfate (glucosamine) 3-O-sulfotransferase 1	-1.82	0.0087
ACP5	acid phosphatase 5, tartrate resistant	-1.82	0.0030
NPIPL2	nuclear pore complex interacting protein-like 2	-1.78	0.0134
HBA2	hemoglobin, alpha 2	-1.78	0.0054
ARNTL	aryl hydrocarbon receptor nuclear translocator-like	-1.78	0.0462
INMT	indolethylamine N-methyltransferase	-1.78	0.0099
GSN	gelsolin	-1.77	0.0125
GNA14	guanine nucleotide binding protein (G protein), alpha 14	-1.76	0.0116
AIF1L	allograft inflammatory factor 1-like	-1.75	0.0048
PTGDS	prostaglandin D2 synthase 21kDa (brain)	-1.75	0.0073
TEK	TEK tyrosine kinase, endothelial	-1.74	0.0011
FAM107A	family with sequence similarity 107, member A	-1.74	0.0116
CRHBP	corticotropin releasing hormone binding protein	-1.74	0.0022
HTRA3	HtrA serine peptidase 3	-1.73	0.0017
A2M	alpha-2-macroglobulin	-1.72	0.0033
VWF	von Willebrand factor	-1.72	0.0169
JAM2	junctional adhesion molecule 2	-1.72	0.0347
ITGAX	integrin, alpha X (complement component 3 receptor 4 subunit)	-1.71	0.0158
CRELD1	cysteine-rich with EGF-like domains 1	-1.71	0.0178
CHI3L2	chitinase 3-like 2	-1.69	0.0104
HBA1	hemoglobin, alpha 1	-1.67	0.0192
ITGA6	integrin, alpha 6	-1.66	0.0264
SYNPO2	synaptopodin 2	-1.65	0.0220
CDH5	cadherin 5, type 2 (vascular endothelium)	-1.64	0.0270
ZNF266	zinc finger protein 266	-1.64	0.0318
RAMP3	receptor (G protein-coupled) activity modifying protein 3	-1.64	0.0417
CXCR7	chemokine (C-X-C motif) receptor 7	-1.63	0.0280
ADAMTS1	ADAM metallopeptidase with thrombospondin type 1 motif, 1	-1.62	0.0296
PTPRB	protein tyrosine phosphatase, receptor type, B	-1.61	0.0324
RPS12	ribosomal protein S12	-1.61	0.0357
SLC40A1	solute carrier family 40 (iron-regulated transporter), member 1	-1.60	0.0414
PDK4	pyruvate dehydrogenase kinase, isozyme 4	-1.59	0.0456
ADAM33	ADAM metallopeptidase domain 33	-1.57	0.0432
BMPER	BMP binding endothelial regulator	-1.56	0.0467
EMCN	endomucin	-1.53	0.0406

Table III- 5. Complete list of differentially expressed genes (DEGs) between the BAVr (BAV1-BAV3) and BAVc (BAV4, BAV5) groups (p<0.05 with post-hoc Bonferroni correction), sorted by fold change.

DEGs in BAVr versus BAVc			
Gene symbol	**Gene annotation**	**Fold change**	**Adjusted p-value**
IGFN1	immunoglobulin-like and fibronectin type III domain containing 1	22.06	0.0022
ENTPD2	ectonucleoside triphosphate diphosphohydrolase 2	22.05	0.0132
CBLN1	cerebellin 1 precursor	20.11	1.97E-04
FAM123A	family with sequence similarity 123A	13.73	0.0244
TRDN	triadin	13.04	2.15E-05
OTOGL	otogelin-like	12.90	0.0305
VSTM2A	V-set and transmembrane domain containing 2A	11.08	0.0132
CTSE	cathepsin E	10.99	1.94E-06
SLC6A20	solute carrier family 6 (proline IMINO transporter), member 20	10.50	2.59E-04
KISS1	KiSS-1 metastasis-suppressor	10.10	3.20E-04
CNTFR	ciliary neurotrophic factor receptor	9.69	2.16E-09
NPPC	natriuretic peptide C	9.09	6.47E-08
NKAIN2	Na+/K+ transporting ATPase interacting 2	9.04	0.0250
COL9A1	collagen, type IX, alpha 1	8.45	0.0498
MYOC	myocilin, trabecular meshwork inducible glucocorticoid response	7.86	6.90E-08
DES	desmin	7.47	8.82E-11
CADM2	cell adhesion molecule 2	6.08	1.48E-04
PLCH1	phospholipase C, eta 1	6.01	4.93E-05
ADCYAP1R1	adenylate cyclase activating polypeptide 1 (pituitary) receptor type I	5.79	1.50E-04
CHL1	cell adhesion molecule with homology to L1CAM	5.61	0.0443
SCN7A	sodium channel, voltage-gated, type VII, alpha	5.60	4.93E-05
PPP1R1B	protein phosphatase 1, regulatory (inhibitor) subunit 1B	5.55	3.19E-08
ITLN1	intelectin 1 (galactofuranose binding)	5.52	0.0132
SMTNL2	smoothelin-like 2	5.40	2.84E-06
ATP1A2	ATPase, Na+/K+ transporting, alpha 2 polypeptide	5.26	1.39E-08
KIF1A	kinesin family member 1A	5.20	5.40E-04
COL6A6	collagen, type VI, alpha 6	5.16	7.21E-11
OTC	ornithine carbamoyltransferase	5.10	0.0075
COCH	coagulation factor C homolog, cochlin (Limulus polyphemus)	5.04	1.22E-04
ACTC1	actin, alpha, cardiac muscle 1	4.99	1.66E-04
HLA-DRB5	major histocompatibility complex, class II, DR beta 5	4.81	7.72E-08
IGSF10	immunoglobulin superfamily, member 10	4.80	3.22E-08
HMGCLL1	3-hydroxymethyl-3-methylglutaryl-CoA lyase-like 1	4.73	0.0358
PRODH	proline dehydrogenase (oxidase) 1	4.71	0.0019
WNT9B	wingless-type MMTV integration site family, member 9B	4.66	2.63E-04
ST6GALNAC1	ST6 euraminyl-2,3-beta-galactosyl-1,3)-N-acetylgalactosaminide alpha-2,6-sialyltransferase 1	4.42	3.94E-06

Table III-5 continued

DEGs in BAVr versus BAVc			
Gene symbol	**Gene annotation**	**Fold change**	**Adjusted p-value**
GFAP	glial fibrillary acidic protein	4.41	1.41E-09
NWD1	NACHT and WD repeat domain containing 1	4.12	0.0019
PTGDS	prostaglandin D2 synthase 21kDa (brain)	4.08	2.19E-07
SPOCK3	sparc/osteonectin, cwcv and kazal-like domains proteoglycan (testican) 3	4.06	6.47E-06
PRLR	prolactin receptor	4.04	0.0019
SCARA5	scavenger receptor class A, member 5 (putative)	3.97	2.55E-07
CECR2	cat eye syndrome chromosome region, candidate 2	3.88	0.0116
IL1RL1	interleukin 1 receptor-like 1	3.80	7.81E-04
ALDH3A1	aldehyde dehydrogenase 3 family, member A1	3.77	0.0025
TMEM132C	transmembrane protein 132C	3.74	9.49E-05
ALDH1A1	aldehyde dehydrogenase 1 family, member A1	3.73	3.89E-05
MED12L	mediator complex subunit 12-like	3.69	6.94E-05
LAMC3	laminin, gamma 3	3.60	5.93E-06
SOX10	SRY (sex determining region Y)-box 10	3.60	0.0182
COL4A3	collagen, type IV, alpha 3 (Goodpasture antigen)	3.57	4.54E-05
PPP1R39	protein phosphatase 1, regulatory subunit 39	3.51	0.0047
CLDN10	claudin 10	3.47	0.0378
ERAP2	endoplasmic reticulum aminopeptidase 2	3.41	3.01E-06
C2orf88	chromosome 2 open reading frame 88	3.37	0.0023
PTPN20A	protein tyrosine phosphatase, non-receptor type 20A	3.37	0.0376
ABCC9	ATP-binding cassette, sub-family C (CFTR/MRP), member 9	3.36	0.0111
PDE4B	phosphodiesterase 4B, cAMP-specific	3.34	0.0302
LCNL1	lipocalin-like 1	3.31	0.0256
MYH14	myosin, heavy chain 14, non-muscle	3.27	8.48E-04
THNSL2	threonine synthase-like 2 (S. cerevisiae)	3.22	0.0111
CHRDL1	chordin-like 1	3.20	2.67E-04
SFRP1	secreted frizzled-related protein 1	3.19	3.13E-04
PLIN1	perilipin 1	3.08	0.0439
ACTG2	actin, gamma 2, smooth muscle, enteric	3.06	8.48E-04
MET	met proto-oncogene (hepatocyte growth factor receptor)	3.05	0.0377
LIFR	leukemia inhibitory factor receptor alpha	3.05	1.08E-04
MYH10	myosin, heavy chain 10, non-muscle	3.03	0.0016
ERBB3	v-erb-b2 erythroblastic leukemia viral oncogene homolog 3 (avian)	3.00	0.0227
CNTN1	contactin 1	2.99	0.0363
CLDN11	claudin 11	2.99	0.0013
TBX20	T-box 20	2.98	0.0012
NDNF	neuron-derived neurotrophic factor	2.88	0.0420
AKR1C2	aldo-keto reductase family 1, member C2 (dihydrodiol dehydrogenase 2; bile acid binding protein)	2.88	0.0024

Table III-5 continued

DEGs in BAVr versus BAVc			
Gene symbol	**Gene annotation**	**Fold change**	**Adjusted p-value**
CPAMD8	C3 and PZP-like, alpha-2-macroglobulin domain containing 8	2.88	0.0069
RIMS4	regulating synaptic membrane exocytosis 4	2.82	4.21E-04
PLIN4	perilipin 4	2.81	0.0217
ZEB1	zinc finger E-box binding homeobox 1	2.80	0.0345
AIF1L	allograft inflammatory factor 1-like	2.79	0.0025
CPA3	carboxypeptidase A3 (mast cell)	2.79	0.0409
KIF26A	kinesin family member 26A	2.79	0.0378
GFRA1	GDNF family receptor alpha 1	2.76	0.0032
MAPT	microtubule-associated protein tau	2.69	0.0039
C7	complement component 7	2.69	3.89E-04
DOK6	docking protein 6	2.66	0.0432
PKHD1L1	polycystic kidney and hepatic disease 1 (autosomal recessive)-like 1	2.62	0.0019
EMILIN3	elastin microfibril interfacer 3	2.61	0.0056
MATN2	matrilin 2	2.61	5.13E-04
PIR	pirin (iron-binding nuclear protein)	2.49	0.0441
PI16	peptidase inhibitor 16	2.47	0.0286
ANGPTL7	angiopoietin-like 7	2.44	0.0360
PDZRN4	PDZ domain containing ring finger 4	2.42	0.0267
PKP2	plakophilin 2	2.41	0.0402
ABCA8	ATP-binding cassette, sub-family A (ABC1), member 8	2.40	0.0154
PTPRB	protein tyrosine phosphatase, receptor type, B	2.35	0.0129
SAMD5	sterile alpha motif domain containing 5	2.29	0.0500
PLEKHA6	pleckstrin homology domain containing, family A member 6	2.27	0.0254
TPSAB1	tryptase alpha/beta 1	2.27	0.0300
BMPER	BMP binding endothelial regulator	2.26	0.0069
NSG1	Neuron-specific protein family member 1	2.25	0.0135
LGI4	leucine-rich repeat LGI family, member 4	2.21	0.0484
FAM107A	family with sequence similarity 107, member A	2.20	0.0208
NOS3	nitric oxide synthase 3 (endothelial cell)	2.20	0.0305
DHCR24	24-dehydrocholesterol reductase	2.19	0.0233
TNXB	tenascin XB	2.17	0.0203
LDLR	low density lipoprotein receptor	2.17	0.0248
SPTBN1	spectrin, beta, non-erythrocytic 1	2.14	0.0467
HS3ST1	heparan sulfate (glucosamine) 3-O-sulfotransferase 1	2.13	0.0372
MEIS2	Meis homeobox 2	2.10	0.0267
SYNPO2	synaptopodin 2	2.04	0.0462
NDRG2	NDRG family member 2	2.03	0.0332
MMP13	matrix metallopeptidase 13 (collagenase 3)	-299.48	0
CHGA	chromogranin A (parathyroid secretory protein 1)	-51.58	0.0163
GADL1	glutamate decarboxylase-like 1	-46.95	0.0206

Table III-5 continued

DEGs in BAVr versus BAVc			
Gene symbol	**Gene annotation**	**Fold change**	**Adjusted p-value**
IBSP	integrin-binding sialoprotein	-44.35	0
FLT4	fms-related tyrosine kinase 4	-41.38	1.55E-11
CCL7	chemokine (C-C motif) ligand 7	-34.84	0.0341
MEPE	matrix extracellular phosphoglycoprotein	-31.83	0.0425
CBLN4	cerebellin 4 precursor	-29.84	1.32E-04
SP7	Sp7 transcription factor	-28.23	1.99E-05
PRND	prion protein 2 (dublet)	-23.89	1.08E-04
IGLL5	immunoglobulin lambda-like polypeptide 5	-21.10	0
GPIHBP1	glycosylphosphatidylinositol anchored high density lipoprotein binding protein 1	-19.76	0.0203
IGJ	immunoglobulin J polypeptide, linker protein for immunoglobulin alpha and mu polypeptides	-18.75	0
TDO2	tryptophan 2,3-dioxygenase	-18.73	4.37E-04
MMP1	matrix metallopeptidase 1 (interstitial collagenase)	-16.74	0.0022
RP11-1280I22.1	Plasma cell-induced resident endoplasmic reticulum protein	-16.71	0.0014
FOSB	FBJ murine osteosarcoma viral oncogene homolog B	-15.97	0
AQP9	aquaporin 9	-15.68	0.0023
MAT1A	methionine adenosyltransferase I, alpha	-15.24	0.0279
MMP9	matrix metallopeptidase 9 (gelatinase B, 92kDa gelatinase, 92kDa type IV collagenase)	-14.51	0
SPP1	secreted phosphoprotein 1	-14.04	0
CXCL5	chemokine (C-X-C motif) ligand 5	-13.87	0.0016
CCKAR	cholecystokinin A receptor	-13.37	0.0172
CXCL13	chemokine (C-X-C motif) ligand 13	-13.36	0.0185
GSTT1	glutathione S-transferase theta 1	-12.58	0
GJB2	gap junction protein, beta 2, 26kDa	-12.02	0.0069
SIRPB1	signal-regulatory protein beta 1	-11.68	0.0038
CYP26A1	cytochrome P450, family 26, subfamily A, polypeptide 1	-11.42	0.0097
TNFRSF18	tumor necrosis factor receptor superfamily, member 18	-11.07	0.0173
C10orf81	chromosome 10 open reading frame 81	-11.00	2.49E-10
CD79A	CD79a molecule, immunoglobulin-associated alpha	-10.81	1.51E-04
FCRL5	Fc receptor-like 5	-9.87	0.0288
CXorf36	chromosome X open reading frame 36	-9.24	3.64E-07
DLL4	delta-like 4 (Drosophila)	-9.18	3.93E-04
DLX5	distal-less homeobox 5	-8.73	6.04E-05
C1QTNF8	C1q and tumor necrosis factor related protein 8	-8.63	9.40E-04
GZMB	granzyme B (granzyme 2, cytotoxic T-lymphocyte-associated serine esterase 1)	-8.58	0.0089
KCNK2	potassium channel, subfamily K, member 2	-8.46	2.77E-04
S100A8	S100 calcium binding protein A8	-8.41	0.0104
COL10A1	collagen, type X, alpha 1	-8.26	4.61E-10
POU2AF1	POU class 2 associating factor 1	-8.25	5.45E-07

Table III-5 continued

DEGs in BAVr versus BAVc			
Gene symbol	**Gene annotation**	**Fold change**	**Adjusted p-value**
COL2A1	collagen, type II, alpha 1	-7.91	0.0012
TNFSF11	tumor necrosis factor (ligand) superfamily, member 11	-7.89	0.0349
CCL3	chemokine (C-C motif) ligand 3	-7.72	1.58E-06
ACAN	aggrecan	-7.69	0
COL11A1	collagen, type XI, alpha 1	-7.49	2.74E-08
LRRC15	leucine rich repeat containing 15	-7.30	3.30E-13
SDC1	syndecan 1	-7.06	3.05E-07
CHI3L1	chitinase 3-like 1 (cartilage glycoprotein-39)	-7.04	1.24E-11
FCN1	ficolin (collagen/fibrinogen domain containing) 1	-6.48	0.0123
RNASE2	ribonuclease, RNase A family, 2 (liver, eosinophil-derived neurotoxin)	-6.18	0.0077
TMEM200A	transmembrane protein 200A	-6.09	2.00E-07
SLAMF7	SLAM family member 7	-6.04	1.58E-06
NELL2	NEL-like 2 (chicken)	-5.94	1.44E-04
BGLAP	bone gamma-carboxyglutamate (gla) protein	-5.74	2.93E-04
TREM1	triggering receptor expressed on myeloid cells 1	-5.67	9.11E-06
HBA1	hemoglobin, alpha 1	-5.59	8.82E-11
GALNT3	putative sodium/glutamine symporter GlnT	-5.55	0.0039
KCNJ15	potassium inwardly-rectifying channel, subfamily J, member 15	-5.53	0.0172
SIGLEC14	sialic acid binding Ig-like lectin 14	-5.46	7.79E-04
SLC2A5	solute carrier family 2 (facilitated glucose/fructose transporter), member 5	-5.39	4.25E-05
HBA2	hemoglobin, alpha 2	-5.35	3.55E-11
TM4SF18	transmembrane 4 L six family member 18	-5.34	2.15E-04
CCL14	chemokine (C-C motif) ligand 14	-5.27	0.0022
IRF4	interferon regulatory factor 4	-5.27	2.67E-04
CPXM1	carboxypeptidase X (M14 family), member 1	-5.17	0.0031
ADAMTS16	ADAM metallopeptidase with thrombospondin type 1 motif, 16	-5.00	0.0336
HBB	hemoglobin, beta	-4.95	6.57E-10
PTP4A3	protein tyrosine phosphatase type IVA, member 3	-4.93	5.79E-08
DERL3	Der1-like domain family, member 3	-4.79	1.84E-04
GNLY	granulysin	-4.76	0.0420
FOS	FBJ murine osteosarcoma viral oncogene homolog	-4.68	5.56E-10
CA12	carbonic anhydrase XII	-4.62	4.99E-07
PLVAP	plasmalemma vesicle associated protein	-4.48	3.93E-09
ADRA2A	adrenergic, alpha-2A-, receptor	-4.39	1.92E-07
PAX8	paired box 8	-4.26	1.17E-04
SLC11A1	solute carrier family 11 (proton-coupled divalent metal ion transporters), member 1	-4.25	5.34E-06
SIGLEC5	sialic acid binding Ig-like lectin 5	-4.22	0.0065
AOC2	amine oxidase, copper containing 2 (retina-specific)	-4.08	0.0366
FCGR1B	Fc fragment of IgG, high affinity Ib, receptor (CD64)	-3.98	8.55E-05

Table III-5 continued

DEGs in BAVr versus BAVc			
Gene symbol	**Gene annotation**	**Fold change**	**Adjusted p-value**
FPR1	formyl peptide receptor 1	-3.88	3.82E-04
ISM1	isthmin 1 homolog (zebrafish)	-3.79	0.0011
GPR84	G protein-coupled receptor 84	-3.75	0.0119
SERPINA1	serpin peptidase inhibitor, clade A (alpha-1 antiproteinase, antitrypsin), member 1	-3.69	1.93E-04
FCGR1A	Fc fragment of IgG, high affinity Ia, receptor (CD64)	-3.67	4.14E-06
PIM2	pim-2 oncogene	-3.67	3.82E-04
TNC	tenascin C	-3.63	1.23E-04
GPR68	G protein-coupled receptor 68	-3.60	0.0017
SOCS3	suppressor of cytokine signalling 3	-3.55	3.28E-06
CCL8	chemokine (C-C motif) ligand 8	-3.55	0.0035
HLA-DQA1	major histocompatibility complex, class II, DQ alpha 1	-3.53	4.17E-06
PDGFRL	platelet-derived growth factor receptor-like	-3.51	0.0022
SLPI	secretory leukocyte peptidase inhibitor	-3.50	0.0077
GPR88	G protein-coupled receptor 88	-3.45	0.0241
ABP1	amiloride binding protein 1 (amine oxidase (copper-containing))	-3.39	0.0154
RGS16	regulator of G-protein signalling 16	-3.39	0.0056
IL21R	interleukin 21 receptor	-3.29	0.0307
VCAM1	vascular cell adhesion molecule 1	-3.28	4.93E-05
DDX11	DEAD/H (Asp-Glu-Ala-Asp/His) box polypeptide 11	-3.25	8.84E-04
DPYSL4	dihydropyrimidinase-like 4	-3.22	0.0225
CCL21	chemokine (C-C motif) ligand 21	-3.21	0.0019
SLAMF6	SLAM family member 6	-3.19	0.0164
F3	coagulation factor III (thromboplastin, tissue factor)	-3.16	0.0190
TSPAN11	tetraspanin 11	-3.14	7.69E-05
STMN2	stathmin-like 2	-3.12	0.0017
SCG2	secretogranin II	-3.12	1.50E-05
KIAA1199	KIAA1199	-3.10	2.83E-04
ST14	suppression of tumorigenicity 14 (colon carcinoma)	-3.09	0.0182
TIMD4	T-cell immunoglobulin and mucin domain containing 4	-3.08	0.0311
NDUFA4L2	NADH dehydrogenase (ubiquinone) 1 alpha subcomplex, 4-like 2	-3.07	7.77E-05
ADAM12	ADAM metallopeptidase domain 12	-3.03	9.05E-04
CLEC5A	C-type lectin domain family 5, member A	-3.02	0.0371
FCGR3B	Fc fragment of IgG, low affinity IIIb, receptor (CD16b)	-2.97	0.0480
APOC1	apolipoprotein C-I	-2.96	0.0381
IFI30	interferon, gamma-inducible protein 30	-2.93	3.99E-04
S100A9	S100 calcium binding protein A9	-2.92	0.0180
ENPP1	ectonucleotide pyrophosphatase/phosphodiesterase 1	-2.86	7.33E-05
HIST2H2BF	histone cluster 2, H2bf	-2.86	0.0500
SLC16A3	solute carrier family 16, member 3 (monocarboxylic acid transporter 4)	-2.83	0.0048
FCGR3A	Fc fragment of IgG, low affinity IIIa, receptor (CD16a)	-2.79	3.38E-04

Table III-5 continued

DEGs in BAVr versus BAVc			
Gene symbol	**Gene annotation**	**Fold change**	**Adjusted p-value**
C4A	complement component 4A (Rodgers blood group)	-2.76	0.0075
CD300C	CD300c molecule	-2.76	0.0446
SERPINE1	serpin peptidase inhibitor, clade E (nexin, plasminogen activator inhibitor type 1), member 1	-2.71	2.61E-04
CADM1	cell adhesion molecule 1	-2.70	0.0065
C4B	complement component 4B (Chido blood group)	-2.70	0.0101
CCL18	chemokine (C-C motif) ligand 18 (pulmonary and activation-regulated)	-2.68	6.98E-05
KCNN4	potassium intermediate/small conductance calcium-activated channel, subfamily N, member 4	-2.68	0.0074
HAPLN3	hyaluronan and proteoglycan link protein 3	-2.65	8.48E-04
PDPN	podoplanin	-2.61	0.0016
THY1	Thy-1 cell surface antigen	-2.61	0.0048
FNDC1	fibronectin type III domain containing 1	-2.60	0.0228
CTHRC1	collagen triple helix repeat containing 1	-2.55	0.0168
IGFBP2	insulin-like growth factor binding protein 2, 36kDa	-2.50	0.0025
RPSAP58	ribosomal protein SA pseudogene 58	-2.43	0.0291
RGS2	regulator of G-protein signalling 2, 24kDa	-2.40	0.0254
FCGBP	Fc fragment of IgG binding protein	-2.37	0.0084
SYT12	synaptotagmin XII	-2.35	0.0110
ASPN	asporin	-2.33	0.0195
POU2F2	POU class 2 homeobox 2	-2.32	0.0300
C1orf162	chromosome 1 open reading frame 162	-2.31	0.0300
SPOCK1	sparc/osteonectin, cwcv and kazal-like domains proteoglycan (testican) 1	-2.30	0.0152
FZD8	frizzled family receptor 8	-2.30	0.0235
PLAUR	plasminogen activator, urokinase receptor	-2.26	0.0169
LILRB2	leukocyte immunoglobulin-like receptor, subfamily B (with TM and ITIM domains), member 2	-2.26	0.0450
IFITM10	interferon induced transmembrane protein 10	-2.26	0.0019
JUNB	jun B proto-oncogene	-2.24	0.0173
FAP	fibroblast activation protein, alpha	-2.21	0.0111
THBS2	thrombospondin 2	-2.19	0.0290
CD93	CD93 molecule	-2.17	0.0497
JUN	jun proto-oncogene	-2.10	0.0407
TP53I11	tumor protein p53 inducible protein 11	-2.09	0.0357
C5AR1	complement component 5a receptor 1	-2.08	0.0218
OGN	osteoglycin	-2.07	0.0500
XBP1	X-box binding protein 1	-2.06	0.0233

Table III- 6. Selected genes-of-interest comparison between the subgroups.

	BAVr vs TAV fold change	adjusted p-value	BAVr vs BAVc fold change	adjusted p-value	BAVc vs TAV fold change	adjusted p-value
***ACAN*#**	-4.56	5.37E-09	-7.69	0	1.86	0.0059
ADAMTS9	-2.90	0.0490	-	ns	-	ns
BGLAP	-6.32	5.22E-05	-5.74	2.93E-04	-	ns
BMP3	-20.01	0.0043	-	ns	-	ns
CHAD	2.52	0.0015	-	ns	-	ns
***CHI3L1*#**	-6.76	1.20E-10	-7.04	1.24E-11	-	ns
CHIT1	-7.79	9.26E-08	-	ns	-2.93	1.40E-06
CLU	3.11	2.56E-04	-	ns	-	ns
COL11A1	-10.92	0	-7.49	2.74E-08	-	ns
COL2A1	-9.10	1.34E-04	-7.91	0.0012	-	ns
***COL6A6*#**	3.47	1.24E-05	5.16	7.21E-11	-	ns
DLL4	-8.53	8.56E-05	-9.18	3.93E-04	-	ns
EMILIN3	2.19	0.0170	2.61	0.0056	-	ns
GATA4	2.33	0.0079	-	ns	-	ns
GFAP	3.57	5.38E-07	4.41	1.41E-09	-	ns
GREM1	-5.43	0.0074	-	ns	-	ns
GZMB	-7.66	0.0068	-8.58	0.0089	-	ns
HAND2	2.08	0.0110	-	ns	-	ns
HMOX1	-2.15	0.0105	-	ns	-	ns
***IBSP*#**	-39.43	0	-44.35	0	-	ns
ITGAL	-2.42	0.0195	-	ns	-	ns
ITGAX	-3.63	3.16E-07	-	ns	-1.71	0.0158
***LAMC3*#**	3.38	6.39E-06	3.60	5.93E-06	-	ns
LBH	-2.25	0.0148	-	ns	-	ns
MMP1	-11.69	0.0072	-16.74	0.0022	-	ns
***MMP13*#**	-186.53	0	-299.48	0	-	ns
***MMP7*#**	-29.87	5.54E-06	-	ns	-3.19	0.0224
***MMP9*#**	-32.29	0	-14.51	0	-2.30	4.66E-08
MYH10	3.41	0.0050	3.03	0.0016	-	ns
PLAUR	-2.09	0.0384	-2.26	0.0169	-	ns
PTGDS	2.41	0.0112	4.08	2.19E-07	-1.75	0.0073
SOX10	3.63	0.0110	3.60	0.0182	-	ns
SP7	-36.34	2.78E-07	-28.23	1.99E-05	-	ns
***SPP1*#**	-20.35	0	-14.04	0	-	ns
TNC	-2.87	8.98E-05	-3.63	1.23E-04	-	ns
TNXB	2.61	0.0052	2.17	0.0203	-	ns

#genes used in RT-qPCR validation analysis; ns = not statistically significant.

Table III- 7A. GO-terms enrichment clusters of DEG in BAVr (BAV1-BAV3) vs TAV.

	GO classification	Specific GO term	Number of genes	Benjamini-Hochberg*	Enrichment score
Upregulated genes	**Cellular constituent**	Extracellular region	18	1.5E-2	6.15
		Extracellular matrix	7	4.3E-2	2.72
		Plasma membrane	21	4.8E-2	1.5
Downregulated genes	**Biological process**	Inflammatory response	24	1.5E-17	19.86
		Homeostatic process, cell-cell signalling	17	2.7E-3	6.78
		Extracellular structure organisation	9	7.2E-4	5.78
		Ossification	7	3.9E-3	4.33
		Leucocyte activation	9	4.3E-3	3.71
		Cell adhesion, biological adhesion	16	1.3E-3	3.2
		Biomineral formation	6	6.3E-4	3.09
		Wound healing	10	3.1E-4	3.07
		Collagen catabolic process	4	6.1E-3	2.81
		Regulation of response to external stimulus	8	2.6E-3	2.79
		Negative regulation of transport	6	2.5E-2	2.42
		Response to steroid hormone stimulus	7	1.2E-2	2.06
		Regulation of cytokine production	7	2.5E-2	1.45
	Cellular constituent	Extracellular region	71	5.1E-24	35.09
		Extracellular matrix	17	3.8E-5	6.9
		Plasma membrane	53	3.6E-4	6.32
		Integral to plasma membrane	20	2.9E-4	5.45
		Extracellular matrix part	8	1.9E-3	2.11
		Platelet alpha granule	5	2.4E-3	1.87
	Molecular function	Chemokine receptor binding	11	3.1E-10	6.78
		Extracellular matrix structural constituent	5	1.4E-2	2.43
		Calcium ion binding	18	6.7E-3	1.61

*Benjamini-Hochberg globally corrected enrichment p-value <0.05 was considered statistically significant.

Table III-7B . GO-terms enrichment clusters of DEGs in BAVr (BAV1-BAV3) vs BAVc (BAV4, BAV5)

	GO classification	Specific GO term	Number of genes	Benjamini-Hochberg*	Enrichment score
Upregulated genes	**Biological process**	Circulatory system process	8	2.2E-3	3.52
		Muscle contraction	6	7.3E-3	2.32
		Regulation of blood pressure	6	7.2E-3	1.96
	Cellular constituent	Extracellular region	35	3.1E-7	12.58
		Extracellular matrix	12	1.3E-3	3.91
		Plasma membrane	34	1.8E-2	3.04
	Molecular function	Cytokine receptor activity	5	2.7E-2	2.76
		Identical protein binding	9	4.0E-2	1.91
Downregulated genes	**Biological process**	Inflammatory response	18	1.6E-10	13.48
		Biological adhesion	23	1.3E-8	7.89
		Cellular calcium ion homeostasis	6	4.9E-2	6.96
		Extracellular structure organisation	7	1.9E-2	5.83
		Ossification	7	6.1E-3	3.57
		Cellular homeostasis	11	3.0E-2	2.91
		Positive regulation of response to stimulus	8	2.0E-2	2.71
		Bone development	7	8.2E-3	2.69
		Positive regulation of immune response	6	4.1E-2	2.38
		Response to cAMP	4	3.0E-2	2.27
		Cell-cell adhesion	8	3.5E-2	2.03
		Cell motion	10	3.8E-2	1.39
	Cellular constituent	Extracellular region	64	1.9E-20	31.1
		Proteinaceous extracellular matrix	17	3.5E-6	11.22
		Plasma membrane	55	6.6E-6	6.99
		Integral to plasma membrane	21	2.3E-5	5.83
	Molecular function	Cytokine activity	11	2.4E-5	6.96
		Protein complex binding	7	4.4E-3	5.66
		Glycosaminoglycan binding	7	2.3E-3	4.68
		Extracellular matrix structural constituent	5	4.9E-3	2.03
		Metalloendopeptidase acitivity	6	2.0E-2	1.97

*Benjamini-Hochberg globally corrected enrichment p-value <0.05 was considered statistically significant.

Table III-7C. GO-terms enrichment clusters of DEGs in BAVc (BAV4, BAV5) vs TAV.

	GO classification	Specific GO term	Number of genes	Benjamini-Hochberg*	Enrichment score
Upregulated genes	**Biological process**	Antigen processing and presentation	4	7.8E-2	4.44
		Rhythmic process	6	5.7E-3	2.87
	Cellular constituent	Extracellular region	19	7.0E-4	5.81
		MHC class II protein complex	3	4.3E-3	4.44
		Plasma membrane	20	4.6E-2	2.13
	Molecular function	MHC class II receptor activity	3	1.2E-3	4.44
		Transcription factor activity	10	1.9E-2	2.87
Downregulated genes	**Biological process**	Response to wounding	10	2.3E-2	3.75
		Biological adhesion, cell adhesion	12	2.3E-2	3.42
		Regulation of cGMP biosynthetic process	3	4.7E-2	2.16
		Cellular homeostasis	10	3.3E-2	2.05
		Regulation of inflammatory response	5	2.5E-2	1.97
		Circulatory system process	7	1.6E-2	1.83
	Cellular constituent	Extracellular region	47	3.8E-12	25.08
		Intrinsic to plasma membrane	18	2.0E-4	5.04
		Plasma membrane part	32	8.8E-5	4.06
		Proteinaceous extracellular matrix	10	2.0E-2	3.71
	Molecular function	Endopeptidase activity	12	3.6E-2	3.27
		Carbohydrate binding	9	2.6E-2	2.14

*Benjamini-Hochberg globally corrected enrichment p-value <0.05 was considered statistically significant.

Table III- 8. Validation cohort characteristics.

	TAV	BAVr	BAVc
Patients number, n	6	9	12
RNA samples[#], n	8	10	13
Male gender (%)	6 (100)	8 (89)	11 (92)
Mean age (SD)	69 (9)	54 (16)	65 (6)
Background			
Caucasian	5	7	12
Mediterranean	0	1	0
Middle Eastern	1	0	0
Asian	0	1	0
Leaflet calcification (patients, n)	+++ (6)	– (6) + (3)	+++ (12)
BAV morphology (patients, n)	n/a	R-L fusion (6) R-N fusion (1) True BAV (2)	R-L fusion (9) R-N fusion (1) True BAV (2)
Predominant valve dysfunction (patients, n)	Severe AS (6)	Moderate or severe AR (6) Mild AR* (2) Mild AS* (1)	Severe AS (12)

*surgically unsuitable for either repair or preservation; [#]when residual sample was available, RNA was extracted from a different portion of the leaflet and used for validation analysis; AS, aortic stenosis; AR, aortic regurgitation; TAV, tricuspid aortic valve; BAVr, bicuspid aortic valve with leaflet redundancy and either no calcification or minimal calcification; BAVc, BAV with severe valve calcification; leaflet calcification: +++ for heavily calcified leaflets (>2/3 leaflet area), + for mild calcification (<1/3 leaflet area), and – for no calcification ; BAV morphology: R-L fusion, functionally bicuspid due to fusion of right and left coronary leaflets; R-N fusion, functionally bicuspid due to fusion of right and noncoronary leaflets; true BAV, anatomically bicuspid with 2 equal sized leaflets and the absence of raphe; n/a, not applicable.

Table III- 9. Gene lists comprising the different Venn diagram compartments (A-G) as depicted in Figure 5.6.

Group	No. genes	Genes list
A	71	*ACE,ADAMTS9,ADCYAP1,ALOX5AP,AMPD1,AOAH,APOC2,ATP6V0D2,BMP3,CCL4, CD3E,CD52,CHAD,CHST1,CHST15,CHST9,CLU,CPEB1,CR1,EBF2,EMR1,EPB41L4B, EYA1,FAIM3,FCRL3,FMO3,GATA4,GBP3,GREM1,HAND2,HLA-DOB,HMOX1,IL1RN, ITGAL,KIAA1217,KIRREL3,KLK4,LAPTM5,LBH,LTB,LYZ,MATK,MFAP5,MS4A1, MYO1G,NFIA,NTRK2,NUP210,PLA2G2D,PLAU,PNOC,PPBP,RBP1,S100B,SCUBE1, SDS,SEMA6B,SLC14A1,SLC44A3,SLC6A1,SLC7A2,SMOC1,SMOC2,SPIB,SRGN, TCEAL2,TM4SF19,TMEM119,TMEM56,TREM2,TRHDE*
B	91	*ACTG2,ADAMTS16,ADCYAP1R1,ALDH3A1,ANGPTL7,AOC2,ASPN,C2orf88,C4A,C4B, C5AR1,CBLN1,CCL8,CD300C,CD93,CECR2,CHGA,CLDN10,CNTN1,COL9A1,CPXM1, CTHRC1,CYP26A1,DOK6,ENTPD2,ERBB3,FAM123A,FAP,FCGBP,FCGR3A,FCGR3B, FCN1,FZD8,GADL1,GNLY,GPR84,GPR88,HAPLN3,HIST2H2BF,IFITM10,IGFBP2, IGFN1,ITLN1,JUNB,KIF26A,KISS1,LDLR,LGI4,LILRB2,MATN2,MEIS2,MEPE,MET, MYH14,NDNF,NDRG2,OTC,OTOGL,PDE4B,PDGFRL,PDPN,PIR,PKHD1L1,PLEKHA6, PLIN1,POU2F2,PPP1R39,PRLR,PRODH,PTPN20A,RGS2,RNASE2,S100A8,SAMD5, SIGLEC14,SIGLEC5,SIRPB1,SLC16A3,SMTNL2,SOCS3,SPOCK1,SPTBN1,SYT12, TBX20,THBS2,THY1,TNFRSF18,TNFSF11,VSTM2A,XBP1,ZEB1*
C	113	*ABCC8,ADAM33,ADAMTS1,ADIPOQ,ANK3,APOE,AQP2,ARHGEF15,ARNTL, C17orf97,C1QTNF3,C1orf51,C4orf48,CCDC163P,CCDC85B,CDH5,CDH6,CHRFAM7A, COL13A1,COMP,CRELD1,CRHBP,CST1,CTSG,CXCR7,CYP4B1,DACH1,DBP, DDX-39B,DEFA1,DKK1,DYNC1LI2,EGFLAM,EMCN,ESAM,ESPNL,FCN3,FMN2, GAP43, GNA14,GOLGA8B,GPC5,GPR116,GPX7,GSN,GSTM1,HDC,HLA-B, HLA-DQB1, HLADQB2,HMCN1,HSPA12B,HTRA3,HYAL2,INMT,ITGA6,JAKMIP2,JAM2, KIAA1683, KIT,LPL,LRRC37A2,LTBP2,LTF,MASP1,MATN4,MIR3654,MLC1,MS4A2, MTRNR2L9, NOS1,NPIPL2,NPR1,NR1D1,NR1D2,NTM,OCLN,PCDHB5,PDK4,PDPR, PER1,PLP1, POLR2J2,POLR2J3,POU6F2,PRRT4,PTHL,RAMP3,RASA4,RASA4B, RGS5,RNASE3, RPS12,RRP7A,SCO2,SELE,SEMA3F,SIGLEC6,SLC40A1,SLC6A4, SLCO2A1,SSTR5, TEF,TEK,TIE1,TMTC2,TPSD1,TSPAN10,UPK3BL,VWF,WNT7A, ZFAT,ZNF266*
D	114	*ABCA8,ADRA2A,AKR1C2,APOC1,AQP9,BGLAP,C10orf81,C1orf162,CA12,CADM1, CADM2,CBLN4,CCL14,CCL18,CCL21,CCL3,CCL7,CHI3L1,CLDN11,CLEC5A, COL10A1,COL11A1,COL2A1,COL4A3,COL6A6,CPAMD8,CXCL13,CXCL5,CXorf36, DHCR24,DLL4,DLX5,EMILIN3,ENPP1,ERAP2,F3,FCGR1A,FCGR1B,FLT4,FPR1, GALNT3,GFAP,GJB2,GPIHBP1,GPR68,GZMB,HBB,HMGCLL1,IBSP,IFI30,IGSF10, IL1RL1,IL21R,IRF4,ISM1,KCNJ15,KCNK2,KCNN4,KIAA1199,KIF1A,LAMC3,LCNL1, LRRC15,MAPT,MAT1A,MED12L,MMP1,MMP13,MYH10,NDUFA4L2,NELL2,NPPC, NSG1,NWD1,OGN,PDZRN4,PIM2,PKP2,PLAUR,PLCH1,PLVAP,POU2AF1,PRND, PTP4A3,RGS16,RIMS4,S100A9,SCN7A,SDC1,SERPINA1,SERPINE1,SFRP1, SLAMF6,SLAMF7,SLC11A1,SLC2A5,SLC6A20,SLPI,SOX10,SP7,SPOCK3,SPP1, ST14,STMN2,TDO2,TM4SF18,TMEM132C,TMEM200A,TNC,TNXB,TP53I11,TREM1, TSPAN11,VCAM1*
E	20	*A2M,ACP5,APLN,CCL19,CHI3L2,CHIT1,CMA1,CXCL9,GLRX,GPHA2,GZMK,HLF, ITGAX,MMP7,MMRN1,MTRNR2L8,MUC20,RASSF6,SGCA,VMO1*
F	41	*ABCC9,ABP1,ACTC1,ADAM12,AIF1L,ALDH1A1,BMPER,C1QTNF8,C7,CCKAR,CHL1, CHRDL1,COCH,CPA3,DDX11,DES,DPYSL4,FAM107A,FNDC1,FOS,FOSB,GFRA1, GSTT1,HLA-DQA1,HS3ST1,JUN,LIFR,NKAIN2,NOS3,PAX8,PI16,PLIN4,PTPRB, RPSAP58,SCG2,ST6GALNAC1,SYNPO2,THNSL2,TPSAB1,TRDN,WNT9B*
G	19	*ACAN,ATP1A2,CD79A,CNTFR,CTSE,DERL3,FCRL5,HBA1,HBA2,HLA-DRB5,IGJ, IGLL5,MMP9,MYOC,PPP1R1B,PTGDS,RP11-1280I22.1,SCARA5,TIMD4*

REFERENCES

REFERENCES

ACHARYA, A., HANS, C. P., KOENIG, S. N., NICHOLS, H. A., GALINDO, C. L., GARNER, H. R., MERRILL, W. H., HINTON, R. B. & GARG, V. 2011. Inhibitory role of Notch1 in calcific aortic valve disease. *PloS one,* 6**,** e27743.

AICHER, D., URBICH, C., ZEIHER, A., DIMMELER, S. & SCHAFERS, H. J. 2007. Endothelial nitric oxide synthase in bicuspid aortic valve disease. *Ann Thorac Surg,* 83**,** 1290-4.

AIRAKSINEN, M. S. & SAARMA, M. 2002. The GDNF family: signalling, biological functions and therapeutic value. *Nat Rev Neurosci,* 3**,** 383-94.

ALBERS, C. A., NEWBURY-ECOB, R., OUWEHAND, W. H. & GHEVAERT, C. 2013. New insights into the genetic basis of TAR (thrombocytopenia-absent radii) syndrome. *Curr Opin Genet Dev,* 23**,** 316-23.

ALI, S. A. & ALMAN, B. 2012. RNA extraction from human articular cartilage by chondrocyte isolation. *Anal Biochem,* 429**,** 39-41.

ALTMANN, A., WEBER, P., BADER, D., PREUSS, M., BINDER, E. B. & MULLER-MYHSOK, B. 2012. A beginners guide to SNP calling from high-throughput DNA-sequencing data. *Hum Genet,* 131**,** 1541-54.

AMIEL, J., LAUDIER, B., ATTIE-BITACH, T., TRANG, H., DE PONTUAL, L., GENER, B., TROCHET, D., ETCHEVERS, H., RAY, P., SIMONNEAU, M., VEKEMANS, M., MUNNICH, A., GAULTIER, C. & LYONNET, S. 2003. Polyalanine expansion and frameshift mutations of the paired-like homeobox gene PHOX2B in congenital central hypoventilation syndrome. *Nat Genet,* 33**,** 459-61.

ANGRIST, M., BOLK, S., HALUSHKA, M., LAPCHAK, P. A. & CHAKRAVARTI, A. 1996. Germline mutations in glial cell line-derived neurotrophic factor (GDNF) and RET in a Hirschsprung disease patient. *Nat Genet,* 14**,** 341-4.

ANTONINI-CANTERIN, F., CARERJ, S., DI BELLO, V., DI SALVO, G., LA CARRUBBA, S., VRIZ, O., PAVAN, D., BALBARINI, A., NICOLOSI, G. L. & RESEARCH GROUP OF THE ITALIAN SOCIETY OF

CARDIOVASCULAR, E. 2009. Arterial stiffness and ventricular stiffness: a couple of diseases or a coupling disease? A review from the cardiologist's point of view. *Eur J Echocardiogr,* 10**,** 36-43.

ARRINGTON, C. B., BLEYL, S. B., MATSUNAMI, N., BONNELL, G. D., OTTERUD, B. E., NIELSEN, D. C., STEVENS, J., LEVY, S., LEPPERT, M. F. & BOWLES, N. E. 2012. Exome analysis of a family with pleiotropic congenital heart disease. *Circ Cardiovasc Genet,* 5**,** 175-82.

ARRINGTON, C. B., SOWER, C. T., CHUCKWUK, N., STEVENS, J., LEPPERT, M. F., YETMAN, A. T. & BOWLES, N. E. 2008. Absence of TGFBR1 and TGFBR2 mutations in patients with bicuspid aortic valve and aortic dilation. *Am J Cardiol,* 102**,** 629-31.

BAGNALL, R. D., DAS, K. J., DUFLOU, J. & SEMSARIAN, C. 2014. Exome analysis-based molecular autopsy in cases of sudden unexplained death in the young. *Heart Rhythm,* 11**,** 655-62.

BAGNALL, R. D., TSOUTSMAN, T., SHEPHARD, R. E., RITCHIE, W. & SEMSARIAN, C. 2012. Global microRNA profiling of the mouse ventricles during development of severe hypertrophic cardiomyopathy and heart failure. *PLoS One,* 7**,** e44744.

BAHUAU, M., PELET, A., VIDAUD, D., LAMIREAU, T., LEBAIL, B., MUNNICH, A., VIDAUD, M., LYONNET, S. & LACOMBE, D. 2001. GDNF as a candidate modifier in a type 1 neurofibromatosis (NF1) enteric phenotype. *J Med Genet,* 38**,** 638-43.

BAMSHAD, M. J., NG, S. B., BIGHAM, A. W., TABOR, H. K., EMOND, M. J., NICKERSON, D. A. & SHENDURE, J. 2011. Exome sequencing as a tool for Mendelian disease gene discovery. *Nat Rev Genet,* 12**,** 745-55.

BARKER, A. J., MARKL, M., BURK, J., LORENZ, R., BOCK, J., BAUER, S., SCHULZ-MENGER, J. & VON KNOBELSDORFF-BRENKENHOFF, F. 2012. Bicuspid aortic valve is associated with altered wall shear stress in the ascending aorta. *Circ Cardiovasc Imaging,* 5**,** 457-66.

BENSON, D. W. 2008. Thar's tendons in them thar valves! *Circ Res,* 103**,** 914-5.

BENSON, D. W. 2010. Genetic origins of pediatric heart disease. *Pediatr Cardiol,* 31**,** 422-9.

BIBEN, C., WEBER, R., KESTEVEN, S., STANLEY, E., MCDONALD, L., ELLIOTT, D. A., BARNETT, L., KOENTGEN, F., ROBB, L., FENELEY, M. & HARVEY, R. P. 2000. Cardiac septal and valvular dysmorphogenesis in mice heterozygous for mutations in the homeobox gene Nkx2-5. *Circ Res,* 87**,** 888-95.

BLUNDER, S., MESSNER, B., ASCHACHER, T., ZELLER, I., TURKCAN, A., WIEDEMANN, D., ANDREAS, M., BLUSCHKE, G., LAUFER, G., SCHACHNER, T. & BERNHARD, D. 2012. Characteristics of TAV- and BAV-associated thoracic aortic aneurysms--smooth muscle cell biology, expression profiling, and histological analyses. *Atherosclerosis,* 220**,** 355-61.

BONACHEA, E. M., CHANG, S. W., ZENDER, G., LAHAYE, S., FITZGERALD-BUTT, S., MCBRIDE, K. L. & GARG, V. 2014 [Epub ahead of print]. Rare GATA5 sequence variants identified in individuals with bicuspid aortic valve. *Pediatr Res*.

BONDERMAN, D., GHAREHBAGHI-SCHNELL, E., WOLLENEK, G., MAURER, G., BAUMGARTNER, H. & LANG, I. M. 1999. Mechanisms underlying aortic dilatation in congenital aortic valve malformation. *Circulation,* 99**,** 2138-43.

BONOW, R. O., CARABELLO, B. A., CHATTERJEE, K., DE LEON, A. C., JR., FAXON, D. P., FREED, M. D., GAASCH, W. H., LYTLE, B. W., NISHIMURA, R. A., O'GARA, P. T., O'ROURKE, R. A., OTTO, C. M., SHAH, P. M., SHANEWISE, J. S. & AMERICAN COLLEGE OF CARDIOLOGY/AMERICAN HEART ASSOCIATION TASK FORCE ON PRACTICE, G. 2008. 2008 focused update incorporated into the ACC/AHA 2006 guidelines for the management of patients with valvular heart disease: a report of the American College of Cardiology/American Heart Association Task Force on Practice Guidelines (Writing Committee to revise the 1998 guidelines for the management of patients with valvular heart disease). Endorsed by the Society of Cardiovascular Anesthesiologists, Society for Cardiovascular Angiography and Interventions, and Society of Thoracic Surgeons. *J Am Coll Cardiol,* 52**,** e1-142.

BORZI, R. M., OLIVOTTO, E., PAGANI, S., VITELLOZZI, R., NERI, S., BATTISTELLI, M., FALCIERI, E., FACCHINI, A., FLAMIGNI, F., PENZO, M., PLATANO, D., SANTI, S., FACCHINI, A. & MARCU, K. B. 2010. Matrix metalloproteinase 13 loss associated with impaired extracellular matrix remodeling disrupts chondrocyte differentiation by concerted effects on multiple regulatory factors. *Arthritis Rheum,* 62**,** 2370-81.

BOSSE, Y., MIQDAD, A., FOURNIER, D., PEPIN, A., PIBAROT, P. & MATHIEU, P. 2009. Refining molecular pathways leading to calcific aortic valve stenosis by studying gene expression profile of normal and calcified stenotic human aortic valves. *Circ Cardiovasc Genet,* 2**,** 489-98.

BRIEN, P., PUGAZHENDHI, D., WOODHOUSE, S., OXLEY, D. & PELL, J. M. 2013. P38alpha MAPK Regulates Adult Muscle Stem Cell Fate By Restricting Progenitor Proliferation During Postnatal Growth And Repair. *Stem Cells*.

BUTCHER, J. T. & MARKWALD, R. R. 2007. Valvulogenesis: the moving target. *Philos Trans R Soc Lond B Biol Sci,* 362**,** 1489-503.

CAMPER, L., HOLMVALL, K., WANGNERUD, C., ASZODI, A. & LUNDGREN-AKERLUND, E. 2001. Distribution of the collagen-binding integrin alpha10beta1 during mouse development. *Cell Tissue Res,* 306**,** 107-16.

CAVALCANTE, J. L., LIMA, J. A., REDHEUIL, A. & AL-MALLAH, M. H. 2011. Aortic stiffness: current understanding and future directions. *J Am Coll Cardiol,* 57**,** 1511-22.

CECCONI, M., MANFRIN, M., MORACA, A., ZANOLI, R., COLONNA, P. L., BETTUZZI, M. G., MORETTI, S., GABRIELLI, D. & PERNA, G. P. 2005. Aortic dimensions in patients with bicuspid aortic valve without significant valve dysfunction. *Am J Cardiol,* 95**,** 292-4.

CHAKRABORTY, S., COMBS, M. D. & YUTZEY, K. E. 2010. Transcriptional regulation of heart valve progenitor cells. *Pediatr Cardiol,* 31**,** 414-21.

CHARRON, F. & NEMER, M. 1999. GATA transcription factors and cardiac development. *Semin Cell Dev Biol,* 10**,** 85-91.

CHEEK, J. D., WIRRIG, E. E., ALFIERI, C. M., JAMES, J. F. & YUTZEY, K. E. 2012. Differential activation of valvulogenic, chondrogenic, and

osteogenic pathways in mouse models of myxomatous and calcific aortic valve disease. *J Mol Cell Cardiol,* 52**,** 689-700.

CHOI, M., SCHOLL, U. I., JI, W., LIU, T., TIKHONOVA, I. R., ZUMBO, P., NAYIR, A., BAKKALOGLU, A., OZEN, S., SANJAD, S., NELSON-WILLIAMS, C., FARHI, A., MANE, S. & LIFTON, R. P. 2009. Genetic diagnosis by whole exome capture and massively parallel DNA sequencing. *Proc Natl Acad Sci U S A,* 106**,** 19096-101.

CHURKO, J. M., MANTALAS, G. L., SNYDER, M. P. & WU, J. C. 2013. Overview of high throughput sequencing technologies to elucidate molecular pathways in cardiovascular diseases. *Circ Res,* 112**,** 1613-23.

CLEMENTZ, A. G., ROGOWSKI, A., PANDYA, K., MIELE, L. & OSIPO, C. 2011. NOTCH-1 and NOTCH-4 are novel gene targets of PEA3 in breast cancer: novel therapeutic implications. *Breast Cancer Res,* 13**,** R63.

COMBS, M. D. & YUTZEY, K. E. 2009. Heart valve development: regulatory networks in development and disease. *Circ Res,* 105**,** 408-21.

CRIPE, L., ANDELFINGER, G., MARTIN, L. J., SHOONER, K. & BENSON, D. W. 2004. Bicuspid aortic valve is heritable. *J Am Coll Cardiol,* 44**,** 138-43.

DE LA POMPA, J. L. & EPSTEIN, J. A. 2012. Coordinating tissue interactions: Notch signaling in cardiac development and disease. *Dev Cell,* 22**,** 244-54.

DE WIT, A., VIS, K. & JEREMY, R. W. 2013. Aortic stiffness in heritable aortopathies: relationship to aneurysm growth rate. *Heart Lung Circ,* 22**,** 3-11.

DELLA CORTE, A., BANCONE, C., CONTI, C. A., VOTTA, E., REDAELLI, A., DEL VISCOVO, L. & COTRUFO, M. 2012. Restricted cusp motion in right-left type of bicuspid aortic valves: A new risk marker for aortopathy. *J Thorac Cardiovasc Surg,* 144**,** 360-369 e1.

DELLA CORTE, A., DE SANTO, L. S., MONTAGNANI, S., QUARTO, C., ROMANO, G., AMARELLI, C., SCARDONE, M., DE FEO, M., COTRUFO, M. & CAIANIELLO, G. 2006. Spatial patterns of matrix protein expression in dilated ascending aorta with aortic regurgitation:

congenital bicuspid valve versus Marfan's syndrome. *J Heart Valve Dis,* 15**,** 20-7; discussion 27.

DELLA CORTE, A., QUARTO, C., BANCONE, C., CASTALDO, C., DI MEGLIO, F., NURZYNSKA, D., DE SANTO, L. S., DE FEO, M., SCARDONE, M., MONTAGNANI, S. & COTRUFO, M. 2008. Spatiotemporal patterns of smooth muscle cell changes in ascending aortic dilatation with bicuspid and tricuspid aortic valve stenosis: focus on cell-matrix signaling. *J Thorac Cardiovasc Surg,* 135**,** 8-18, 18 e1-2.

DEN REIJER, P. M., SALLEE, D., 3RD, VAN DER VELDEN, P., ZAAIJER, E. R., PARKS, W. J., RAMAMURTHY, S., ROBBIE, T. Q., DONATI, G., LAMPHIER, C., BEEKMAN, R. P. & BRUMMER, M. E. 2010. Hemodynamic predictors of aortic dilatation in bicuspid aortic valve by velocity-encoded cardiovascular magnetic resonance. *J Cardiovasc Magn Reson,* 12**,** 4.

DESHPANDE, J. & KINARE, S. G. 1991. The bicuspid aortic valve--an autopsy study. *Indian J Pathol Microbiol,* 34**,** 112-8.

DETAINT, D., MICHELENA, H. I., NKOMO, V. T., VAHANIAN, A., JONDEAU, G. & SARANO, M. E. 2014. Aortic dilatation patterns and rates in adults with bicuspid aortic valves: a comparative study with Marfan syndrome and degenerative aortopathy. *Heart,* 100**,** 126-34.

DEVAN, A. E., ANTON, M. M., COOK, J. N., NEIDRE, D. B., CORTEZ-COOPER, M. Y. & TANAKA, H. 2005. Acute effects of resistance exercise on arterial compliance. *J Appl Physiol (1985),* 98**,** 2287-91.

DOLAN, J. M., MENG, H., SINGH, S., PALUCH, R. & KOLEGA, J. 2011. High fluid shear stress and spatial shear stress gradients affect endothelial proliferation, survival, and alignment. *Ann Biomed Eng,* 39**,** 1620-31.

DUCHARME, V., GUAUQUE-OLARTE, S., GAUDREAULT, N., PIBAROT, P., MATHIEU, P. & BOSSE, Y. 2013. NOTCH1 genetic variants in patients with tricuspid calcific aortic valve stenosis. *J Heart Valve Dis,* 22**,** 142-9.

EDEP, M. E., SHIRANI, J., WOLF, P. & BROWN, D. L. 2000. Matrix metalloproteinase expression in nonrheumatic aortic stenosis. *Cardiovasc Pathol,* 9**,** 281-6.

ENGIN, F., YAO, Z., YANG, T., ZHOU, G., BERTIN, T., JIANG, M. M., CHEN, Y., WANG, L., ZHENG, H., SUTTON, R. E., BOYCE, B. F. & LEE, B. 2008. Dimorphic effects of Notch signaling in bone homeostasis. *Nat Med,* 14**,** 299-305.

EVANGELISTA, A. 2014. Imaging aortic aneurysmal disease. *Heart,* 100**,** 909-915.

FAZEL, S. S., MALLIDI, H. R., LEE, R. S., SHEEHAN, M. P., LIANG, D., FLEISCHMAN, D., HERFKENS, R., MITCHELL, R. S. & MILLER, D. C. 2008. The aortopathy of bicuspid aortic valve disease has distinctive patterns and usually involves the transverse aortic arch. *J Thorac Cardiovasc Surg,* 135**,** 901-7, 907 e1-2.

FEDAK, P. W. 2008. Bicuspid aortic valve syndrome: heterogeneous but predictable? *Eur Heart J,* 29**,** 432-3.

FEDAK, P. W., DE SA, M. P., VERMA, S., NILI, N., KAZEMIAN, P., BUTANY, J., STRAUSS, B. H., WEISEL, R. D. & DAVID, T. E. 2003. Vascular matrix remodeling in patients with bicuspid aortic valve malformations: implications for aortic dilatation. *J Thorac Cardiovasc Surg,* 126**,** 797-806.

FEDAK, P. W., VERMA, S., DAVID, T. E., LEASK, R. L., WEISEL, R. D. & BUTANY, J. 2002. Clinical and pathophysiological implications of a bicuspid aortic valve. *Circulation,* 106**,** 900-4.

FERNANDES, S., KHAIRY, P., GRAHAM, D. A., COLAN, S. D., GALVIN, T. C., SANDERS, S. P., SINGH, M. N., BHATT, A. & LACRO, R. V. 2012. Bicuspid aortic valve and associated aortic dilation in the young. *Heart,* 98**,** 1014-9.

FERNANDEZ, B., DURAN, A. C., FERNANDEZ-GALLEGO, T., FERNANDEZ, M. C., SUCH, M., ARQUE, J. M. & SANS-COMA, V. 2009. Bicuspid aortic valves with different spatial orientations of the leaflets are distinct etiological entities. *J Am Coll Cardiol,* 54**,** 2312-8.

FOFFA, I., MURZI, M., MARIANI, M., MAZZONE, A. M., GLAUBER, M., AIT ALI, L. & ANDREASSI, M. G. 2012. Angiotensin-converting enzyme insertion/deletion polymorphism is a risk factor for thoracic aortic

aneurysm in patients with bicuspid or tricuspid aortic valves. *J Thorac Cardiovasc Surg*.

FOLKERSEN, L., WAGSATER, D., PALOSCHI, V., JACKSON, V., PETRINI, J., KURTOVIC, S., MALEKI, S., ERIKSSON, M. J., CAIDAHL, K., HAMSTEN, A., MICHEL, J. B., LISKA, J., GABRIELSEN, A., FRANCO-CERECEDA, A. & ERIKSSON, P. 2011. Unraveling the divergent gene expression profiles in bicuspid and tricuspid aortic valve patients with thoracic aortic dilatation - the ASAP study. *Mol Med*.

FONDARD, O., DETAINT, D., IUNG, B., CHOQUEUX, C., ADLE-BIASSETTE, H., JARRAYA, M., HVASS, U., COUETIL, J. P., HENIN, D., MICHEL, J. B., VAHANIAN, A. & JACOB, M. P. 2005. Extracellular matrix remodelling in human aortic valve disease: the role of matrix metalloproteinases and their tissue inhibitors. *Eur Heart J,* 26**,** 1333-41.

FORSELL, C., BJORCK, H. M., ERIKSSON, P., FRANCO-CERECEDA, A. & GASSER, T. C. 2014. Biomechanical Properties of the Thoracic Aneurysmal Wall: Differences Between Bicuspid Aortic Valve and Tricuspid Aortic Valve Patients. *Ann Thorac Surg*.

GARG, V. 2006. Molecular genetics of aortic valve disease. *Curr Opin Cardiol,* 21**,** 180-4.

GARG, V., KATHIRIYA, I. S., BARNES, R., SCHLUTERMAN, M. K., KING, I. N., BUTLER, C. A., ROTHROCK, C. R., EAPEN, R. S., HIRAYAMA-YAMADA, K., JOO, K., MATSUOKA, R., COHEN, J. C. & SRIVASTAVA, D. 2003. GATA4 mutations cause human congenital heart defects and reveal an interaction with TBX5. *Nature,* 424**,** 443-7.

GARG, V., MUTH, A. N., RANSOM, J. F., SCHLUTERMAN, M. K., BARNES, R., KING, I. N., GROSSFELD, P. D. & SRIVASTAVA, D. 2005. Mutations in NOTCH1 cause aortic valve disease. *Nature,* 437**,** 270-4.

GILISSEN, C., HOISCHEN, A., BRUNNER, H. G. & VELTMAN, J. A. 2011. Unlocking Mendelian disease using exome sequencing. *Genome Biol,* 12**,** 228.

GIRDAUSKAS, E., BORGER, M. A., SECKNUS, M. A., GIRDAUSKAS, G. & KUNTZE, T. 2011a. Is aortopathy in bicuspid aortic valve disease a congenital defect or a result of abnormal hemodynamics? A critical

reappraisal of a one-sided argument. *Eur J Cardiothorac Surg,* 39**,** 809-14.

GIRDAUSKAS, E., DISHA, K., BORGER, M. A. & KUNTZE, T. 2012. Relation of bicuspid aortic valve morphology to the dilatation pattern of the proximal aorta: focus on the transvalvular flow. *Cardiol Res Pract,* 2012**,** 478259.

GIRDAUSKAS, E., SCHULZ, S., BORGER, M. A., MIERZWA, M. & KUNTZE, T. 2011b. Transforming growth factor-beta receptor type II mutation in a patient with bicuspid aortic valve disease and intraoperative aortic dissection. *Ann Thorac Surg,* 91**,** e70-1.

GOH, G. & CHOI, M. 2012. Application of whole exome sequencing to identify disease-causing variants in inherited human diseases. *Genomics Inform,* 10**,** 214-9.

GROTENHUIS, H. B., OTTENKAMP, J., WESTENBERG, J. J., BAX, J. J., KROFT, L. J. & DE ROOS, A. 2007. Reduced aortic elasticity and dilatation are associated with aortic regurgitation and left ventricular hypertrophy in nonstenotic bicuspid aortic valve patients. *J Am Coll Cardiol,* 49**,** 1660-5.

GURVITZ, M., CHANG, R. K., DRANT, S. & ALLADA, V. 2004. Frequency of aortic root dilation in children with a bicuspid aortic valve. *Am J Cardiol,* 94**,** 1337-40.

HALL, J. G. 1987. Thrombocytopenia and absent radius (TAR) syndrome. *J Med Genet,* 24**,** 79-83.

HARVEY, R. P. 1996. NK-2 homeobox genes and heart development. *Dev Biol,* 178**,** 203-16.

HATZARAS, I., TRANQUILLI, M., COADY, M., BARRETT, P. M., BIBLE, J. & ELEFTERIADES, J. A. 2007. Weight lifting and aortic dissection: more evidence for a connection. *Cardiology,* 107**,** 103-6.

HILTUNEN, J. O., LAURIKAINEN, A., AIRAKSINEN, M. S. & SAARMA, M. 2000. GDNF family receptors in the embryonic and postnatal rat heart and reduced cholinergic innervation in mice hearts lacking ret or GFRalpha2. *Dev Dyn,* 219**,** 28-39.

HINTON, R. B., JR., LINCOLN, J., DEUTSCH, G. H., OSINSKA, H., MANNING, P. B., BENSON, D. W. & YUTZEY, K. E. 2006. Extracellular matrix remodeling and organization in developing and diseased aortic valves. *Circ Res,* 98**,** 1431-8.

HINTON, R. B., MARTIN, L. J., RAME-GOWDA, S., TABANGIN, M. E., CRIPE, L. H. & BENSON, D. W. 2009. Hypoplastic left heart syndrome links to chromosomes 10q and 6q and is genetically related to bicuspid aortic valve. *J Am Coll Cardiol,* 53**,** 1065-71.

HINTON, R. B. & YUTZEY, K. E. 2011. Heart valve structure and function in development and disease. *Annu Rev Physiol,* 73**,** 29-46.

HITZ, M. P., LEMIEUX-PERREAULT, L. P., MARSHALL, C., FEROZ-ZADA, Y., DAVIES, R., YANG, S. W., LIONEL, A. C., D'AMOURS, G., LEMYRE, E., CULLUM, R., BIGRAS, J. L., THIBEAULT, M., CHETAILLE, P., MONTPETIT, A., KHAIRY, P., OVERDUIN, B., KLAASSEN, S., HOODLESS, P., AWADALLA, P., HUSSIN, J., IDAGHDOUR, Y., NEMER, M., STEWART, A. F., BOERKOEL, C., SCHERER, S. W., RICHTER, A., DUBE, M. P. & ANDELFINGER, G. 2012. Rare copy number variants contribute to congenital left-sided heart disease. *PLoS Genet,* 8**,** e1002903.

HOLMES, K. W., LEHMANN, C. U., DALAL, D., NASIR, K., DIETZ, H. C., RAVEKES, W. J., THOMPSON, W. R. & SPEVAK, P. J. 2007. Progressive dilation of the ascending aorta in children with isolated bicuspid aortic valve. *Am J Cardiol,* 99**,** 978-83.

HOLTZINGER, A. & EVANS, T. 2007. Gata5 and Gata6 are functionally redundant in zebrafish for specification of cardiomyocytes. *Dev Biol,* 312**,** 613-22.

HOPE, M. D., HOPE, T. A., CROOK, S. E., ORDOVAS, K. G., URBANIA, T. H., ALLEY, M. T. & HIGGINS, C. B. 2011. 4D flow CMR in assessment of valve-related ascending aortic disease. *JACC Cardiovasc Imaging,* 4**,** 781-7.

HOPE, M. D., WRENN, J., SIGOVAN, M., FOSTER, E., TSENG, E. E. & SALONER, D. 2012. Imaging biomarkers of aortic disease: increased growth rates with eccentric systolic flow. *J Am Coll Cardiol,* 60**,** 356-7.

HUNTINGTON, K., HUNTER, A. G. & CHAN, K. L. 1997. A prospective study to assess the frequency of familial clustering of congenital bicuspid aortic valve. *J Am Coll Cardiol,* 30**,** 1809-12.

IKONOMIDIS, J. S., RUDDY, J. M., BENTON, S. M., JR., ARROYO, J., BRINSA, T. A., STROUD, R. E., ZEESHAN, A., BAVARIA, J. E., GORMAN, J. H., 3RD, GORMAN, R. C., SPINALE, F. G. & JONES, J. A. 2012. Aortic dilatation with bicuspid aortic valves: cusp fusion correlates to matrix metalloproteinases and inhibitors. *Ann Thorac Surg,* 93**,** 457-63.

IUNG, B. & VAHANIAN, A. 2011. Epidemiology of valvular heart disease in the adult. *Nat Rev Cardiol,* 8**,** 162-72.

JACKSON, V., PETRINI, J., CAIDAHL, K., ERIKSSON, M. J., LISKA, J., ERIKSSON, P. & FRANCO-CERECEDA, A. 2011. Bicuspid aortic valve leaflet morphology in relation to aortic root morphology: a study of 300 patients undergoing open-heart surgery. *Eur J Cardiothorac Surg,* 40**,** e118-24.

JAIN, R., ENGLEKA, K. A., RENTSCHLER, S. L., MANDERFIELD, L. J., LI, L., YUAN, L. & EPSTEIN, J. A. 2011. Cardiac neural crest orchestrates remodeling and functional maturation of mouse semilunar valves. *J Clin Invest,* 121**,** 422-30.

KEANE, M. G., WIEGERS, S. E., PLAPPERT, T., POCHETTINO, A., BAVARIA, J. E. & SUTTON, M. G. 2000. Bicuspid aortic valves are associated with aortic dilatation out of proportion to coexistent valvular lesions. *Circulation,* 102**,** III35-9.

KERN, C. B., WESSELS, A., MCGARITY, J., DIXON, L. J., ALSTON, E., ARGRAVES, W. S., GEETING, D., NELSON, C. M., MENICK, D. R. & APTE, S. S. 2010. Reduced versican cleavage due to Adamts9 haploinsufficiency is associated with cardiac and aortic anomalies. *Matrix Biol,* 29**,** 304-16.

KIM, D., PERTEA, G., TRAPNELL, C., PIMENTEL, H., KELLEY, R. & SALZBERG, S. L. 2013. TopHat2: accurate alignment of transcriptomes in the presence of insertions, deletions and gene fusions. *Genome Biol,* 14**,** R36.

KIRK, E. P., SUNDE, M., COSTA, M. W., RANKIN, S. A., WOLSTEIN, O., CASTRO, M. L., BUTLER, T. L., HYUN, C., GUO, G., OTWAY, R., MACKAY, J. P., WADDELL, L. B., COLE, A. D., HAYWARD, C., KEOGH, A., MACDONALD, P., GRIFFITHS, L., FATKIN, D., SHOLLER, G. F., ZORN, A. M., FENELEY, M. P., WINLAW, D. S. & HARVEY, R. P. 2007. Mutations in cardiac T-box factor gene TBX20 are associated with diverse cardiac pathologies, including defects of septation and valvulogenesis and cardiomyopathy. *Am J Hum Genet,* 81**,** 280-91.

KO, S. M., SONG, M. G. & HWANG, H. K. 2012. Bicuspid aortic valve: spectrum of imaging findings at cardiac MDCT and cardiovascular MRI. *AJR Am J Roentgenol,* 198**,** 89-97.

KODO, K., NISHIZAWA, T., FURUTANI, M., ARAI, S., YAMAMURA, E., JOO, K., TAKAHASHI, T., MATSUOKA, R. & YAMAGISHI, H. 2009. GATA6 mutations cause human cardiac outflow tract defects by disrupting semaphorin-plexin signaling. *Proc Natl Acad Sci U S A,* 106**,** 13933-8.

KOGENARU, S., QING, Y., GUO, Y. & WANG, N. 2012. RNA-seq and microarray complement each other in transcriptome profiling. *BMC Genomics,* 13**,** 629.

KOULLIAS, G. J., KORKOLIS, D. P., RAVICHANDRAN, P., PSYRRI, A., HATZARAS, I. & ELEFTERIADES, J. A. 2004. Tissue microarray detection of matrix metalloproteinases, in diseased tricuspid and bicuspid aortic valves with or without pathology of the ascending aorta. *Eur J Cardiothorac Surg,* 26**,** 1098-103.

KRUGER, R. P., AURANDT, J. & GUAN, K. L. 2005. Semaphorins command cells to move. *Nat Rev Mol Cell Biol,* 6**,** 789-800.

KUHLENBAUMER, G., HULLMANN, J. & APPENZELLER, S. 2011. Novel genomic techniques open new avenues in the analysis of monogenic disorders. *Hum Mutat,* 32**,** 144-51.

KURTOVIC, S., PALOSCHI, V., FOLKERSEN, L., GOTTFRIES, J., FRANCO-CERECEDA, A. & ERIKSSON, P. 2011. Diverging alternative splicing fingerprints in the transforming growth factor-beta signaling pathway identified in thoracic aortic aneurysms. *Mol Med,* 17**,** 665-75.

KUTTY, S., KAUL, S., DANFORD, C. J. & DANFORD, D. A. 2010. Main pulmonary artery dilation in association with congenital bicuspid aortic valve in the absence of pulmonary valve abnormality. *Heart,* 96**,** 1756-61.

KUURE, S., SAINIO, K., VUOLTEENAHO, R., ILVES, M., WARTIOVAARA, K., IMMONEN, T., KVIST, J., VAINIO, S. & SARIOLA, H. 2005. Crosstalk between Jagged1 and GDNF/Ret/GFRalpha1 signalling regulates ureteric budding and branching. *Mech Dev,* 122**,** 765-80.

LA GERCHE, A., CLAESSEN, G., VAN DE BRUAENE, A., PATTYN, N., VAN CLEEMPUT, J., GEWILLIG, M., BOGAERT, J., DYMARKOWSKI, S., CLAUS, P. & HEIDBUCHEL, H. 2013. Cardiac MRI: a new gold standard for ventricular volume quantification during high-intensity exercise. *Circ Cardiovasc Imaging,* 6**,** 329-38.

LAFOREST, B., ANDELFINGER, G. & NEMER, M. 2011. Loss of Gata5 in mice leads to bicuspid aortic valve. *J Clin Invest,* 121**,** 2876-87.

LAFOREST, B. & NEMER, M. 2011. GATA5 interacts with GATA4 and GATA6 in outflow tract development. *Dev Biol,* 358**,** 368-78.

LEE, K. F., SIMON, H., CHEN, H., BATES, B., HUNG, M. C. & HAUSER, C. 1995. Requirement for neuregulin receptor erbB2 in neural and cardiac development. *Nature,* 378**,** 394-8.

LEE, T. C., ZHAO, Y. D., COURTMAN, D. W. & STEWART, D. J. 2000. Abnormal aortic valve development in mice lacking endothelial nitric oxide synthase. *Circulation,* 101**,** 2345-8.

LEWIS, N. P. & HENDERSON, A. H. 1990. Calcific aortic stenosis in twins: a clue to its pathogenesis? *Eur Heart J,* 11**,** 90-1.

LIN, C. J., LIN, C. Y., CHEN, C. H., ZHOU, B. & CHANG, C. P. 2012a. Partitioning the heart: mechanisms of cardiac septation and valve development. *Development,* 139**,** 3277-99.

LIN, C. Y., LIN, C. J., CHEN, C. H., CHEN, R. M., ZHOU, B. & CHANG, C. P. 2012b. The secondary heart field is a new site of calcineurin/Nfatc1 signaling for semilunar valve development. *J Mol Cell Cardiol,* 52**,** 1096-102.

LIN, H. Y., BENDER, J. A., DING, Y., CHUNG, Y. C., HINTON, A. M., PENNELL, M. L., WHITEHEAD, K. K., RAMAN, S. V. & SIMONETTI, O. P. 2012c. Shared velocity encoding: a method to improve the temporal resolution of phase-contrast velocity measurements. *Magn Reson Med,* 68**,** 703-10.

LINCOLN, J., LANGE, A. W. & YUTZEY, K. E. 2006. Hearts and bones: shared regulatory mechanisms in heart valve, cartilage, tendon, and bone development. *Dev Biol,* 294**,** 292-302.

LINCOLN, J. & YUTZEY, K. E. 2011. Molecular and developmental mechanisms of congenital heart valve disease. *Birth Defects Res A Clin Mol Teratol,* 91**,** 526-34.

LIU, A. C., JOAG, V. R. & GOTLIEB, A. I. 2007. The emerging role of valve interstitial cell phenotypes in regulating heart valve pathobiology. *Am J Pathol,* 171**,** 1407-18.

LU, B. C., CEBRIAN, C., CHI, X., KUURE, S., KUO, R., BATES, C. M., ARBER, S., HASSELL, J., MACNEIL, L., HOSHI, M., JAIN, S., ASAI, N., TAKAHASHI, M., SCHMIDT-OTT, K. M., BARASCH, J., D'AGATI, V. & COSTANTINI, F. 2009. Etv4 and Etv5 are required downstream of GDNF and Ret for kidney branching morphogenesis. *Nat Genet,* 41**,** 1295-302.

MAHADEVIA, R., BARKER, A. J., SCHNELL, S., ENTEZARI, P., KANSAL, P., FEDAK, P. W., MALAISRIE, S. C., MCCARTHY, P., COLLINS, J., CARR, J. & MARKL, M. 2014. Bicuspid aortic cusp fusion morphology alters aortic three-dimensional outflow patterns, wall shear stress, and expression of aortopathy. *Circulation,* 129**,** 673-82.

MAJUMDAR, R., YAGUBYAN, M., SARKAR, G., BOLANDER, M. E. & SUNDT, T. M., 3RD 2006. Bicuspid aortic valve and ascending aortic aneurysm are not associated with germline or somatic homeobox NKX2-5 gene polymorphism in 19 patients. *J Thorac Cardiovasc Surg,* 131**,** 1301-5.

MARIAN, A. J. 2012. Molecular genetic studies of complex phenotypes. *Transl Res,* 159**,** 64-79.

MARKWALD, R. R., NORRIS, R. A., MORENO-RODRIGUEZ, R. & LEVINE, R. A. 2010. Developmental basis of adult cardiovascular diseases: valvular heart diseases. *Ann N Y Acad Sci,* 1188**,** 177-83.

MART, C. R. M., B.E. 2013. Shape of the dilated aorta in children with bicuspid aortic valve. *Ann Pediatr Cardiol,* 6**,** 126-131.

MARTIN, L. J., RAMACHANDRAN, V., CRIPE, L. H., HINTON, R. B., ANDELFINGER, G., TABANGIN, M., SHOONER, K., KEDDACHE, M. & BENSON, D. W. 2007. Evidence in favor of linkage to human chromosomal regions 18q, 5q and 13q for bicuspid aortic valve and associated cardiovascular malformations. *Hum Genet,* 121**,** 275-84.

MCCARTHY, M. I. & HIRSCHHORN, J. N. 2008. Genome-wide association studies: potential next steps on a genetic journey. *Hum Mol Genet,* 17**,** R156-65.

MCKELLAR, S. H., MICHELENA, H. I., LI, Z., SCHAFF, H. V. & SUNDT, T. M., 3RD 2010. Long-term risk of aortic events following aortic valve replacement in patients with bicuspid aortic valves. *Am J Cardiol,* 106**,** 1626-33.

MCKELLAR, S. H., TESTER, D. J., YAGUBYAN, M., MAJUMDAR, R., ACKERMAN, M. J. & SUNDT, T. M., 3RD 2007. Novel NOTCH1 mutations in patients with bicuspid aortic valve disease and thoracic aortic aneurysms. *J Thorac Cardiovasc Surg,* 134**,** 290-6.

MELINA, G., RAJAPPAN, K., AMRANI, M., KHAGHANI, A., PENNELL, D. J. & YACOUB, M. H. 2002. Aortic distensibility after aortic root replacement assessed with cardiovascular magnetic resonance. *J Heart Valve Dis,* 11**,** 67-74; discussion 74.

MENSAH, G. A. 2009. The Burden of Valvular Heart Disease. *In:* OTTO, C. M. & BONOW, R. O. (eds.) *Valvular Heart Disease: A Companion to Braunwald's Heart Disease.* 3 ed.: Elsevier Inc.

METAFRATZI, Z. M., EFREMIDIS, S. C., SKOPELITOU, A. S. & DE ROOS, A. 2002. The clinical significance of aortic compliance and its assessment with magnetic resonance imaging. *J Cardiovasc Magn Reson,* 4**,** 481-91.

MICHELENA, H. I., DESJARDINS, V. A., AVIERINOS, J. F., RUSSO, A., NKOMO, V. T., SUNDT, T. M., PELLIKKA, P. A., TAJIK, A. J. & ENRIQUEZ-SARANO, M. 2008. Natural history of asymptomatic patients with normally functioning or minimally dysfunctional bicuspid aortic valve in the community. *Circulation,* 117**,** 2776-84.

MICHELENA, H. I., KHANNA, A. D., MAHONEY, D., MARGARYAN, E., TOPILSKY, Y., SURI, R. M., EIDEM, B., EDWARDS, W. D., SUNDT, T. M., 3RD & ENRIQUEZ-SARANO, M. 2011. Incidence of aortic complications in patients with bicuspid aortic valves. *JAMA,* 306**,** 1104-12.

MOHAMED, S. A., AHERRAHROU, Z., LIPTAU, H., ERASMI, A. W., HAGEMANN, C., WROBEL, S., BORZYM, K., SCHUNKERT, H., SIEVERS, H. H. & ERDMANN, J. 2006. Novel missense mutations (p.T596M and p.P1797H) in NOTCH1 in patients with bicuspid aortic valve. *Biochem Biophys Res Commun,* 345**,** 1460-5.

MOHAMED, S. A., HANKE, T., SCHLUETER, C., BULLERDIEK, J. & SIEVERS, H. H. 2005. Ubiquitin fusion degradation 1-like gene dysregulation in bicuspid aortic valve. *J Thorac Cardiovasc Surg,* 130**,** 1531-6.

MOHAMED, S. A., RADTKE, A., SARAEI, R., BULLERDIEK, J., SORANI, H., NIMZYK, R., KARLUSS, A., SIEVERS, H. H. & BELGE, G. 2012. Locally Different Endothelial Nitric Oxide Synthase Protein Levels in Ascending Aortic Aneurysms of Bicuspid and Tricuspid Aortic Valve. *Cardiol Res Pract,* 2012**,** 165957.

MOLKENTIN, J. D. 2000. The zinc finger-containing transcription factors GATA-4, -5, and -6. Ubiquitously expressed regulators of tissue-specific gene expression. *J Biol Chem,* 275**,** 38949-52.

MONTANARO, L., PARISINI, P., GREGGI, T., DI SILVESTRE, M., CAMPOCCIA, D., RIZZI, S. & ARCIOLA, C. R. 2006. Evidence of a linkage between matrilin-1 gene (MATN1) and idiopathic scoliosis. *Scoliosis,* 1**,** 21.

MORDI, I. & TZEMOS, N. 2012. Bicuspid aortic valve disease: a comprehensive review. *Cardiol Res Pract,* 2012**,** 196037.

MORENO, P. R., ASTUDILLO, L., ELMARIAH, S., PURUSHOTHAMAN, K. R., PURUSHOTHAMAN, M., LENTO, P. A., SHARMA, S. K., FUSTER, V. & ADAMS, D. H. 2011. Increased macrophage infiltration and neovascularization in congenital bicuspid aortic valve stenosis. *J Thorac Cardiovasc Surg,* 142**,** 895-901.

MORRISEY, E. E., IP, H. S., TANG, Z. & PARMACEK, M. S. 1997. GATA-4 activates transcription via two novel domains that are conserved within the GATA-4/5/6 subfamily. *J Biol Chem,* 272**,** 8515-24.

NAGY, E., ANDERSSON, D. C., CAIDAHL, K., ERIKSSON, M. J., ERIKSSON, P., FRANCO-CERECEDA, A., HANSSON, G. K. & BACK, M. 2011. Upregulation of the 5-lipoxygenase pathway in human aortic valves correlates with severity of stenosis and leads to leukotriene-induced effects on valvular myofibroblasts. *Circulation,* 123**,** 1316-25.

NG, S. B., NICKERSON, D. A., BAMSHAD, M. J. & SHENDURE, J. 2010. Massively parallel sequencing and rare disease. *Hum Mol Genet,* 19**,** R119-24.

NIESSEN, K. & KARSAN, A. 2008. Notch signaling in cardiac development. *Circ Res,* 102**,** 1169-81.

NIGAM, V., SIEVERS, H. H., JENSEN, B. C., SIER, H. A., SIMPSON, P. C., SRIVASTAVA, D. & MOHAMED, S. A. 2010. Altered microRNAs in bicuspid aortic valve: a comparison between stenotic and insufficient valves. *J Heart Valve Dis,* 19**,** 459-65.

NIGAM, V. & SRIVASTAVA, D. 2009. Notch1 represses osteogenic pathways in aortic valve cells. *J Mol Cell Cardiol,* 47**,** 828-34.

NISTRI, S., GRANDE-ALLEN, J., NOALE, M., BASSO, C., SIVIERO, P., MAGGI, S., CREPALDI, G. & THIENE, G. 2008. Aortic elasticity and size in bicuspid aortic valve syndrome. *Eur Heart J,* 29**,** 472-9.

NISTRI, S., SORBO, M. D., MARIN, M., PALISI, M., SCOGNAMIGLIO, R. & THIENE, G. 1999. Aortic root dilatation in young men with normally functioning bicuspid aortic valves. *Heart,* 82**,** 19-22.

NKOMO, V. T., ENRIQUEZ-SARANO, M., AMMASH, N. M., MELTON, L. J., 3RD, BAILEY, K. R., DESJARDINS, V., HORN, R. A. & TAJIK, A. J. 2003. Bicuspid aortic valve associated with aortic dilatation: a community-based study. *Arterioscler Thromb Vasc Biol,* 23**,** 351-6.

NKOMO, V. T., GARDIN, J. M., SKELTON, T. N., GOTTDIENER, J. S., SCOTT, C. G. & ENRIQUEZ-SARANO, M. 2006. Burden of valvular heart diseases: a population-based study. *Lancet,* 368**,** 1005-11.

NORRIS, R. A., MORENO-RODRIGUEZ, R. A., SUGI, Y., HOFFMAN, S., AMOS, J., HART, M. M., POTTS, J. D., GOODWIN, R. L. & MARKWALD, R. R. 2008. Periostin regulates atrioventricular valve maturation. *Dev Biol,* 316**,** 200-13.

PADANG, R., BAGNALL, R. D., RICHMOND, D. R., BANNON, P. G. & SEMSARIAN, C. 2012a. Rare non-synonymous variations in the transcriptional activation domains of GATA5 in bicuspid aortic valve disease. *J Mol Cell Cardiol,* 53**,** 277-81.

PADANG, R., BAGNALL, R. D. & SEMSARIAN, C. 2012b. Genetic basis of familial valvular heart disease. *Circ Cardiovasc Genet,* 5**,** 569-80.

PADANG, R., BANNON, P. G., JEREMY, R., RICHMOND, D. R., SEMSARIAN, C., VALLELY, M., WILSON, M. & YAN, T. D. 2013. The genetic and molecular basis of bicuspid aortic valve associated thoracic aortopathy: a link to phenotype heterogeneity. *Ann Cardiothorac Surg,* 2**,** 83-91.

PADANG, R., DENNIS, M., SEMSARIAN, C., BANNON, P. G., TANOUS, D. J., CELERMAJER, D. S. & PURANIK, R. 2014. Detection of serious complications by MR imaging in asymptomatic young adults with repaired coarctation of the aorta. *Heart Lung Circ,* 23**,** 332-8.

PALOSCHI, V., KURTOVIC, S., FOLKERSEN, L., GOMEZ, D., WAGSATER, D., ROY, J., PETRINI, J., ERIKSSON, M. J., CAIDAHL, K., HAMSTEN, A., LISKA, J., MICHEL, J. B., FRANCO-CERECEDA, A. & ERIKSSON, P. 2011. Impaired splicing of fibronectin is associated with thoracic aortic aneurysm formation in patients with bicuspid aortic valve. *Arterioscler Thromb Vasc Biol,* 31**,** 691-7.

PANAYOTOVA, R., MACNAB, A. & WATERWORTH, P. D. 2013. A pilot project of familial screening in patients with bicuspid aortic valve disease. *J Heart Valve Dis,* 22**,** 150-5.

PATNALA, R., CLEMENTS, J. & BATRA, J. 2013. Candidate gene association studies: a comprehensive guide to useful in silico tools. *BMC Genet,* 14**,** 39.

PETERKIN, T., GIBSON, A., LOOSE, M. & PATIENT, R. 2005. The roles of GATA-4, -5 and -6 in vertebrate heart development. *Semin Cell Dev Biol,* 16**,** 83-94.

PHILLIPS, H. M., MAHENDRAN, P., SINGH, E., ANDERSON, R. H., CHAUDHRY, B. & HENDERSON, D. J. 2013. Neural crest cells are required for correct positioning of the developing outflow cushions and pattern the arterial valve leaflets. *Cardiovasc Res,* 99**,** 452-60.

PIERPONT, M. E., BASSON, C. T., BENSON, D. W., JR., GELB, B. D., GIGLIA, T. M., GOLDMUNTZ, E., MCGEE, G., SABLE, C. A., SRIVASTAVA, D. & WEBB, C. L. 2007. Genetic basis for congenital heart defects: current knowledge: a scientific statement from the American Heart Association Congenital Cardiac Defects Committee, Council on Cardiovascular Disease in the Young: endorsed by the American Academy of Pediatrics. *Circulation,* 115**,** 3015-38.

PISANO, C., MARESI, E., BALISTRERI, C. R., CANDORE, G., MERLO, D., FATTOUCH, K., BIANCO, G. & RUVOLO, G. 2011. Histological and genetic studies in patients with bicuspid aortic valve and ascending aorta complications. *Interact Cardiovasc Thorac Surg,* 14**,** 300-6.

PONTICOS, M., PARTRIDGE, T., BLACK, C. M., ABRAHAM, D. J. & BOU-GHARIOS, G. 2004. Regulation of collagen type I in vascular smooth muscle cells by competition between Nkx2.5 and deltaEF1/ZEB1. *Mol Cell Biol,* 24**,** 6151-61.

POSCH, M. G., GRAMLICH, M., SUNDE, M., SCHMITT, K. R., LEE, S. H., RICHTER, S., KERSTEN, A., PERROT, A., PANEK, A. N., AL KHATIB, I. H., NEMER, G., MEGARBANE, A., DIETZ, R., STILLER, B., BERGER, F., HARVEY, R. P. & OZCELIK, C. 2010. A gain-of-function TBX20 mutation causes congenital atrial septal defects, patent foramen ovale and cardiac valve defects. *J Med Genet,* 47**,** 230-5.

PRAKASH, S. K., BOSSE, Y., MUEHLSCHLEGEL, J. D., MICHELENA, H. I., LIMONGELLI, G., DELLA CORTE, A., PLUCHINOTTA, F. R., RUSSO, M. G., EVANGELISTA, A., BENSON, D. W., BODY, S. C., MILEWICZ, D. M. & INVESTIGATORS, B. A. 2014. A roadmap to investigate the genetic basis of bicuspid aortic valve and its complications: insights from the International BAVCon (Bicuspid Aortic Valve Consortium). *J Am Coll Cardiol,* 64**,** 832-9.

PRATLEY, R., NICKLAS, B., RUBIN, M., MILLER, J., SMITH, A., SMITH, M., HURLEY, B. & GOLDBERG, A. 1994. Strength training increases resting metabolic rate and norepinephrine levels in healthy 50- to 65-yr-old men. *J Appl Physiol (1985),* 76**,** 133-7.

PURANIK, R., TSANG, V. T., PURANIK, S., JONES, R., CULLEN, S., BONHOEFFER, P., HUGHES, M. L. & TAYLOR, A. M. 2009. Late magnetic resonance surveillance of repaired coarctation of the aorta. *Eur J Cardiothorac Surg,* 36**,** 91-5; discussion 95.

QUENOT, J. P., BOICHOT, C., PETIT, A., FALCON-EICHER, S., D'ATHIS, P., BONNET, C., WOLF, J. E., LOUIS, P. & BRUNOTTE, F. 2005. Usefulness of MRI in the follow-up of patients with repaired aortic coarctation and bicuspid aortic valve. *International journal of cardiology,* 103**,** 312-6.

RAASTAD, T., GLOMSHELLER, T., BJORO, T. & HALLEN, J. 2001. Changes in human skeletal muscle contractility and hormone status during 2 weeks of heavy strength training. *Eur J Appl Physiol,* 84**,** 54-63.

RAJAMANNAN, N. M. 2011. Bicuspid aortic valve disease: the role of oxidative stress in Lrp5 bone formation. *Cardiovasc Pathol,* 20**,** 168-76.

REAMON-BUETTNER, S. M. & BORLAK, J. 2004. TBX5 mutations in non-Holt-Oram syndrome (HOS) malformed hearts. *Hum Mutat,* 24**,** 104.

RICCI, M., XU, Y., HAMMOND, H. L., WILLOUGHBY, D. A., NATHANSON, L., RODRIGUEZ, M. M., VATTA, M., LIPSHULTZ, S. E. & LINCOLN, J. 2012. Myocardial alternative RNA splicing and gene expression profiling in early stage hypoplastic left heart syndrome. *PLoS One,* 7**,** e29784.

ROBICSEK, F., THUBRIKAR, M. J., COOK, J. W. & FOWLER, B. 2004. The congenitally bicuspid aortic valve: how does it function? Why does it fail? *Ann Thorac Surg,* 77**,** 177-85.

ROGER, V. L., GO, A. S., LLOYD-JONES, D. M., BENJAMIN, E. J., BERRY, J. D., BORDEN, W. B., BRAVATA, D. M., DAI, S., FORD, E. S., FOX, C. S., FULLERTON, H. J., GILLESPIE, C., HAILPERN, S. M., HEIT, J. A., HOWARD, V. J., KISSELA, B. M., KITTNER, S. J., LACKLAND, D. T., LICHTMAN, J. H., LISABETH, L. D., MAKUC, D. M., MARCUS, G. M., MARELLI, A., MATCHAR, D. B., MOY, C. S., MOZAFFARIAN, D.,

MUSSOLINO, M. E., NICHOL, G., PAYNTER, N. P., SOLIMAN, E. Z., SORLIE, P. D., SOTOODEHNIA, N., TURAN, T. N., VIRANI, S. S., WONG, N. D., WOO, D. & TURNER, M. B. 2012. Heart disease and stroke statistics--2012 update: a report from the American Heart Association. *Circulation,* 125**,** e2-e220.

RUDDY, J. M., JONES, J. A., STROUD, R. E., MUKHERJEE, R., SPINALE, F. G. & IKONOMIDIS, J. S. 2010. Differential effect of wall tension on matrix metalloproteinase promoter activation in the thoracic aorta. *J Surg Res,* 160**,** 333-9.

RUSANESCU, G., WEISSLEDER, R. & AIKAWA, E. 2008. Notch signaling in cardiovascular disease and calcification. *Curr Cardiol Rev,* 4**,** 148-56.

RUSSO, C. F., CANNATA, A., LANFRANCONI, M., VITALI, E., GARATTI, A. & BONACINA, E. 2008. Is aortic wall degeneration related to bicuspid aortic valve anatomy in patients with valvular disease? *J Thorac Cardiovasc Surg,* 136**,** 937-42.

SANS-COMA, V., CARMEN FERNANDEZ, M., FERNANDEZ, B., DURAN, A. C., ANDERSON, R. H. & ARQUE, J. M. 2012. Genetically alike Syrian hamsters display both bifoliate and trifoliate aortic valves. *J Anat,* 220**,** 92-101.

SCHAEFER, B. M., LEWIN, M. B., STOUT, K. K., GILL, E., PRUEITT, A., BYERS, P. H. & OTTO, C. M. 2008. The bicuspid aortic valve: an integrated phenotypic classification of leaflet morphology and aortic root shape. *Heart,* 94**,** 1634-8.

SCHNABEL, R. B., BACCARELLI, A., LIN, H., ELLINOR, P. T. & BENJAMIN, E. J. 2012. Next steps in cardiovascular disease genomic research--sequencing, epigenetics, and transcriptomics. *Clin Chem,* 58**,** 113-26.

SCHOEN, F. J. 2008. Evolving concepts of cardiac valve dynamics: the continuum of development, functional structure, pathobiology, and tissue engineering. *Circulation,* 118**,** 1864-80.

SCHOTT, J. J., BENSON, D. W., BASSON, C. T., PEASE, W., SILBERBACH, G. M., MOAK, J. P., MARON, B. J., SEIDMAN, C. E. & SEIDMAN, J. G. 1998. Congenital heart disease caused by mutations in the transcription factor NKX2-5. *Science,* 281**,** 108-11.

SEGAT, D., FRIE, C., NITSCHE, P. D., KLATT, A. R., PIECHA, D., KORPOS, E., DEAK, F., WAGENER, R., PAULSSON, M. & SMYTH, N. 2000. Expression of matrilin-1, -2 and -3 in developing mouse limbs and heart. *Matrix Biol,* 19**,** 649-55.

SEO, J. B., CHUNG, W. Y., KIM, S. H., KIM, M. A. K. & ZO, J. H. 2013. Immediate impact of exercise on arterial stiffness in humans. *World J Cardiovasc Dis,* 3**,** 40-45.

SHENOY, C., MARON, M. S. & PANDIAN, N. G. 2014. Cardiovascular magnetic resonance imaging for bicuspid aortic valve syndrome: the time is now. *Eur Heart J Cardiovasc Imaging,* 15**,** 612-4.

SHI, L. M., TAO, J. W., QIU, X. B., WANG, J., YUAN, F., XU, L., LIU, H., LI, R. G., XU, Y. J., WANG, Q., ZHENG, H. Z., LI, X., WANG, X. Z., ZHANG, M., QU, X. K. & YANG, Y. Q. 2014. GATA5 loss-of-function mutations associated with congenital bicuspid aortic valve. *Int J Mol Med,* 33**,** 1219-26.

SHIBATA, S. & LEVINE, B. D. 2011. Biological aortic age derived from the arterial pressure waveform. *J Appl Physiol (1985),* 110**,** 981-7.

SIEVERS, H. H. & SCHMIDTKE, C. 2007. A classification system for the bicuspid aortic valve from 304 surgical specimens. *J Thorac Cardiovasc Surg,* 133**,** 1226-33.

SIU, S. C. & SILVERSIDES, C. K. 2010. Bicuspid aortic valve disease. *J Am Coll Cardiol,* 55**,** 2789-800.

SOHNS, J. M., UNTERBERG-BUCHWALD, C., KOWALLICK, J. T., STEINMETZ, M., SCHULTE, C., STABB, W., JOSEPH, A., MERBOLDT, K. D., VOIT, D., ZHANG, S., UECKER, M., FRAHM, J. & LOTZ, J. 2013. Real-time cardiac phase contrast MRI blood flow including Valsalva and Mueller maneuver. Initial experiences. *J Cardiovasc Magn Reson,* 15 (Suppl 1)**,** E17.

SRIVASTAVA, D. & OLSON, E. N. 2000. A genetic blueprint for cardiac development. *Nature,* 407**,** 221-6.

TABOR, H. K., RISCH, N. J. & MYERS, R. M. 2002. Candidate-gene approaches for studying complex genetic traits: practical considerations. *Nat Rev Genet,* 3**,** 391-7.

TADROS, T. M., KLEIN, M. D. & SHAPIRA, O. M. 2009. Ascending aortic dilatation associated with bicuspid aortic valve: pathophysiology, molecular biology, and clinical implications. *Circulation,* 119**,** 880-90.

TAKEUCHI, J. K., MILEIKOVSKAIA, M., KOSHIBA-TAKEUCHI, K., HEIDT, A. B., MORI, A. D., ARRUDA, E. P., GERTSENSTEIN, M., GEORGES, R., DAVIDSON, L., MO, R., HUI, C. C., HENKELMAN, R. M., NEMER, M., BLACK, B. L., NAGY, A. & BRUNEAU, B. G. 2005. Tbx20 dose-dependently regulates transcription factor networks required for mouse heart and motoneuron development. *Development,* 132**,** 2463-74.

THOMAS, P. S., SRIDURONGRIT, S., RUIZ-LOZANO, P. & KAARTINEN, V. 2012. Deficient signaling via Alk2 (Acvr1) leads to bicuspid aortic valve development. *PLoS One,* 7**,** e35539.

TIAN, L. & CHESLER, N. C. 2012. In vivo and in vitro measurements of pulmonary arterial stiffness: A brief review. *Pulm Circ,* 2**,** 505-17.

TOWNE, M. C., BEGGS, A. H. & AGRAWAL, P. B. 2013. Efficiency of whole exome/genome sequencing for achieving a diagnosis in rare presentations (abstract). *American Society of Human Genetics 2013 Meeting.* Boston.

TOYOFUKU, T., YOSHIDA, J., SUGIMOTO, T., YAMAMOTO, M., MAKINO, N., TAKAMATSU, H., TAKEGAHARA, N., SUTO, F., HORI, M., FUJISAWA, H., KUMANOGOH, A. & KIKUTANI, H. 2008. Repulsive and attractive semaphorins cooperate to direct the navigation of cardiac neural crest cells. *Dev Biol,* 321**,** 251-62.

TUTAR, E., EKICI, F., ATALAY, S. & NACAR, N. 2005. The prevalence of bicuspid aortic valve in newborns by echocardiographic screening. *Am Heart J,* 150**,** 513-5.

TZEMOS, N., THERRIEN, J., YIP, J., THANASSOULIS, G., TREMBLAY, S., JAMORSKI, M. T., WEBB, G. D. & SIU, S. C. 2008. Outcomes in adults with bicuspid aortic valves. *JAMA* 300**,** 1317-25.

VALLELY, M. P., SEMSARIAN, C. & BANNON, P. G. 2008. Management of the ascending aorta in patients with bicuspid aortic valve disease. *Heart Lung Circ,* 17**,** 357-63.

VANDESOMPELE, J., DE PRETER, K., PATTYN, F., POPPE, B., VAN ROY, N., DE PAEPE, A. & SPELEMAN, F. 2002. Accurate normalization of real-time quantitative RT-PCR data by geometric averaging of multiple internal control genes. *Genome Biol,* 3**,** RESEARCH0034.

VERMA, S. & SIU, S. C. 2014. Aortic dilatation in patients with bicuspid aortic valve. *N Engl J Med,* 370**,** 1920-9.

WALSH, E. C. & STAINIER, D. Y. 2001. UDP-glucose dehydrogenase required for cardiac valve formation in zebrafish. *Science,* 293**,** 1670-3.

WARD, C. 2000. Clinical significance of the bicuspid aortic valve. *Heart,* 83**,** 81-5.

WARE, J. S., ROBERTS, A. M. & COOK, S. A. 2012. Next generation sequencing for clinical diagnostics and personalised medicine: implications for the next generation cardiologist. *Heart,* 98**,** 276-81.

WIRRIG, E. E. & YUTZEY, K. E. 2011. Transcriptional regulation of heart valve development and disease. *Cardiovasc Pathol,* 20**,** 162-7.

WIRRIG, E. E. Y., K.E. 2013. Developmental pathways in CAVD, Calcific Aortic Valve Disease. *In:* AIKAWA, E. (ed.) *Cardiology and Cardiovascular Medicine.* InTech.

WOODWARD, E. R., ENG, C., MCMAHON, R., VOUTILAINEN, R., AFFARA, N. A., PONDER, B. A. & MAHER, E. R. 1997. Genetic predisposition to phaeochromocytoma: analysis of candidate genes GDNF, RET and VHL. *Hum Mol Genet,* 6**,** 1051-6.

YANAGAWA, B., LOVREN, F., PAN, Y., GARG, V., QUAN, A., TANG, G., SINGH, K. K., SHUKLA, P. C., KALRA, N. P., PETERSON, M. D. & VERMA, S. 2012. miRNA-141 is a novel regulator of BMP-2-mediated calcification in aortic stenosis. *J Thorac Cardiovasc Surg,* 144**,** 256-62.

YASUDA, H., NAKATANI, S., STUGAARD, M., TSUJITA-KURODA, Y., BANDO, K., KOBAYASHI, J., YAMAGISHI, M., KITAKAZE, M., KITAMURA, S. & MIYATAKE, K. 2003. Failure to prevent progressive dilation of ascending aorta by aortic valve replacement in patients with bicuspid aortic valve: comparison with tricuspid aortic valve. *Circulation,* 108 Suppl 1**,** II291-4.